



# MONASH University

## **The Application of Ultrasound in the Imaging of Impingements of the Shoulder and Native and Post-Arthroplastic Hip**

*David John Robinson*

*BAppSci (Medical Imaging) Grad Dip (CompSci) DMU (Gen, Vasc)*

A thesis submitted for the degree of *Doctor of Philosophy* at

Monash University in 2018

Department of Medical Imaging and Radiation Sciences

Faculty of Medicine, Nursing and Health Sciences

This page intentionally left blank

# Table of Contents

<b>TABLE OF CONTENTS .....</b>	<b>III</b>
<b>COPYRIGHT NOTICE .....</b>	<b>VIII</b>
<b>DECLARATION .....</b>	<b>IX</b>
<b>LIST OF CONFERENCE PRESENTATIONS .....</b>	<b>XIII</b>
<b>LIST OF ABBREVIATIONS .....</b>	<b>XIV</b>
LIST OF FIGURES .....	XVI
<b>LIST OF TABLES .....</b>	<b>XIX</b>
<b>ACKNOWLEDGEMENTS.....</b>	<b>XX</b>
<b>ABSTRACT .....</b>	<b>1</b>
<b>CHAPTER 1 INTRODUCTION .....</b>	<b>5</b>
1.1 IMPINGEMENT AND ENTRAPMENT SYNDROMES .....	5
1.2 PREVALENCE OF IMPINGEMENT AND ENTRAPMENT SYNDROMES.....	5
1.3 CURRENT IMAGING TECHNIQUES FOR IMPINGEMENT AND ENTRAPMENT SYNDROMES.....	8
1.3.1 Current imaging in Quadrilateral Space Syndrome .....	9
1.3.2 Current imaging for detection and quantification of FAI.....	13
1.3.3 Current imaging of Adverse Local Tissue Reaction .....	15
1.4 PURPOSE OF THESIS.....	16
<b>CHAPTER 2 ANATOMY OF THE SHOULDER AND HIP .....</b>	<b>18</b>
2.1 ANATOMY OF THE SHOULDER JOINT .....	18
2.1.1 Osteology of the Shoulder joint .....	18
2.1.2 Angiology of the Proximal Upper Limb .....	19
2.1.3 Neurology of the Proximal Upper Limb.....	22
2.1.4 The Quadrilateral space.....	27

2.1.5 <i>The Thoracic Outlet</i> .....	28
2.2 ANATOMY OF THE HIP JOINT .....	29
2.2.1 <i>Osteology of the Hip joint</i> .....	29
2.2.2 <i>Angiology of the Hip</i> .....	31
2.2.3 <i>Arthrology</i> .....	34
2.2.4 <i>Neurology of the Hip</i> .....	40
<b>CHAPTER 3 LITERATURE REVIEW</b> .....	<b>43</b>
3.1 QUADRILATERAL SPACE SYNDROME (QSS).....	43
3.1.1 <i>Fibrous bands</i> .....	43
3.1.2 <i>Shoulder translation with movement</i> .....	45
3.1.3 <i>Mass lesions</i> .....	45
3.1.4 <i>Other causes</i> .....	45
3.2 NATURAL HISTORY OF QSS.....	47
3.2.1 <i>Pathophysiology of QSS</i> .....	48
3.2.2 <i>Thoracic Outlet Syndrome</i> .....	50
3.3 DIAGNOSIS OF QSS.....	53
3.4 PATHOPHYSIOLOGY OF PRIMARY OSTEOARTHRITIS OF THE HIP .....	72
3.4.1 <i>Natural History of Hip Dysmorphia</i> .....	75
3.4.2 <i>Femoroacetabular Impingement</i> .....	77
3.4.3 <i>Diagnosis of Femoroacetabular Impingement</i> .....	83
3.4.4 <i>Treatment of Femoroacetabular impingement</i> .....	93
3.5 POST-ARTHROPLASTIC IMPINGEMENT .....	96
3.5.1 <i>Adverse Local Tissue Reaction around hip replacements – ALTR</i> .....	96
3.5.2 <i>Current Imaging of the Post-Arthroplastic Hip</i> .....	97
3.5.3 <i>Ultrasound</i> .....	99
<b>CHAPTER 4 ULTRASOUND OF THE POSTERIOR CIRCUMFLEX HUMERAL ARTERY</b> .....	<b>101</b>
4.1 DECLARATION FOR THESIS CHAPTER.....	103



4.2 SUMMARY .....	105
4.3 INTRODUCTION .....	105
4.4 METHODS .....	108
4.4.1 Patient Selection .....	108
4.4.2 Ultrasound Technique.....	108
4.5 RESULTS.....	113
4.6 DISCUSSION .....	116
4.7 CONCLUSION .....	117
 <b>CHAPTER 5 OCCLUSION AND STENOSIS OF THE POSTERIOR CIRCUMFLEX HUMERAL ARTERY:</b>	
<b>DETECTION WITH ULTRASOUND IN A NORMAL POPULATION.....</b>	<b>119</b>
5.1 DECLARATION FOR THESIS CHAPTER.....	120
5.2 ABSTRACT .....	122
5.3 INTRODUCTION .....	123
5.4 PATIENTS AND METHODS .....	124
5.5 ULTRASOUND TECHNIQUE.....	125
5.6 STATISTICAL ANALYSIS .....	127
5.7 RESULTS.....	127
5.8 DISCUSSION .....	131
 <b>CHAPTER 6 ULTRASOUND DETERMINATION OF THE FEMORAL HEAD-NECK ALPHA ANGLE .....</b>	
<b>6.1 DECLARATION FOR THESIS CHAPTER.....</b>	<b>138</b>
<b>6.2 ABSTRACT .....</b>	<b>141</b>
<b>6.3 INTRODUCTION .....</b>	<b>143</b>
<b>6.4 MATERIALS AND METHODS .....</b>	<b>146</b>
<b>6.5 RESULTS.....</b>	<b>150</b>
<b>6.6 DISCUSSION .....</b>	<b>155</b>
<b>6.7 CONCLUSION .....</b>	<b>159</b>

<b>CHAPTER 7 ULTRASOUND SCREENING FOR ADVERSE LOCAL TISSUE REACTION AFTER HIP</b>	
<b>ARTHROPLASTY .....</b>	<b>160</b>
7.1 DECLARATION FOR THESIS CHAPTER.....	162
7.2 ABSTRACT .....	165
7.3 INTRODUCTION.....	166
7.4 METHODS .....	167
7.4.1 X-ray protocol.....	168
7.4.2 Ultrasound protocol .....	168
7.5 RESULTS.....	171
7.6 DISCUSSION .....	177
<b>CHAPTER 8 DISCUSSION.....</b>	<b>184</b>
8.1 ULTRASOUND AS AN ANGIOGRAPHY TOOL IN THE ASSESSMENT OF THE PCHA .....	184
8.2 COMPARISON OF MEASUREMENT OF THE HIP ALPHA ANGLE BETWEEN ULTRASOUND AND 3DCT.....	188
8.3 ULTRASOUND FOR EARLY ALTR DETECTION .....	192
<b>CHAPTER 9 CONCLUSION .....</b>	<b>196</b>
<b>CHAPTER 10 REFERENCES .....</b>	<b>198</b>
<b>APPENDIX 1 ULTRASOUND OF THE POSTERIOR CIRCUMFLEX HUMERAL ARTERY .....</b>	<b>210</b>
EXPLANATORY STATEMENT .....	211
PATIENT QUESTIONNAIRE .....	214
CONSENT FORM .....	216
SUGGESTED AMENDMENTS .....	217
<i>Exclusion criteria</i> .....	217
<i>Pulsatility Index (PI)</i> .....	217
<i>Number of males and females</i> .....	217
<i>Students t-test</i> .....	217
<i>Results table.</i> .....	217
<i>Reliability of scanning method</i> .....	218

**APPENDIX 2 ULTRASOUND DETERMINATION OF THE FEMORAL HEAD-NECK ALPHA ANGLE..... 219**

HUMAN ETHICS CERTIFICATE OF APPROVAL .....	219
EXPLANATORY STATEMENT .....	221
CONSENT FORM .....	224
SUGGESTED AMENDMENTS .....	225
<i>Results contingency table: Ultrasound determination of the Femoral Head-Neck alpha angle</i> .....	225
<i>IntraClass Correlation Coefficient</i> .....	225
<i>Doppler Settings</i> .....	225

**APPENDIX 3 ULTRASOUND OF THE ILIOPSOAS BURSA ..... 227**

EXPLANATORY STATEMENT .....	227
CONSENT FORM .....	230
SUGGESTED AMENDMENTS .....	231
<i>Exclusion criteria</i> .....	231
<i>Ultrasound measurements</i> .....	231
<i>Threshold of normal</i> .....	231

## **Copyright Notice**

© David John Robinson (2018).

Except as provided in the Copyright Act 1968, this thesis may not be reproduced in any form without the written permission of the author.

## **Declaration**

In accordance with Monash University Doctorate Regulation 17.2 Doctor of Philosophy and Research Master's regulations the following declarations are made:

I hereby declare that this thesis contains no material which has been accepted for the award of any other degree or diploma at any university or equivalent institution and that, to the best of my knowledge and belief, this thesis contains no material previously published or written by another person, except where due reference is made in the text of the thesis.

This thesis includes four original papers published in peer reviewed journals. The core theme of the thesis is to evaluate the utility of ultrasound in the detection of impingement syndromes affecting the shoulder and hip.

The ideas, development and writing up of all the papers in the thesis were the principal responsibility of myself, the candidate, working within the Department of Medical Imaging and Radiation Sciences under the main supervision of A/Prof Michal Schneider, and clinical co-supervision of Drs Steven Lee and Paul Marks.

The inclusion of co-authors reflects the fact that the work is based on active collaboration between researchers and acknowledges input into team-based research.

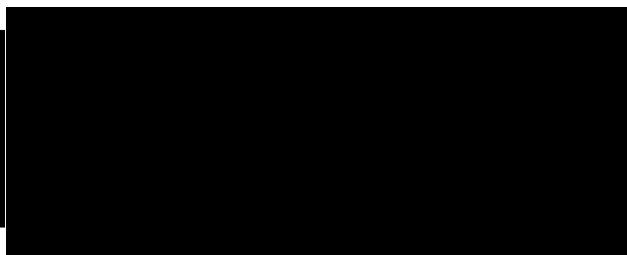
In the case of chapters 4, 5, 6 and 7 my contribution to the work involved the following:

		Status			Co-
Thesis Chapter	Publication Title	(published, in press, accepted or returned for revision, submitted)	Nature and % of student contribution	Co-author name(s) Nature and % of Co-author's contribution*	author(s), Monash student Y/N*
4	Ultrasound of the posterior circumflex humeral artery	Published	80% Concept, collecting data, data analysis, writing published draft	1) Dr. Paul Marks Concept and input into manuscript 10% 2) A/Prof Michal Schneider Input into manuscript 10%	No  No
5	Occlusion and stenosis of the posterior circumflex humeral artery in a normal population	Published	75% Concept, collecting data, data analysis, writing published draft	1) Dr Paul Marks Concept and input into manuscript 10% 3) A/Prof Michal Schneider Input into manuscript 15%	No  No

6	Ultrasound determination of the femoral head-neck alpha angle	Published	75% Concept, data collection and analysis, writing submitted draft	1) Dr. Steven Lee Input into manuscript 10% 2) Dr Paul Marks Concept and input into manuscript 5% 3) A/Prof Michal Schneider Input into manuscript 10%	No  No  No
7	Ultrasound screening for adverse local tissue reaction after hip arthroplasty	Published	75% Concept, collecting data, data analysis, writing published draft	1) Dr Steven Lee Input into manuscript 10% 2) Dr Paul Marks Concept and input into manuscript 5% 3) A/Prof Michal Schneider Input into manuscript 10%	No  No  No

I have renumbered sections of submitted or published papers in order to generate a consistent presentation within the thesis.

**Student signature:**

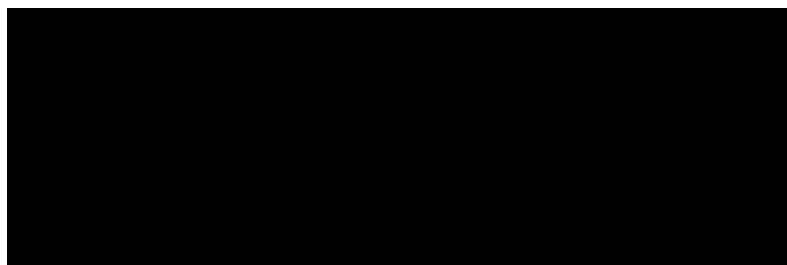


**Date:** 27 September 2018

Print Name.....David John Robinson

The undersigned hereby certify that the above declaration correctly reflects the nature and extent of the student's and co-authors' contributions to this work. In instances where I am not the responsible author I have consulted with the responsible author to agree on the respective contributions of the authors.

**Main Supervisor signature:**



**Date:** 28 November 2018



## List of Conference Presentations

### **Ultrasound of the Posterior Circumflex Humeral Artery**

**Robinson DJ, Marks P, Schneider-Kolsky ME**

Oral Presentation

12<sup>th</sup> World Congress of the World Federation for Ultrasound in Medicine and Biology

30 August – 3 September 2009

Sydney Convention & Exhibition Centre, Sydney, Australia

### **Two methods of calculating alpha angle in computed tomography assessment of femoroacetabular impingement**

**Robinson DJ, Lee S, Marks P, Schneider ME**

Poster Presentation

Combined Scientific Meeting – Australasian Society of Medical Imaging and Radiation Therapy

Imaging and Radiation in personalised medicine

4 – 7 September 2014

Melbourne Convention and Exhibition Center, Australia

### **Ultrasound of the Hip Replacement**

**Robinson DJ, Lee S, Marks P, Schneider M**

Oral Presentation

Concurrent session 1B – Musculoskeletal Lower Limb

44<sup>th</sup> Annual Scientific Meeting of the Australasian Society for Ultrasound in Medicine

17 – 19 October 2014

Crown Promenade, Melbourne, Australia

### **Ultrasound of the post-arthroplastic hip**

**Robinson, DJ, Lee S, Marks P, Schneider, M**

Oral Presentation

Musculoskeletal Series: Ultrasound RC304 – 05

101<sup>st</sup> Scientific Assembly and Annual Meeting

Radiological Society of North America

November 29 – December 4, 2015

McCormick Place, Chicago, USA.

### **Reliable Measurement of the Femoral Head-neck Alpha Angle Utilizing Ultrasound**

**Robinson DJ, Lee S, Marks P, Schneider M**

Poster presentation MK345-SD-TUA4

101<sup>st</sup> Scientific Assembly and Annual Meeting

Radiological Society of North America

November 29 – December 4, 2015

McCormick Place, Chicago, USA.

### **Ultrasound Post Hip Arthroplasty**

**Robinson DJ, Lee S, Schneider M**

Oral Presentation

3<sup>rd</sup> Annual Radiologists Conference

Healthcare Imaging Services – National Imaging Conference “A Clear View”

Grand Hyatt Melbourne, Vic Australia

September 08 – September 10, 2017

## List of Abbreviations

<u><math>\alpha</math> angle</u>	<u>alpha angle, measured at the femoral head-neck junction</u>
ABER	abduction and external rotation (of the arm)
ALTR	adverse local tissue reaction
AT	acceleration time
aTOS	arterial thoracic outlet syndrome
BHR	Birmingham Hip Replacement
EDV	end diastolic velocity
FABER	flexion abduction and external rotation – Patrick test
FADIR	flexion adduction and internal rotation – anterior impingement test
FAI	femoroacetabular impingement
MR	magnetic resonance
MRI	magnetic resonance imaging
MARS MRI	metal artefact reduction sequencing MRI
nTOS	neurogenic thoracic outlet syndrome
OA	osteoarthritis
PCHA	posterior circumflex humeral artery
<u>PCC</u>	<u>Pearson correlation coefficient</u>
PSV	peak systolic velocity
QSS	quadrilateral space syndrome
RI	resistive index
SCFE	slipped capital femoral epiphysis
TOS	thoracic outlet syndrome
US	ultrasound
vTOS	venous thoracic outlet syndrome
XR	plain x-ray
XIV	

3DCT

three-dimensional computed tomography

# List of Figures

FIGURE 1-1: ULTRASOUND OF THE MEDIAN NERVE AT THE WRIST. ....	9
FIGURE 1-2: MAGNETIC RESONANCE ANGIOGRAM OF THE PCHA. ....	10
FIGURE 1-3: DOPPLER ULTRASOUND OF A RADIAL ARTERY STENOSIS. ....	12
FIGURE 1-4: THE ALPHA ANGLE DESCRIBED BY NÖTZLI ET AL (2002). ....	14
FIGURE 1-5: 3DCT (LEFT) AND MRI (RIGHT) OF THE HIP DEMONSTRATING THE AXIAL PLANE USED FOR CALCULATION OF THE ALPHA ANGLE. ....	15
FIGURE 2-1: BONY ANATOMY OF THE SHOULDER. THREE-DIMENSIONAL COMPUTED TOMOGRAM OF THE RIGHT SHOULDER, VIEWED FROM ANTEROLATERAL. ....	19
FIGURE 2-2: CORONAL VIEW OF THE RIGHT SHOULDER - DETAILED ANATOMY OF THE THORACIC OUTLET.....	21
FIGURE 2-3: ARTERIAL ANATOMY OF THE LEFT SHOULDER VIEWED FROM BEHIND.....	22
FIGURE 2-4: DETAILED ANATOMY OF THE BRACHIAL PLEXUS (RIGHT SHOULDER FROM THE FRONT). ....	25
FIGURE 2-5: THE ANATOMY OF THE QUADRILATERAL SPACE (LEFT SHOULDER VIEWED FROM BEHIND). ....	26
FIGURE 2-6: SCHEMATIC REPRESENTATION OF THE COURSE OF THE AXILLARY NERVE BEYOND THE QUADRILATERAL SPACE. ....	27
FIGURE 2-7: THE QUADRILATERAL SPACE OF THE LEFT SHOULDER, VIEWED FROM BEHIND.....	28
FIGURE 2-8: ANATOMY OF THE ANTERIOR FEMORAL NECK. ....	30
FIGURE 2-9: THE COMMON FEMORAL ARTERY.....	33
FIGURE 2-10: THE HIP JOINT. ....	36
FIGURE 2-11: THE LIGAMENTS OF THE ANTERIOR HIP JOINT. ....	37
FIGURE 2-12: THE ILIOPSOAS BURSA SHOWN HERE IN BLUE OVERLYING THE HIP JOINT. ....	40
FIGURE 2-13: THE FEMORAL NERVE. PASSING OVER THE CONJOINT ILIOPSOAS TENDON ANTERIOR TO THE HIP JOINT.....	41
FIGURE 2-14: THE GENITOFEMORAL NERVE AND ITS' BRANCHES .....	42
FIGURE 3-1: MAGNETIC RESONANCE IMAGE OF A PATIENT WITH A GANGLION PROJECTING FROM THE INFERIOR LABRUM.....	47
FIGURE 3-2: ANTEROPOSTERIOR (LEFT) AND LATERAL (WITH 15 DEGREES' DOWN TILT (RIGHT)) PLAIN X-RAY OF THE RIGHT SHOULDER. ....	55

FIGURE 3-3: SAGITTAL PROTON DENSITY MRI SCAN OF THE SHOULDER OF A PATIENT REFERRED FOR SHOULDER PAIN. ....	59
FIGURE 3-4: POSTERIOR CIRCUMFLEX HUMERAL ARTERY ULTRASOUND. ....	67
FIGURE 3-5: TRANSVERSE ULTRASOUND OF POSTERIOR RIGHT SHOULDER. ....	69
FIGURE 3-6: TRANSVERSE ULTRASOUND OF THE POSTERIOR RIGHT SHOULDER. ....	70
FIGURE 3-7: NORMAL HIP (LEFT) COMPARED TO HIP DEMONSTRATING A SMALL BUMP (BLACK ARROW-RIGHT) AT THE SUPEROLATERAL JUNCTION OF THE FEMORAL HEAD AND NECK. ....	74
FIGURE 3-8: THE CAM EFFECT. ....	80
FIGURE 3-9: PINCER IMPINGEMENT. ....	82
FIGURE 3-10: THE CLOCK-FACE NOMENCLATURE OF RAKHRA ....	88
FIGURE 3-11: FORTY-THREE-YEAR-OLD FEMALE WITH HIP AND GROIN PAIN ....	91
FIGURE 3-12: CT SCAN OF A BIRMINGHAM HIP RESURFACING SHOWING METAL ARTEFACT DEGRADING THE IMAGE OF THE PERIPROSTHETIC SOFT TISSUES. ....	98
FIGURE 4-1: ASSESSMENT OF THE LEFT PCHA. ....	111
FIGURE 4-2: PATIENT POSITIONING FOR ULTRASOUND SCANNING OF THE LEFT POSTERIOR CIRCUMFLEX HUMERAL ARTERY. ....	112
FIGURE 4-3: POSTERIOR CIRCUMFLEX HUMERAL ARTERY (PCHA) ULTRASOUND. ....	113
FIGURE 4-4: TENDON OF THE TERES MINOR PASSING ACROSS THE POSTERIOR HUMERAL HEAD ....	114
FIGURE 4-5: TYPICAL PULSED DOPPLER SIGNAL OBTAINED FROM THE POSTERIOR CIRCUMFLEX HUMERAL ARTERY IN NEUTRAL POSITION. ....	116
FIGURE 5-1 PCHA EMERGING FROM THE QUADRILATERAL SPACE. FLOW IS TOWARDS THE TRANSDUCER. ....	126
FIGURE 5-2 SCANNING THE PCHA WITH THE ARM IN ABER. ....	127
FIGURE 5-3 TYPICAL DOPPLER VALUES OF THE PCHA IN NEUTRAL POSITION. ....	130
FIGURE 5-4 (A AND B) NORMAL PCHA DOPPLER TRACE IN NEUTRAL POSITION. ....	131
FIGURE 6-1: DIAGRAM OF THE ALPHA ANGLE CALCULATION FROM THE AXIAL OBLIQUE IMAGE AS DESCRIBED BY BEAULÈ ....	144
FIGURE 6-2: COMPUTED TOMOGRAPHY AXIAL OBLIQUE IMAGE OF THE RIGHT HIP OF A 36-Y-OLD FEMALE REFERRED FOR POSSIBLE FEMOROACETABULAR IMPINGEMENT. ....	147
FIGURE 6-3: ULTRASOUND IMAGE OF THE ANTERIOR FEMORAL HEAD AND NECK USED FOR CALCULATION OF	

THE ALPHA ANGLE. ....	148
FIGURE 6-4 RESULTS. BLAND-ALTMAN SCATTER PLOT OF THE MEAN OF THE COMPUTED TOMOGRAPHY (CT) AND ULTRASOUND MEASUREMENTS OF THE ALPHA ANGLE (X-AXIS) VERSUS THE MEAN ABSOLUTE DIFFERENCE BETWEEN THE CT AND THE ULTRASOUND MEASUREMENTS OF THE ALPHA ANGLE (Y-AXIS). .....	154
FIGURE 6-5 LEFT HIP ULTRASOUND AND COMPUTED TOMOGRAPHY (CT) (INSERT) PERFORMED FOR GROIN PAIN OF A 63-Y-OLD FEMALE.....	158
FIGURE 7-1: ANTERIOR AXIAL OBLIQUE ULTRASOUND OF A 44-Y-OLD MAN WITH AN ASYMPTOMATIC RIGHT- SIDED MITCH RESURFACING IN SITU FOR 5 Y .....	169
FIGURE 7-2: ANTERIOR SAGITTAL ULTRASOUND OF A 76-Y-OLD MALE PATIENT WITH AN ASYMPTOMATIC REVISION UNCEMENTED ACCOLADE THR IN SITU FOR 7 Y .....	172
FIGURE 7-3: ANTERIOR LONGITUDINAL ULTRASOUND OF A 75-Y-OLD MAN WITH RIGHT-SIDED BHR IN SITU FOR 8 Y .....	174
FIGURE 7-4: ULTRASOUND OF A 77-Y-OLD MALE PATIENT WITH AN ASYMPTOMATIC REVISION LEFT THR IN SITU FOR 8 Y.....	178
FIGURE 7-5: ANTERIOR AXIAL OBLIQUE ULTRASOUND OF A 65-Y-OLD WOMAN WITH AN ASYMPTOMATIC LEFT BHR IN SITU FOR 7 Y .....	179
FIGURE 7-6: SIXTY-SEVEN-YEAR-OLD FEMALE PATIENT WITH AN ASYMPTOMATIC RIGHT BHR RESURFACING IN SITU FOR 12 Y. ....	181

List of Tables

TABLE 5-1: DOPPLER ULTRASOUND EVALUATION OF PCHA BLOOD FLOW IN ASYMPTOMATIC SHOULDERS (N/N (%)..... 129

TABLE 5-2 ULTRASOUND CHARACTERISTICS OF THE PCHA ACCORDING TO ARM POSITION AND DOMINANCE. .... 131

TABLE 6-2: MEASURED ALPHA ANGLE FOR EACH HIP CALCULATED FROM CT AND THREE SEPARATE ULTRASOUND IMAGES (N = 39) WITH MEAN DIFFERENCE BETWEEN ULTRASOUND AND CT ..... 151

List of Equations

EQUATION 3-1: FORMULA FOR FEMORAL HEAD-NECK OFFSET RATIO..... 86

EQUATION 6-1 FORMULA FOR ACCURACY..... 150

## Acknowledgements

The present study was carried out at The Avenue X-ray & MRI, Windsor, Australia, between [2010](#) and [2018](#). My deepest appreciation is extended to my three supervisors, A/Prof Michal Schneider, Deputy Head and Director of Research, Department of Medical Imaging and Radiation Sciences, Monash University, Melbourne, Dr Paul Marks MBBS FRANZCR in the early stages of the work, and latterly Dr Steven Lee MBBS FRANCR. Their encouragement, enthusiasm and outstanding advice during these years have enabled me to complete this thesis. In particular, the encouragement and conceptual advice of Dr Marks at first instilled the idea that I might formalise my natural curiosity in clinical ultrasound applications into a research degree. A very big thank you to A/Prof Schneider who accepted me as a research student in spite my vague research proposal, lack of an honours degree and ignorance of the logistics of research degrees, not to mention my snails-pace progress and lack of regular communication. Their patient, professional and cheerful approach is something that I will carry with me for the remainder of my career.

I am grateful to the staff at The Avenue who have never once complained about me being consumed by data collection or running late for the ultrasound list, especially Chief Ben Tawfik, Patrick Ho and David in CT, and Genevieve , Claire and the rest of the front desk team. Also thank you to Healthcare Imaging Services for allowing me time off in many half-day increments to pursue my studies, especially Marie Mould, Nick Bourke and Cliona Cunningham. To the other sonographers, Justine Armstrong, Geri, Khoi and Tuyet thank you for covering me – I owe you.

My sincere and undying gratitude is due to my wife Morayma for her forbearance and love, and to my loving children Matthew, Sami and Sofia for their patience and understanding for my dark moods and short temper. They are a constant reminder that the love and support of



family is all. All the time that I have hitherto set aside for this thesis is now yours. I owe you all.

Finally, I would like to thank all the kind people who participated in the research. Their generous donation of time allowed this research to be completed. This critical information is now added to the global body of knowledge.

This page intentionally left blank

## Abstract

This thesis is comprised of studies that investigate the use of ultrasound to detect and characterise several impingement and entrapment syndromes affecting the shoulder and hip. These conditions can be intermittent, clinically silent and may be associated with vocational activity, such as Quadrilateral Space Syndrome (QSS) of the shoulder (1, 2). They may also cause clinically and financially significant long-term harm, for example severe osteoarthritis (OA) that requires early hip replacement in the case of Femoroacetabular Impingement (FAI) or early revision of a hip replacement (1). Adverse Local Tissue Reaction (ALTR) after hip replacement surgery contributes to a 9% revision burden for hip replacement in Australia and make up 13% of all revisions in the U.K. (3, 4).

Diagnosis of impingement and entrapment syndromes can be difficult and delays in diagnosis can result in irreversible and costly damage to the nerve or joint mechanism in question, and may lead to major disability (5-7). Until recently, the diagnosis of these conditions relied on clinical assessment, and imaging examinations depending on the patient needs' and availability of equipment (8).

Medical imaging is playing an increasing role in the investigation and diagnosis of impingement syndromes (9). Currently accepted modalities include plain x-ray (XR), x-ray angiography, Magnetic Resonance Imaging (MRI), including MR angiography (MRA), metal artefact reduction MRI (MARS MRI) and computed tomography (CT) including three-dimensional CT (3DCT) (10-13). It is essential that these conditions are detected at an early stage using imaging modalities that can provide accurate diagnosis and are able to monitor progression and assessment of the pathology during and after treatment. Access to many of these modalities is, however, restricted in regional and rural centres and in second and third-world countries, in particular to MRI (9, 14). Imaging modalities such as MRI, MRA and CT are unsuitable for monitoring the course of the disease or for serial follow-up after treatment

(4).

There is a need for cheap, non-invasive, non-ionising, readily available and affordable soft tissue imaging techniques which can reliably and accurately detect and characterize impingement and entrapment syndromes of the shoulder and hip. Ultrasound has the potential to provide this imaging technique.

The purpose of this thesis was to:

1. Investigate the ability and accuracy of ultrasound to detect arterial impingement of the PCHA as a proxy for entrapment of the axillary nerve in the quadrilateral space,
2. Demonstrate the usefulness of ultrasound in providing objective evidence of FAI when CT is not available or not appropriate by comparing an ultrasound measurement of the femoral head-neck alpha angle to an established imaging standard.
3. Characterize the typical ultrasound findings associated with the post-arthroplastic hip, with particular reference to the shape of the anterior hip capsule, the presence of fluid or solid material about the femoral neck and the iliopsoas bursa, as well as size of the iliopsoas tendon in a group of patients undergoing routine biennial review of arthroplastic hips.

This thesis begins with an introduction to impingement syndromes and their diagnosis,  
followed by a chapter describing the anatomy of the shoulder and hip. Chapter three is a  
literature review of the specific syndromes examined in this thesis. Chapter four describes a study assessing the ability of ultrasound to perform angiography of the posterior circumflex humeral artery (PCHA) of the shoulder. Our findings demonstrate that stenosis of this artery secondary to impingement with arm abduction and external rotation (ABER) can serve as a proxy for entrapment of the axillary nerve in the quadrilateral space in QSS (10). Chapter five

describes a second study using ultrasound to determine the rate of stenosis and occlusion in the normal population, an investigation that MRA or XR angiography are unable to perform due to availability, ionising radiation, expense and/or invasiveness. We have for the first time demonstrated that the rate of impingement of the PCHA with ABER amongst the normal population is 16%. These two studies confirm the primary hypothesis of this thesis, that ultrasound can be used for the diagnosis of impingement and entrapment syndromes of the shoulder especially when other modalities are not available or are too costly.

Having shown that ultrasound can reliably assist in the detection of impingement of the PCHA at the shoulder, we were interested in assessing its suitability in detection of impingements that occur at the hip. Current imaging applications are problematic in terms of cost and availability, radiation burden amongst the young adult population in the case of FAI, or the ability to resolve soft tissues adjacent to orthopaedic hardware in the case of MARS MRI after hip arthroplasty.

Femoral head-neck asphericity manifests as a bony “bump” at the superior capital epiphysis. It is thought to cause impingement between the femoral head-neck and the acetabulum, resulting in damage to the labrum and articular cartilage and potentially leading to OA (15). 3DCT is considered the preferred imaging modality in the objective quantification of femoral head-neck asphericity of the hip through measurement of the alpha ( $\alpha$ ) angle (12). Chapter six presents the third study presented in this thesis, comparing ultrasound-derived measurements of the alpha angle with the gold-standard 3DCT, and highlights that ultrasound can indeed provide objective evidence of cam-type FAI.

The prosthetic hip has a unique impingement that affects the longevity of the implant and can cause significant morbidity. ALTR directly results in implant failure through aseptic loosening and makes revision surgery more difficult and reduces the rate of revision success

(16, 17). Imaging of the prosthetic hip has been recommended by several international bodies for regular general screening of the hip after arthroplasty, however areas adjacent to prosthetic hardware are not readily imaged even when using MARS MRI. (18, 19). The role of ultrasound in such circumstances has not been fully evaluated.

Chapter seven demonstrates that ultrasound can detect ALTR earlier than any other currently accepted modality. Ultrasound appears to be better suited to regular screening for ALTR than currently accepted modalities.

Chapter eight discusses the findings resulting from the different studies reported in this thesis.

Chapter nine concludes this thesis. Taken together, our studies have demonstrated that ultrasound has a complementary role alongside currently accepted modalities in the assessment of impingement and entrapment syndromes of the shoulder and hip. Ultrasound has the potential to make earlier diagnosis as an adjunct to established modalities or alone when other imaging modalities are not available or considered too costly, thereby providing access to appropriate imaging, across a wider patient cohort, reducing costs and improving short- and long term outcomes after interventions for shoulder or hip impingements.

I hope that this thesis will encourage the use of ultrasound as a first line of investigation for impingement syndromes and that it will encourage further research into the potential applications of this modality for these and other impingement syndromes.

# ***Chapter 1*** Introduction

## **1.1 Impingement and Entrapment Syndromes**

An impingement is a mechanical encroachment upon or collision between two objects (20, 21). Nerve entrapment occurs secondary to compression either acutely, or over time with repeated short intervals of mechanical constriction (9). A range of impingement and entrapment syndromes exist involving tendons, nerves, arteries, veins and bony surfaces within a spectrum of musculoskeletal pathologies (9). Progressive encroachment can result in oedema, haemorrhage, fibrosis, tendinosis and bony cortical damage depending upon the structure involved (9, 15, 22). While some of these syndromes are well-recognised clinical entities, imaging technologies such as MRI and ultrasound are increasingly being used in an attempt to provide prompt accurate diagnosis in other cases (8). Ongoing advances in technologies and resolution have seen medical imaging playing an increasing role in the diagnosis and treatment planning for these pathologies (9).

## **1.2 Prevalence of Impingement and Entrapment Syndromes**

Shoulder impingement is a very common problem, with lifetime prevalence reported to range from 7 – 67% (23). Clinical assessment of shoulder impingement has only moderate sensitivity and specificity, with large inter-observer variability (24). It should be noted that widely different definitions of shoulder pain contribute to the variation in reported prevalence rates (23). Assessment and management of the painful shoulder is based on the Neer concept of subacromial impingement, where interaction of the anterior supraspinatus tendon, acromion, coracoacromial ligament and the acromioclavicular joint progressively damages the

rotator cuff (24). Imaging is required to supplement clinical assessment, with the benefits of ultrasound well recognised, with studies showing no statistical difference between ultrasound and MRI for detecting full or partial-thickness rotator cuff tears or tear size (23-25).

Peripheral neuropathies are also common, with about 20 million people in the United States (6.5%) suffering some form of peripheral neuropathy (26). Approximately 8-9% of Medicare (United States) recipients have peripheral neuropathy as their primary or secondary diagnosis (26). Neuropathy secondary to mechanical impingement or entrapment is less common. The incidence of carpal tunnel syndrome, the most common entrapment syndrome, has been reported to be 2.7% in the United States (27).

Quadrilateral space syndrome, a mechanical entrapment of the axillary nerve in the quadrilateral space of the shoulder is an uncommon syndrome thought to occur secondary to either prolonged repetitive trauma in overhead athletes or manual labourers, or secondary to shoulder trauma, with the reported incidence after anterior shoulder dislocation ranging from 5% to 55% (28, 29). Axillary nerve compression may also be caused by space-occupying lesions such as tumours, cysts and inflammatory processes, or dynamically, by narrowing of anatomic tunnels and passages through which the nerve travels during athletic or vocational endeavour (30).

The bony articulation of the hip can also be subject to an impingement syndrome where the femoral head-neck junction impacts upon the acetabular labrum. Impingement occurs due to a non-spherical extra-articular protuberance of bone at the femoral head-neck junction impacting the acetabulum, usually with flexion of the leg upon the trunk in adduction - known as femoroacetabular impingement (FAI) (5, 31). This mechanical bony impingement at the hip can result in damage to the articular cartilage and cartilaginous labrum, possibly leading to



OA (32). It has been suggested that up to 65% of OA of the hip has an identifiable anatomical variation as a cause (33). FAI has been shown in a number of studies to occur mainly in younger patients (20-40 years) with an estimated incidence of approximately 10-20% (1, 31). Early severe OA can lead to joint degeneration and loss of function and ultimately require hip arthroplasty (5). The number of hip replacements in Australia has risen from 5829 in the year 2000, to 46646 in the year 2016 at an estimated average cost of \$25,000 per hip replacement in Victoria (3, 34).

Impingement can also occur at the hip after hip replacement arthroplasty, with a small number of patients developing a progressive soft tissue reaction to wear debris associated with the orthopaedic hardware (16, 18, 35). ALTR can cause soft tissue necrosis and aseptic loosening, the major factor in early prosthesis failure (36). The problem is sufficient to cause recall of some types of hip prostheses, such as the Articular Surface Replacement, which demonstrated a failure rate of 25% and 48.8% at six years for resurfacing and total hip prostheses respectively (36).

Resurfacing hip prostheses, where the native femoral neck is preserved and a prosthetic cap is fixed to the top of a remodelled femoral head have a unique impingement syndrome. In this case, ALTR causes osteolysis and thinning of the native femoral neck ultimately resulting in femoral neck fracture (37, 38).

Early detection of ALTR to prosthetic hip wear debris is vital to improve the success of revision surgery for hip replacement (18). Several national bodies have recommended regular medical imaging follow-up of hip prostheses specifically to detect ALTR early and improve revision outcomes (18, 39). The revision burden of hip arthroplasty in Australia in 2016 was reported as 8.9% (40). Significant differences currently exist in the recommended guidelines

for follow-up of hip arthroplasty between the five major authorities (USA, Europe, UK, Canada, Australia) in both frequency and imaging technique (4). Much of the current worldwide guidance is not evidence-based, with most protocols lacking the sensitivity to detect asymptomatic ALTR lesions (4).

### **1.3 Current Imaging Techniques for Impingement and Entrapment**

#### **Syndromes**

All medical imaging techniques are currently utilised to some degree in the detection and characterisation of impingement and entrapment syndromes of the shoulder and hip (9, 12, 41). Each modality however, has its own limitations. Mainstays of medical imaging such as x-ray and CT are unable to depict soft tissue structures such as nerves and ligaments or demonstrate postural-based impingement or compression of soft tissues such as those which occur in QSS (Figure 3-2). X-ray and CT are often contraindicated due to radiation dose concerns for younger patients or when screening large asymptomatic populations. X-ray arteriography for detecting vascular compression is invasive as it requires intravenous administration of radio-opaque contrast and is rarely used today (29).

MRI, MR angiography and MARS MRI are widely used in a number of cases, however, they are relatively expensive and are not always available, and in the case of angiography, can be invasive. MRI is unable to demonstrate the axillary nerve in the quadrilateral space or soft tissues adjacent to orthopaedic hardware (19, 42).

Ultrasound can directly visualise some nerve abnormalities and provide information on the nature of impingement or constriction of a nerve, particularly in cases where the clinical picture is confusing or equivocal (42). In carpal tunnel syndrome, the most common upper

limb impingement syndrome, focal calibre changes of the median nerve can be directly visualised by ultrasound imaging (Figure 1-1).

High-resolution ultrasound has become an efficient, reliable, and low-cost alternative to MRI for detection of entrapment and compressive neuropathies (9). Ultrasound has many advantages over the more established modalities. Ultrasound images are not affected by orthopaedic hardware or metallic implants, have better spatial and contrast resolution, and are able to be performed dynamically, giving functional information and have a flexible field of view (43).

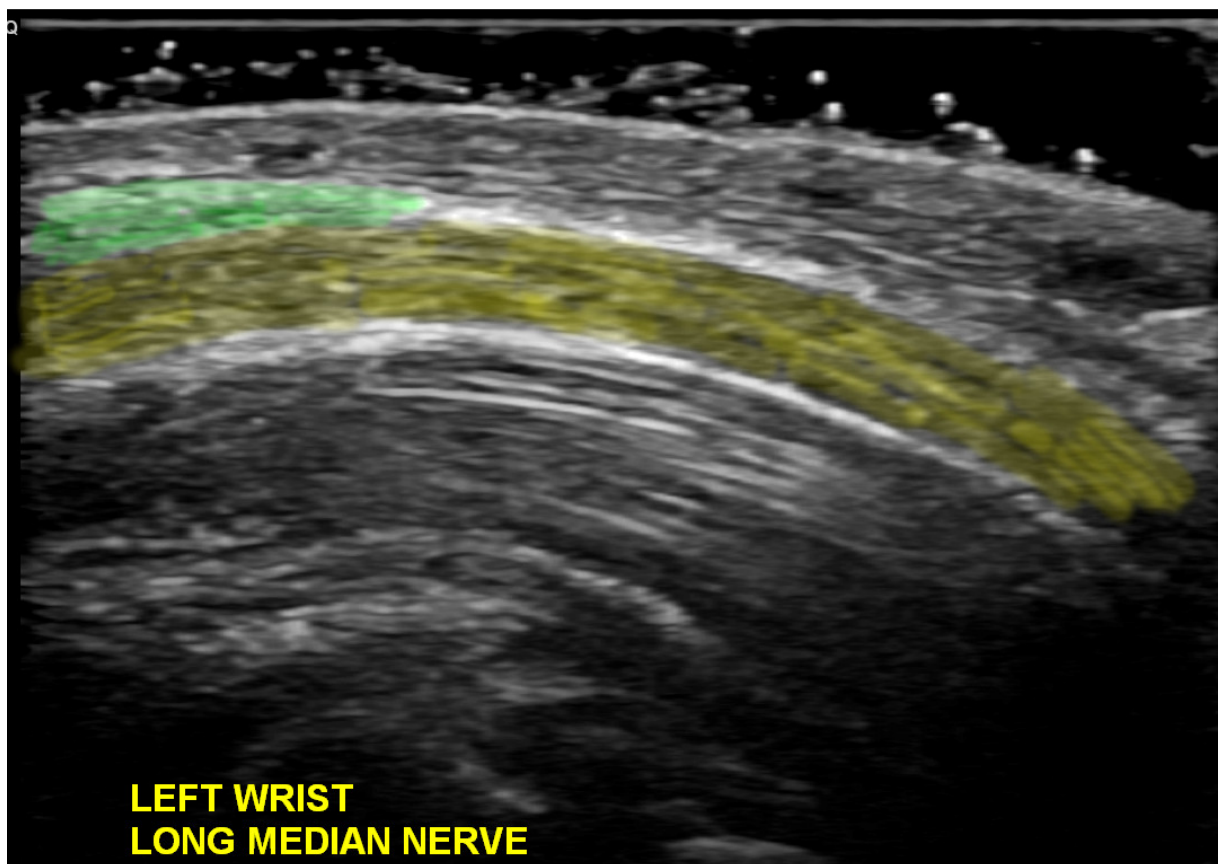


Figure 1-1: Ultrasound of the median nerve at the wrist. The median nerve (yellow shading) is impinged upon by the flexor retinaculum (green shading) at the carpal tunnel of the wrist in Carpal Tunnel Syndrome. Source: David Robinson, The Avenue X-ray & MRI

### 1.3.1 Current imaging in Quadrilateral Space Syndrome

For patients presenting with suspected QSS, diagnosis relies upon angiographic

demonstration of compression of the PCHA on abduction and external rotation (ABER) of the arm as evidence of mechanical compromise of the axillary nerve in the quadrilateral space (44-46). MRA has supplanted arteriography as the standard of diagnosis for QSS (Figure 1-2) (2, 46).

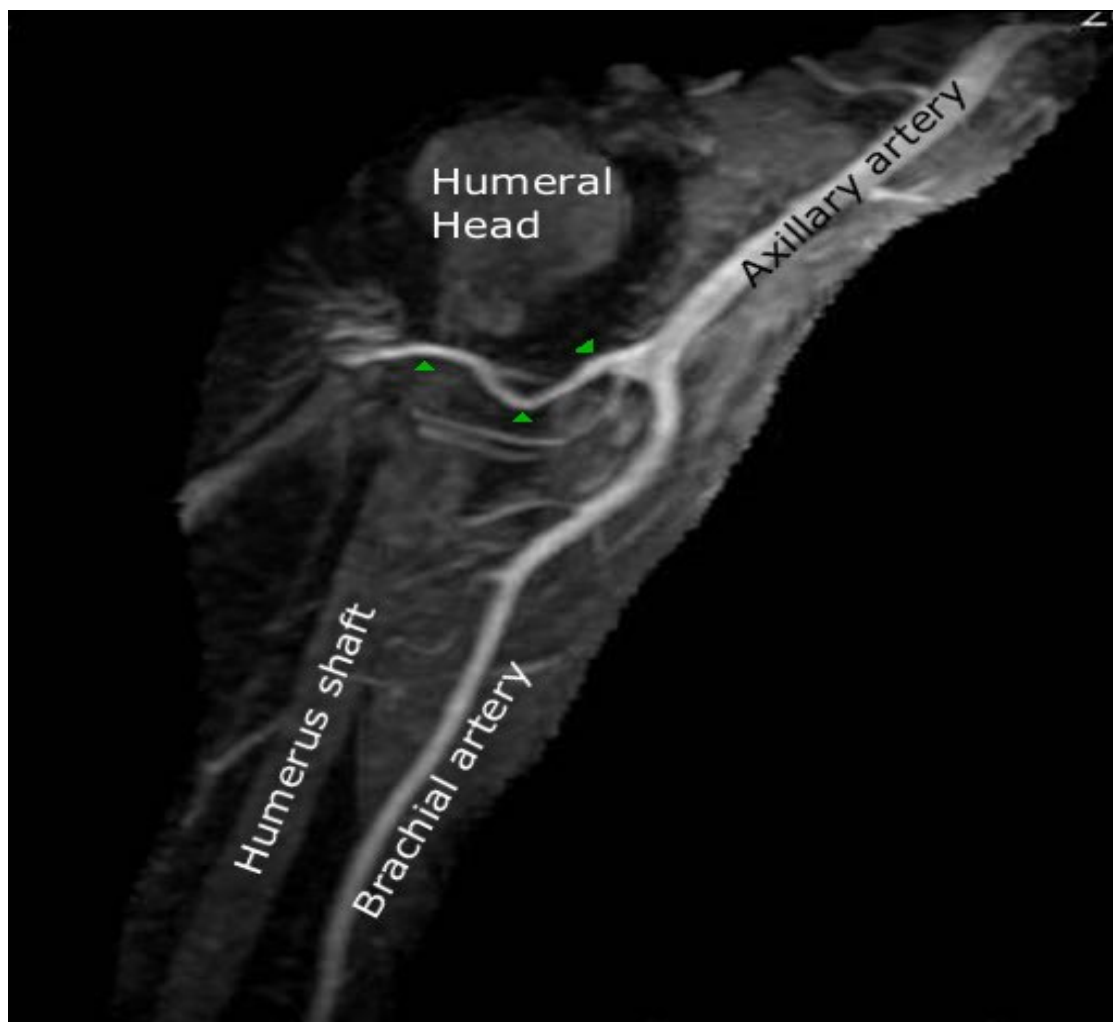


Figure 1-2: Magnetic Resonance Angiogram of the PCHA. The artery is highlighted by the green arrowheads passing behind the surgical neck of the humerus. This procedure is difficult to perform and is invasive, requiring [contrast administration](#). Source: Dr. Paul Marks, The Avenue Radiology, Windsor.

MRA is, however, difficult to perform [and](#) is invasive and relatively expensive, not available in all areas and requires the patient to maintain the arm in an uncomfortable position for an extended length of time (2). MRA is now considered amongst other imaging modalities such

as CT angiography and XR angiography for young people with evidence of upper limb ischaemia and/or neurogenic features depending upon clinician preference and likely diagnosis (2, 47).

#### **1.3.1.1 Doppler Ultrasound**

Currently, ultrasound has no role in the diagnosis of QSS, however, Doppler ultrasound techniques for the assessment of peripheral arteries may be applied to the PCHA to detect compression and occlusion of the PCHA with ABER.

Doppler ultrasound is capable of the quantitative assessment of blood flow and blood flow velocity within blood vessels. It is routinely used to assess arterial stenoses and occlusions compromising blood flow in the upper and lower limbs, most commonly when examining cases of suspected atherosclerosis, arterial embolus or thrombosis (48-50). Doppler ultrasound is the modality of choice in the assessment of the subclavian artery in suspected thoracic outlet syndrome (51). When the diameter of an artery is reduced by atherosclerotic disease or external compression, some identifiable characteristics of the Doppler frequency spectrum will change (Figure 1-3)(49). Changes detectable with spectral Doppler ultrasound include increased flow velocity and turbulence immediately distal to a stenosis (49).

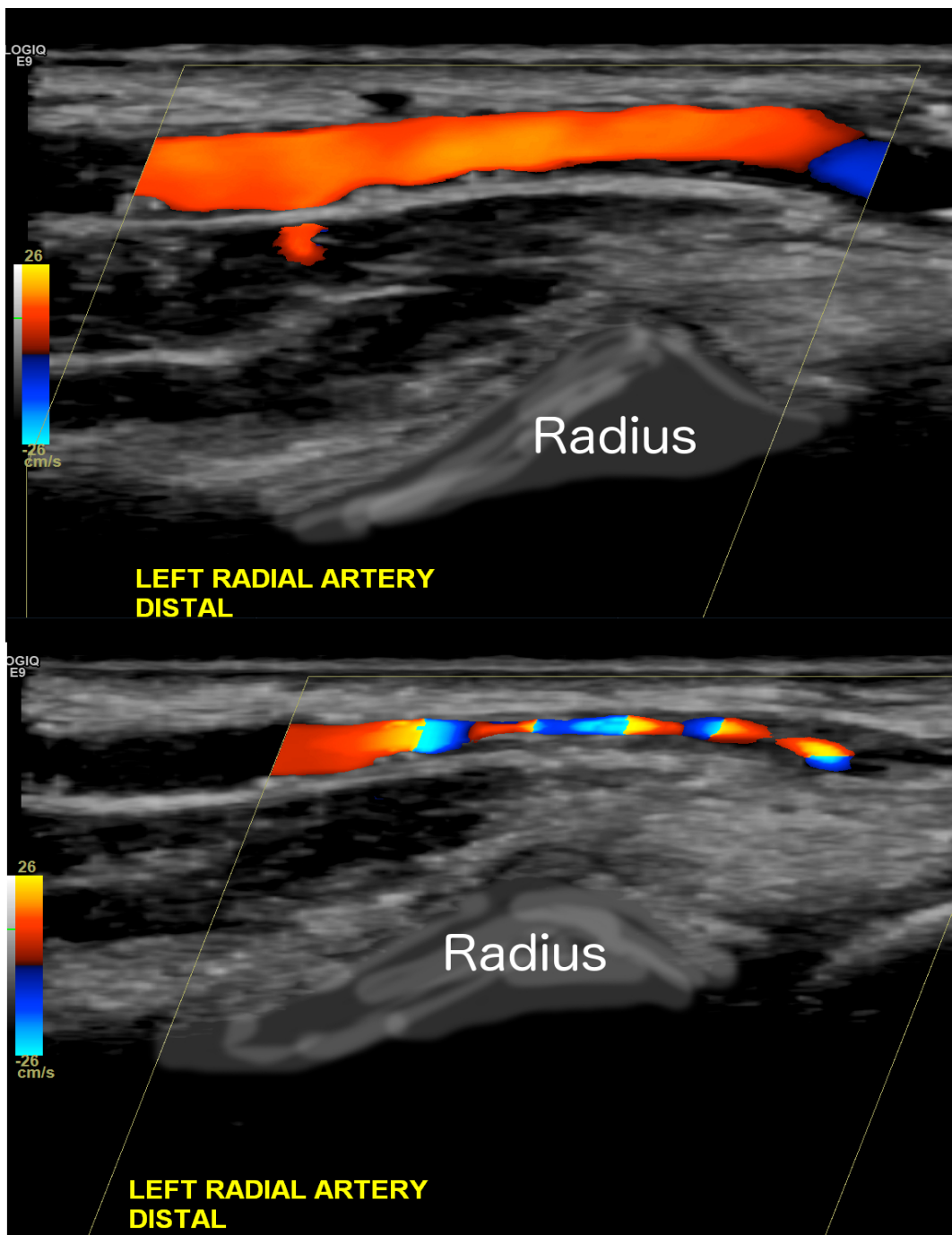


Figure 1-3: Doppler ultrasound of a radial artery stenosis. Color Doppler ultrasound shows a widely patent radial artery with uniform color filling at the wrist (upper image). Stenosis (lower image) demonstrates narrowing of the flow channel and color mosaicism representing increased velocities and turbulence, the hallmarks of arterial stenosis on Doppler ultrasound. Stenosis in this case is artificially generated by compressing the artery with the transducer against the radius bone. Source: David Robinson, The Avenue X-ray & MRI.

Sensitivity and specificity of duplex scanning for haemodynamically significant lesions

(>50% stenosis) of peripheral arteries have been found to be 98%, with a positive predictive value of 94% and negative predictive value of 92% (52). Duplex sonography is comparable to the gold standard arteriography for the detection of arterial lesions and determining the degree of stenosis for peripheral artery disease (52).

### **1.3.2 Current imaging for detection and quantification of FAI**

A quantitative measurement of the loss of normal sphericity of the femoral head-neck junction in FAI was first described by Nötzli et al in 2002 using MRI to calculate a femoral head-neck alpha angle (11). Thirty-nine patients with groin pain, decreased internal rotation and a positive impingement test were compared with 35 asymptomatic control subjects of similar age (group average age 30 and 35 years respectively) and the angle between the waist and neck at the femoral head-neck junction (alpha angle) was calculated and compared (Figure 1-4) (11). The mean alpha angle in the control group was  $42.0^{\circ} \pm 2.2^{\circ}$  (range  $33^{\circ}$  to  $48^{\circ}$ ) and  $74.0^{\circ} \pm 5.4^{\circ}$  (range  $55^{\circ}$  to  $95^{\circ}$ ) in the patients ( $p < 0.001$ ) (11).

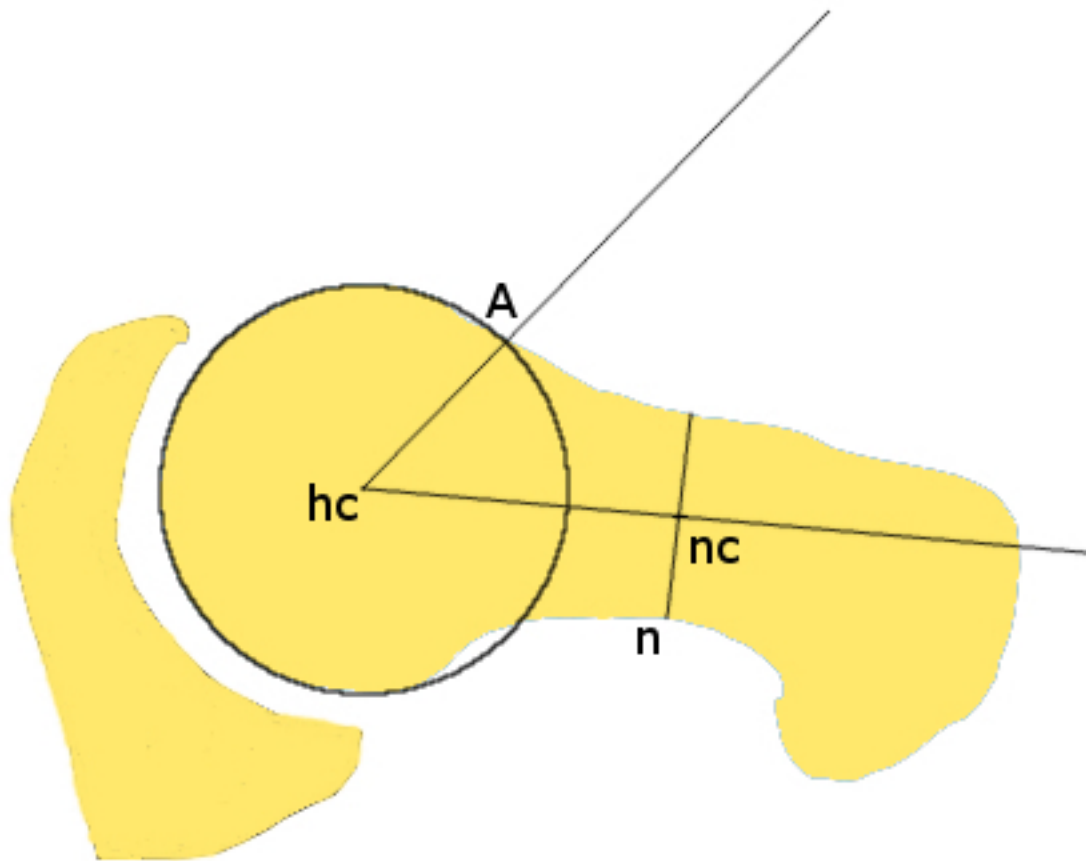


Figure 1-4: The alpha angle described by Nötzli et al (2002). A circular template is placed over the femoral head. A line is drawn from the center of the femoral head (hc) laterally through the center of the narrowest part of the femoral neck (point nc on line n). Another line is drawn from the center of the femoral head through the point at which the femoral head-neck contour exits the circular template (point A). The angle between the lines hc-A and hc-nc is the alpha angle. Source: Nötzli et al (2002) (11), adapted by David Robinson, The Avenue X-ray & MRI.

Subsequent investigations by Beaulé et al (2005) using 3DCT found similar results to those of Nötzli et al (12).





Figure 1-5: 3DCT (left) and MRI (right) of the hip demonstrating the axial plane used for calculation of the alpha angle. The CT image on the left has had the alpha angle calculated according to the method of Beaulé (49.2 degrees). The superior bone-soft tissue contrast of the CT is preferred in our institution for calculation of the alpha angle. Source: David Robinson, The Avenue X-ray & MRI

Current imaging techniques for hip FAI are problematic in the target patient group, typically a young asymptomatic population, due to cost and availability of MRI and CT scanning. MRI for evaluation of FAI is of limited availability and relatively expensive, similar to MRI for QSS. In the case of CT and plain X-ray, unnecessary radiation exposure in young people causes concern when there may be no clinically evident pathology early in the disease process (11, 12, 53). There is a need for new imaging techniques and classification of the FAI hip ahead of the onset of OA to justify surgical intervention in essentially asymptomatic young adults (5).

### **1.3.3 Current imaging of Adverse Local Tissue Reaction**

The areas adjacent to a hip prosthesis are not readily imaged using MRI or MRI with metal artefact reduction sequencing (MARS MRI) protocols (54). MRI is contraindicated for some types of ferrous implants as safety has not been evaluated. Further, it is expensive and not widely available and thus not suitable for the screening of an asymptomatic well-functioning

prosthesis (19, 55).

There is a need to develop tolerable, low-cost imaging protocols for routine follow-up of all patients after hip replacement surgery. The Medicines and Healthcare products Regulatory Agency of the UK and the United States FDA recommend ultrasound in the follow-up of hip prostheses (18, 19, 39). Ultrasound provides superior imaging of the periprosthetic soft tissues of the post-arthroplastic hip as it is unaffected by metal artefact from the prosthesis and is able to easily and reliably characterize soft tissue masses (54, 56). Ultrasound is ideally suited to convenient regular follow-up of hip arthroplasty patients, including screening for ALTR in asymptomatic groups.

## **1.4 Purpose of thesis**

The central theme of this research is the evaluation of ultrasound techniques for the detection and assessment of a number of impingement and entrapment syndromes affecting the shoulder and hip.

The purpose of this thesis is to:

- i. Investigate the use of ultrasound in the detection of arterial impingement of the PCHA as a proxy for mechanical impingement of the axillary nerve in the quadrilateral space,
- ii. To demonstrate the usefulness of ultrasound in providing objective evidence of FAI when CT is not available or not appropriate by comparing an ultrasound measurement of the femoral head-neck alpha angle to an established imaging standard, and
- iii. To characterize the typical ultrasound findings with particular reference to the shape of the anterior hip capsule, the presence of fluid or solid material about the femoral neck and the iliopsoas bursa, as well as size of the iliopsoas tendon in a group of patients undergoing routine biennial review of arthroplastic hips.

The work described in this thesis is presented as a series of published papers linked together according to the central thesis by assessing the ability of ultrasound to detect the PCHA, determining the rate of occlusion of the PCHA in a normal population, comparing ultrasound measurement of the femoral head-neck alpha angle to 3DCT as the established standard, and using ultrasound to assess characteristics of the soft tissues surrounding hip prostheses.

The results of this research will enable clinicians with limited access to sophisticated, invasive and expensive modalities such as MRI arteriography and 3DCT to diagnose and commence treatment of impingements earlier, especially in younger patients without concerns regarding radiation burden and potentially, before major irreversible soft tissue damage occurs. Earlier detection provides a wider range of options for patient management which may reduce the need for expensive and invasive treatments with concomitant improvement of outcomes.

The new applications of ultrasound described in this thesis add objective medical imaging evidence of disease and will result in better management and reduced morbidity.

## ***Chapter 2* Anatomy of the Shoulder and Hip**

### **2.1 Anatomy of the Shoulder joint**

#### **2.1.1 Osteology of the Shoulder joint**

The shoulder joint is a multi-axial spheroidal joint, made up of the hemi-spherical head of the upper arm bone – the humerus, and the shallow glenoid cavity of the scapula (57). The humerus is a long bone with an expanded round head proximally having an ovoid shape, forming less than half of a sphere, directed medially backwards and upwards when the arm is by the side (57, 58). There is an anatomical neck, adjoining the margin of the head and visible as a slight constriction at the margin of the rounded spherical head (58). There is also a surgical neck visible as a tapered region where the upper part of the bone joins the shaft, inferior to the anatomical neck (57, 58). A groove approximately 4mm deep passes through the anatomical neck containing the long head of the biceps tendon, and dividing the anterolateral aspect into greater and lesser tubercles (Figure 2-1) (58).

The scapula is a large flattened triangular bone on the posterolateral aspect of the thorax. The lateral angle of this triangle narrows to form the scapula neck, which then connects the glenoid to the scapula (57). The pear-shaped concave glenoid cavity is deepened by a fibrocartilaginous rim attached to its margins known as the glenoid labrum (58)

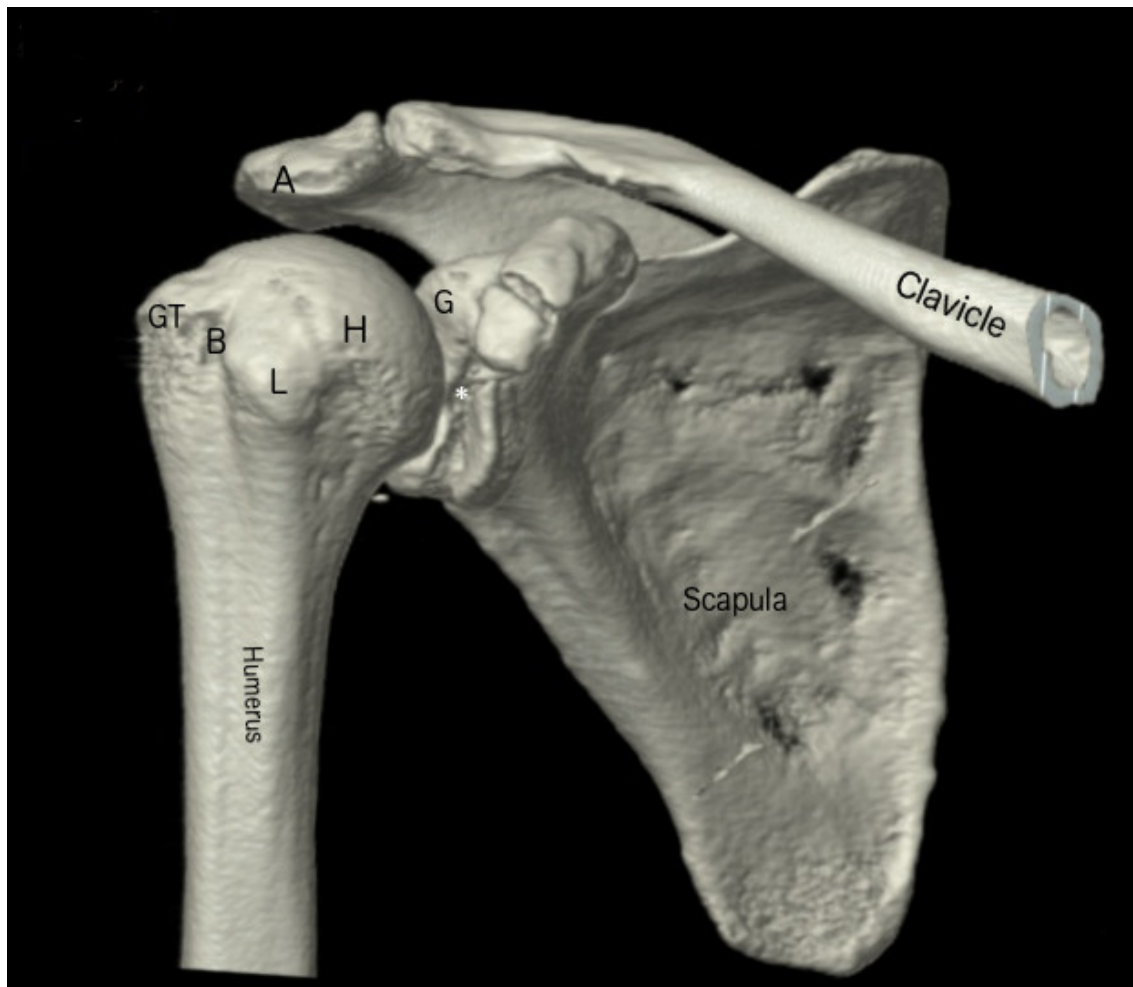


Figure 2-1: Bony anatomy of the shoulder. Three-dimensional computed tomogram of the right shoulder, viewed from anterolateral. Fracture of the scapula glenoid, denoted by the white asterisk. A – acromion, B – bicipital groove, G – glenoid, H – humeral head, L – lesser tuberosity, GT – greater tuberosity. Source: The Avenue X-ray & MRI.

## 2.1.2 Angiology of the Proximal Upper Limb

### 2.1.2.1 The Subclavian artery

The second part of the subclavian artery is very short and usually lies behind the scalenus anterior muscle (Figure 2-2) (57). Occasionally the artery perforates the scalenus anterior muscle and extremely rarely lies in front of this muscle. The third part of the subclavian artery runs downwards and laterally from the lateral margin of the scalenus anterior, behind the clavicle to the lateral border of the first rib to become the axillary artery (57, 59). The

relations of the first part of the subclavian artery are different for left and right sides, however posteriorly and inferiorly both sides apply closely to the pleura and apex of the lung and both sides lie deep to the skin and the clavicular attachment of the sternocleidomastoid muscle (57).

#### **2.1.2.2 The Axillary artery**

The axillary artery is a continuation of the subclavian artery that begins at the outer border of the first rib distal and inferior to the clavicle (59). The pectoralis minor muscle crosses the vessel and divides it into three parts – proximal, posterior (to the pectoralis minor) and distal. The first part of the axillary artery lies deep to the clavicular fibres of the pectoralis major muscle (57). The posterior part lies behind the pectoralis major and minor muscles and in front of the posterior cord of the brachial plexus (57). The cords of the brachial plexus surround the posterior (second) part on three sides, posterior, medial and lateral and separate it from contact with adjacent axillary vein and muscles (57).

It is the third part of the axillary artery gives rise to the PCHA at the lower border of the subscapularis muscle which lies posterior to the axillary artery at this point (Figure 2-2) (57).

#### **2.1.2.3 The Posterior Circumflex Humeral Artery (PCHA)**

The PCHA is larger than the anterior circumflex humeral artery, with the average transverse diameter measuring 3.7mm (60). It branches from the third part of the axillary artery just below the lower border of the subscapularis muscle and passes backwards with the axillary nerve via the quadrilateral space (Figure 2-3) (57). The PCHA branches from a common trunk with the deep brachial artery from the axillary artery in 19% of individuals (61). It passes in a curved shape posteriorly to the neck of the humerus to give branches to the deltoid, teres major and minor, and long and lateral heads of triceps muscles, before anastomosing with the anterior circumflex humeral artery (Figure 2-5) (57, 61).

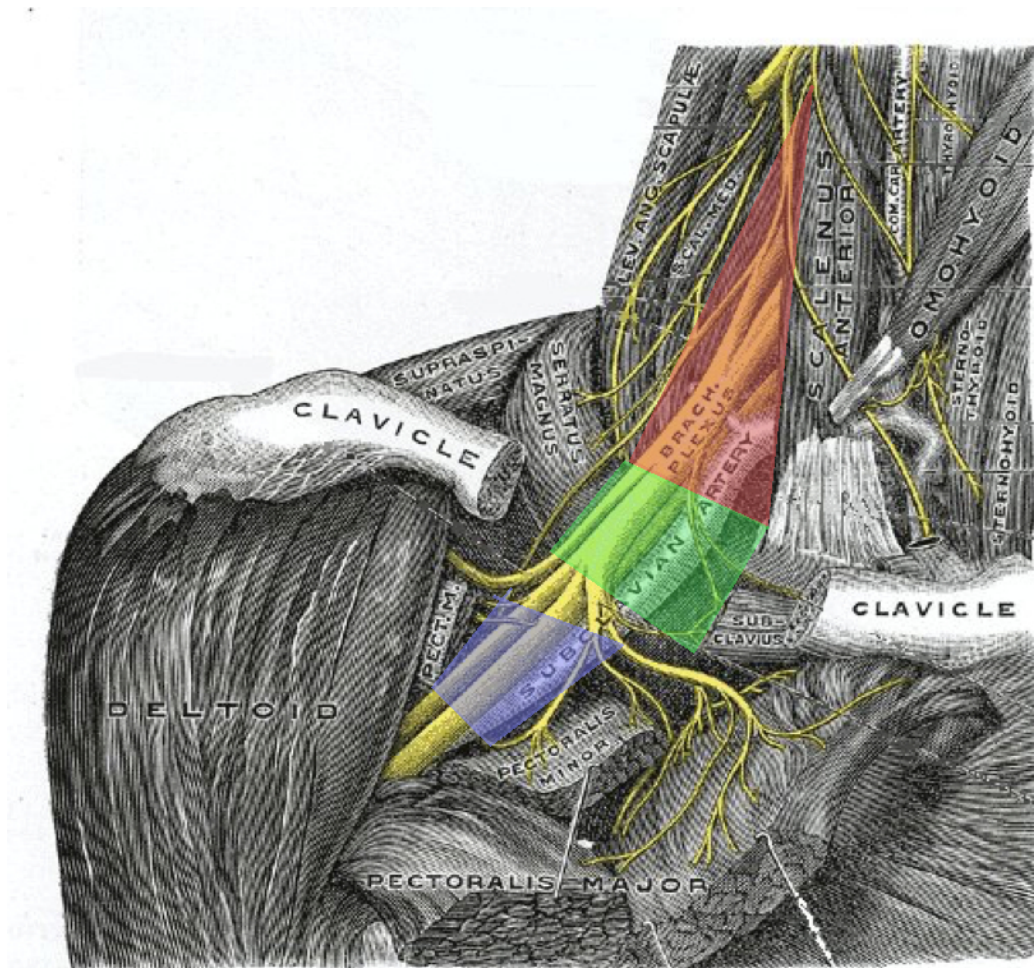


Figure 2-2: Coronal view of the right shoulder - detailed anatomy of the thoracic outlet. The subclavian artery and brachial plexus can be seen passing through the scalene triangle (red), costoclavicular space (green) and retropectoralis minor space (blue). The clavicle has been cut and the pectoralis muscles retracted for visualisation. Source: Gray, H. Anatomy of the human body, 1918 (57). Adapted by David Robinson, The Avenue X-ray & MRI.



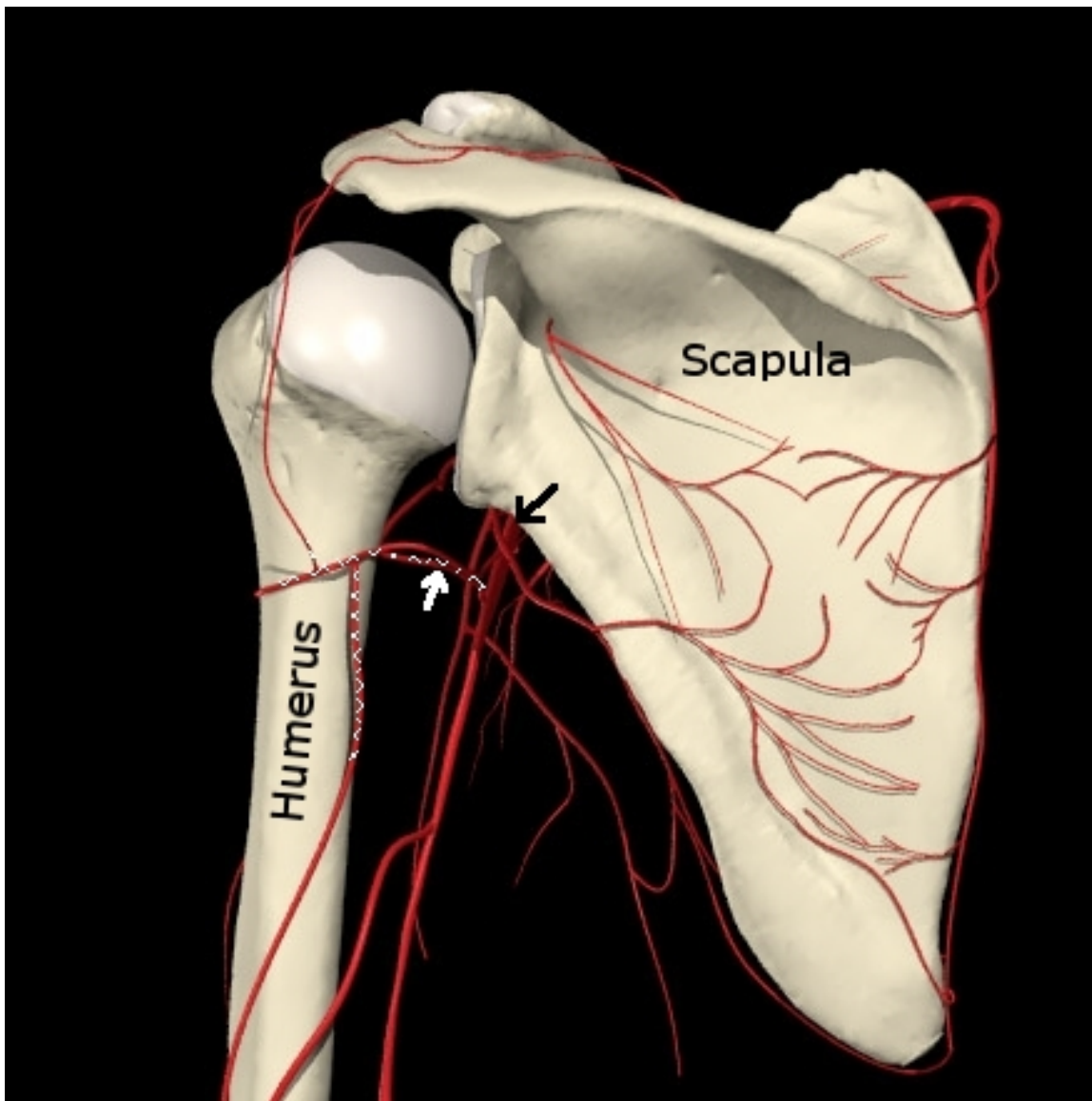


Figure 2-3: Arterial anatomy of the left shoulder viewed from behind. The Posterior Circumflex Humeral Artery (white cross hatch) arises from the posterior aspect of the axillary artery (black arrow) to pass backwards through the quadrilateral space accompanying the axillary nerve (not shown). Source: Primal Pictures, [www.anatomy.tv](http://www.anatomy.tv) (62).

### 2.1.3 Neurology of the Proximal Upper Limb

#### 2.1.3.1 The Brachial Plexus

The brachial plexus is formed by the union of the ventral rami of the lower four cervical nerves (C5 to C8) and the greater part of the ventral ramus of the first thoracic nerve (T1) (63). The plexus emerges between the scalenus anterior and scalenus medius muscles at first



above the third part of the subclavian artery and then posterior to the artery (Figure 2-2). The cords surround the second part of the axillary artery on three sides with the posterior cord behind (57). The lower four cervical nerves and the first thoracic nerve form the roots of the plexus, and while nearly almost equal in size, are subject to some variation in the way in which the plexus is formed; the most constant arrangement is C5 and C6 to unite to form an upper trunk, C8 and T1 unite behind the scalenus anterior muscle to form a lower trunk, and C7 forms the middle trunk of the plexus (Figure 2-4) (57, 63). The three trunks pass downwards and laterally, and just above or behind the clavicle each splits into an anterior and a posterior division (63). The posterior divisions of all three trunks unite to form the posterior cord of the plexus, which is situated at first above and then behind the axillary artery (Figure 2-4 & Figure 2-5) (57). The anterior divisions of the upper and middle trunk unite to form a cord situated on the lateral side of the axillary artery called the lateral cord of the plexus (63). The anterior division of the lower trunk passes down at first behind and then on the medial side of the axillary artery to form the medial cord of the brachial plexus (57).

#### **2.1.3.2 The Axillary Nerve**

The axillary nerve arises from the posterior cord of the brachial plexus, derived from C5 and C6 (Figure 2-4) (57, 64). It descends inferolaterally anterior to the subscapularis muscle to the lower border of the subscapularis muscle, and just lateral to the pectoralis minor muscle it arises and winds backwards in intimate relation to the lower part of the articular capsule of the shoulder joint, to pass through the quadrilateral space (51, 57, 64, 65). The nerve is the most superior structure in the space, extending on average 10mm from the glenoid labrum but as little as 2.5mm in some cases (66). The nerve follows Hilton's law where the nerve supplying the muscles extending across and acting upon a joint also innervate the joint (64). The axillary nerve divides into anterior (superior) and posterior (inferior) branches, usually in the quadrilateral space (64, 66). It is the anterior branch that is accompanied by the posterior

circumflex humeral vessels, taking a tortuous path around the surgical neck of the humerus posteriorly deep to the deltoid muscle, supplying the anterior and middle deltoid muscle and providing a number of cutaneous branches (Figure 2-5 & Figure 2-6) (57, 64, 66). The posterior branch supplies the teres minor and the posterior part of the deltoid muscle, and continues as the upper lateral cutaneous nerve of the arm, supplying the skin over the lower part of the deltoid and the upper long head of triceps muscle (Figure 2-5 & Figure 2-6) (57, 64).

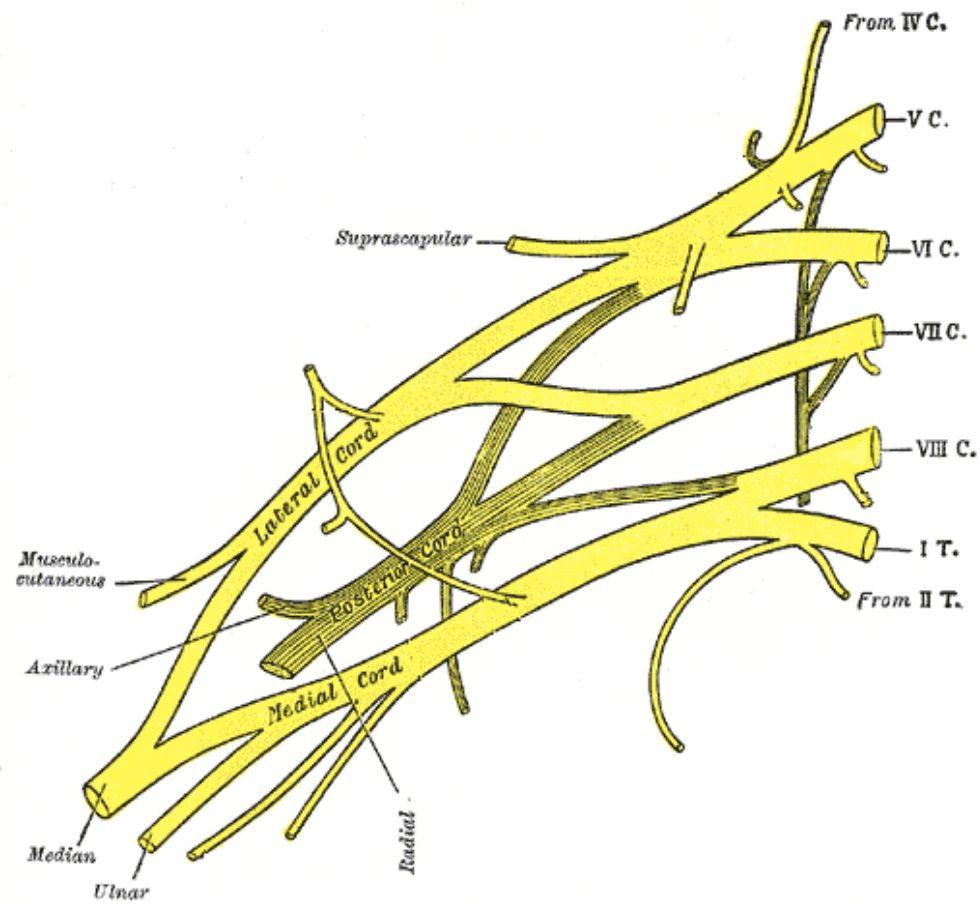


Figure 2-4: Detailed anatomy of the Brachial Plexus (Right shoulder from the front). The axillary nerve arises from the posterior cord. Source: Gray, H. Anatomy of the human body, 1918 (54) adapted by David Robinson, The Avenue X-ray & MRI.

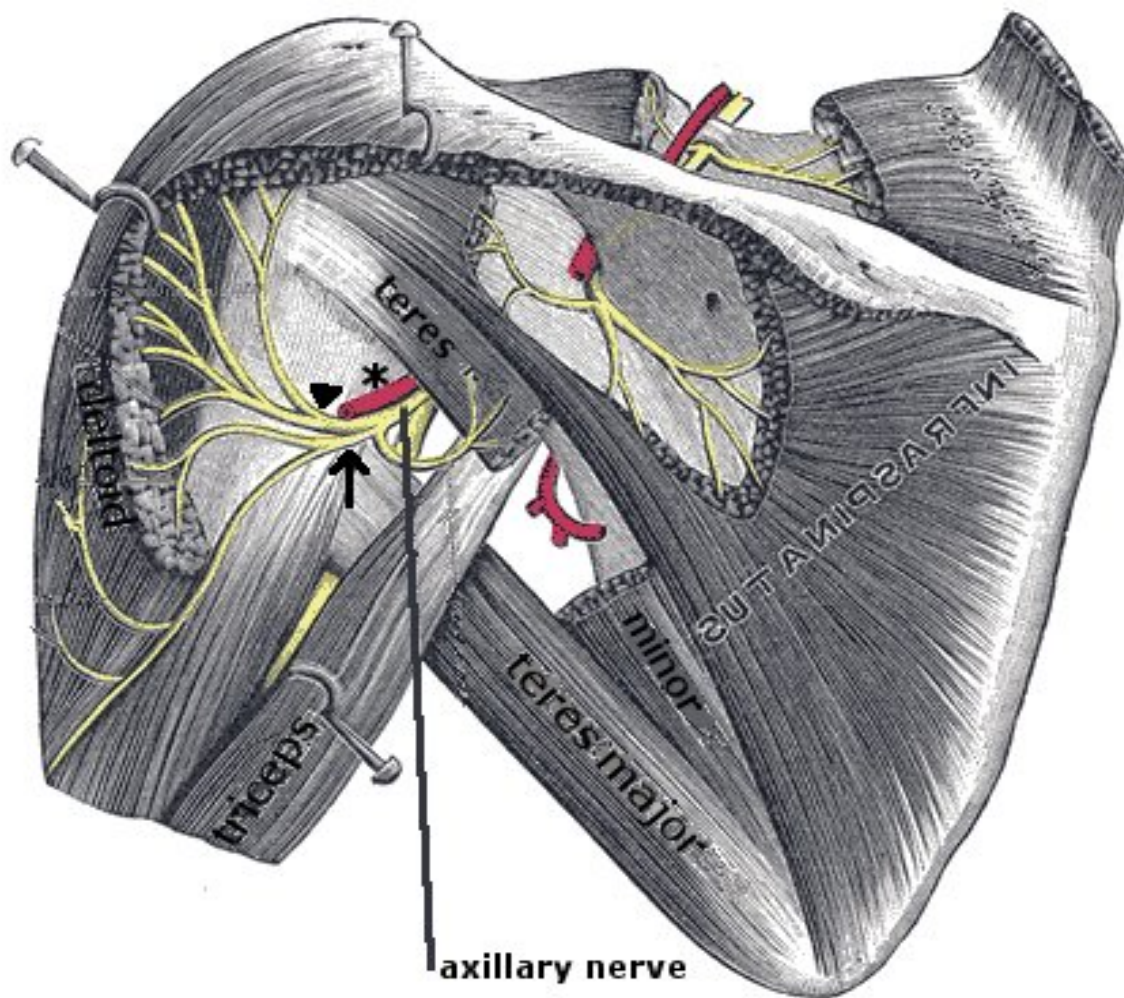


Figure 2-5: The anatomy of the quadrilateral space (left shoulder viewed from behind). The PCHA (\*) can be seen accompanying the anterior branch of the axillary nerve (yellow) through the quadrilateral space. The division of the nerve into anterior (arrowhead) and posterior (arrow) branches can be seen. Source: Gray, H. Anatomy of the human body, 1918 (57) adapted by David Robinson, The Avenue X-ray & MRI

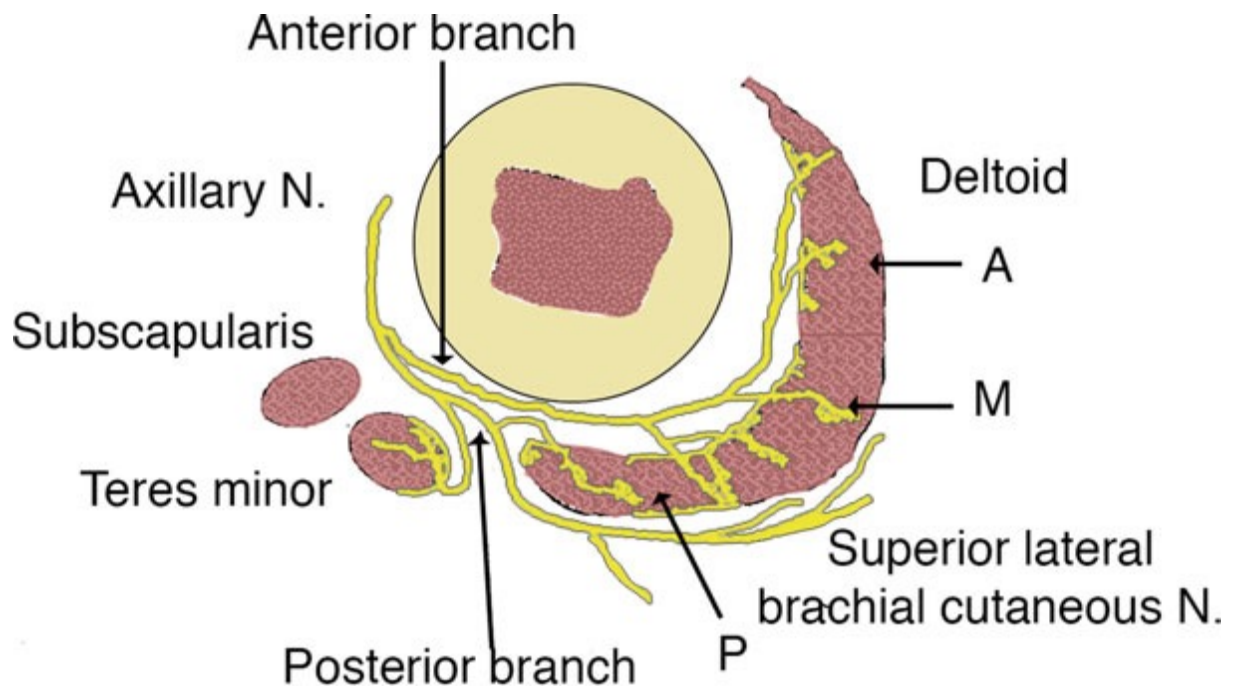


Figure 2-6: Schematic representation of the course of the axillary nerve beyond the quadrilateral space. A - anterior deltoid, M - middle deltoid, P - posterior deltoid. Source: Galley (2015)(64).

#### 2.1.4 The Quadrilateral space

The quadrilateral space is bounded superiorly by the teres minor, medially by the long head of triceps muscle, laterally by the neck of the humerus and inferiorly by the teres major (Figure 2-7) (57, 67).

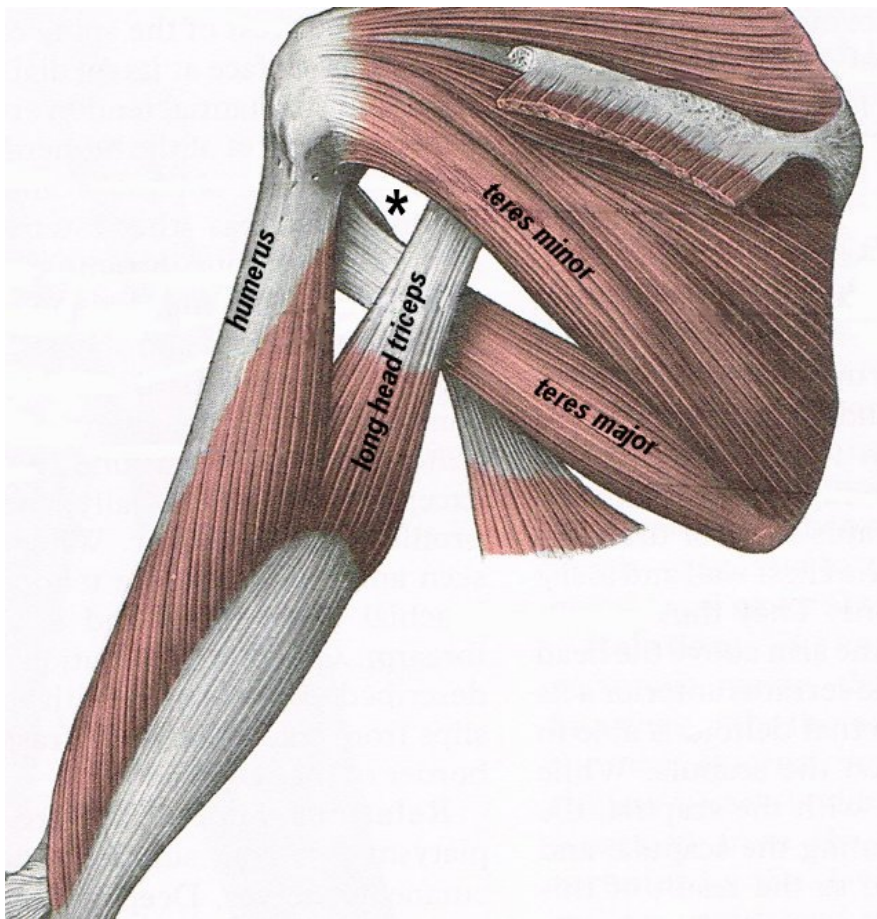


Figure 2-7: The quadrilateral space of the left shoulder, viewed from behind. The deltoid muscle has been removed. The quadrilateral space (\*) lies just below the joint capsule and medial to the surgical neck of the humerus. Source: Williams PL, Warwick R E (Ed.s.) Grays Anatomy 36<sup>th</sup> Ed 1980 (57) adapted by David Robinson, The Avenue X-ray & MRI.

### 2.1.5 The Thoracic Outlet

Three compartments form what is known as the thoracic outlet. The interscalene triangle is the most proximal (medial) composed of the anterior scalene muscle, middle scalene muscle behind and the first rib inferiorly (57). The triangle passes the subclavian artery inferior-most, and the three trunks of the brachial plexus. The costoclavicular space is formed by the clavicle superiorly, the subclavius muscle anteriorly, and posteriorly by the first rib and middle scalene muscle (51, 57). The costoclavicular space passes the subclavian vein anterior-most, the subclavian artery immediately behind, and the brachial plexus (Figure 2-2). The retropectoralis minor space is the most lateral of the three compartments, being bordered by



the pectoralis minor muscle anteriorly, subscapularis muscle posterior and superior, and by the anterior chest wall posteriorly and inferiorly (Figure 2-2) (57). The arrangement of the neurovascular structures within the retropectoralis minor space is similar to the costoclavicular space (51).

## **2.2 Anatomy of the hip joint**

### **2.2.1 Osteology of the Hip joint**

#### **2.2.1.1 The Acetabulum**

The acetabulum of the pelvic innominate bone is a deep hemispherical cavity on the lateral aspect, with the opening directed laterally, downwards approximately 45 degrees and forwards approximately 15 degrees (57, 68). The sides of the cup present an articular (lunate) surface, widest superiorly by which the weight of the trunk is passed onto the femur bone when erect (57). This horse-shoe-shaped strip is covered with articular cartilage and provides the surface upon which the femur articulates within the hip joint (68).

#### **2.2.1.2 The Femur**

The femur is the longest and strongest bone of the body. Its proximal end comprises a rounded articular head projecting medially on a short neck of bone, with a greater and lesser trochanter (57). The head of the femur is half to two thirds of a sphere directed upwards, medially and slightly forwards to articulate with the acetabulum (Figure 2-8) (57, 68). It is entirely covered in hyaline cartilage, thickest anterosuperiorly (68). The neck of the femur is about 5cm long and connects the head and the shaft at an angle of about 125°-135° (the angle of inclination) allowing the leg to swing clear of the pelvis (57, 68). The neck of the femur is narrowest at its middle and is wider at the lateral extent than medially (57). The anterior

surface of the neck is flattened and is marked at its' junction with the femoral shaft by a prominent rough ridge termed the intertrochanteric line (57). This anterior surface of the neck is entirely intra-capsular and the capsular/ligamentous structure extend to the intertrochanteric line on the anterior aspect (57, 68).



Figure 2-8: Anatomy of the anterior femoral neck. Source: Williams & Warwick, Gray's Anatomy, 36th ed.(57).

Ossification of the femur occurs from five centres, in the shaft, head, greater and lesser trochanters and the distal end (57). The epiphyseal line between the neck and head is known as the capital or upper femoral epiphysis (57, 69). The epiphyses fuse independently with the



capital epiphysis fusing during the fourteenth year in females and the seventeenth year in males (57).

## **2.2.2 Angiology of the Hip**

### **2.2.2.1 The Femoral Artery**

The femoral artery is a continuation of the external iliac artery beginning behind the inguinal ligament midway between the anterior superior iliac spine and symphysis pubis (57, 59). It passes inferiorly anteromedial to the hip joint. It is separated behind from the tendon of the psoas major by the femoral sheath – a downward prolongation of the iliac fascia of the abdomen (57). It is separated from the capsule of the hip joint by the tendon of the psoas major. The nerve to the pectineus muscle passes medially behind the proximal end of the artery (57). Immediately lateral to the artery lies the femoral nerve (57).

### **2.2.2.2 Arteria Profunda Femoris**

The Arteria Profunda Femoris is large branch of the femoral artery, usually from the lateral side approximately 3.5 cm (between 2.5 and 5 cm) below the inguinal ligament (48, 57). This artery passes at first laterally but then turns medial and passes behind the femoral artery and vein to the medial side of the femur to descend and anastomose with the muscular branches of the popliteal artery (57). The origin of the arteria profunda femoris is somewhat variable and it may sometimes arise from the medial side and more rarely, from the posterior aspect of the femoral artery (48, 57, 59)

### **2.2.2.3 The Lateral Circumflex Femoral Artery**

The Lateral Circumflex Femoral artery arises as a lateral branch of the arteria profunda femoris and continues laterally between the divisions of the femoral nerve and behind the

sartorius and rectus femoris and divides into ascending, transverse and descending branches (48, 57). Occasionally the lateral circumflex femoral artery may also arise directly from the femoral artery (57). The ascending branch passes superiorly along the intertrochanteric line to the lateral side of the hip where it anastomoses with the superior gluteal and deep circumflex iliac arteries and forms an anastomotic ring with the medial circumflex femoral artery from which the femoral head and neck are supplied (48, 57).

#### **2.2.2.4 The Medial Circumflex Femoral Artery**

This artery usually arises from the posteromedial aspect of the profunda but also frequently from the femoral artery (48, 57). After supplying the adductor muscles it then passes medially around the femur between the pectineus and psoas major to divide into transverse and ascending branches (57). The ascending branch passes obliquely upward towards the trochanteric fossa to anastomose with the gluteal and lateral circumflex femoral arteries (57).

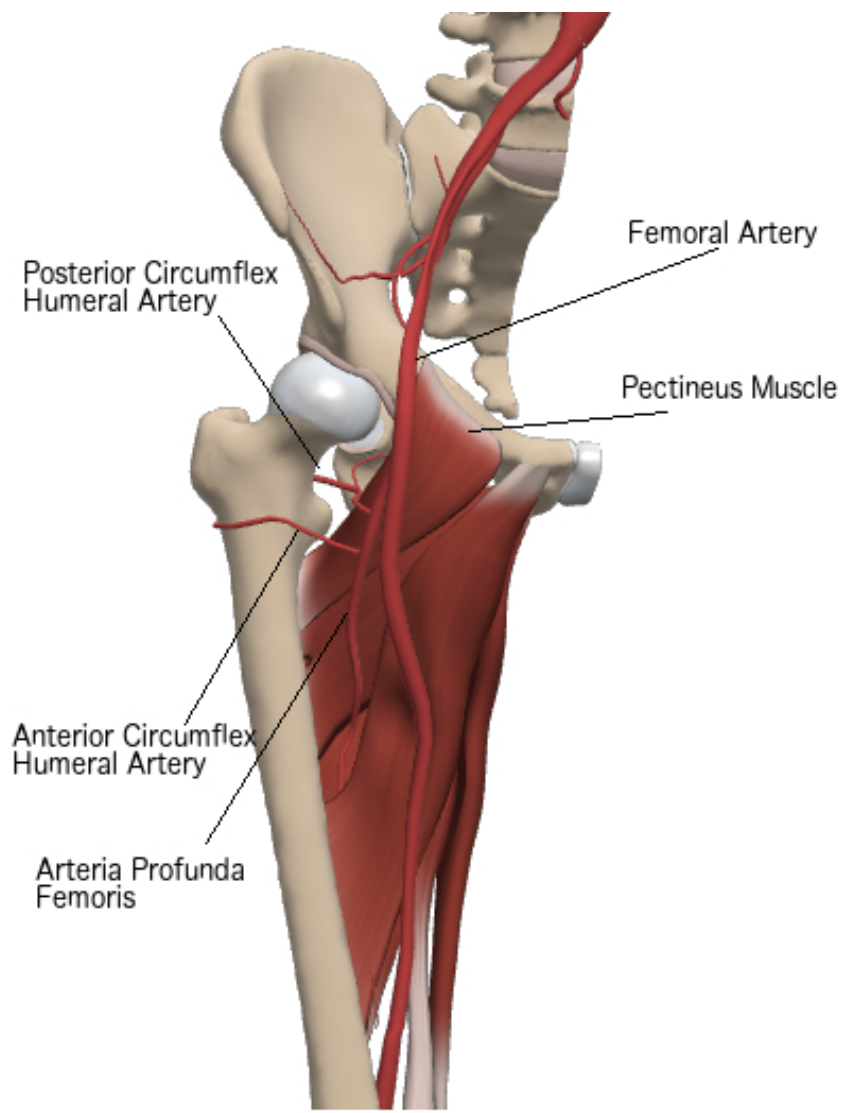


Figure 2-9: The Common Femoral Artery. The Anterior and Posterior Circumflex Humeral arteries can be seen branching from the Arteria Profunda Femoris, in turn a branch of the Common Femoral Artery. Source: (62). Adapted by David Robinson, The Avenue X-ray & MRI.

#### **2.2.2.5 The Common Femoral Vein**

The Common Femoral Vein accompanies and lies medial to the femoral artery at the level of the hip, occupying the middle compartment of the femoral sheath (57, 59). It receives numerous muscular tributaries as well as the vena profunda femoris vein from posterior, and the great saphenous vein proximally, entering its anterior aspect (57, 59). The lateral and medial circumflex femoral veins are also usually tributaries (57).

### **2.2.3 Arthrology**

The hip is a multi-axial ball-and-socket joint where the head of the femur (ball) articulates with the cup-shaped fossa (socket) of the acetabulum (Figure 2-10) (57, 68). The articular surfaces are not completely congruent and the close-pack position (maximal articular surface congruency/stability) occurs at full extension and some medial rotation, allowing the human to stand erect with minimal muscular effort (57, 70). At full extension, the iliofemoral ligament has an anchoring function assisting the maintenance of a standing position (68). The articular surfaces are spheroidal and the femoral head is completely covered with articular cartilage except for a small roughened pit called the fovea capitis, to which the ligament of the head is attached (57). The depth of the acetabulum is increased by a fibro-cartilagenous rim – the acetabular labrum (57, 68).

#### **2.2.3.1 Fibrous capsule**

The fibrous capsule is a strong and dense fibrous covering attached in front to the outer margin of the labrum surrounding the neck of the femur and attached in front to the intertrochanteric line and above to the base of the neck of the femur (57). The fibrous capsule is much thicker anteriorly and at the upper part where the greatest amount of resistance is required, particularly during standing (57, 71). The anterior part is reinforced by the iliofemoral ligament (57, 68). It is covered in front by the psoas major and iliacus muscles and separated from them by a bursa (57).

#### **2.2.3.2 Acetabular labrum**

The acetabular labrum is a fibro-cartilagenous ring composed of type I collagen attached to the margin of the bony acetabulum (57, 72, 73). The inner articular two thirds are essentially

avascular, while the outer one third derives an adequate blood supply from the hip capsule (medial and lateral circumflex femoral arteries) (72). The free edge of the labrum is turned in and embraces the head of the femur closely such that the head of the femur is held in place even if the fibrous capsule is divided (57, 68). The primary function seems to be to act as a sealing mechanism to trap synovial fluid, keeping the femoral and acetabular articular surfaces separate even when under load (72).

Ramified free nerve endings involved in tactile and pain sense are found throughout all parts of the labrum, but are more numerous in the superior and anterior quarters of the labrum (74). Eighty-six percent of sensory end-organs including those involved in pressure, deep sensation and temperature sense are found in the superficial layer (74). The labrum is innervated with free nerve endings with and without end-organ mechanoreceptors, suggesting both a nociceptive (pain) and proprioceptive (positional) role for the labrum of the hip joint (73, 74).

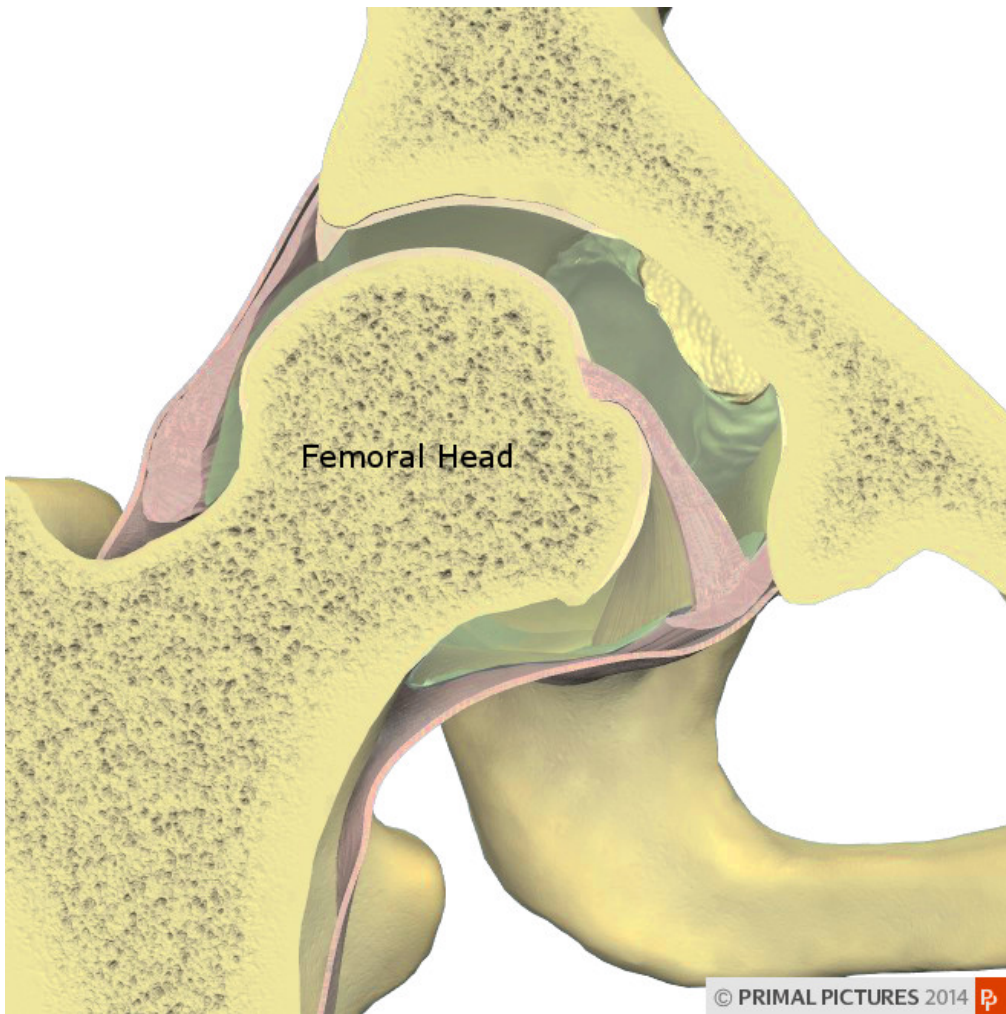


Figure 2-10: The hip joint. Source: Primal Pictures Ltd. (62).

### 2.2.3.3 Iliofemoral ligament

The iliofemoral ligament is triangular in shape and the strongest of all the ligaments of the body, lying in front of the joint and blended with the capsule (57, 68). It forms an inverted “Y”, with the apex of the triangle attached to the lower part of the anterior inferior iliac spine and its base to the intertrochanteric line of the femur (Figure 2-11) (57). The medial aspect is essentially vertical in orientation and attached to the lower part of the trochanteric line. The lateral aspect of the iliofemoral ligament is oblique and attached to the upper part of the same trochanteric line (57, 68, 71). This lateral band is sometimes referred to as the iliotrochanteric ligament.

#### 2.2.3.4 Pubofemoral ligament

The pubofemoral ligament is also triangular with its base at the iliopectineal eminence and the superior ramus of the os pubis of the pelvic innominate bone (57). It blends with the fibrous capsule and the deep surface of the medial aspect of the iliofemoral ligament (57).

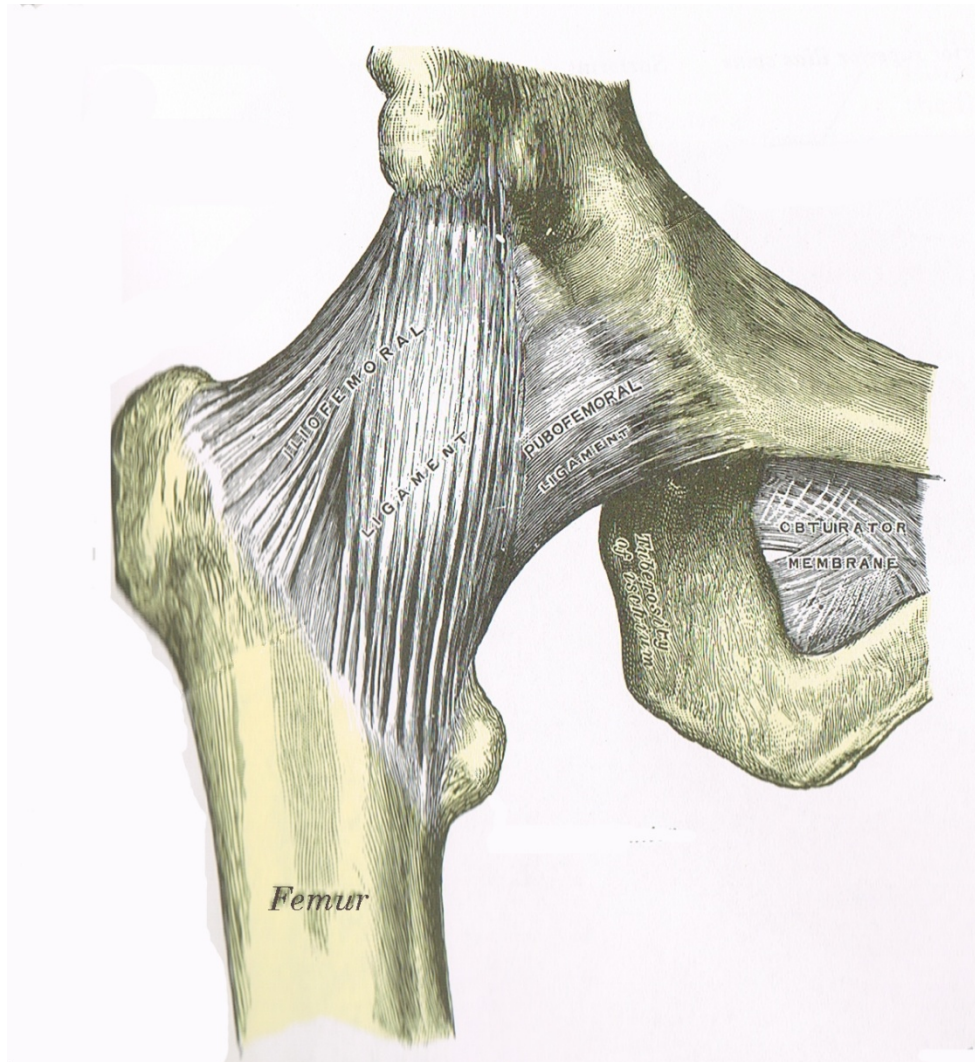


Figure 2-11: The ligaments of the anterior hip joint. Source: Williams & Warwick, Gray's Anatomy, 36th ed. 1918 (57).

#### 2.2.3.5 Psoas Major

A long fusiform muscle lateral to the lumbar region of the vertebral column, it arises from the

transverse processes of the lumbar vertebra, the intervertebral discs of T12 to L5 and the tendinous arches (57, 75). It descends along the pelvic brim, continues posterior to the inguinal ligament and anterior to the capsule of the hip joint before converging into a tendon and receiving on its lateral side nearly all of the fibres of the iliacus muscle and then attaching to the lesser trochanter of the femur (57). Its medial border at the level of the hip joint is partially overlapped by the femoral vein lying anteromedially (57).

#### **2.2.3.6 Psoas Minor**

Absent in 40% of individuals, it originates from the bodies of T12 and L1 and inserts onto the iliopectineal eminence of the innominate bone and the iliac fascia (75). Although not continuing to the lesser trochanter of the femur, the psoas minor muscle when present is nevertheless considered part of the iliopsoas compartment, lying ventral to the psoas major (75).

#### **2.2.3.7 Iliacus**

A triangular sheet of muscle arising from the inner lip of the iliac crest, the superior two-thirds of the concavity of the iliac fossa and the upper surface of the lateral part of the sacrum (57). Most of its fibres converge into the lateral side of the tendon of the psoas major but some attach directly to the femur distally and in front of the lesser trochanter (57). It receives some fibres from the upper part of the capsule of the hip joint (57, 71).

#### **2.2.3.8 The iliopsoas bursa**

Also called the subtendinous iliac bursa it separates the iliacus and psoas tendons from the



pubis and the capsule of the hip joint and is present bilaterally in 98% of adults (Figure 2-12) (57, 76). During the dissection of seven cadavers the bursa was found to extend from the level of inguinal ligament just lateral to its midpoint, downwards and slightly laterally over the thin part of the hip joint capsule between the iliofemoral and pubofemoral ligaments to the level of the neck of the femur just above the lesser trochanter (77). Its average dimensions were measured at 5.5cm long by 2cm wide and it is usually of equal width from the superior to the inferior aspect, but sometimes it is wider at the cephalic end (77). The distal limit of the bursa coincides with the insertion of the psoas tendon onto the lesser trochanter (76). Its function is to reduce friction between the iliopsoas muscle and the underlying hip joint during hip movements (77). The bursa occasionally (among 14% of adults) communicates with the hip joint through a circular aperture between the pubofemoral ligament and the vertical band of the iliofemoral ligament (57, 76). This communication can be congenital or acquired (78). In cases where the communication between the joint and the bursa is acquired, repeated friction and chronic synovitis can result in tears in the synovial membrane over time and allow fluid to pass into the bursa, causing it to enlarge (78). Common disorders associated with an enlarged iliopsoas bursa are mainly of chronic nature and associated with increased production of synovial fluid (and increased intra-articular pressure) including OA, Rheumatoid arthritis, osteonecrosis and total hip replacement (78). Superiorly, the bursa, when enlarged may extend into the pelvic cavity below the inguinal ligament (76). When it enlarges the bursa dissects anteriorly between the iliopsoas tendon and the pectineus muscle, posterolateral to the femoral vessels to reach the femoral ring immediately behind the inguinal ligament (57, 76). The bursa may also enlarge posterolaterally with a thin portion of the bursa dissecting between the iliac muscle and the ilium bone (78).

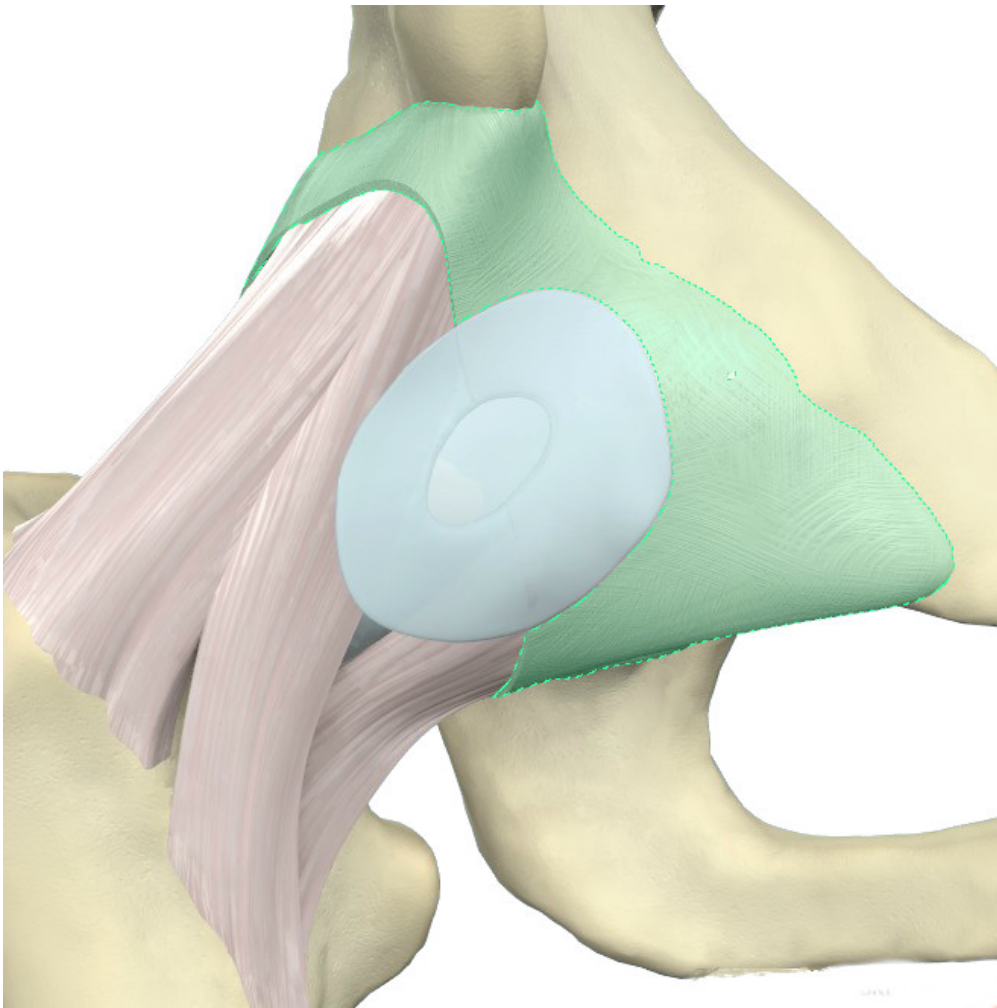


Figure 2-12: The Iliopsoas Bursa shown here in blue overlying the hip joint. The joint capsule is partly cut away (green) to reveal the ligaments. Source: Primal Pictures Ltd (62) (62).

## **2.2.4 Neurology of the Hip**

### **2.2.4.1 The Femoral Nerve**

The femoral nerve is the largest branch of the lumbar plexus, arising from the dorsal branches of the ventral rami of the second, third and fourth lumbar nerves (57). It descends through the substance of the psoas major and passes inferiorly between the psoas major and the iliacus deep to the iliac fascia and passes behind the inguinal ligament before dividing into an anterior and posterior trunk (57). It lies lateral to the femoral artery and is separated from it by part of the psoas major behind the inguinal ligament (57).

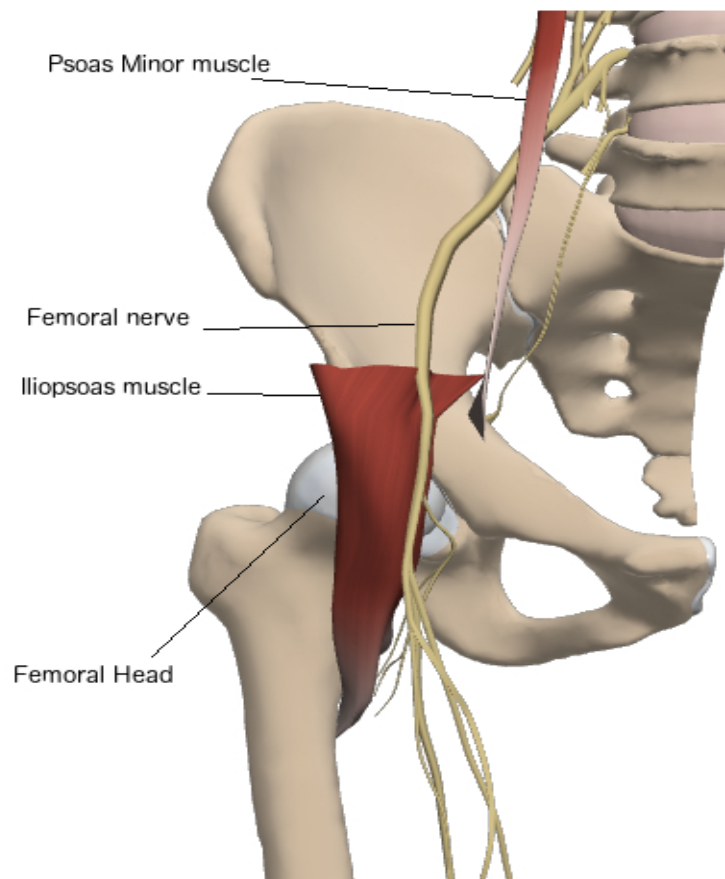


Figure 2-13: The Femoral Nerve. Passing over the conjoint iliopsoas tendon anterior to the hip joint.

Source: (62). [Adapted by David Robinson, The Avenue X-Ray & MRI.](#)

#### 2.2.4.2 The Saphenous Nerve

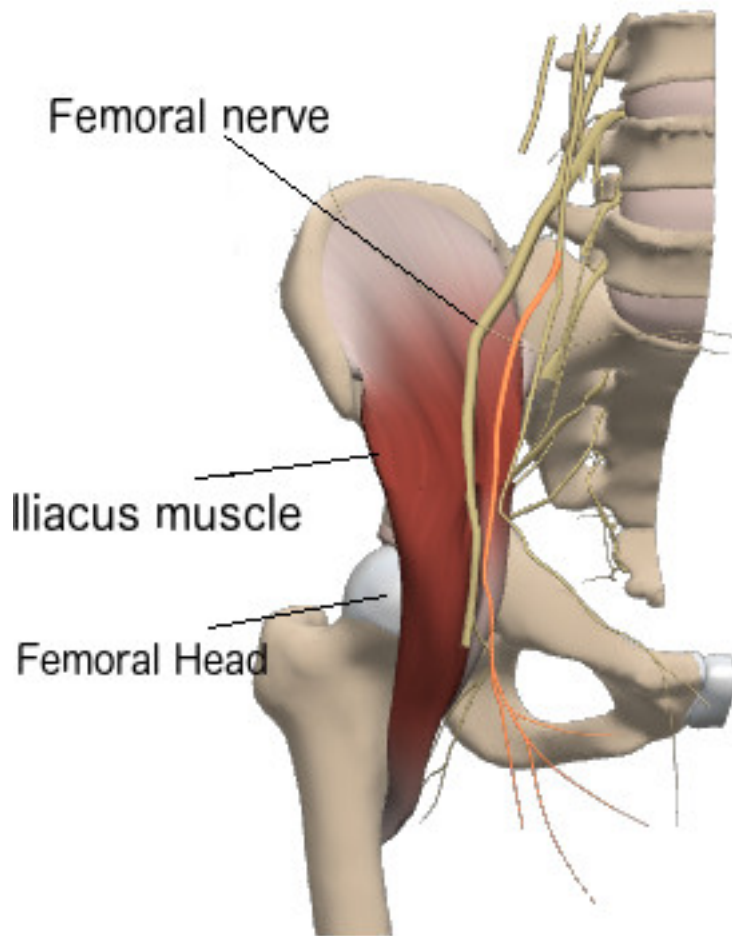
The saphenous nerve is the largest cutaneous branch of the femoral nerve (57). It descends on the lateral side of the femoral artery and enters the adductor canal where it crosses the artery from its lateral to medial side (57).

#### 2.2.4.3 The Genitofemoral Nerve

This nerve arises from the first and second lumbar nerves and passes obliquely downwards and forwards through the psoas major and then on the surface of that muscle before dividing at a variable distance above the inguinal ligament into the genital and femoral branches (57).

The femoral branch descends on the lateral side of the external iliac artery and enters the

femoral sheath lateral to the femoral artery (57). It then pierces the anterior layer of the femoral sheath to supply the skin over the upper part of the femoral triangle (57).



---

Figure 2-14: The Genitofemoral Nerve and its' branches, passing obliquely downward over the surface of the iliopsoas shown here in orange. The Femoral Nerve (yellow) is labelled for clarity. **Source:** (62). Adapted by David Robinson, The Avenue X-Ray & MRI.

## ***Chapter 3 Literature review***

### **3.1 Quadrilateral Space Syndrome (QSS)**

Peripheral neuropathies of the shoulder are all considered entrapment syndromes and account for 2% of shoulder sports-related pain (66). Many cases relate to a physical phenomenon where the nerve is stretched or encased into a fibrous or osteofibrous space such as the quadrilateral space (66). Quadrilateral Space Syndrome, where the axillary nerve is compromised within the quadrilateral space, was first reported in 1983 (10). The discovery of the syndrome originated from a critical review beginning in 1967 of the results of surgery to relieve thoracic outlet syndrome (10). This review found a high percentage of poor results where the subclavian artery was surgically decompressed without relief of symptoms.

#### **3.1.1 Fibrous bands**

Originally it was believed that the syndrome was caused by compression neuropathy of the axillary nerve within the quadrilateral space by anomalous fibrous bands traversing the space.

Similar fibrous bands were not found at the dissection of an unknown number of cadavers (10). The condition is considered to be very uncommon, affecting less than two percent of the population, with only sixteen articles published in more than 30 years reporting 37 additional cases leading up the new classification in 2015 by the Mayo clinic (2, 26, 27, 45, 79, 80).

Initially, the diagnosis of the condition was made by subclavian XR arteriography, where abduction of as little as 60 degrees caused occlusion of the PCHA (10). The subclavian/axillary angiogram in these patients had already been established as normal.

Impingement upon the PCHA was thought to be indicative of compression of the neurovascular bundle and hence pathognomonic of the condition. In the original study by Cahill, all asymptomatic shoulders showed a normal patent PCHA on ABER (10). Eighteen cases were operated on, with eight describing a dramatic improvement in symptoms, a further eight had improvement but with continued symptoms at night and two had no improvement (10).

Successful surgical decompression to release the axillary nerve can be tested at surgery by palpating the reappearance of PCHA pulsations with the arm in ABER (10, 79, 81, 82).

Some authors have speculated that the fibrous bands, usually occurring between the long head of triceps and the teres major, are caused by repetitive low-grade trauma to the shoulder, such as might occur among athletes engaged in activities requiring repetitive overhead movement (66, 81). QSS usually affects young active people such as young adult athletes undertaking repeated overhead actions such as throwers and swimmers (32, 79, 81, 83). Employment activities (such as cleaning, painting) may also be a source of similar repetitive trauma (29, 84). The syndrome is not found in the elderly and less active individuals, supporting this hypothesis (81). In the original study Cahill and Palmer described the condition as “practically always in the dominant extremity” (10). Other subsequent reports have not remarked upon dominance or otherwise of the affected limb (29, 45, 82, 84, 85).

Examination of a series of eight cadavers (16 shoulders, including three male and five female, of unknown age) in 2006 found fibrous bands traversing the quadrilateral space in 14/16 (88%) shoulders (67). In most cases there were multiple bands, suggesting that these fibrous bands are perhaps a common finding (67).

At surgery on symptomatic patients, the axillary nerve has been noted by some to be surrounded by fibrous tissue and tethered to the long head of the triceps (86). Examination of

a series of four cadavers in 1995 revealed that the axillary nerve slid freely over the surface of the tendinous part of the origin of the long head of triceps in presumably normal shoulders (86). MacClelland and Paxinos in their series of dissections found that the fibrous bands, when present, reduced the cross-sectional area of the quadrilateral space during both internal and external rotation (67).

### **3.1.1-3.1.2 Shoulder translation with movement**

The axillary nerve itself passes underneath the shoulder articular capsule in close relation to the lower part of the humeral head (57, 65). This creates the possibility that movement of the humeral head (particularly inferior displacement) can give rise to axillary nerve compression neuropathy independent of conditions within the quadrilateral space. Humeral head decentering either secondary to trauma or due to instability (glenoid labral pathology or rotator cuff tear) may give rise to QSS (30, 79, 87-89).

### **3.1.2-3.1.3 Mass lesions**

Tears of the glenoid labrum may be accompanied by the development of paralabral ganglion cysts. Inferior labral ganglion cysts may impinge upon the axillary nerve in the quadrilateral space giving rise to QSS (87). Mass lesions have been reported to be a cause of extrinsic compression of the axillary nerve leading to QSS (Figure 3-1). Hung et al (2014) reported a case of a 48 year old female with a 3cm Schwannoma of the axillary nerve in the quadrilateral space causing symptoms of QSS. This finding was confirmed by histopathological examination (80). More recently the description of QSS has been further defined as compression of the axillary nerve within the quadrilateral space by tumours, cysts or teres minor muscle hypertrophy (83).

### **3.1.3-3.1.4 Other causes**

Other possible causes of axillary nerve compression neuropathy suggested in the past include

compression/shear between the teres major and minor during extended athletic endeavour or extreme abduction, hypertrophy of the teres minor and/or subscapularis, as well as varicocoeles within the quadrilateral space (30, 79).

Some upper extremity vascular disorders in athletes may be caused by arterial embolic syndromes that are also secondary to impingement (90). Muscle hypertrophy in throwing athletes and fatigue-induced translational events may incite impingement on neurovascular structures (90).

Impingement of the PCHA with ABER can damage the artery wall, giving rise to aneurysm and thrombus formation. The PCHA is particularly prone to mechanical injury as it passes around the neck of the humerus (91). Forceful overhead motion such as found among high-performance overhead athletes is postulated to cause a traction effect on the artery, leading to intimal injury, degeneration and aneurysm formation (47, 91). In a series of three professional volleyball players, Atema et al (2012) found that all had ischemia of the hand due to arterial emboli originating from an injured PCHA resulting in thrombosis passing retrograde to the axillary artery and thence to the distal small arteries (91).





Figure 3-1: Magnetic Resonance Image of a patient with a ganglion projecting from the inferior labrum (white arrow). The ganglion lies adjacent to the axillary nerve and posterior circumflex humeral artery. Source: Dr. Paul Marks, The Avenue Radiology, Windsor, 2010.

### **3.2 Natural history of QSS**

The natural history of QSS is unknown but the condition is thought to be self-limiting.

Progression of the condition is halted or reversed by sufferers ceasing the provocative activity or changing behaviours (10, 79). QSS may resolve with non-operative management provided there is no expanding lesion compressing the nerve within the quadrilateral space (79).

Behaviour modification, rest, and abstaining from activities that exacerbate symptoms and non-steroidal anti-inflammatory medications can often provide excellent symptomatic relief (2, 10, 79).

Any lesion causing axillary nerve impingement may remain undiscovered where surgical intervention is not required, although space-occupying lesions such as ganglia and neuromata may be apparent with modern medical imaging (80, 87, 88). Fibrous bands such as those discovered by Cahill and Palmer cannot be imaged with any known technique at this time (10, 66).

The prognosis with non-operative treatment is difficult to assess because most reports only discuss those patients who underwent surgery (92). The axillary nerve does not appear to sustain injury from normal upper limb movements such as excursion and longitudinal tensile stress causing lengthening (2). The nerve sheath (epineurium) has circumferential collagen fibers that allow it to withstand more force than it transmits to the nerve core (endoneurium) protecting the core from injury during movements such as ABER (2). It is chronic fixed nerve traction that displaces the nerve in transverse and longitudinal dimensions leading to long-term damage to axons and myelin (2). Cahill and Palmer in their original report found that seventy percent of patients (42/60) with compressed PCHA on angiography did not have symptoms sufficient to justify surgery (10). The indications for surgery included persistent symptoms despite non-operative management and confirmation of the diagnosis by a positive arteriogram or the presence of an aneurysm (2, 79).

### **3.2.1 Pathophysiology of QSS**

Symptoms of QSS are varied but have been described as dull aching or burning pain over the lateral and posterior aspects of the shoulder, vague weakness affecting deltoid and teres minor muscles, and pain with applied pressure to the quadrilateral space posteriorly (67, 79).

Symptom onset is typically slow and intermittent and pain and paraesthesia is poorly

localized and has a non-dermatomal distribution (10). Symptoms are often exacerbated with overhead activity, in particular ABER (79). Affected persons may notice reduced abduction strength or an inability to raise their arm (79). Affected athletes may fatigue quickly during exercise, especially with overhead activity and/or heavy lifting (79). There may also be numbness/paraesthesia of the lateral arm, and if the syndrome is well advanced the patient may note atrophy or asymmetry of the deltoid muscle mass (2, 79). Employment activities (such as cleaning, painting) may also be a source of similar repetitive trauma (29, 45). The diagnosis is difficult when history and physical examination alone are relied upon, and in many cases no definite diagnosis can be reached (44, 93). Many individuals will present with unexplained pain for months or years (92). Delays in diagnosis may result in inappropriate treatment, prolonged disability and potentially irreversible muscular fatty atrophy of the deltoid and teres minor muscles, as well as permanent damage to the axillary nerve (85, 87, 88).

Shoulder pain in the young athletic population is very common and may have a variety of causes (92). QSS may be confused with other shoulder pathology such as rotator cuff tears, capsulitis or impingement, also common in the relevant demographic (79, 87). The differential diagnosis may also include thoracic outlet syndrome and cervical radiculopathy, osteoarthritis and adhesive capsulitis (79, 92).

Based on only one symptomatic patient, Mochizuki suggested that occlusion of the PCHA on MRA is not specific for a diagnosis of QSS when compared with six healthy volunteers (46). Mochizuki et al (1994) found stenoses near the origin of the PCHA in 80% of the healthy volunteers (46)

Two hundred and eighty elite volleyball players were scanned with ultrasound via the axilla to determine the incidence of PCHA aneurysm and vessel characteristics of the PCHA and the deep brachial artery (61). The mean transverse PCHA diameter was 3.7mm (60). The

prevalence of aneurysm was 4.6% (13/280), all detected in the proximal PCHA (61). The PCHA arose from the axillary artery in 81% (228/280), or from a common trunk (with the deep brachial artery or other artery) in 19% (52/280) (61). In the normal anatomical variants, the artery showed a curved course dorsally toward the humeral head in 93% (211/228), potentially aiding identification with ultrasound (61).

While investigating a series of nine cases of QSS a new classification system with two new categories of QSS was suggested by the authors, namely vascular and neurogenic QSS (2). Vascular QSS (vQSS) results from repeated mechanical stress during ABER leading to intimal injury and damage to the vessel wall which in turn can result in thrombus and aneurysm formation of the PCHA, with subsequent distal embolism (2). Sufferers typically present with coolness of the digits, cold intolerance and cyanosis of one or more of the upper extremity digits (2).

Neurogenic QSS (nQSS) involves a fixed anatomic anomaly causing extrinsic compression of the axillary nerve resulting in permanent scarring and adhesions (2). Sufferers of nQSS present with more typical symptoms of QSS, including paresis, paraesthesia, poorly localized shoulder pain and tenderness of the posterior shoulder over the quadrilateral space (2). The forward elevation, abduction and external rotation (ABER) test is a sensitive provocative test, with symptoms becoming apparent if the position is held for 1-2 minutes (28).

### **3.2.2 Thoracic Outlet Syndrome**

Thoracic outlet syndrome (TOS) is complex of symptoms of the upper extremity including pain, parathesias, numbness and weakness of the arm and hand secondary to neurovascular compression in the thoracic outlet (94, 95). TOS is one of the differential diagnoses of QSS, and the age range of affected persons is remarkably similar at between 20-40 years of age (51). The condition is caused by compression of the neurovascular structures at the thoracic

outlet somewhere between the scalene triangle and the inferior border of the axilla (94). The costoclavicular space is by far the most frequent site of arterial compression, while the retro-pectoralis minor space has, by comparison, rarely been reported as a site of compression (51, 96). The brachial plexus, subclavian vein and subclavian artery may all be affected by external compression, leading to the separate distinctions of TOS, namely arterial TOS (aTOS), venous TOS (vTOS) and neurogenic TOS (nTOS) (48, 97). The neurogenic type (nTOS) is the most common type of all cases of TOS (95%), usually occurring secondary to trauma, and can be diagnosed during a clinical examination (48, 97). Arterial TOS, the first type to be recognised in 1821, comprises less than five percent of TOS cases and is most commonly due to osseous abnormalities such as cervical ribs, anomalous first ribs and callous formation secondary to fracture of the clavicle or first rib (48, 94). The subclavian vein, implicated in venous TOS does not cross the interscalene triangle, but runs in front of the anterior scalene muscle (57, 98). A cervical or anomalous first rib, or hypertrophied scalene muscle will thus not cause vTOS (98). Venous TOS makes up less than five percent of all TOS cases (98).

Classification of aTOS or nTOS is difficult. They may occur concurrently (51). Because of the anatomical proximity of the subclavian artery and brachial plexus, compression of one structure can be considered to be indicative of compression of the other, and some of the pathophysiologic mechanisms are related (51, 94). Doppler ultrasound of the subclavian artery and vein in the costoclavicular space was carried out among five patients with clinically suspected thoracic outlet syndrome and five healthy volunteers as controls (99). Patients were examined in the sitting position with the arm in neutral position, 90 degrees of abduction, 120 degrees and hyperabduction and again upon release of abduction (99). All control patients showed no Doppler changes at 120 degrees of abduction, whereas all symptomatic patients showed Doppler ultrasound changes characteristic of stenosis such as

increased peak systolic velocity (PSV) and turbulent flow (99). The observed Doppler ultrasound changes included turbulence and a more than doubling of peak systolic velocity with some cases demonstrating complete cessation of flow (99). No significant changes in velocities were found during these manoeuvres among control subjects (99).

Many asymptomatic people exhibit upper extremity pulse deficits with positional movements of the arm. Evidence of thoracic outlet arterial compression has been reported to be common in asymptomatic persons (48, 100). Photoplethysmography was used to determine objectively the presence of vascular arterial compression during provocative tests in 130 asymptomatic individuals and evidence was found of vascular compression in 60% (78/130) of these volunteers ( $p < 0.005$ ) (100). In particular, occlusion was most common (10% - 13/130) during hyperabduction of the arm (100). Doppler ultrasound was performed on 20 asymptomatic volunteers and the results showed significant compression of the subclavian artery (at least doubling of the peak systolic velocity or complete cessation of flow with hyperabduction) in four (20%) of the patients, including one with bilateral occlusion (101).

Stapleton et al in 2009 using Doppler ultrasound attempted to establish the normal subclavian artery responses to a series of provocative manoeuvres, including 120 degrees of abduction and 90 degrees of external rotation (102). The study demonstrated a heterogeneous response of peak systolic velocity and specifically, lack of flow with abduction in six of 31 (19%) patients ( $p = 0.008$ ) (102).

It is therefore apparent that the hyperabduction of the arm (beyond 90 degrees) could dramatically affect blood flow in the subclavian/axillary artery in up to half of asymptomatic individuals (48, 51, 100-102). As the PCHA is a branch of the third part of the axillary artery in 81% of individuals, aTOS affecting flow in the axillary artery will also affect flow in the PCHA (48, 61). Doppler ultrasound characteristics of the PCHA in such a situation would not be representative of external forces acting on the PCHA within the quadrilateral space.

### 3.3 Diagnosis of QSS

#### 3.3.1.1 Clinical diagnosis

It has been suggested that physical examination alone may be sufficient to diagnose QSS (29). Clinical presentation is, however, varied and inconsistent and the syndrome may present with variable symptoms, including poorly localized shoulder pain, paraesthesias and point tenderness on the posterior aspect of the shoulder over the quadrilateral space (10, 30, 79, 84). Symptoms are usually exacerbated with the affected arm held in ABER. QSS may be confused with other shoulder pathology such as rotator cuff tears, capsulitis or impingement, and TOS which are also common in the relevant demographic (79, 87, 92). The rarity of QSS requires that other diagnostic tests (such as ultrasound) be performed to rule out other more common causes of shoulder pain that may mimic the condition (2, 79).

#### 3.3.1.2 Electromyography

Some authors have suggested that electromyography (EMG) with reduced conduction velocity of the axillary nerve or reduced deltoid muscle potentials may be specific for diagnosis (86). The posterior branch of the axillary nerve supplies two primary motor endpoints in the teres minor muscle and the posterior part of the deltoid muscle (57, 89).

In a series of four patients with QSS, four abnormal electro diagnostic studies, manifesting as reduced conduction velocity of the axillary nerve were observed (86). In another series of five patients with surgically proven QSS, three of four had “positive” electro diagnostic studies indicating axillary nerve compromise, while the fifth did not have EMG performed but had a positive angiogram (29). However, only one had reduced motor conduction of the axillary nerve. In neither of these two studies was there mention of normal controls. There was no report of improved conduction velocity after surgery in either series reported despite all

patients reporting improvement of symptoms and sensory deficits, after six months of follow-up of the four patients in the series by Chen, and an unspecified duration in the series reported by Francel (29, 86). The small sample sizes in these two studies make it difficult to generalise these findings for the community at large.

Nerve conduction studies may not be helpful especially early in disease progression due to the intermittent nature of the nerve impingement, and may not become positive until chronic atrophic changes and muscular atrophy are present (79). Electro diagnostic studies can therefore be normal in cases of axillary nerve compression syndromes (66, 92). Such studies are also invasive and can be unreliable in isolating the teres minor nerve (89). Quality electromyography suffers from poor availability, with costs for a single test of multiple nerves up to several hundred dollars (103).

### **3.3.1.3 X-Ray**

X-ray is usually the first medical imaging tool used in the assessment of patients with shoulder symptoms. QSS may occur secondary to direct trauma to the posterior shoulder or compression caused by bony outgrowths such as callus post fracture of the humerus or scapula (79, 104). The role of X-ray is particularly important after trauma or in the follow-up of traumatic shoulder pathology. Differential diagnoses of QSS include degenerative OA of the glenohumeral joint and OA of the acromioclavicular joint which are detectable with plain x-ray (Figure 3-2) (79). Long-term effects of humeral head instability may be seen on plain x-rays and suggest a mechanism for axillary nerve impingement, but instability may also be detectable with careful clinical examination (105). The most common cause of QSS are the fibrous bands first described by Cahill and Palmer and soft tissue structures such as these are not detectable with plain x-ray (79).



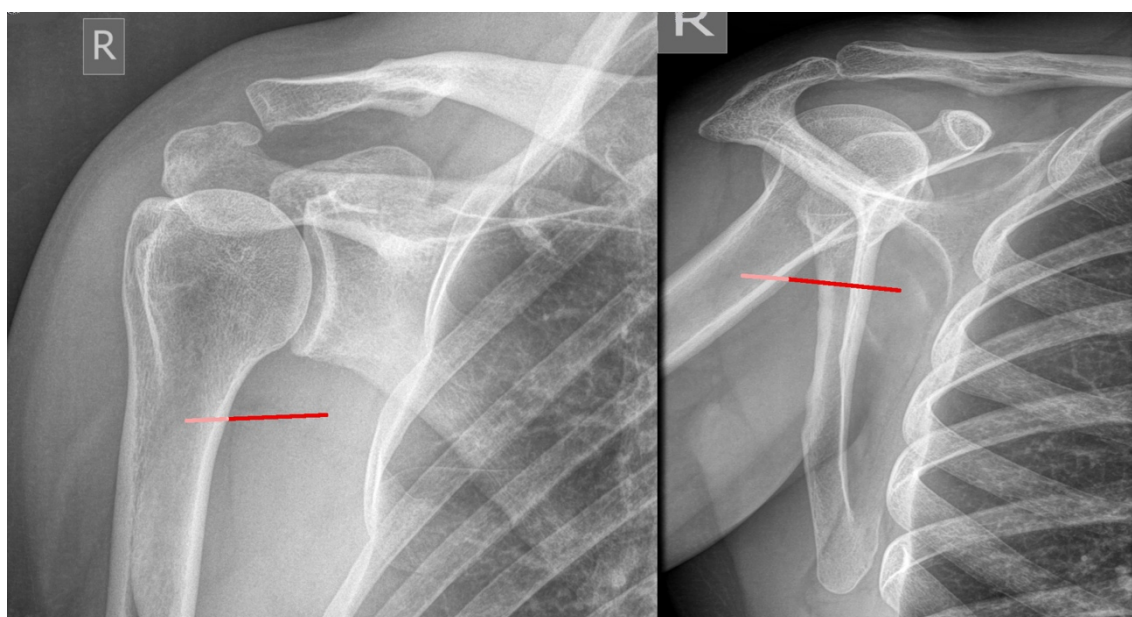


Figure 3-2: Anteroposterior (left) and lateral (with 15 degrees' down tilt (right)) plain x-ray of the right shoulder. The shoulder appears normal. The quadrilateral space is represented by the red line passing from medial to lateral and slightly superior to inferior below the humeral head. Plain x-ray is unable to demonstrate soft-tissue abnormalities in this area. Source: David Robinson, The Avenue X-ray & MRI

### 3.3.1.4 Angiography

Angiographic imaging of the PCHA was part of the initial description of the condition by Cahill and Palmer in 1983. They noticed occlusion of the PCHA in ABER, and postulated that this intermittent arterial occlusion was representative of pathological impingement upon the axillary nerve (10). Although occlusion of the PCHA upon abduction and external rotation was the original description, arteriographic evidence of external compression of the PCHA (i.e. stenosis of the PCHA) has since been included as evidence of impingement upon the axillary nerve in the quadrilateral space (106). No other imaging modalities were described in the original report of Cahill and Palmer (10). Angiography of the subclavian artery is no longer performed at our institution, due to the invasive nature, radiation burden, time constraints and better alternatives.

~~More recently, PCHA compromise in the setting of clinical suspicion of QSS has been~~

~~evaluated by magnetic resonance (MR) angiography (Figure 1-2) (102). MR angiography is able to not only assess impingement of the PCHA in abduction and external rotation, but can also eliminate other causes of shoulder symptoms, such as rotator cuff disease and glenohumeral joint osteoarthritis (84). MR angiography may also demonstrate other causes of axillary nerve compromise such as ganglia, fracture or dislocation (82, 103). MR angiography of the PCHA has since become widely utilized in the assessment of QSS (43, 76).~~

~~However, MR angiography of the PCHA is usually the final imaging tool used in the pursuit of the cause of shoulder pain, where the clinical picture is consistent with QSS. MR angiography of the PCHA is performed predominantly amongst athletes in whom axillary nerve decompression surgery is being considered. In the general population when readily available and cheap imaging options such as x-ray and ultrasound have not revealed the cause of symptoms, patients are often managed conservatively with physical therapy and behavioural changes, without referral for MR angiography (10, 27).~~

~~Doubt has been cast on the specificity for QSS during PCHA occlusion on abduction and external rotation on MR angiography. In a study of one patient with QSS and six healthy volunteers the PCHA was found to be stenotic near the origin in 80% of the healthy volunteers (43). Positive findings on angiography was thus not specific for QSS (43). The evidence for PCHA compromise representing axillary nerve impingement is thus not strong, as published studies have used limited sample sizes and had few asymptomatic volunteers to serve as controls.~~

### **3.3.1.5 MRI**

The fibrous inter-muscular bands thought responsible for extrinsic compression of the axillary nerve have not been revealed to date with MRI imaging (66). Axillary neuropathy caused by impingement of the nerve within the quadrilateral space will cause denervation atrophy of the

teres minor muscle and posterior deltoid muscle (89). Fatty atrophy of the teres minor or posterior deltoid muscle detected on MRI has been considered to be a diagnostic marker of the syndrome provided there is an intact teres minor tendon and rotator cuff (Figure 3-3) (85). MRI evidence of atrophy includes decreased muscle bulk and fatty infiltration. MRI enables assessment of the teres minor muscle for the presence of isolated fatty atrophy (79, 85, 106, 107). MRI uses no intravenous contrast material and assesses the fat content of the muscle in question, rather than mechanical impingement upon the PCHA. Tears of the teres minor tendon causing atrophy are extremely rare, however there is no proof that isolated teres minor atrophy without oedema is related to QSS (66, 107). In such cases this finding should be considered an isolated finding, and the patients symptoms are probably related to another lesion (66).

Teres minor atrophy however, occurs mainly in older patients approximately 60 years of age (and older) who do not fit the expected clinical presentation of QSS (89). Teres minor atrophy has been found to be associated with humeral head decentering secondary to rotator cuff tears (88, 89). Two hundred and seventeen consecutive shoulder MRI examinations were performed on patients with shoulder symptoms referred from the general population over a period of three months (89). Five and a half percent (12/217) had isolated teres minor atrophy without teres minor tendon tear. Ten of these patients (83%) had rotator cuff tears – nine had full thickness tears and one high-grade partial thickness tear. One 26 year-old patient had an isolated posterior labral tear and one 32 year old patient had no associated pathology (89).

In a retrospective review of all shoulder MRI examinations performed over a two year period at one institution, a three percent (61/2563) incidence of isolated teres minor denervation was reported (106). None of these patients had a clinical history consistent with QSS. The average patient age was not stated. Associated findings included a tear of at least one of the tendons of the rotator cuff (n=47), glenohumeral joint capsular injury (n=14) and labral tears (n=44)

(106).

Another retrospective review of an imaging database over a 67-month period using keywords “quadrilateral” and “teres” identified patients with atrophy or abnormal signal in the teres minor muscle (107). Patients were predominantly referred for evaluation of rotator cuff tear. Of 2436 reports, 19 (0.8%) were found to have focal atrophy or an abnormally increased T2 signal in the teres minor muscle (107). The mean age of patients in this study was 52 years (range 26-83), and only one had atrophy of the teres minor muscle, the only abnormality identified on MRI (107). The remainder of the examinations found associated labral tears (6/19 (31.6%)), rotator cuff tears (11/19 (57.9%)) and humeral fractures (2/19 (10.5%)) (107). No patients underwent further imaging evaluation of the quadrilateral space to confirm compression of the neurovascular bundle or surgery on the quadrilateral space (107).

Fatty atrophy of teres minor is not an uncommon finding on MRI of shoulders in our institution. It leaves the practitioner with a dilemma. Is the change due to disuse, tear or denervation from QSS? Hence, a cheap and available confirmatory test is needed.

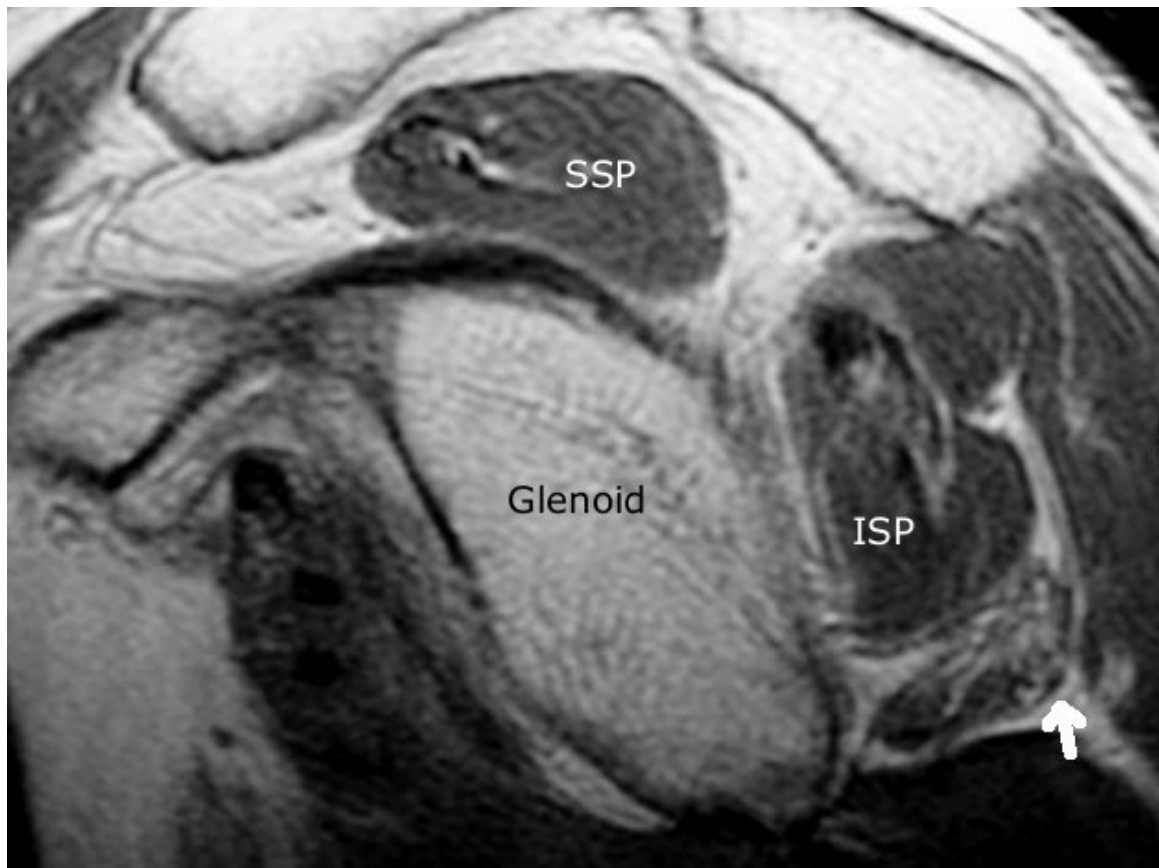


Figure 3-3: Sagittal proton density MRI scan of the shoulder of a patient referred for shoulder pain. Coronal view with anterior aspect to left of the image. Incidentally noted teres minor fatty atrophy manifests as white streaking within the teres minor (white arrow) when compared to adjacent infraspinatus muscle (ISP). SSP – supraspinatus muscle. Source: Dr. Paul Marks, The Avenue Radiology, Windsor.

More recently, PCHA compromise in the setting of clinical suspicion of QSS has been evaluated by magnetic resonance (MR) angiography (Figure 1-2) (106). MR angiography is able to not only assess impingement of the PCHA in abduction and external rotation, but can also eliminate other causes of shoulder symptoms, such as rotator cuff disease and glenohumeral joint osteoarthritis (87). MR angiography may also demonstrate other causes of axillary nerve compromise such as ganglia, fracture or dislocation (85, 107). MR angiography of the PCHA has since become widely utilized in the assessment of QSS (46, 79).

However, MR angiography of the PCHA is usually the final imaging tool used in the pursuit of the cause of shoulder pain, where the clinical picture is consistent with QSS. MR

angiography of the PCHA is performed predominantly amongst athletes in whom axillary nerve decompression surgery is being considered. In the general population when readily available and cheap imaging options such as x-ray and ultrasound have not revealed the cause of symptoms, patients are often managed conservatively with physical therapy and behavioural changes, without referral for MR angiography (10, 30).

Doubt has been cast on the specificity for QSS during PCHA occlusion on abduction and external rotation on MR angiography. In a study of one patient with QSS and six healthy volunteers the PCHA was found to be stenotic near the origin in 80% of the healthy volunteers (46). Positive findings on angiography was thus not specific for QSS (46). The evidence for PCHA compromise representing axillary nerve impingement is thus not strong, as published studies have used limited sample sizes and had few asymptomatic volunteers to serve as controls.

Both MR angiography and MRI in the diagnosis of QSS have a number of disadvantages. MR angiography is time consuming, invasive, relatively expensive, not available in all areas and requires the patient to maintain the arm in the most uncomfortable position for an extended length of time. MR contrast agents are not suitable for patients with known chronic renal disease. The sensitivity of MR angiography–detected PCHA stenosis or occlusion has been called into question in a study of just six healthy volunteers (46). Two of 10 (20%) of the PCHA of the volunteers’ shoulders were normal, while the others (80%) appeared stenotic near the origins (46). The incidence of PCHA stenosis amongst a healthy population without symptoms of QSS is thus not known.

MRI-detected fatty muscular atrophy is a non-specific sign and the sensitivity for diagnosis of QSS has not been evaluated until 2004 (107). Fatty atrophy of the teres minor can have a variety of possible causes such as prior surgical intervention, glenohumeral translational events, ageing, lack of use, diabetes and brachial plexus and nerve root pathologies (106-108).

Despite the less invasive nature of MRI for isolated fatty atrophy of the teres minor muscle, this finding does not appear specific enough to suggest a diagnosis of QSS.

### **3.3.1.6 Ultrasound**

Historically the role of ultrasound in the investigation of shoulder pain has been in the detection of other pathologies with a similar clinical presentation to QSS, such as rotator cuff tears, tendinopathy or subacromial bursitis. Rotator cuff tears and subacromial bursitis are common amongst the population suspected of having QSS (79, 87). Ultrasound is widely available and regularly combined with plain x-ray in the initial workup for patients with shoulder symptoms. Ultrasound is also particularly well suited for follow up of cases post treatment due to the lack of ionizing radiation, or risk of contrast allergy reactions, the relatively low cost and wide availability.

The intra-observer variability of ultrasound of rotator cuff tears has been reported to be low in a study of 61 patients with shoulder pain, with two radiologists in full agreement in 92% of cases (109). In a study of 46 sports participants, measurements of the subacromial space, the subacromial bursa, the supraspinatus tendon and dynamic impingement were performed by two physiotherapists using a standardised ultrasound protocol (110). Intra- and inter-rater reliability were all above 0.80 (range 0.82–0.99) with no systematic bias. For the dynamic impingement examination, the overall agreement was 98% and 93%, with Kappa of 0.96 and 0.82, for intra- and inter-rater reliability, respectively (110).

#### **3.3.1.6.1 Shear Wave Elastography**

Shear-wave elastography uses an acoustic radiation force of a focussed ultrasonic push pulse sequence to induce tissue oscillation (shear waves), which propagate perpendicular to the ultrasound beam (111, 112). The shear wave velocity is related to mechanical properties of the examined tissue such as fiber direction (relative to the shear wave propagation

direction) and tissue elasticity (112). Shear-wave elastography has been investigated as a functional tool, for example in the assessment of functional recovery of injured tendons (113). Shear-wave elastography is not available at our clinical practice.

Axial strain elastography provides a more objective, semi-quantitative measure of the intrinsic tissue elasticity by comparing shear-wave elastography images before and after freehand transducer compression (111, 113).

Shear-wave propagation has been assessed to determine if wave velocity correlates to muscle fatty degeneration (112). Twenty-eight patients with a history of rotator cuff repair (median time after surgery 2.3 ( $\pm$  0.7) years) and fourteen patients with tears managed without surgery (N=42) had shear wave velocity measurements of the supraspinatus compared with MR spectroscopy measurements of fat/water ratio for fatty degeneration (112). Pearsons' rank correlation test showed good correlation of 0.82 ( $p = 0.00008$ ), however it should be noted that four patients had no shear-wave data collected due to the overlying soft tissue thickness exceeding two centimetres (112).

Recent studies suggest that axial-strain sonoelastography is able to distinguish between asymptomatic and diseased tendons, however these techniques have not yet been included for routine use in clinical practice due to the level of artefacts, operator dependency, lack of standardization and inability to quantify the data (113). A primary limitation of shear-wave elastography is the lack of depth penetration and small size of the area for analysis, meaning that assessment of deep structures such as the iliopsoas tendon of the hip is not currently possible (111). The current clinical application of shear-wave sonoelastography is predominantly as an adjunct to conventional ultrasound (111). Shear – wave elastography has no role in the evaluation of peripheral arteries. It is not clear how measurements of tissue elasticity would aid the detection of arterial occlusion or stenosis, or dysmorphia of femoral head-neck junction. It should be noted that fatty degeneration of the



Teres Minor muscle is a late-stage manifestation of QSS, and that the objective of diagnostic imaging is to diagnose QSS before this irreversible process begins.

### 3.3.1.6.1 3.3.1.6.2 Ultrasound Colour mapping

Colour Doppler ultrasound adds directional colour mapping to an image, aiding in the identification of blood vessels and localisation of stenosis and occlusions. A large area of the two-dimensional grey scale (B mode) image is assessed for evidence of Doppler shifts, and then those regions where a shift has been detected are colour coded (114). In this way, the motion of red blood cells within blood vessels can be mapped in colour onto the B-mode image. This is especially useful for smaller blood vessels (such as the PCHA) that are not always apparent on the grey-scale images (114).

A new technique called Power Doppler uses the strength or amplitude of the Doppler signal, rather than the frequency and direction (115). This technique demonstrates improved sensitivity to blood flow due to the better dynamic range and independence to the angle of insonation (115). Directional Power Doppler combines the amplitude of the Doppler signal with the signal phase to provide directional coding using different colours similar to colour Doppler. Power Doppler is mainly used in clinical applications that are poorly imaged with colour Doppler, such as decreased flow characteristic of ischaemia, or inflammatory hyperaemia (115). Assessment of occlusion and stenosis of peripheral blood vessels has historically been performed using colour Doppler imaging (48, 59, 116).

### 3.3.1.6.2 3.3.1.6.3 Ultrasound of the Posterior Circumflex Humeral Artery - PCHA

Ultrasound in axillary neuropathy has been described in two papers aimed at localising the axillary nerve in the axillary space (42, 117). The axillary nerve itself is difficult to visualize

with ultrasound even when using modern high-frequency transducers because of its small size of less than 4 millimetres (61, 117). Doppler ultrasound techniques may be applied to the evaluation of the PCHA where there is suspicion of QSS. Colour Doppler ultrasound of the PCHA as a useful technique to provide indirect information about the location of the adjacent axillary nerve was reported in an education exhibit and literature review in 2003 (117). Colour Doppler imaging can be used to identify the PCHA, and thus the adjacent axillary nerve via the axillary space (42). An attempt to visualise the PCHA via the axillary space was made by Brestas et al (2006) who examined one patient with a three-month history of shoulder pain, no rotator cuff tear, and increased echogenicity of the teres minor (45). The PCHA was visualised via the axillary space with the arm abducted to 90 degrees and the elbow flexed (45). They found loss of Doppler flow signals of the PCHA and reported a “tight” stenosis of the PCHA near its’ origin (45). It is not certain whether the PCHA completely occluded in this patient. The technique described by Brestas examined the origin of the PCHA, presumably just before the PCHA enters the quadrilateral space, thus occlusion of the artery cannot be verified using this technique.

#### ~~3.3.1.6.3~~ 3.3.1.6.4 Ultrasound Spectral Doppler (duplex)

Spectral Doppler ultrasound uses electronic timing in the reception of echoes to provide a sample volume along a single line of sight within the ultrasound image that can be precisely placed in within the blood vessel under examination (114, 116). The Doppler information thus obtained is displayed as a graph of the frequency content of the Doppler shift (vertical axis) against time (horizontal axis) (114). The amplitude of the various frequency components are displayed on a brightness scale (114). Analysis of the resulting frequency spectrum can provide quantitative information on blood flow within a blood vessel, including:

- Peak Systolic velocity (PSV) – maximum blood velocity at cardiac end-systole. PSV may only be calculated when the angle of the ultrasound beam to the vessel lumen is known.

- End-diastolic velocity (EDV) - minimum blood velocity at cardiac end-diastole. This evaluation also requires angle correction.
- Systolic Acceleration time (AT) – the time interval between the beginning of systole and peak systole (114). Stenosis of a vessel results in reduced acceleration rate of blood flow during systole, manifesting as reduced slope of the upstroke part of the spectral waveform (a prolonged acceleration time) (114).
- Resistive Index (RI) – a measure of the resistance to blood flow, defined by the expression  $(PSV - EDV) / PSV$  (114, 116). A higher RI means a small end-diastolic flow relative to PSV, i.e. greater resistance to flow.
- Pulsatility Index (PI) – a measure of the resistance to blood flow, defined by the expression  $(PSV-EDV) / \text{Time-average Velocity}$ . Higher PI means a greater difference between maximum and minimum blood flow velocity (116).

In order to calculate an absolute value such as blood flow velocity (centimetres per second – cm/sec) in PSV and EDV the direction of flow relative to the direction of propagation of the sound beam must be known. It is only where the vessel lumen can be visualized on B-mode that the angle can be accurately determined and the absolute value of velocity calculated.

Blood flowing within an artery can be considered to be composed of an infinite number of hollow cylinders each of which slides across the other (116). Cylinders adjacent to the vessel wall are not moving, whereas those closest to the centre have the fastest flow velocity (116). The velocity of blood flow is therefore not uniform across any blood vessel, with red blood cells near the vessel walls moving more slowly than those in the centre of the stream, known as a parabolic flow profile (114, 116). Having a large Doppler sample box relative to the vessel being insonated will acquire Doppler signals from across the entire vessel. This results in a wide range of velocities being detected and subsequently a degree of spectral broadening

as the full range of velocities is detected and displayed on the spectral display.

When the reduction in diameter is small these spectral changes are subtle and difficult to detect (and may remain within the normal range). Examples include deceleration spectral broadening, loss of the systolic window and a mild increase in PSV (49, 52, 116, 118, 119). Stenoses of up to 20% produce only spectral broadening but no PSV changes (118). This makes the detection of up to 20% stenoses in small vessels difficult. Stenoses up to 50% will show more marked spectral broadening and an up to 100% increase in PSV (118).

A stenosis of sufficient calibre to reduce blood flow is termed a “hemodynamically significant” stenosis, equal to a  $\geq 50\%$  diameter reduction, or a  $\geq 75\%$  area reduction (59). Arterial lesions of more than 50% diameter stenosis are considered to be hemodynamically significant because such levels of lumen narrowing preclude the arterial segment from providing the amount of blood flow demanded of it (120). Hemodynamically significant arterial lesions display more dramatic changes in the ultrasound Doppler spectrum including more than doubling of the PSV above normal at and immediately beyond the stenosis (49, 116). As the degree of lumen narrowing increases, the PSV continues to increase in an almost linear fashion making PSV a useful index of the degree of stenosis (120).

Beyond a significant stenosis, the Doppler frequency spectrum may show resumption of normal PSV values, however the acceleration time (AT) becomes prolonged. This prolonged acceleration time and PSV values below normal result in a spectral Doppler waveform called “tardus parvus”. AT and RI measured on the Doppler spectrum are useful parameters because it is not necessary to calculate vector angles as is required for the calculation of PSV and EDV (114). A large section of the vessel is thus not required to be visualized in order to accurately

calculate the vector angle and thus velocity. Stenosis of the PCHA in abduction and external rotation manifest as changes in PSV and AT on spectral Doppler ultrasound and may be useful parameters in cases of suspected QSS.

Ultrasound of the PCHA in abduction and external rotation in cases of suspected QSS may make the diagnosis of QSS simpler, cheaper, less time-consuming and more comfortable for the patient (Figure 3-4). Ultrasound also has the added advantage over other imaging modalities because of the ability to carry out the examination in real time and to repeat immediately any low quality or non-diagnostic examination.

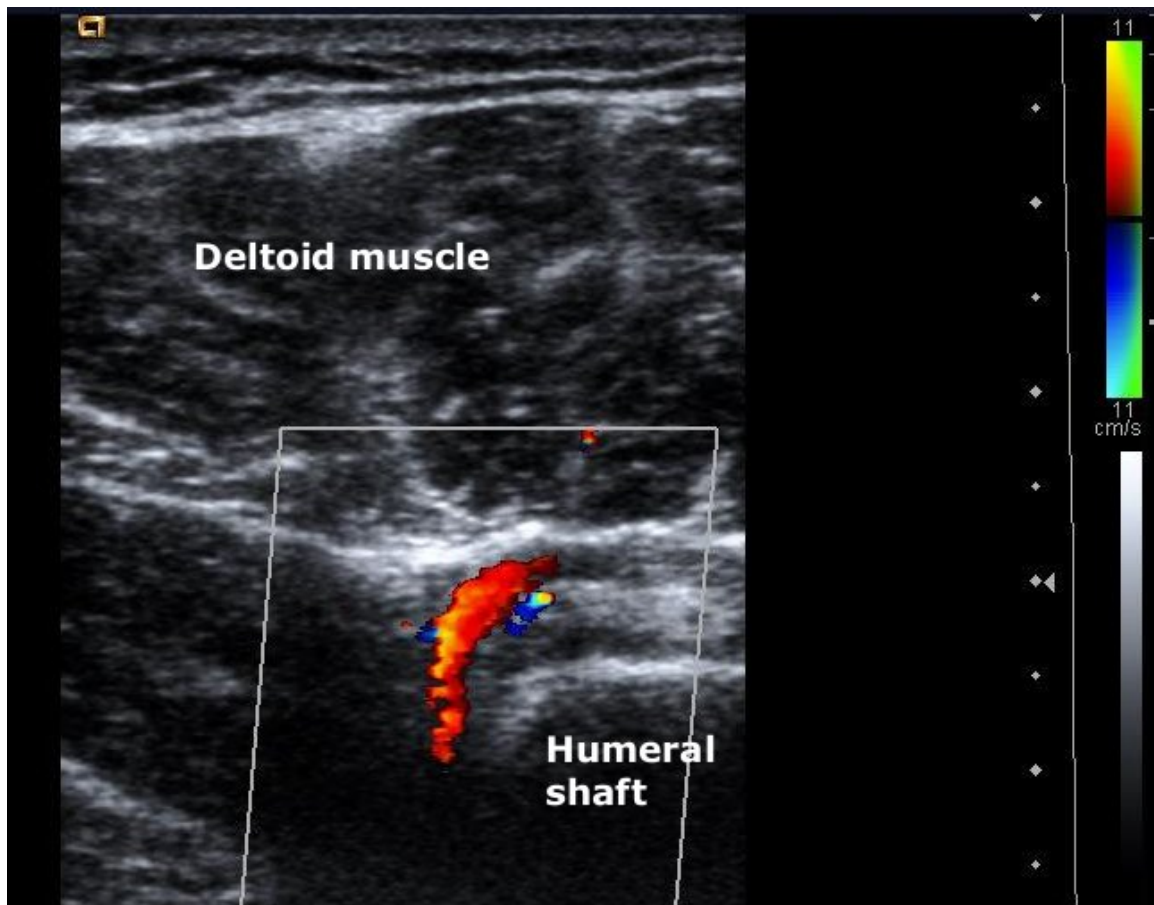


Figure 3-4: Posterior circumflex humeral artery ultrasound. The PCHA (coloured red) passing behind the neck of the humerus is seen on this transverse colour Doppler ultrasound. Blood flow direction is toward the transducer. Source: David Robinson, The Avenue X-ray & MRI

### 3.3.1.7 The Teres Minor Muscle

Ultrasound may be able to detect teres minor atrophy, with the echogenicity of the affected muscle increasing (corresponding to increasing numbers of fat cells) relative to adjacent unaffected muscles (121). The increase in fatty content increases the number of ultrasound reflective interfaces and subsequently echogenicity (121). Decreased muscle bulk and increased echogenicity, with increased sound beam attenuation may be an indicator of muscle atrophy, potentially secondary to denervation (88, 122).

Reports by two radiologists regarding the visibility of muscle contour, pennate pattern, central tendon and muscle echogenicity of supraspinatus and infraspinatus muscles on ultrasound were evaluated using MRI as the reference standard in 65 consecutive patients with possible rotator cuff tears (123). For radiologist 1 and 2 the accuracy of ultrasound in depicting fatty atrophy of supraspinatus muscle was 75% (49 of 65) and 72% (47 of 65), sensitivity was 89% (eight of nine) and 100% (nine of nine), and specificity was 73% (41 of 56) and 68% (38 of 56), respectively. The accuracy of ultrasound in depicting fatty atrophy of infraspinatus muscle was 85% (55 of 65) and 80% (52 of 65), sensitivity was 58% (11 of 19) and 63% (12 of 19), and specificity was 96% (44 of 46) and 87% (40 of 46), respectively ( $p < 0.001$ ) (123). The authors claimed that ultrasound was moderately accurate in the diagnosis of rotator cuff muscle atrophy when compared to MRI (Figure 3-5 & Figure 3-6) (123).

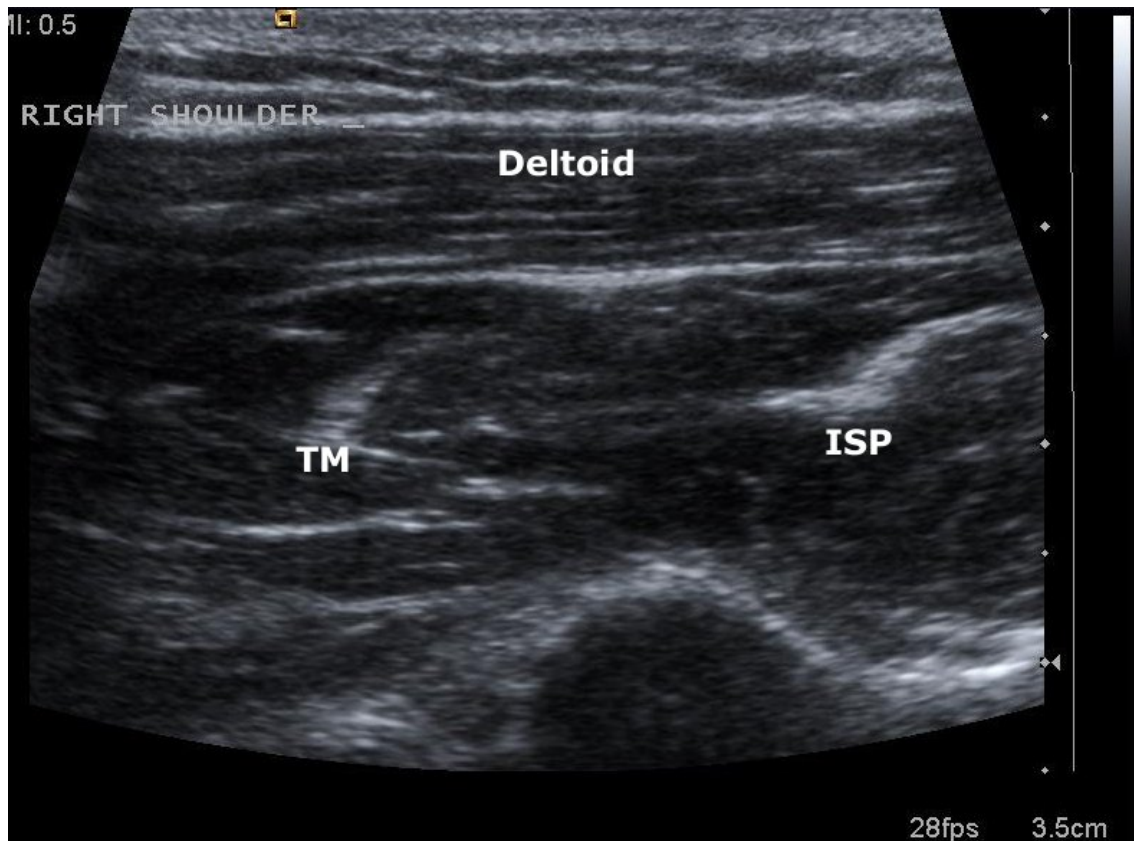


Figure 3-5: Transverse ultrasound of posterior right shoulder. The echogenicity of adjacent teres minor (TM) and infraspinatus (ISP) muscles is comparable with no evidence of fatty atrophy. Source: David Robinson, The Avenue X-ray & MRI.

Teres minor atrophy in isolation (without concomitant rotator cuff tear) has previously been noted (retrospectively) in four percent among 199 routine shoulder ultrasound examinations (88). In the case reported by Brestas, there was a diffuse increase in echogenicity of the teres minor with a slight reduction in muscle bulk, confirmed on MRI (45).



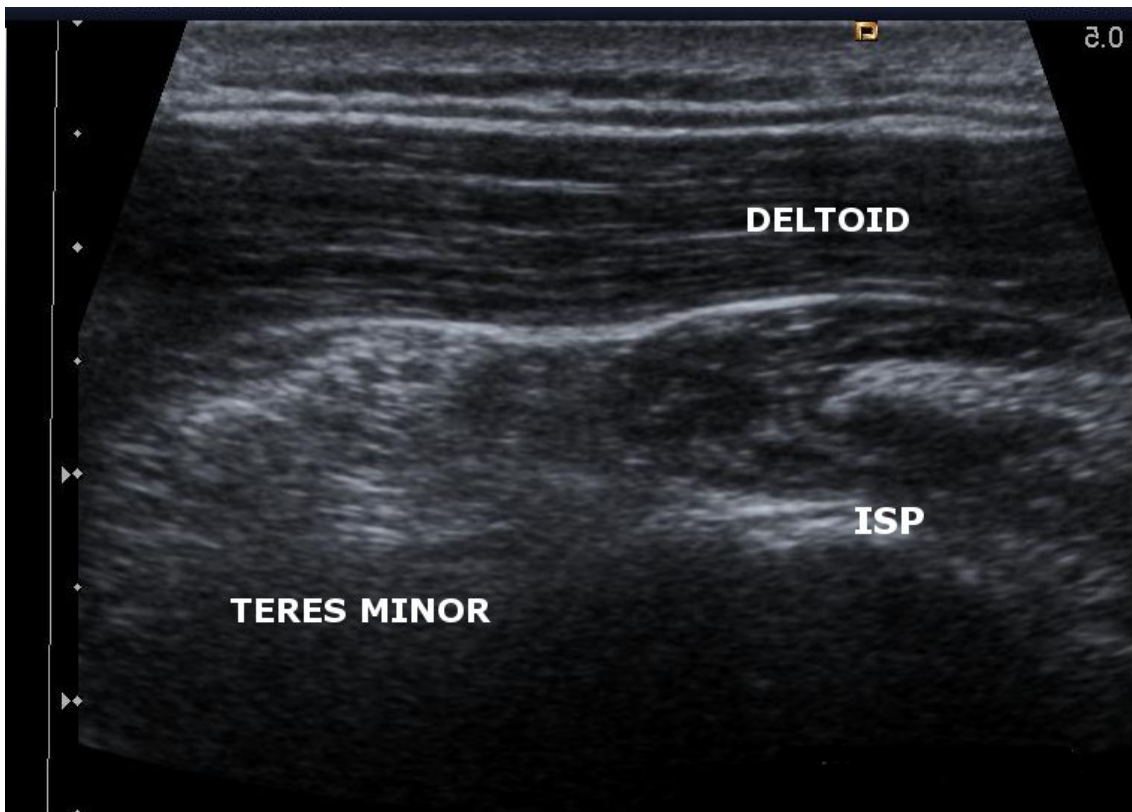


Figure 3-6: Transverse ultrasound of the posterior right shoulder. The echogenicity of the teres minor muscle is increased and bulk reduced consistent with fatty atrophy. ISP – infraspinatus muscle.  
Source: David Robinson, The Avenue X-ray & MRI

The hip also manifests a number of mechanical impingement syndromes that may also be occupational or sports related, as in the case of FAI and may result in considerable patient morbidity and expense during rehabilitation. Young, active patients presenting clinically with groin pain from hip impingement have a wide differential diagnosis, similar to the shoulder joint. The most common pathologies considered at the hip include inguinal hernia and muscle or tendon tear. In these cases, where the problem is considered to be soft tissue related, the first imaging investigation is often ultrasound. Other imaging modalities are limited because of radiation burden for young patients or the ability to resolve soft tissues adjacent to orthopaedic hardware. As a consequence, diagnosis is often delayed.

Ultrasound currently has no role in the assessment of OA of the hip, and the use of ultrasound



in the assessment of impingements such as FAI at the hip has not been widely reported on.

### **3.4 Pathophysiology of Primary Osteoarthritis of the hip**

The diagnosis of hip OA has been long understood to manifest on plain x-rays as narrowing of the joint space, roughened texture and flattening (mushrooming) of an upwardly and outwardly displaced femoral head, and lengthening of the acetabulum through an osteophyte (124). The aetiology of this process has been divided into Secondary OA, where the condition has some known (usually traumatic) cause, and primary OA, where some unknown intrinsic defect of the joint cartilage predisposes sufferers to early joint degeneration (125). However, it has been suggested as early as 1933 that mild mechanical imperfections of the joint may be the cause of early OA, such that all OA is in fact secondary (124).

In a series of x-rays of 25 adult controls and 200 randomly chosen patients with primary OA, minor abnormalities could be detected by examination of pelvic radiographs (33). The researchers found that evidence of minor anatomic abnormalities such as acetabular dysplasia and femoral head “tilt” deformity was present in the 200 patients’ pelvic radiographs, possibly resulting from minor asymptomatic disruption to the proximal femoral epiphysis ( $p < 0.001$ ) (33). Several other radiological studies have since reported that unrecognized mild hip abnormalities are causally related to OA (22, 69, 126-128).

In an attempt to further define the essential x-ray characteristics of the normal adult hip, one hundred and thirty patients with a diagnosis of OA due to “idiopathic arthritis” and 30 male and 30 female controls with no x-ray evidence of hip OA were studied (127). Four characteristics of the hip acetabulum were evaluated including the slope of the acetabulum, the acetabular roof, depth of the acetabulum and the centre-edge angle (127). Sixty-three of

the 130 patients (48%) had acetabular dysplasia when compared with the controls (127). In another study the researchers studied radiographs of 75 patients with slipped capital femoral epiphysis (SCFE) and 187 patients with Legg-Perthes disease before comparing the findings with radiographs of 75 patients with primary OA (69). The configuration of the femoral head and neck was examined for evidence of the association between a minimally slipped epiphysis and Legg-Perthes disease with idiopathic, or primary OA (69). The researchers first assessed femoral head sphericity, the position of the femoral head relative to the axis of the femoral neck and the contour of the femoral neck (69). The authors coined the term “pistol-grip deformity for characteristic changes to the femoral head and neck that occur after both minimally SCFE and Legg-Perthes disease that include:

1. Flattening of the normally concave surface of the lateral femoral neck
2. A bump on the anterolateral surface of the femoral neck
3. Increased concavity of the posteromedial surface of the femoral neck with the formation of a hook at the junction of the articular surface of the femoral head and neck (Figure 3-7) (69).

Striking similarities were observed between the characteristics of hips with primary OA and the hips of patients with known childhood hip disease, with 40% demonstrating the pistol-grip deformity (69). The researchers found that the pistol-grip deformity occurred much more frequently in males, appearing in 66% of patients with primary OA but only in 10% of the equivalent females (69). The deformities frequently occurred on the contralateral asymptomatic hips of those patients with known childhood hip disease (69).

This “femoral” abnormality appears to be most dominant amongst young men and may be produced by several aetiologies, including SCFE, Legg-Calve-Perthes disease, multiple epiphyseal dysplasia, and spondyloepiphyseal dysplasia and may also be produced post

femoral neck fracture when the femoral head remains in a retroverted or varus position (5, 69, 127, 129, 130)

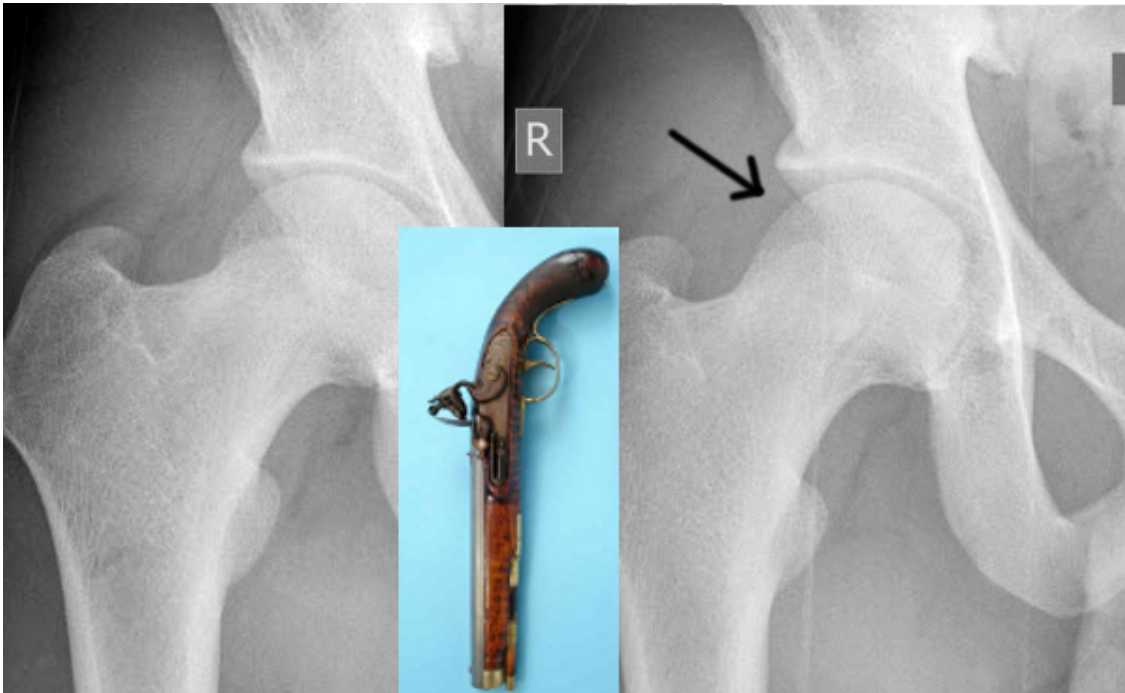


Figure 3-7: Normal hip (left) compared to hip demonstrating a small bump (black arrow-right) at the superolateral junction of the femoral head and neck. The resulting change in femoral head-neck morphology is said to represent the handle of an old-fashioned pistol (insert) – pistol grip deformity. Source: Ty Seaton, Richmond Diagnostic Imaging.

Fifteen patients with anterior FAI attributable to a non-spherical femoral head and 15 age and gender-matched controls were examined using MR arthrography (131). The results showed a statistically significant difference between patients and control subjects in head-neck offset ( $p = 0.011 - 0.049$ ) and lateral epiphyseal extension ( $p = 0.0002 - 0.041$ ) suggesting a growth abnormality of the capital physis as a cause of the femoral head asphericity (131). Femoral head asphericity may be a developmental disorder as SCFE as a cause of the pistol-grip deformity was not supported by the findings since no hips were observed to have a posterior tilt of the epiphysis (131).

A study of 327 cases of OA for which adequate clinical, radiological and anatomical data

were available, showed that only a small fraction had no detectable abnormality of the joint, with just 27 (8.3%) falling into this category (125). The integrity of the articular cartilage appears to be intimately dependent upon the architectural integrity of the joint as a whole suggesting that OA is almost always associated with some underlying, but not immediately obvious abnormality of the joint (125). More than 90% of patients with primary OA appeared to have abnormalities of the hip joint, most commonly mild acetabular displacement and/or pistol grip deformity (125).

Most cases of primary OA are in fact secondary OA, with mild developmental abnormalities having been overlooked in earlier radiographic studies (33, 125, 127, 129, 131).

### **3.4.1 Natural History of Hip Dysmorphia**

A number of studies have found a relationship between hip dysmorphia and the onset of OA through biomechanical damage to the hip joint. Twenty-nine symptomatic adults were examined clinically, as well as with x-ray and CT. The “acetabular rim syndrome” was described in all patients as a dysplastic acetabulum that is a precursor to OA of the hip (22). Dysplastic acetabulae appeared to be either shallow or have a “short roof” that does not adequately cover the femoral head, predisposing the hip to damage to the articular cartilage that leads to instability and progressive damage to the entire joint over time (22). On clinical examination during passive flexion, adduction and internal rotation of the thigh, the proximal and anterior part of the femoral neck are brought into contact with the rim of the acetabulum at the point where damage to the cartilage is likely to be found (22).

Dysmorphia was also demonstrated in a small retrospective review of 30 patients with primary OA, with 97% (29/30) having at least one abnormal measurement on the AP or cross-table lateral x-ray (128).

In a dated study conducted between 1915 and 1952, 31 hips among 28 patients with SCFE were observed over a mean period of 41 years (range 26 – 54 years) without interventional treatment (132). The severity of the displacement of the femoral head was graded as mild, moderate or severe using the difference between the head-shaft angle between the two sides on the first radiographs available for review (132). The progression of SCFE to OA was observed over the study period in all 13 patients with moderate or severe grade slips (132).

The link between the presence of “slip” morphology and the development of OA was further demonstrated in a study of 2665 adult human skeletons from the Cleveland city morgue. Slip morphology unrelated to age was reported to be a major risk factor (31/83 – 37%) for development of high-grade OA (133). Post-slip morphology appears to expose the prominent anterosuperior metaphyseal portion of the femoral neck to the anterior surface of the acetabulum during flexion and internal rotation, producing wear or damage of the hip joint cartilage (133).

In a clinical and radiological study (anteroposterior x-ray and CT), 310 adult patients (620 hips) referred due to hip pain of at least one hip were studied and a dysmorphic orientation of the acetabulum was discovered in 43 of 446 (9.6%) abnormal exams, where the mouth of the acetabulum was rotated posteriorly (retroverted) (134).

This pathological orientation results in the anterolateral cover of the femoral head being more extensive (65%) than usual (49%) (134). During flexion of the hip, the anterior wall and anterosuperior roof of a retroverted acetabulum appear to be vulnerable to impingement between them and the femoral neck, causing significant degenerative change.

Further support for these observations was provided by intraoperative examinations of 13 consecutive adolescents (14 hips) with SCFE (135). The findings showed that a prominent

femoral metaphysis restricts the normal range of movement (ROM) and that labrum and cartilage damage are the result of an impingement (mechanical jamming) between the metaphysis and the superomedial acetabular rim triggering arthrosis (135).

While minor structural abnormalities may not cause damage to the articular labrum and cartilage in normal activity profiles, the increased range of movement demanded in many sporting activities may result in impingement and joint damage at the limits of the range of motion (134, 136). The tilt deformity on AP pelvic x-ray is more common in physically active individuals (126). This association of sporting activity and joint damage has been confirmed in a study investigating patients undergoing osteoplasty for FAI who reported developing pain with sports participation (137). Three hundred and one patients presented for surgery for FAI. Just 24% reported a traumatic event preceding pain onset, but 91% reported symptoms with high-demand sports (137). In another similar study, 292 patients presenting with mechanical hip pathology were examined clinically and radiologically with three x-ray views, demonstrating that 70% of patients played some type of sport with 30% participating at a high-level competition (regional or national level) and just 19% reporting trauma as the initial cause of their pain (138). This supports the view that the wide range of movement required in competitive sports may exacerbate damage from dysplasia (138).

The studies discussed above indicate that hip dysplasia is more common than has been previously appreciated and that dysmorphia provides a mechanism for impingement and joint damage that may lead to OA, particularly in activities where the full range of hip motion is tested such as during many competitive sporting activities.

### **3.4.2 Femoroacetabular Impingement**

An impingement syndrome at the bony articulation of the hip occurs where the femoral head-

neck junction impinges upon the acetabular labrum (Figure 3-8).

Although this is a mild deformity, if unrecognized in early life, it may prove to be a major cause of OA in later years (11). Early intervention to eliminate the abnormality or manage the condition may prevent the onset of OA and preserve the integrity of the joint (32, 125).

The idea that an impingement between the femoral head or neck and the acetabulum might cause damage to the joint mechanism that leads to the onset of OA has been further developed when using MRI (139). The researchers compared the femoral head-neck offset of 24 patients with a painful hip and a labrum abnormality confirmed by MRI with 24 asymptomatic controls and found a statistically significant reduction in the concave taper from the anterior femoral head to neck ( $p = 0.002$ ) (139). The authors postulated that the proximal femur abuts the labrum lining the acetabular rim or possibly intrudes underneath the acetabular rim (the cam effect) even during the normal range of movement, causing damage and eventually OA over time (Figure 3-8) (139).

In a review of their clinical experience spanning more than 10 years and 600 surgical hip dislocations, damage to the hip cartilage from FAI apparently occurs due to normal movement of the hip and not axial loading as previously believed, thus supporting the idea of FAI causing OA (15). Two distinct types of FAI were identified by the authors based on the observed pattern of labral and chondral injuries (15). Cam impingement seemed to result from a femoral head with increased radius jamming into the acetabulum during forward flexion (15). Pincer impingement is the result of linear contact between the acetabular rim and the femoral head-neck junction, often the result of an acetabular abnormality (15).

#### **3.4.2.1 Cam-type FAI**

This type of impingement occurs due to a non-spherical extra-articular protuberance of bone



at the femoral head-neck junction impacting the acetabulum and causing damage to the articular cartilage and cartilaginous labrum, usually with flexion of the leg upon the trunk in adduction (5, 15, 31, 135). It is called cam impingement due to the action of the non-spherical portion of the femoral head jamming onto the acetabulum (Figure 3-8) (5).

A similar non-spherical pathomorphology was found in 13 consecutive adolescents with SCFE during surgery to correct a reduced femoral head-neck offset (135). The same series showed cartilage defects at the superomedial acetabulum without corresponding femoral head cartilage damage (135). Flexion of the hip joint and additional internal rotation caused impingement of the metaphyseal area against the superomedial acetabulum and labrum (135). Surgical observations have described an “outside in” abrasion of the acetabular cartilage and/or avulsion from the labrum, leading in turn to tear or detachment of the un-involved labrum (15). The majority of hip motion occurs between neutral and 90 degrees of flexion making the most at-risk area of the hip the anterosuperior quadrant of the acetabular rim (15, 72, 140). In order to evaluate the relationship between a decrease in femoral head-neck offset and increase of the lateral epiphyseal extension, and an unusual orientation of the capital physeal scar, MR arthrography was carried out among patients with FAI attributable to a non-spherical femoral head and compared to gender and age-matched controls (131). The findings suggested a growth abnormality of the capital physis as a cause of the dysplastic femoral head-neck, such as delayed separation of the common physis or eccentric closure of the capital epiphysis rather than SCFE (131). The study by Siebenrock et al (2004) supported the idea that the reduced head-neck offset is a developmental disorder rather than the result of a slipped capital epiphysis (129, 131).

Damage to the labrum, acetabulum and femoral head was evaluated after surgical dislocation in 149 hips (141). The authors hypothesized that the pattern of articular damage for cam and pincer impingement is different (141). In cam type impingement damage occurred mainly at

the anterosuperior part of the acetabulum and was made worse by internal rotation, however in pincer-type impingement damage occurred circumferentially about the entire acetabulum and movement was limited by the over-covering acetabular rim impacting with the femoral neck (141). This study provided evidence that both cam and pincer impingement have a specific pattern of damage, however, they often occurred together in the same hip with just 26 of the 149 (17%) hips demonstrating pure cam impingement and 16/149 (11%) pure pincer impingement (141).

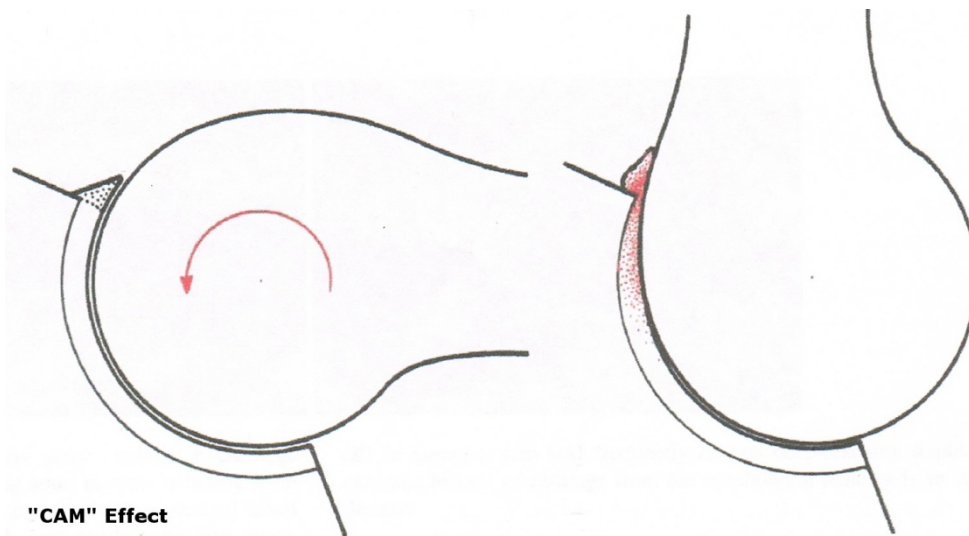


Figure 3-8: The cam effect. As the non-spherical femoral head rotates with flexion, the anterior labrum is impinged causing damage. Source Ganz et al (2008) (5).

The cam impingement was described as causing an avulsion of the acetabular cartilage from the labrum and subsequently the subchondral bone destroying cartilage and causing an approximation of the femoral head into the acetabulum leading to joint space narrowing (5). Cam impingement appears to be more prevalent in young male patients (5, 12, 131, 139, 140).

A quantitative method to describe the concavity of the femoral head-neck junction was first described in 2002 and the ability of the method to distinguish between patients with positive impingement tests and asymptomatic hips with a normal examination was tested (11). The

group compared MR examinations of 39 patients with groin pain, decreased internal rotation and positive impingement test with 35 asymptomatic control subjects (11). The anterior margin of the waist of the femoral head-neck junction was defined and measured using an angle (Figure 1-4) (11). The findings demonstrated a significant difference in the measurement of this alpha ( $\alpha$ ) angle, measuring  $74.0 (\pm 5.4)$  degrees in symptomatic patients and  $42.0 (\pm 2.2)$  degrees in the control group ( $p < 0.001$ ) (11). Measurement of the  $\alpha$  angle has also been performed with radiography, CT scan and MRI, with only CT able to repeat reliably the original findings of MRI (11, 12, 41, 53, 139).

### **3.4.2.2 Pincer-type FAI**

Pincer impingement, in contrast to cam impingement, occurs when there is contact anteriorly between the femoral neck and an extended acetabulum causing over-coverage of the femoral head (5). This was demonstrated in a series of 170 consecutive patients admitted for reconstructive surgery of the hip with a diagnosis of degenerative joint disease (127). The hips were evaluated using four characteristics of the acetabulum (127):

1. Slope of the acetabulum – the angle between a horizontal line and a line connecting the lateral edge of the acetabular roof and the floor of the acetabular fossa.
2. Acetabular roof- angle between a line parallel to the lateral edge of the acetabulum and a line tangent to the roof of the acetabulum
3. Depth of the acetabulum – measure of the perpendicular distance from the deepest point of the articular surface of the acetabulum to a line connecting the lateral edge of the acetabular roof and the floor of the acetabular fossa.
4. Center-edge (CE) angle - angle between two lines radiating from the center of the femoral head, one passing through the outer edge of the acetabular roof and the other connecting the centers of the two femoral heads (127)

A large proportion of the hips with no history of hip disease and therefore suffering “idiopathic” OA (63/130 (48%)) were found to have acetabular dysplasia when compared to controls (127). Fifty of the 63 (79%) hips with acetabular dysplasia were female (127).

The alignment of the acetabulum rather than morphology can also provide a mechanism for pincer impingement. In this case, the mouth of the acetabulum inclines more posterolaterally giving rise to a more extensive anterolateral cover of the femoral head and impingement between the femoral neck and the anterosuperior acetabular rim (134). The movement in such hips appears to be limited by an over-covering acetabular rim causing damage at the limits of movement by the femoral neck impacting against the labrum (Figure 3-9) (141).

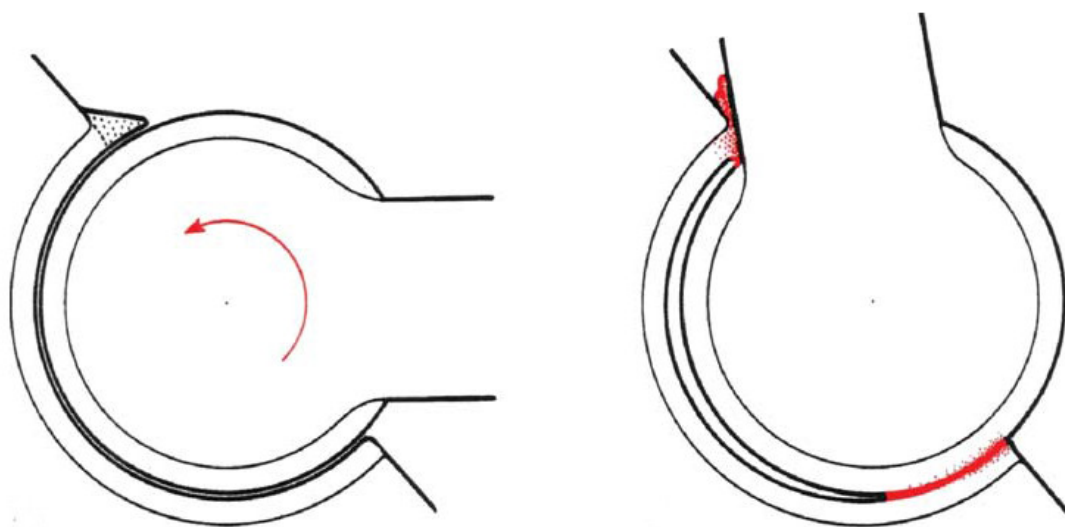


Figure 3-9: Pincer Impingement. This type of FAI, results from linear impact due to the acetabular over-coverage. The femoral head is round (contrast with Figure 3-8) however the extended acetabular rim causes impact between the femoral head-neck junction and the acetabular rim. Source: Ganz et al (2008) (5) .

The over-coverage of the normal femoral head and neck by the dysplastic or malpositioned acetabulum results in impingement between the femoral neck and the acetabular rim, known as pincer impingement (Figure 3-9) (5). In pincer-type FAI the labrum fails leading to fissuring and ganglion formation, the acetabular cartilage degenerates becoming thinner until bone apposition

occurs (5). OA as a result of pincer impingement is a slower process than cam FAI affecting mainly females at a later age (5, 127, 141).

### **3.4.3 Diagnosis of Femoroacetabular Impingement**

#### **3.4.3.1 Clinical diagnosis**

More than 80% of patients with FAI present with pain in the groin which is often mistaken for other pathologies such as hernia or muscular injury as patients are often young and physically active (15, 22, 137, 138, 142). Groin symptoms may radiate to the medial thigh and patients often demonstrate the “C” sign, where the ipsilateral hand is cupped above the greater trochanter with the fingers gripping into the anterior groin describing deep interior hip pain (143). Symptoms of FAI are often initially intermittent and include pain and stiffness particularly after strenuous or prolonged exercise, or sitting for a prolonged period, becoming more constant as the disease progresses (15, 142, 144).

Many patients will describe a lack of flexibility in comparison to the contralateral hip, or stiffness which manifests as a reduction in the degree of flexion and internal rotation of the joint (22, 134, 142, 143). The hallmark of FAI is diminished internal rotation caused by the altered bony joint architecture and this range of motion is further reduced when OA is present, although patients with OA tend to be older (137, 143). Passive movement of the thigh into maximum flexion, adduction and internal rotation (FADIR - the anterior impingement test) brings the femoral head-neck junction into contact with the rim of the acetabulum, recreating the impingement thought responsible for the damage to the articular labrum and cartilage and is almost always positive in cases of FAI (15, 22, 72, 137). The FABER test (Patrick test) involves flexion, abduction and external rotation of the hip such that the ankle is placed on the contralateral distal thigh just above the knee, demonstrating an increased distance between the

knee and the examination table when compared to the unaffected leg if positive for FAI (72, 137, 145). A positive McCarthy sign occurs when the patients' symptoms are reproduced when the flexed hip is passively extended in external rotation and then internally rotated. This may be a sign of an acetabular labral tear (72). Resisted extension, such as rising from a sitting position is uncomfortable for many sufferers (143).

Diagnosis is often delayed or incorrect and treatment including surgical treatment is often inappropriate (136, 137). In the early stages of the condition patients with FAI do not display any of the classic radiological signs of hip OA such as joint space narrowing, subchondral sclerosis, osteophyte formation or cyst formation (31). The time from symptom onset to diagnosis was found to be more than three years in one study of 52 hips with radiographic structural abnormalities consistent with FAI (136). Seven of the 52 (13%) hips were found to have had prior surgery at another site without improvement (136).

### **3.4.3.2 Diagnostic imaging:**

#### **3.4.3.2.1 X-ray**

The first group to define the x-ray characteristics of the dysplastic hip suggested that hip OA was the result of minor anatomical abnormalities resulting in incongruity of joint surfaces. The results showed that such hips had a tilt deformity of the femoral head on AP x-rays of the pelvis that indicated an abnormal relationship between the femoral head and neck (33). This minor deformity was thought to be related to prior injury to the femoral head-neck, as seen in SCFE or epiphysiolysis (33, 69, 125). Standard AP pelvic x-rays were first used to perform four measurements of the acetabulum to define the essential characteristics of normal and dysplastic hips in 1974 (127). A large proportion of women thought to have idiopathic OA were found to have previously unrecognized acetabular dysplasia (127).

It has been claimed that the AP pelvis plain x-ray can be used to demonstrate the pistol-grip

deformity, head tilt deformity, and a lateral bump (145).

A number of studies over the years have attempted to further characterise and quantify abnormal hip morphology prior to the development of OA using measurements derived from x-ray. Subjective qualitative findings of FAI such as the pistol-grip deformity are common in the young adult population, particularly males, with 21.5% of males and 3.3% of females having the pistol-grip deformity (146).

Thirty patients with idiopathic arthritis were retrospectively compared with 54 normal controls using nine measurements from x-ray images of the AP and cross-table lateral pelvis (128). Twenty nine (97%) had at least one abnormal measurement and up to seven abnormal measurements in one hip, whereas there were no abnormal measurements in the control group (128).

X-ray has also been used to measure the alpha angle of the femoral head-neck junction. Six x-ray projections were performed on 21 desiccated femurs to determine the best view for depicting the asphericity of the femoral head-neck junction and to determine alpha angle (147). The Alpha angle was highest during the Dunn view with 45 degrees flexion ( $71^{\circ} \pm 10^{\circ}$ ) and smallest in the cross-table  $15^{\circ}$  external rotation ( $51^{\circ} \pm 7^{\circ}$ ) (147). In a review article Rylander et al (2010) suggested that special lateral views of the femoral neck would better visualize the anterosuperior lesion on the femoral neck, such as 15 degree internally rotated lateral, Dunn view and the modified Dunn view (72).

Other authors have claimed that the non-spherical osseous abnormality of the femoral head is usually located anterolaterally or anterosuperiorly on the head-neck junction in a sagittal plane and is thus not normally visible in standard anteroposterior (AP) radiographs, but is best demonstrated with 15 degrees of internal rotation, a lateral view of the femur such as the Dunn view, a cross-table lateral or frog-leg lateral (5, 11, 41, 53, 145, 148).

Studies have however shown that many x-ray derived measurements including femoral head asphericity and head-neck offset have poor agreement, or that the abnormalities may be missed altogether (149-151). X-ray derived alpha angles may vary by up to 30 degrees depending on radiographic projection used and the anterosuperior location of the deformity means that some views may miss the asphericity (147, 152). Osteophytes at the femoral neck may produce an elevated alpha angle called a “false cam” effect, putting the validity of the alpha angle derived from x-ray into doubt (153). The inter- and intra-observer reliability of the alpha angle derived from plain radiography has been found to range from excellent to poor, with the measurement only becoming abnormal in some studies when the bump is placed anteriorly (154-156).

#### 3.4.3.2.2 Magnetic Resonance Imaging

MRI has also been evaluated in the assessment of morphological abnormalities of the hip. 3D MRI was used to compare the femoral head-neck offset of patients with positive impingement test and labral damage confirmed on MRI, with asymptomatic controls of similar age distribution (139). A statistically significant reduction in the head-neck offset was found in the anterior aspect of the femoral neck between patients and control subjects ( $p=0.002$ ) which occurred mainly in the anterior and lateral aspects, leading to a shallow taper between the head and neck (139). The offset ratio was defined as:

Equation 3-1: Formula for femoral head-neck offset ratio.

$$OR = \frac{(Femoral\ head\ radius - Femoral\ neck\ radius)}{Femoral\ head\ radius\ calculated\ from\ the\ area\ of\ the\ femoral\ head\ contour}$$

MR arthrography has also been used to assess hip morphology in 15 patients with anterior femoroacetabular impingement and 15 age and gender-matched controls by measuring the



femoral head-neck offset at 16 points around the axis of the femoral neck (131). A statistically significant reduction in femoral head-neck offset in the patients' group at the anterosuperior quadrant (4.3mm versus 7.6mm,  $p=0.011$  to  $p=0.049$ ) was reported (131).

For better detection of superiorly-located lesions radial reconstruction of the femoral head-neck from MR arthrograms was performed on 41 patients clinically suspected of having FAI (157). The head-neck junction was divided into a clock face where superior was denoted 12 o'clock and anterior 3 o'clock in order to compare the alpha angle obtained from oblique axial images (equivalent to the 3 o'clock vector - anterior head neck junction) to the maximal alpha angle obtained between 12 o'clock to 3 o'clock (Figure 3-10) (157). The mean maximal radial reconstruction alpha angle (70.5 degrees) was higher than the oblique axial method (53.4 degrees), with the highest alpha angles occurring at the 1 o'clock and 2 o'clock vectors (157). Alpha angles are generally found to be greater in males corresponding to the finding that the femoral head-neck physeal extension is more common amongst males (5, 12, 139, 140).

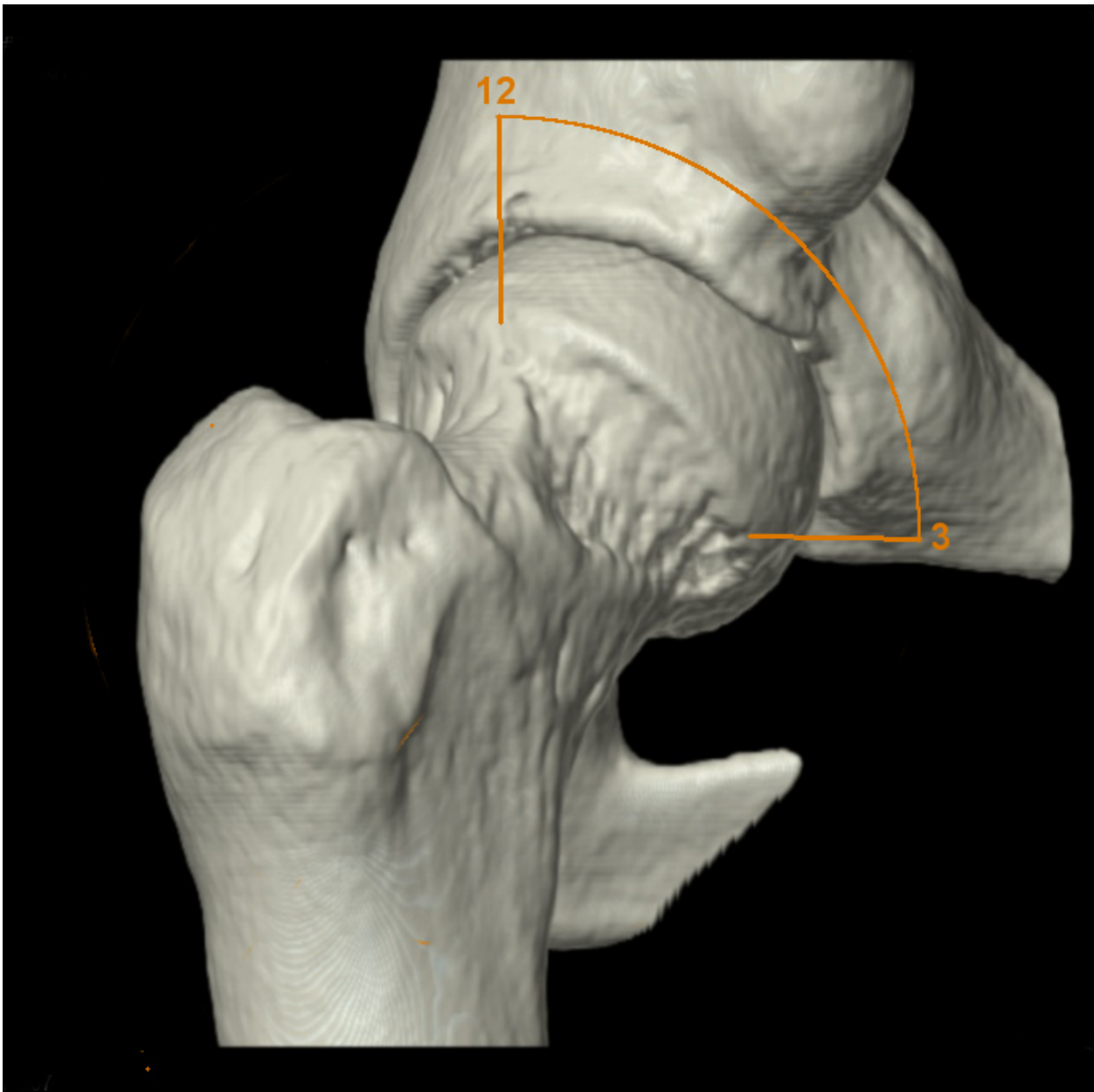


Figure 3-10: The clock-face nomenclature of Rakhra et al. The superior head-neck junction is denoted to be 12 o'clock, and the anterior-most head-neck junction is 3 o'clock. 3DCT of an 18 year old male post osteoplasty. Source: Rakhra et al (2009) (157), David Robinson, The Avenue X-ray & MRI.

A simple method of describing the concavity of the femoral head-neck junction that could distinguish between those with clinical evidence of cam-type impingement and asymptomatic controls was proposed using MRI imaging in 2002 (11). From an oblique axial image the alpha angle is the angle between two lines, one along the longitudinal axis through the center of the narrowest part of the femoral neck and another from the center of the femoral head to

the point where the femoral head-neck contour leaves a circular femoral head template (Figure 1-4) (11). This approach was tested among 39 patients who presented with groin pain, decreased internal rotation and a positive impingement test. They were compared to 35 asymptomatic control subjects. The mean alpha angle was  $42.0^{\circ} \pm 2.2^{\circ}$  (range  $33^{\circ}$  to  $48^{\circ}$ ) in the control group and  $74.0^{\circ} \pm 5.4^{\circ}$  (range  $55^{\circ}$  to  $95^{\circ}$ ) in the patients ( $p < 0.001$ ) (11). Causes of impingement that are due to a dysmorphic femoral head-neck junction such as a wide neck, formation of osteophytes or displacement of the head posteriorly will cause the alpha angle to be high (11). Notzli et al (2002) suggested a threshold of abnormality of 55 degrees (11).

Some researchers have suggested that the more invasive MR arthrography is not warranted for evaluating intra-articular lesions in the hip (158). Preoperative MRI was performed in 46 patients with clinical suspicion of FAI in order to evaluate the modality in the identification of labral and articular cartilage tears (158). Thirty seven of the 38 (97%) surgically confirmed lesions occurred in the labral-chondral transition zones, 50% of which were placed anterosuperior on the acetabulum (158).

Many authors consider MRI to be the definitive imaging modality because of its contrast resolution, multiplanar imaging ability, 3D depiction of internal hip derangement and the fact that other sources of groin pain such as stress fracture are also readily excluded (155).

The current standard of diagnosis of cam-type impingement is considered to include loss of sphericity of the femoral head-neck junction, manifesting as an elevated alpha angle (31).

#### **3.4.3.2.3 CT (including 3DCT)**

CT and in particular 3DCT is another axial imaging technique that has been assessed as an imaging method for characterising hip morphology. In a study of 310 adult patients (620 hips) referred for symptoms associated with dysplasia arising from at least one hip, AP x-ray and

axial CT were performed to define the orientation of the acetabular opening (134). Of 446/620 (72%) hips symptomatic for dysplasia, 43 (10 %) were found to have an acetabular opening that is inclined more posterolaterally (retroverted) from the sagittal plane (134). It was suggested that the more lateral-lying anterior acetabular edge may result in impingement between it and the femoral neck (134).

The multi-dimensional image post-processing features available with 3DCT of the hip allows global visualization of the bony contours without invasive intra-articular contrast injection almost independently of the patient position (12). MR arthrography and 3DCT were compared among 20 hips with 12 controls. All patients had 3DCT for other indications. The resultant 3DCT calculation of the alpha angle closely reproduced the findings of Notzli et al (2002) when using MRI (11, 12). In this study, the alpha angle was calculated by placing the femoral neck axis line parallel to the anterior femoral neck and used the anterior-facing paraxial section (3 o'clock) to calculate alpha angle (12).

#### **3.4.3.2.4 Ultrasound**

Ultrasound has been used to examine the hip joint and surrounding soft tissues (14, 159). The normal ultrasound appearance of the anterior joint capsule was studied in six cadaveric adult specimens, 58 healthy children and 105 children with unilateral transient synovitis (159). A concave anterior joint capsule where it passes over the femoral neck effectively rules out joint effusion (159). Tendons, ligaments and superficial cortical surfaces of the bony structures of the hip joint can be visualised using ultrasound as the imaging modality (14). Ultrasound has been used as the imaging modality in a number of reported case studies of iliopsoas bursitis on its own or in combination with CT and MR (78, 160).

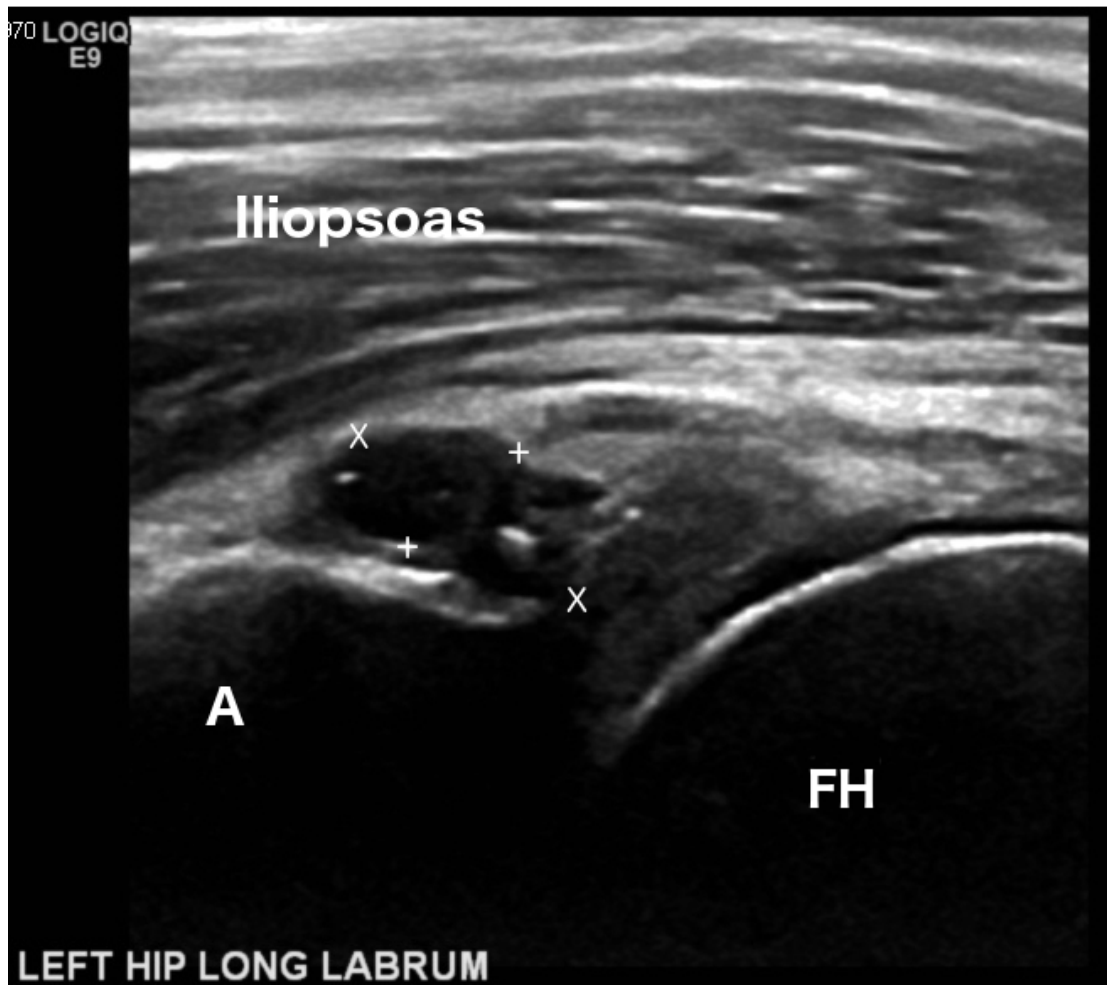


Figure 3-11:Forty-three-year-old female with hip and groin pain. Small cystic structure (denoted by X- X and +-+) representing a paralabral ganglion. This pathology was secondary to damage from FAI. Key: A – acetabulum, FH – femoral head, iliopsoas – conjoint iliopsoas muscle and tendon. Source: David Robinson, The Avenue X-ray & MRI.

Calculation of the  $\alpha$  angle involves fitting a spherical template over the femoral head and then drawing a straight line along the longitudinal axis of the femoral neck (Figure 1-4) (11, 152). Ultrasound is able to provide limited imaging of the anterior and anterolateral femoral head and neck but may be able to demonstrate a sufficient volume of the femoral head to fit the spherical template for calculation of the alpha angle. Previous reports of ultrasound in the assessment of femoral head-neck alpha angle have been performed using undescribed or inconsistent methods for calculating the alpha angles (161, 162). Fifty patients were assessed with MR arthrography and ultrasound and the alpha angles from the two modalities compared

with a strong significant relationship for Reader 1 (Pearson correlation coefficient -PCC 0.891) but poor to moderate agreement for Reader 2 (PCC 0.425) (162). The investigators used two distinct methods of computing the alpha angle for the ultrasound and MR arthrography, where the femoral neck axis line was approximated by a tangential line connecting the distal insertion of the joint capsule to the femoral head contour (162). Alpha angle measurements were compared on 40 patients using ultrasound and MRI, using the method of Notzli for the MRI femoral neck baseline but the method of Beaulé for US, where the femoral neck baseline is parallel to the visible anterior femoral neck cortical surface (11, 12, 161). A high level of agreement was found for the hip in neutral position ( $r=0.67$ ,  $p<0.0001$ ) and agreement was best with 20 degrees of internal rotation ( $r=0.77$ ,  $p<0.0001$ ) but there was poor agreement with 20 degrees of external rotation (161).

The ability to make a diagnosis of FAI, in particular among younger populations, before major joint damage occurs, using a non-ionising, widely available and cost-effective technique for early detection of cam-type FAI would be highly beneficial. Prospective longitudinal long-term follow-up studies that could prove the hypothesis that FAI causes OA of the hip have yet to be performed (5). Ultrasound is ideal for this younger patient demographic. Being able to confirm a link between FAI and later OA would provide justification to surgically restore normal anatomy before major cartilage damage occurs (5). These established imaging techniques are unable to provide useful imaging for such studies. Ultrasound may be helpful in the early assessment of bony impingement syndromes such as FAI. Ultrasound currently has no meaningful role in the assessment of OA of the hip. Ultrasound is unable to demonstrate the bulk of the articular surface due to overlying bone, although it may demonstrate more advanced disease, such as marginal bony erosions and anterior osteophytic changes typical of established OA (14).

### **3.4.4 Treatment of Femoroacetabular impingement**

#### **3.4.4.1 Conservative Treatment**

Proximal femoral head-neck deformities that occur in childhood such as SCFE and Legg-Calve-Perthes disease are known to often develop severe progressive OA secondary to the dysplastic joint (5, 133). However not all radiologically detectable cam defects cause symptoms of FAI (143, 163, 164). This was demonstrated in a study of 755 asymptomatic hips from 429 randomly selected patients having CT scans for other medical indications. Alpha angles were measured from the AP scout view. The results showed that cam-type abnormalities of the hip were not rare with 62/215 (28.84%) males and 63/540 (11.67%) of females regarded as having abnormal femoral head-neck morphology (165). As the impingement that causes damage mainly occurs at extremes of motion such as during energetic sporting activities, more sedentary individuals will not provoke impingement even with abnormal anatomy (15, 135, 143, 166). This was confirmed in a study of 96 patients with radiological evidence of FAI who were retrospectively reviewed for signs of symptoms. Over a mean of 18.5 years (range 10-40 years) 79/96 (82.3%) remained symptom free (167). Regression analysis showed that only the presence of idiopathic OA of the contralateral diseased hip was predictive of development of OA on the asymptomatic side ( $p = 0.039$ ) (167).

Identification of abnormal femoral head-neck anatomy may prompt behaviour modification to avoid the impingement and occurrence of symptoms obviating the need for surgical correction (143, 168). Thirty-seven athletic patients with evidence of mild FAI (alpha angle  $< 60$  degrees measured on XR) were instructed to modify and adapt daily activities to minimize adduction and internal rotation (169). After 25-28 months four patients required surgical intervention after failure of this conservative treatment and six had recurrent pain and discomfort not

severe enough to warrant intervention. The mean ( $\pm$ SD) visual analogue scores for hip pain improved from 6 ( $\pm$ 1) to 2 ( $\pm$ 1) ( $p < 0.01$ ) and mean non-arthritic hip scores improved from 72 ( $\pm$ 4) to 91 ( $\pm$ 5) ( $p < 0.01$ ) (169).

In many cases however, conservative management of activity and symptoms fails as the disease is progressive and affects young physically active individuals (144).

#### **3.4.4.2 Surgical Treatment**

Even though the anatomical abnormalities associated with FAI are subtle radiologically, and may not be clinically important, the apparent biomechanical basis of idiopathic OA suggests that early surgical correction of the anatomical abnormality may delay or even prevent onset of OA (5, 128, 170). Surgical FAI treatment should aim to relieve symptoms where present, enhance activity and function and would be most effective when abnormal hip morphology can be reconstructed to allow improved clearance for normal range of motion before any major acetabular or cartilage damage occurs, thus preserving the natural hip joint (5, 15, 170). Retardation of the development of OA would be of considerable benefit even if such an intervention did not address any symptomatic manifestation of FAI (5).

Thirteen patients were treated by osteochondroplasty of the femoral head-neck region by an anterior approach without dislocation of the femoral head by Sionek et al (2010) revealing an improvement in the Harris outcome classification of pain, range of movement and gait in 12 of the 13 patients (171, 172).

Cam deformities may be treated by osteochondroplasty, labral lesions may be repaired and acetabular over-coverage may be treated by trimming the acetabular rim, however it cannot be said with certainty that surgical intervention will prevent the development of OA and potentially hip joint arthroplasty. Where such secondary damage to the labrum and articular



cartilage exists, surgical treatment should aim to restore normal joint morphology (164).

Such surgical interventions are, however, not without risks. Major complications of hip joint surgery include avascular necrosis, revision to total arthroplasty, femoral head-neck fracture, failure of fixation or inadequate osteotomy requiring revision surgery, deep infection and loss of range of movement by heterotopic ossification (170). The long-term benefits of surgical intervention have not been established (164, 170).

An open surgical approach usually involves dislocation of the femoral head and incurs the risk of avascular necrosis of the femoral head (15). An open surgical approach that involves protecting the femoral head vessels was described by Ganz et al (2003) involving anterior dislocation and removal of any non-spherical portion of the femoral head, removal of any anterior acetabular over-covering rim and any torn or degenerate labrum, with the remaining labrum reattached (15).

#### **3.4.4.3 Surgical treatment - Arthroscopic**

Femoral head dislocation and the risk of femoral head vascular disruption and avascular necrosis can be avoided by an arthroscopic approach using traction to widen and access the joint space (15). An arthroscopic approach offers a less invasive intervention with associated faster recovery and return to activity (173). However, traction of the joint can result in neuropraxia, particularly of the pudendal nerve (174). Osteoplasty of an osseous abnormality requires access to the peripheral compartment of the hip which is more technically demanding, produces greater trauma to the patient and requires a longer operating time (175).

Results have shown, however, that arthroscopic surgery can alleviate symptoms and improve hip functionality with minimal complications in young physically active patients with FAI. Sixty patients who were 16 years or younger with clinical and radiological FAI and positive impingement test or alpha angle > 60 degrees underwent arthroscopic treatment including

labral repair and focal femoral osteoplasty. Of those, only 8/60 (13%) required a revision for persistent pain due to capsulo-labral adhesions (all female) (173).

Similar results were demonstrated in 27 hip arthroscopies among 21 athletically active patients 19 years and younger with positive clinical signs of FAI. They were retrospectively assessed after arthroscopic surgery for complications and improvement of hip function (176). Self-reported ability to engage in the pre-operative level of athletic competition improved in all cases ( $p < 0.001$ ). Positive surgical outcomes have also been reported with regard to changes in the alpha angle. In another study of 55 patients (56 hips) under 40 years of age who underwent hip arthroscopy for symptomatic labral tears associated with FAI, the mean alpha angle decreased from  $68 \pm 10$  degrees to  $40 \pm 4$  degrees ( $p \leq 0.001$ ) (70).

Surgery to repair hip dysmorphia before major joint damage occurs, thereby preventing progression to OA is therefore possible. Arthroscopic surgical correction of cam impingement has been demonstrated to be achievable with minimal complications, even in younger patients for whom such intervention might be questioned.

### **3.5 Post-Arthroplastic Impingement**

For patients who undergo replacement of a hip impingement remains an issue for the prosthetic joint. Impingement by prosthetic wear debris does not always cause symptoms such as groin pain and reduced ROM. Its' sequelae upon both the soft tissues surrounding the joint and the remaining bone, however, has serious consequences for the longevity of the prosthesis and morbidity, should revision surgery be necessary.

#### **3.5.1 Adverse Local Tissue Reaction around hip replacements – ALTR**

Prosthetic hip joints produce wear debris mainly from the bearing surfaces, which is shed as

nanoparticles directly into the joint synovial fluid (16). Other parts of the bearing such as the femoral stem or the trunnion between the femoral head and the upper part of the femoral stem may also shed particulate debris from the implant into the joint or surrounding soft tissues. These particles cause an adverse inflammatory cellular response that can damage bone at the implant interface, altering fixation of the prosthesis and ultimately leading to aseptic loosening (16, 35). Sufficient fluid, necrotic tissue and prosthetic debris may accumulate and form a macroscopic mass, referred to as pseudotumor, or more recently, Adverse Local Tissue Reaction (ALTR).

Large accumulations of phagocytic cells and macrophages can lead to peri-prosthetic osteolysis and reduction in bone stock (16, 35). Soft tissue thickening impinging upon the native femoral neck has been thought to predispose to osteolysis and bone remodelling resulting in thinning of the neck with the potential for subsequent neck fracture (13, 18, 177).

### **3.5.2 Current Imaging of the Post-Arthroplastic Hip**

Early identification of the poorly performing prosthesis provides the option of early revision which is thought to provide a better long-term outcome (18). Follow-up imaging of the symptomatic post-arthroplastic hip is usually performed with serial x-ray and cross-sectional imaging modalities such as CT and MRI. However, these imaging modalities are compromised in their ability to image the soft tissues, mainly due to significant metal artefact from the prosthesis (Figure 3-12) (13, 18, 39, 177). The role and need for regular follow-up imaging has been unclear with respect to asymptomatic, well- functioning hip replacements (4). Current imaging protocols lack the sensitivity to detect ALTR in these prostheses, even though high rates of ALTR have been reported in this cohort (4, 19, 39, 178). Even asymptomatic, well-functioning prostheses should be periodically assessed with cross-sectional imaging to look for evidence of accumulating wear debris that may hasten aseptic

loosening, femoral neck osteolysis and early prosthesis failure (4, 179).

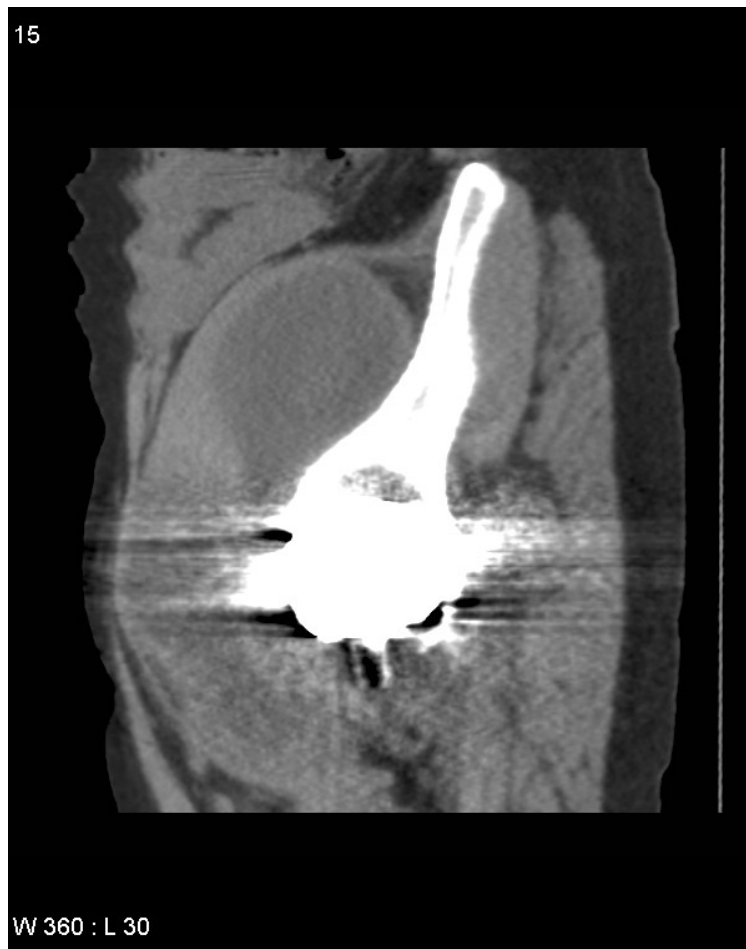


Figure 3-12: CT scan of a Birmingham Hip resurfacing showing metal artefact degrading the image of the periprosthetic soft tissues. Source Dr. Paul Marks, The Avenue X-ray & MRI.

MRI with metal artefact reduction sequencing (MARS) algorithms have been suggested for the assessment of periprosthetic soft tissues (13, 18, 19, 180). MRI is, however, not optimal because the tolerability of some types of metal implants have, to date, not been evaluated (180). MRI is a relatively expensive modality not widely available in all areas, has a prolonged scan time and is contraindicated in patients with some ferromagnetic implants, making MRI unsuitable for screening patients with asymptomatic, well-functioning prostheses (55). Further, the soft tissues adjacent to the native or prosthetic femoral neck are not readily imaged even with MARS MRI (54). Small-volume ALTR adjacent to the implant or native femoral neck in the case of resurfacing can be missed on MRI even when using

metal artefact reduction protocols. Such accumulations have been reported to progress if left untreated (179, 181). There is a need to develop tolerable, low-cost imaging protocols for routine follow-up of all patients after hip replacement surgery.

The United Kingdom Medicines and Healthcare products Regulatory Agency (MHRA) has recommended annual follow-up of metal-on-metal hip replacements for at least five years following hip replacement surgery with medical imaging including ultrasound to evaluate any developing fluid collections and soft tissue masses (178).

### **3.5.3 Ultrasound**

Conditions of the hip and groin previously considered worthwhile investigating with ultrasound include effusions of the native hip and hernias, but not conditions associated with the post-arthroplastic hip such as ALTR and iliopsoas bursitis (182). Ultrasound has been suggested as an imaging modality in symptomatic cases where metal sensitivity is suggested, as a complement to CT imaging in suspected cases of iliopsoas impingement, or combined with diagnostic and therapeutic injection of the iliopsoas bursa in cases of anterior iliopsoas impingement (183-186).

Previous studies examining the utility of ultrasound in the follow-up of hip arthroplasty have focused on large-diameter, metal-on-metal implants and the presence of periprosthetic soft tumour masses and fluid collections, with results varying from poor to almost perfect agreement with MARS MRI (4, 54, 56, 181, 187, 188).

These studies have demonstrated that ultrasound can provide superior imaging of the periprosthetic soft tissues of the post-arthroplastic hip as it is unaffected by metal artefact from the prosthesis and is able to easily and reliably characterize soft tissue masses. Multiple international agencies have recommended annual follow-up of metal-on-metal hip

replacements following hip replacement surgery with ultrasound looking specifically for fluid collections and soft tissue masses that may represent ALTR (19, 178).

Ultrasound is ideally suited for convenient regular follow-up of hip arthroplasty patients.

Whilst ultrasound has been recommended as an imaging modality in the follow-up of hip replacement surgery, few descriptions of typical ultrasound appearances of the major pathologies that may afflict the hip replacement have been published and there is little information to guide operators.

In the following series of chapters, we describe four studies which have evaluated the ability of ultrasound to detect and assess impingement and entrapment syndromes affecting the shoulder and hip. The first two published studies explore the potential of ultrasound to detect QSS of the shoulder. In chapter 4 we evaluated the ability of ultrasound to visualise the PCHA of the shoulder. In chapter 5 we determined the rate of occlusion and stenosis of the PCHA with ABER in the normal population. In chapter 6, the third published study, we assess the ability of ultrasound to quantify the femoral head-neck alpha angle of the hip in the detection of FAI. Finally, in chapter 7 we performed a study of the appearances of ultrasound of the post-arthroplastic hip to evaluate the potential of ultrasound to detect ALTR at the earliest possible stage.

All four studies have been published and each chapter provides an exact copy of the published article.

## ***Chapter 4* Ultrasound of the Posterior Circumflex Humeral Artery**

DJ Robinson,<sup>1</sup> P Marks<sup>1</sup> and ME Schneider-Kolsky<sup>2</sup>

<sup>1</sup>Department of Radiology, The Avenue Hospital, Windsor, Victoria

<sup>2</sup>Department of Medical Imaging & Radiation Sciences, Faculty of Medicine, Nursing and Health Sciences, Monash University, Clayton, Australia

*Journal of Medical Imaging and Radiation Oncology* **54 (3)** (June 2010) 219–223

**doi:**10.1111/j.1754-9485.2010.02162.x

This chapter is an exact copy of the journal paper referred above in which ultrasound was assessed for its ability to demonstrate the PCHA and obtain pulsed Doppler signals in neutral arm position and in ABER.

One of the aims of this thesis is to investigate the usefulness of ultrasound in detecting occlusion and stenosis of the PCHA as a proxy for mechanical impingement of the axillary nerve in QSS. In this chapter, we examine the ability of ultrasound to detect blood flow in the PCHA. Ultrasound is the modality of choice for detecting stenosis and occlusions of peripheral arteries, of which the PCHA is a branch. Ultrasound angiography does not require catheterisation of the vessel or contrast media for visualisation. Fifty volunteers were recruited and an attempt made to detect the PCHA using ultrasound in both neutral arm position, and in abduction and external rotation – the position that causes impingement in QSS. This chapter confirms that ultrasound is viable method to detect stenosis and occlusion

of the PCHA.



## 4.1 Declaration for Thesis Chapter

Declaration by candidate

In the case of Chapter 4, the nature and extent of my contribution to the work was the following:

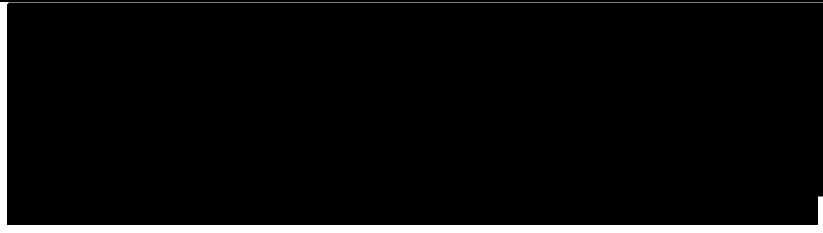

<b>Nature of Contribution</b>	<b>Extent of Contribution</b>
Concept,	70 %
Collecting data,	100 %
Data analysis,	90 %
Writing published draft	90 %

The following co-authors contributed to the work. If co-authors are students at Monash University, the extent of their contribution in percentage terms must be stated:

<b>Name</b>	<b>Nature of Contribution</b>	<b>Extent of Contribution (%) for student Co-authors only</b>
A/Prof Michal Schneider	Intellectual input on data analysis and manuscript editing	N/A
Dr Paul Marks	Intellectual input on study concept and manuscript editing	N/A

The undersigned hereby certify that the above declaration correctly reflects the nature and extent of the candidate's and co-authors' contributions to this work\*.

Candidate's Signature

	Date : 15 November 2018
	Date: 15 November 2018

Main Supervisor's Signature

# Ultrasound of the Posterior Circumflex Humeral Artery

## 4.2 Summary

Quadrilateral space syndrome (QSS) is described as compression neuropathy of the axillary neurovascular bundle in the quadrilateral space of the shoulder. This neurovascular bundle includes the posterior circumflex humeral artery (PCHA). Historically, angiography and more recently magnetic resonance angiography have been used to assess occlusion and stenosis of the PCHA in cases of suspected QSS. These traditional imaging techniques have a number of disadvantages in terms of cost, availability, invasiveness and patient comfort. We undertook to examine the ability of ultrasound to reliably visualise the PCHA. Asymptomatic adult volunteers were recruited from staff, and patients attending the radiology department who presented for pathologies unrelated to the shoulder. We used a new technique to assess blood flow in the PCHA, performing the scan from a posterolateral approach on the upper arm just above the level of the surgical neck of the humerus. This technique enabled the scan to be undertaken with the patient seated comfortably. Fifty volunteers were recruited into the study. The mean (SD) age was 35 (14 years). The PCHA was visualised in all patients. Our method was able to maximise Doppler sensitivity and visualisation of the artery without discomfort to the patient in less than 10 min. Ultrasound can be used to reliably visualise the PCHA.

Ultrasound has potential to be used in the assessment of the PCHA in cases of QSS.

### **Key words:**

axillary neuropathy; posterior circumflex humeral artery; quadrilateral space syndrome; teres minor muscle; ultrasonography

## 4.3 Introduction

Quadrilateral space syndrome (QSS) is defined as compression neuropathy of the axillary nerve in the quadrilateral space (79). The quadrilateral space is bounded superiorly by the capsule of the shoulder joint and subscapularis muscle, medially by the long head of triceps muscle, laterally by the neck of the humerus and inferiorly by the teres major (57)

The axillary nerve is a branch of the posterior cord of the brachial plexus, derived from C5 and C6, and divides into anterior and posterior branches. It is the anterior branch that is accompanied by the posterior circumflex humeral vessels, winding around the surgical neck of the humerus posteriorly deep to the deltoid muscle and supplying it, and providing a number of cutaneous branches (57). The posterior branch supplies the teres minor and the posterior part of the deltoid muscle and continues as the upper lateral cutaneous nerve of the arm, supplying the skin over the lower part of the deltoid and the upper long head of triceps muscle (57).

Symptoms are varied but have been described as dull aching or burning pain over the lateral and posterior aspects of the shoulder, vague weakness affecting deltoid and teres minor muscles, and pain with applied pressure to the quadrilateral space posteriorly (67, 79).

The mechanism of injury to the axillary nerve is considered to be most frequently due to repeated external compression of the neurovascular bundle in the quadrilateral space (79, 85).

Cahill and Palmer in their original study published in 1983 believed that the syndrome was caused by anomalous fibrous bands traversing the quadrilateral space (10).

Other possible causes of the axillary nerve compression neuropathy suggested in the past include compression/shear between the teres major and minor during extended athletic endeavour or extreme abduction, hypertrophy of teres minor and/or subscapularis, and varicocele within the quadrilateral space (30, 79). Sufferers are normally young adult athletes undertaking repeated overhead actions, such as throwers and swimmers (30, 79, 87).

The diagnosis of QSS is difficult when history and physical examination alone are relied upon, and in many cases no definite diagnosis can be reached (10, 189). Many individuals will

present with unexplained pain for months or years (92). Delays in diagnosis may result in inappropriate treatment, prolonged disability, and potentially irreversible muscular fatty atrophy of the deltoid and teres minor muscles, as well as permanent damage to the axillary nerve (85, 87, 106).

Angiographic imaging of the PCHA was part of the initial description of the condition by Cahill and Palmer in 1983 (10). They noticed occlusion of the PCHA in abduction and external rotation, and postulated that this intermittent arterial occlusion was representative of pathological impingement upon the axillary nerve (10). In this original study by Cahill, all asymptomatic shoulders showed a normal patent PCHA on abduction and external rotation (10).

More recently, PCHA compromise in the setting of clinical suspicion of QSS has been evaluated by magnetic resonance (MR) angiography (46). MR angiography of the PCHA is usually the final imaging tool used in the pursuit of the cause of shoulder pain, where the clinical picture is consistent with QSS. MR angiography of the PCHA is performed predominantly among athletes in whom axillary nerve decompression surgery is being considered. MR angiography is time consuming, invasive, relatively expensive, not available in all areas and requires the patient to maintain the arm in the most uncomfortable position (abducted and externally rotated) for an extended length of time.

Historically the role of ultrasound in the investigation of shoulder pain has been in the detection of other pathologies with a similar clinical presentation to QSS, such as rotator cuff tendinopathy and tears or subacromial bursitis. Ultrasound is capable of the quantitative assessment of blood flow within the human body and is routinely used to assess arterial stenoses and occlusions compromising blood flow in the upper and lower limbs in a setting of atherosclerosis, arterial embolus, and thrombosis (48). We hypothesised that Doppler ultrasound techniques may be applied to the evaluation of the PCHA where there is suspicion of QSS. We investigated whether ultrasound colour Doppler may be able to reliably detect

blood flow within the PCHA with a view to providing a simpler, cheaper and more comfortable method of diagnosing QSS.

## **4.4 Methods**

### **4.4.1 Patient Selection**

Volunteers were recruited consecutively from different groups of attendees to the radiology clinic at our institution. Only volunteers over 18 years of age were considered for inclusion. Patients attending the clinic for ultrasound not involving the shoulder were informed by reception staff that a research project was being undertaken into a small artery at the back of the shoulder. Those who expressed an interest in participating were given an information sheet to read while waiting for their ultrasound. If after reading this sheet they agreed to participate they were included in the study.

Additionally, posters briefly describing the study were placed in the patient waiting room and staff common areas, instructing any others who might be interested to ask for an information sheet at the radiology reception. Those who, after reading an information sheet, agreed to participate and provided written consent were included in the study.

All those who volunteered to undergo the scan were initially included. The volunteers were asked to complete a detailed patient questionnaire prior to the scan, providing detail on age, current symptoms if any, significant prior trauma or surgery to the shoulder and any other evidence of glenohumeral instability.

Ethics approval for the project was received from the Standing Committee on Ethics in Research involving Humans at Monash University.

### **4.4.2 Ultrasound Technique**

A Siemens Sonoline Anteres release 5 was the machine of choice for all scans. The assessment of the PCHA requires a vascular transducer to detect the small vessel and relatively weak Doppler signals. A VFX 9-4 linear transducer was used with harmonics on at 4.2MHz and 50 decibel. A single focus was set at an equivalent depth to the inferior glenoid. Lines of sight were set to medium to maintain good frame rate. Colour settings included high write priority, low wall filter (84 Hz) operating at 6.7 MHz to maximise the Doppler signal. In larger patients it was necessary to reduce the Doppler transmit frequency to 5MHz to allow penetration to the target area and good colour fill of the PCHA.

Spectral Doppler settings were used with a dynamic range at 55 decibel, 2mm gate and fast sweep speed to spread out the spectral trace for accurate Doppler measurements. Only two to three spectral peaks were required on the spectral display to perform the measurements.

The scan was performed with the patient erect and seated comfortably. The transducer was placed on the posterolateral arm just above the level of the surgical neck of the humerus [Figure 4-1: & Figure 4-2]. For the left shoulder the patient sat slightly to the right of the ultrasound machine at an angle of approximately 45 degrees to a straight line drawn from front to back through the ultrasound machine, allowing the sonographer access to the control panel. The sonographer positioned himself to the patient's left at an approximately 90 degree angle to the seated patient, assuming the sonographer scans with the right hand [Figure 4-2]. For the right shoulder, the patient was seated in essentially the same location, but rotated 180 degrees (The patient was facing away from the ultrasound machine) so that the right shoulder was nearest to the sonographer. This provides access to the vessels of the right shoulder and the control panel of the machine.

Spectral Doppler traces of both shoulders were acquired in neutral position, and in ABER. Assessment of the PCHA in ABER was achieved by asking the patient to place the palm of their hand on the back of their head, and then repositioning the transducer to maintain the

humeral shaft in a transverse plane. The artery could then be imaged using the same technique as described above.

The Doppler sample box was placed in the most proximal part of the PCHA visible on the B-Mode scan as it emerged from the quadrilateral space. Doppler values were measured once and recorded in both neutral and ABER for peak systolic velocity (PSV), end-diastolic velocity (EDV), resistive index (RI) and acceleration time (AT) in both PCHA and distal subclavian artery [Figure 4-3].

The PCHA branches from the third part of the axillary artery just below the lower border of the subscapularis muscle and passes posteriorly with the axillary nerve via the quadrilateral space, emerging just beneath the teres minor muscle to reach the surgical neck of the humerus (57). It passes posteriorly to the neck of the humerus to give branches to the deltoid, teres major and minor, and long and lateral heads of triceps muscles, before anastomosing with the anterior circumflex humeral artery (57). As it emerges from the quadrilateral space it is ideally positioned for Doppler ultrasound as it passes directly towards a strategically placed transducer, thus maximising the Doppler signals [Figure 4-1: and Figure 4-3]. Approaching the PCHA from behind with the artery passing directly toward the transducer thus maximises the Doppler shift and hence the signal strength and sensitivity to blood flow.



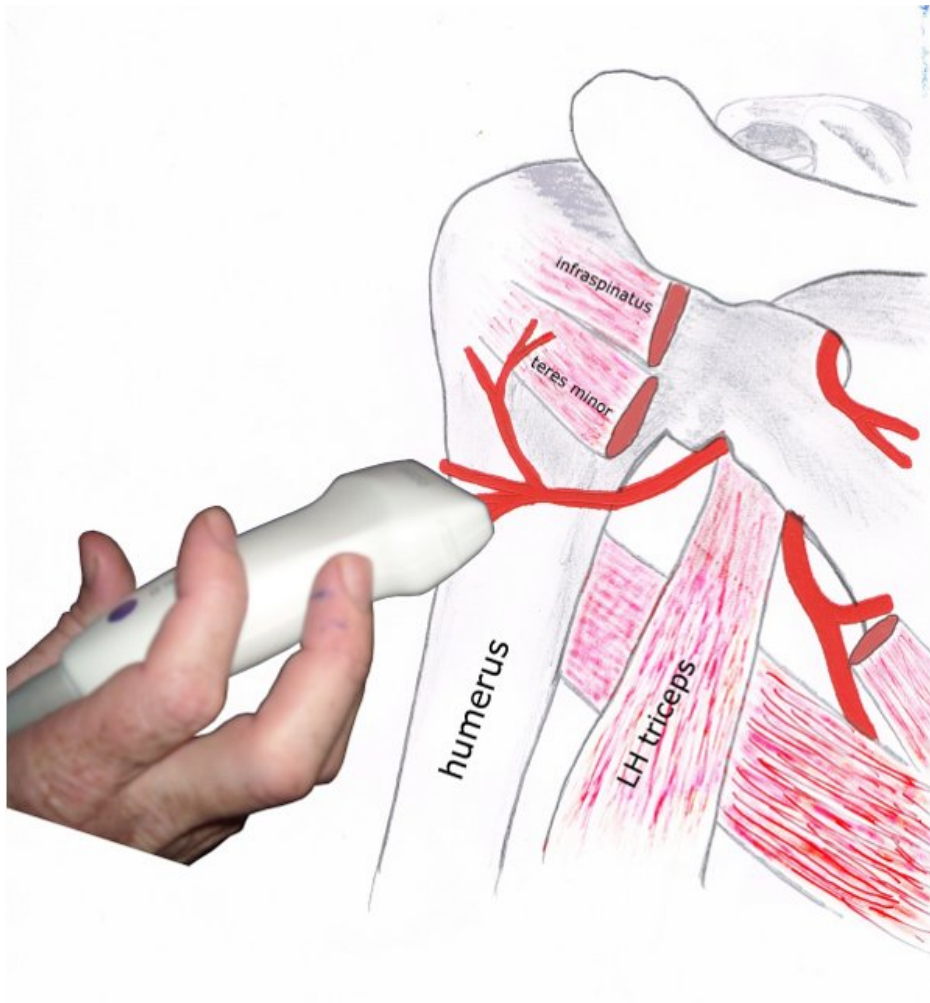


Figure 4-1: Assessment of the left PCHA. The transducer is placed on the posterolateral upper arm in transverse plane. Source: Williams PL, Warwick R Ed.s. Grays Anatomy 36th Ed 1980 (modified).



Figure 4-2: Patient positioning for ultrasound scanning of the left posterior circumflex humeral artery.

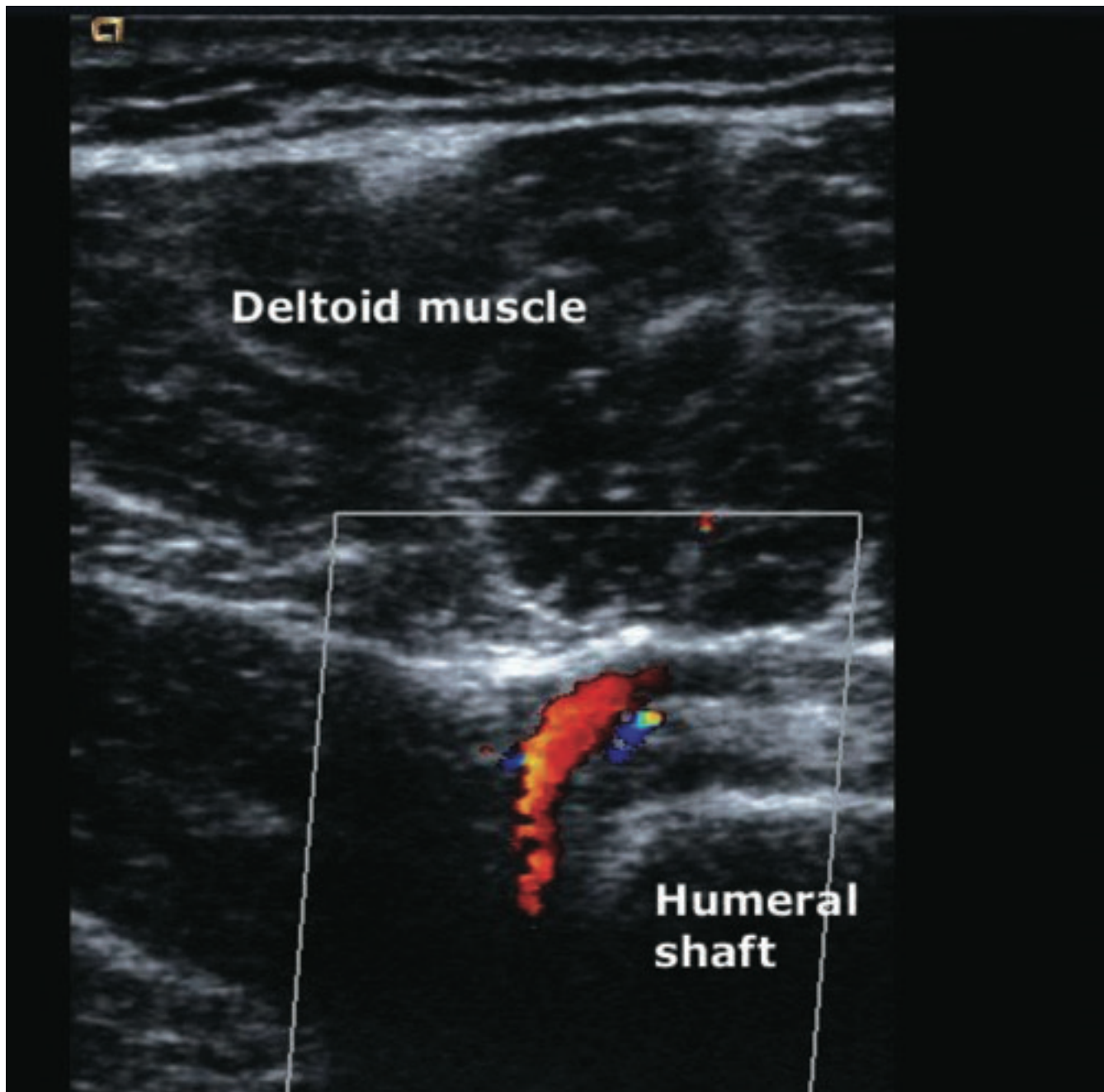


Figure 4-3: Posterior circumflex humeral artery (PCHA) ultrasound. Transverse color Doppler ultrasound of the PCHA. The artery (coloured red) passes behind the neck of the humerus. Flow direction is towards the transducer.

## 4.5 Results

Fifty volunteers were recruited into the study. The mean (SD) age was 35 ( $\pm 14$ ). Using the scanning technique outlined above, the PCHA could be observed in neutral and abduction and

external rotation in all cases.

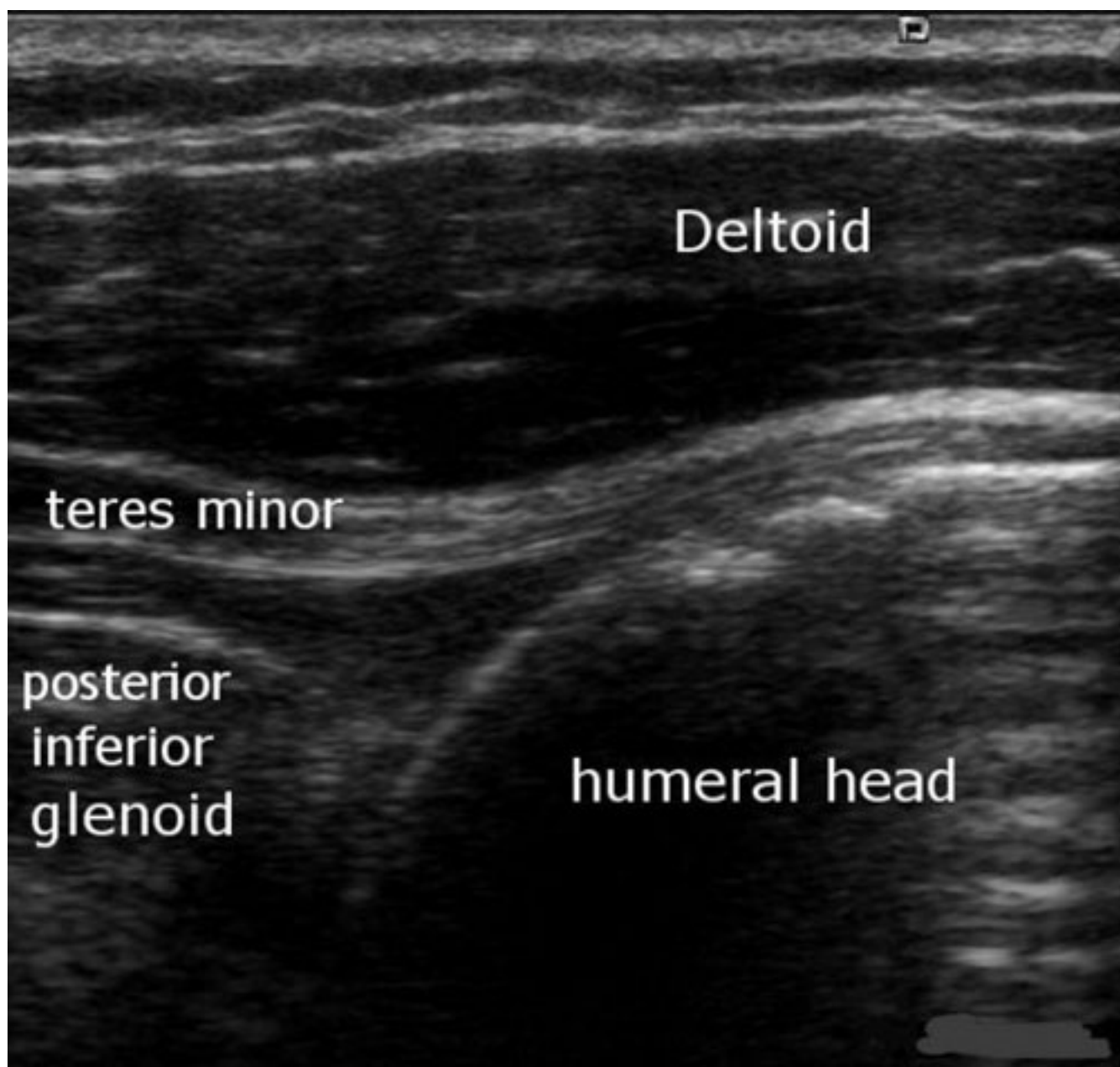


Figure 4-4: Tendon of the teres minor passing across the posterior humeral head. The transducer is in transverse plane with respect to the humeral shaft. The posterior glenoid can be seen to the left of the rounded humeral head. The posterior circumflex humeral artery can be found by passing the transducer directly inferiorly from this point.

The musculotendinous junction of the teres minor was visible when passing over the inferior glenoid and lower part of the humeral head [Figure 4-4]. From this point, moving the transducer inferiorly along the humeral shaft brought the PCHA into view as it emerges from the quadrilateral space. The PCHA was seen as pulsating colour with flow directly towards

the transducer and concavity of the curve towards the humeral shaft [Figure 4-3 and Figure 4-5]. The curvilinear walls of the PCHA were seen closely applied to the posterior humerus in grey scale as well, aiding identification of the artery. Introducing a cephalic angulation of the transducer back towards the glenoid will expose a longer section of the PCHA as it passes inferiorly through the quadrilateral space.

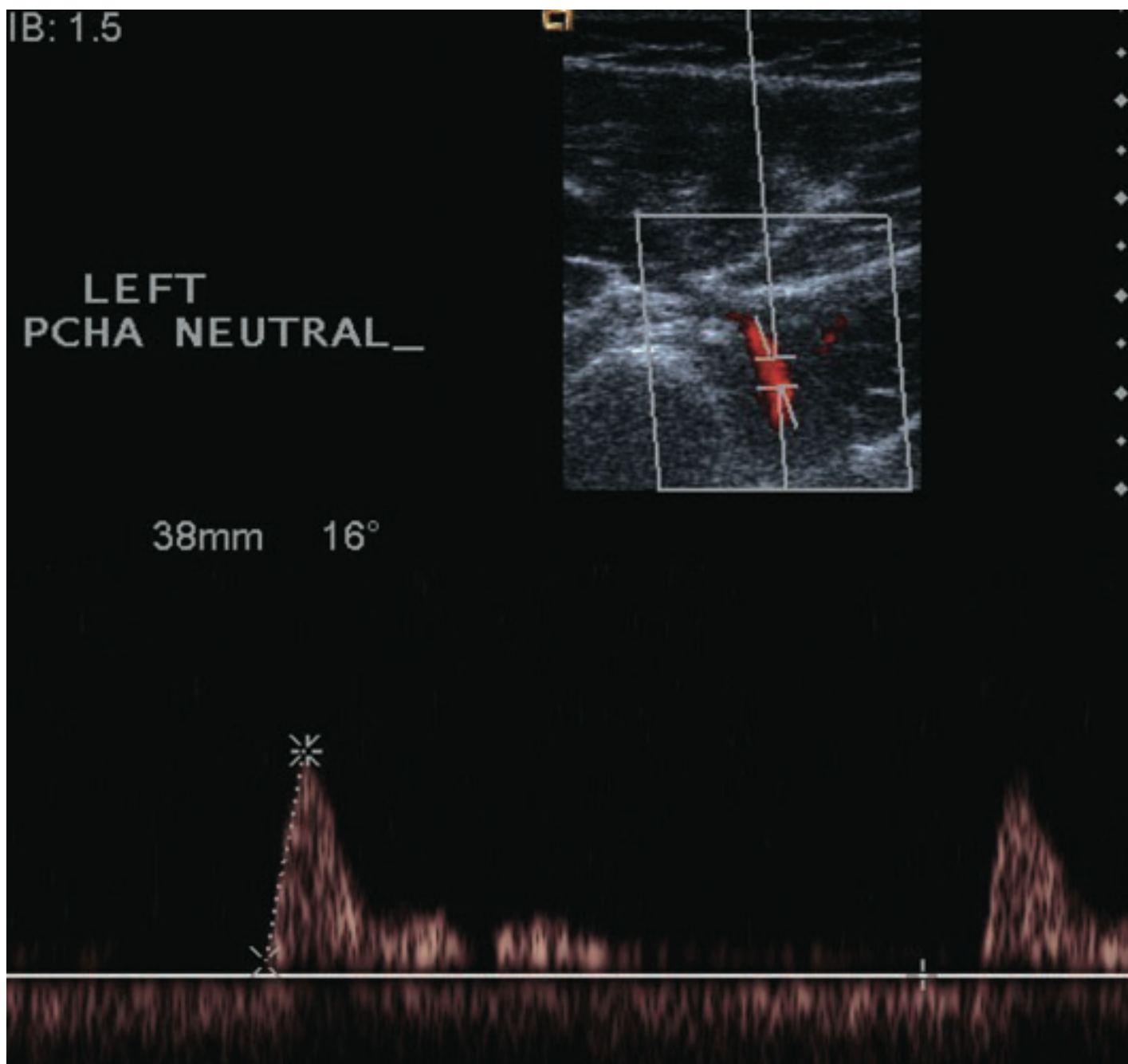


Figure 4-5: Typical pulsed Doppler signal obtained from the posterior circumflex humeral artery in neutral position.

## 4.6 Discussion

Our study has demonstrated that ultrasound can be used successfully to visualize and evaluate the PCHA in asymptomatic patients.

Ultrasound assessment of the PCHA has previously been described in only one case of QSS



(45). This patient was examined with ultrasound via the axillary space with the arm abducted to 90° and the elbow flexed. They found loss of Doppler flow signals of the PCHA and reported a ‘tight’ stenosis of the PCHA near its origin (45).

It is not certain whether the PCHA completely occluded as has been suggested by Cahill and Palmer (10). The technique described by Brestas examined the origin of the PCHA, presumably just before the PCHA enters the quadrilateral space; thus, occlusion of the artery cannot be verified using this technique (45). They did suggest that colour Doppler may help to identify the PCHA and confirm compression of the neurovascular bundle with the arm in stress positions, but they did not carry out this technique.

We have described an alternative method using ultrasound colour Doppler to insonate the PCHA via the posterolateral arm as the PCHA leaves the quadrilateral space. We have found this method to be reliable and reproducible with good patient acceptance.

Assessment of the PCHA in both neutral and abduction and external rotation is easily achieved using our method, allowing comparison of Doppler parameters of the PCHA in both arm positions.

An ultrasound method of assessing the PCHA in cases of suspected QSS has many advantages over current methods. The ultrasound examination can be completed in less than 10 min and can be included in a standard ultrasound examination of the shoulder at no extra cost. Ultrasound is more widely available, it involves no radiation or toxic contrast materials, there is no requirement for catheterisation and the test is able to be readily repeated.

As our study only evaluated asymptomatic volunteers, future studies will need to be carried out among patients with a history of shoulder pain and suspected QSS and evaluate if the PCHA can be equally well visualised and assessed in that patient cohort.

## **4.7 Conclusion**

We have described a new technique using ultrasound to assess the PCHA. The PCHA may be easily and reliably identified via a posterolateral approach on the upper arm. With our technique it is possible to assess the PCHA in both neutral and abducted and externally rotated positions quickly and comfortably.



## ***Chapter 5 Occlusion and stenosis of the posterior circumflex humeral artery: Detection with ultrasound in a normal population***

David John Robinson,<sup>1</sup> Paul Marks<sup>1</sup> and Michal Schneider-Kolsky<sup>2</sup>

<sup>1</sup>The Avenue X-ray and MRI, The Avenue Hospital, Windsor

<sup>2</sup>Department of Medical Imaging and Radiation Sciences, Faculty of Medicine, Nursing and Health Sciences, Monash University, Clayton, Victoria, Australia

*Journal of Medical Imaging and Radiation Oncology* **55** (2011) 479–484

**doi:**10.1111/j.1754-9485.2011.02301.x

This chapter is an exact copy of the journal paper referred above in which ultrasound was used to determine the rate of occlusion of the PCHA with ABER in the normal population.

Due to the nature of imaging modalities previously utilised to examine the PCHA, the rate of occlusion and stenosis of the PCHA with ABER in the normal population is unknown. The specificity of this sign as a proxy for axillary nerve impingement has therefore been called into question. The benefit of using ultrasound to examine the PCHA is that the lack of radiation dose or invasiveness allows testing of a large population of normal volunteers and the true rate of PCHA compromise with ABER can be explored. This chapter reports the findings of our study which has shown a rate of PCHA compromise with ABER in the normal population of 16%.

## 5.1 Declaration for Thesis Chapter

Declaration by candidate

In the case of Chapter 5, the nature and extent of my contribution to the work was the following:

<b>Nature of Contribution</b>	<b>Extent of Contribution</b>
Concept,	70 %
Collecting data,	100 %
Data analysis,	90 %
Writing published draft	90 %

The following co-authors contributed to the work. If co-authors are students at Monash University, the extent of their contribution in percentage terms must be stated:

<b>Name</b>	<b>Nature of Contribution</b>	<b>Extent of Contribution (%) for student Co-authors only</b>
-------------	-------------------------------	---

A/Prof Michal Schneider	Intellectual input on data analysis and manuscript editing	N/A
Dr Paul Marks	Intellectual input on study concept and manuscript editing	N/A

The undersigned hereby certify that the above declaration correctly reflects the nature and extent of the candidate's and co-authors' contributions to this work\*.

Candidate's Signature		Date : 15 November 2018
Main Supervisor's Signature		Date: 15 November 2018

## **Occlusion and stenosis of the posterior circumflex humeral artery:**

### **Detection with ultrasound in a normal population**

#### **5.2 Abstract**

**Introduction:** The posterior circumflex humeral artery (PCHA) travels together with the axillary nerve through the quadrilateral space of the shoulder. Angiographic occlusion of this artery upon abduction and external rotation (ABER) of the arm has been accepted as evidence of mechanical compression of the axillary nerve and thus considered pathognomonic of quadrilateral space syndrome (QSS). The specificity of this sign for QSS has however been called into question as there are, to date, limited data on the incidence of axillary neurovascular compression during ABER in a normal population. We set out to determine the rate of stenosis or occlusion of the PCHA on ABER in healthy volunteers using ultrasound.

**Methods:** Healthy volunteers asymptomatic for shoulder complaints were recruited from patients attending the clinic for ultrasound imaging not related to the shoulder, as well as volunteers among staff. Doppler sampling of the PCHA of both shoulders of participants was conducted in neutral and abduction and externally rotated positions. Each shoulder was treated as a separate entity.

**Results:** Results showed that 15/93 (16%) of shoulders demonstrated Doppler ultrasound evidence of occlusion or significant stenosis in the absence of shoulder complaints.

**Conclusion:** Occlusion or stenosis of the PCHA on ABER is an uncommon finding in an asymptomatic population. Axillary neurovascular compression is unlikely if colour Doppler ultrasound does not show PCHA compromise during ABER.

**Key words:**

axillary neuropathy; posterior circumflex humeral artery; quadrilateral space syndrome; ultrasonography.

### **5.3 Introduction**

The axillary neurovascular bundle passes through the quadrilateral space just below the shoulder joint (57). This neurovascular bundle includes the posterior circumflex humeral artery (PCHA) as well as the axillary nerve (57). Quadrilateral space syndrome (QSS) is defined as compression neuropathy of the axillary nerve in the quadrilateral space (79).

The mechanism of injury to the axillary nerve is considered to be most frequently due to repeated external compression of the neurovascular bundle in the quadrilateral space (79, 85). Affected persons may notice numbness/ parasthesia of the lateral arm, rapid fatigue in athletic activity, reduced abduction strength or an inability to raise their arm (79).

The diagnosis is difficult when history and physical examination alone are relied upon, and in many cases no definite diagnosis can be reached (10, 189). QSS may easily be overlooked in patients suffering from shoulder symptoms as other shoulder pathology such as rotator cuff tears, capsulitis or impingement are much more common (79, 87). Wrong diagnosis may lead to inappropriate patient management and unnecessary and unsuccessful treatment. If the syndrome is well advanced, clinical presentation may include atrophy or asymmetry of the deltoid muscle mass (79).

PCHA compromise in the setting of clinical suspicion of QSS has been evaluated by MR angiography (46). Doubt has been cast upon the specificity for QSS of PCHA occlusion upon abduction and external rotation (ABER) of the arm with MR angiography. Mochizuki, in a study of one patient with QSS and six healthy volunteers, found that PCHA was stenotic near the origin in 80% of the healthy volunteers and that positive MR angiography was thus not specific for QSS (46). Magnetic resonance angiography in the diagnosis of QSS has a number

of disadvantages as a first-line investigative imaging modality. Magnetic resonance angiography is time-consuming, invasive, relatively expensive and not available in all areas. It also requires the patient to maintain the arm in the most uncomfortable position for an extended length of time. Otherwise, more easily available and cheaper imaging modalities are therefore needed to provide initial imaging of this pathology.

Ultrasound is routinely used to assess arterial stenoses and occlusions compromising blood flow in the upper and lower limbs in a setting of atherosclerosis, arterial embolus and thrombosis (48). We designed this study with the aim to use Doppler ultrasound to characterise blood flow within the PCHA and to determine the prevalence with arm ABER of occlusion and arterial stenosis sufficient to cause detectable Doppler spectral changes in healthy, asymptomatic volunteers.

## **5.4 Patients and methods**

Ethics approval for the project was received from the Standing Committee on Ethics in Research Involving Humans at our institution. All patients attending the clinic for ultrasound not involving the shoulder were invited by reception staff to participate in the research project.

Participants were asked to complete a detailed patient questionnaire prior to the scan, providing detail on age, current symptoms if any, significant prior trauma or surgery to either of their shoulders and any other evidence of glenohumeral instability. Volunteers who were younger than 18 years were excluded from the study. Each shoulder was considered a separate entity, and characteristics and results were recorded separately for each. Shoulders of participants that had had prior surgery potentially affecting shoulder stability such as labral or rotator cuff repair were excluded, while the participants' unaffected contralateral shoulder was included. Patients who were deemed suitable for participation in this study gave written

consent.

## 5.5 Ultrasound Technique

A Siemens Sonoline Anteres Release 5 (Siemens, Issaquah, WA, USA) was used for all scans. A VFX 13-5 linear small part transducer was used to assess the shoulder rotator cuff using maximum frequency (11.4 MHz) at 55 dB. A VFX 9-4 transducer was used to assess the distal subclavian artery in neutral and ABER positions for evidence of arterial thoracic outlet syndrome. The assessment of the PCHA also requires a vascular transducer to detect the small vessel and relatively weak Doppler signals. The VFX 9-4 linear transducer was therefore chosen. It was used with harmonics on at 4.2 MHz and 50 dB. The field of view extended over a depth of approximately 4 cm.

Scanning was performed with the patient seated on a swivel chair in front of and to the right of the ultrasound machine. The shoulder being examined was closest to the sonographer. The PCHA was identified on the posterolateral shoulder by scanning in transverse plane inferior to the tendon of teres minor. In this way, the PCHA travels almost directly towards the transducer maximising the Doppler signal (190) (Figure 5-1). Spectral Doppler traces of both shoulders were acquired in neutral position and in ABER. The latter was achieved by asking volunteers to place their palm on the back of their head (Figure 5-2). The Doppler sample box was placed in the most proximal part of the PCHA visible on the B-mode scan as it emerged from the quadrilateral space. Doppler values were measured once and recorded in both neutral and ABER for peak systolic velocity (PSV), end-diastolic velocity (EDV), resistive index (RI) and acceleration time (AT) in both PCHA and distal subclavian artery (Figure 5-3). A significant stenosis was considered to be at least a doubling of PSV on ABER, implying a 50% or greater stenosis from the neutral position. A delayed AT was considered to be greater than 80 ms.

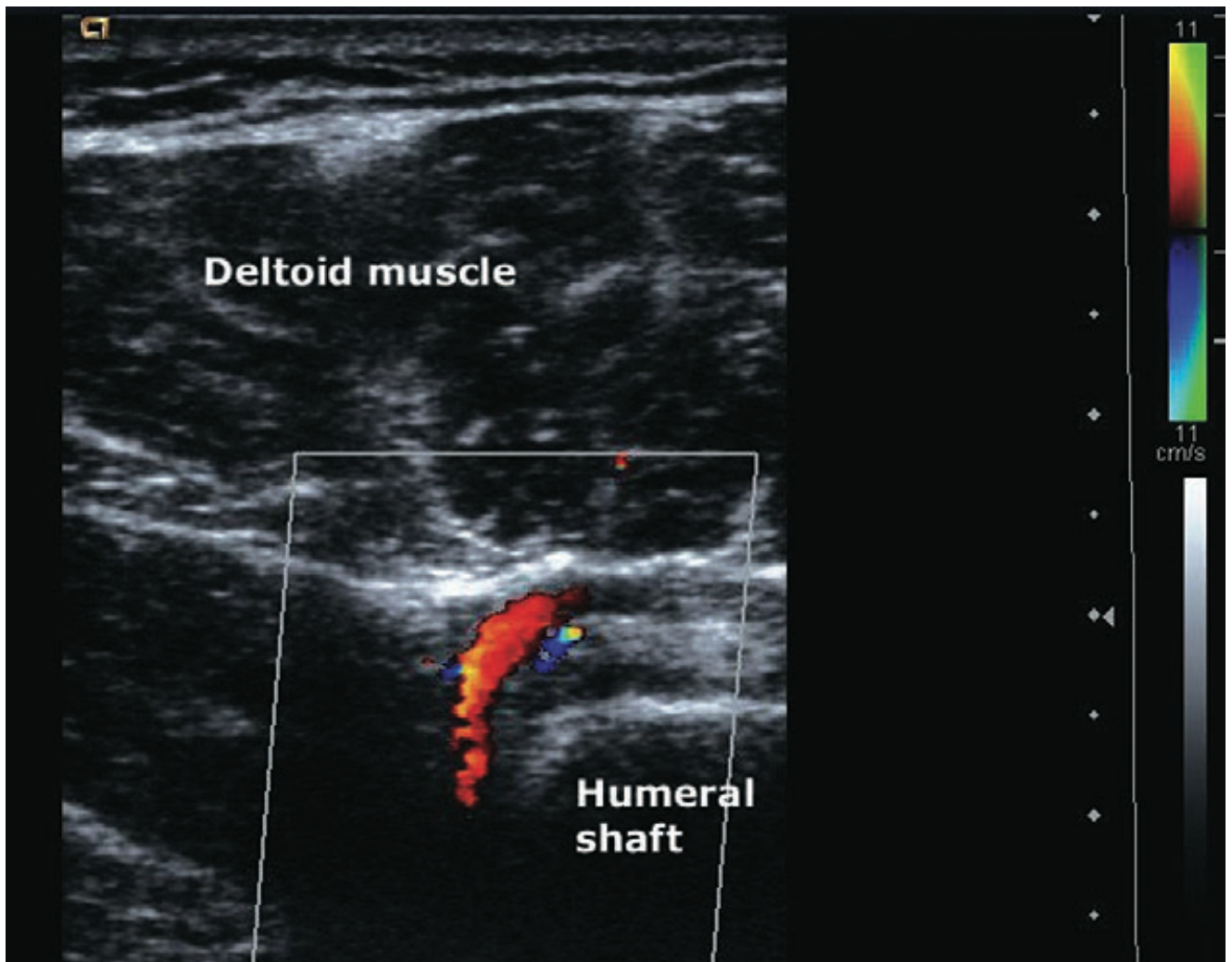


Figure 5-1 PCHA emerging from the quadrilateral space. Flow is towards the transducer. Concavity of the path of the vessel is towards the humeral shaft. (PCHA, posterior circumflex humeral artery).





Figure 5-2 Scanning the PCHA with the arm in ABER. Transducer remains in transverse plane with respect to the humeral shaft. (ABER, abduction and external rotation; PCHA, posterior circumflex humeral artery).

## 5.6 Statistical Analysis

Mean ( $\pm$  standard deviation (SD)) PSV, EDV, RI and AT for the PCHA were recorded and compared between the arm in neutral position and in ABER position using a Student's *t*-test. All analyses were carried out using SPSS (version 16.0, SPSS Inc, Chicago, IL, USA). A *P*-value of  $<0.05$  was considered statistically significant.

## 5.7 Results

Fifty volunteers were recruited into the study. The age range was 20 to 75 years, with a median age of 37 years. There were 33 females and 17 males.

Seven shoulders were not included in the analysis. One 26 year old male had had surgery for repair of a labral tear of the dominant shoulder and this shoulder was excluded from the final results. The contralateral shoulder was included. Another participant, a 22 year old female demonstrated complete loss of flow in both distal subclavian arteries on ABER. Both shoulders of this individual were excluded from the final analysis.

Four participants were noted to have full thickness tears of at least one rotator cuff tendon. All shoulders demonstrating full-thickness tears of any rotator cuff tendon were also excluded.

There were 93 shoulders remaining for the analysis (N=93) (Table 5-1).

Seventy-eight of 93 (83.87%) shoulders showed no evidence of occlusion or significant stenosis of the PCHA on ABER.

The mean PCHA PSV ( $\pm$  SD) for the dominant shoulder in neutral was 29.58 cm/sec ( $\pm$ 8.69 cm/sec). In ABER this changed slightly to 29.81 cm/sec ( $\pm$  19.76 cm/sec) ( $p = 0.932$ ). For the non-dominant shoulder PCHA PSV in neutral was 28.99 ( $\pm$ 9.38) cm/sec, and upon ABER this changed to 25.79 ( $\pm$ 16.80) cm/sec ( $p= 0.217$ ). Eight shoulders demonstrated total occlusion of flow in the PCHA on ABER (8.60%). Of these, three (37.50 %) involved the dominant side. All demonstrated normal blood flow in neutral position.

Average AT was 37.73 ( $\pm$  9.34) msec in neutral and 49.51 ( $\pm$  31.38) msec in ABER ( $p = 0.001$ ). The resistive index average was 0.92 ( $\pm$ 0.07) in neutral and 0.93 ( $\pm$  0.14) in ABER ( $p = 0.66$ ) (Table 5-2).

Two of 93 (2.15 %) shoulders demonstrated a significant stenosis (at least a doubling of PSV from that found in neutral position) of the PCHA on ABER. One of these was a dominant side and the other involved the non-dominant side [Figure 5-4].

Six (6.45%) shoulders demonstrated a prolonged (> 80 msec) acceleration time on abduction and external rotation – just one of these demonstrated evidence of ipsilateral arterial thoracic outlet syndrome (greater than doubling of distal subclavian PSV with ABER). Five of the six stenoses thus most probably occurred within the proximal quadrilateral space and damping of the PCHA Doppler signal was not likely due to subclavian artery external compression.

Delayed acceleration time in the sixth case was discounted as being due to PCHA compromise due to evidence of arterial thoracic outlet syndrome. Three of the remaining five (60%) involved the dominant shoulder.

Table 5-1: Doppler ultrasound evaluation of PCHA blood flow in asymptomatic shoulders (n/N (%)).

PCHA flow	n/N(%)	Reason
Normal	78/93 (83.87%)	-
Abnormal	15/93 (16.13%)	-
Occluded on ABER	8/15 (53.33%)	No detectable Doppler signal
Stenosed on ABER	2/15 (13.33%)	ABER PSV > 2 times neutral PSV
Delayed acceleration	5/15 (33.33%)	AT>80 msec without evidence of aTOS

**Key:** ABER – abduction and external rotation, AT – acceleration time in milliseconds; aTOS – arterial thoracic outlet syndrome.; PCHA – posterior circumflex humeral artery; PSV – Peak systolic velocity.

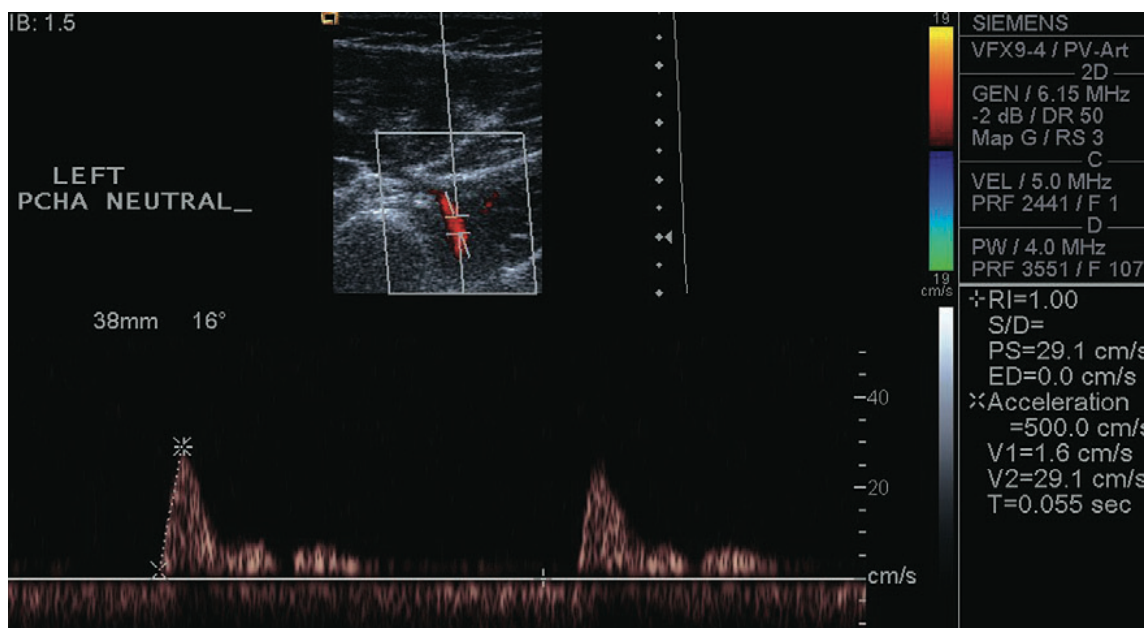
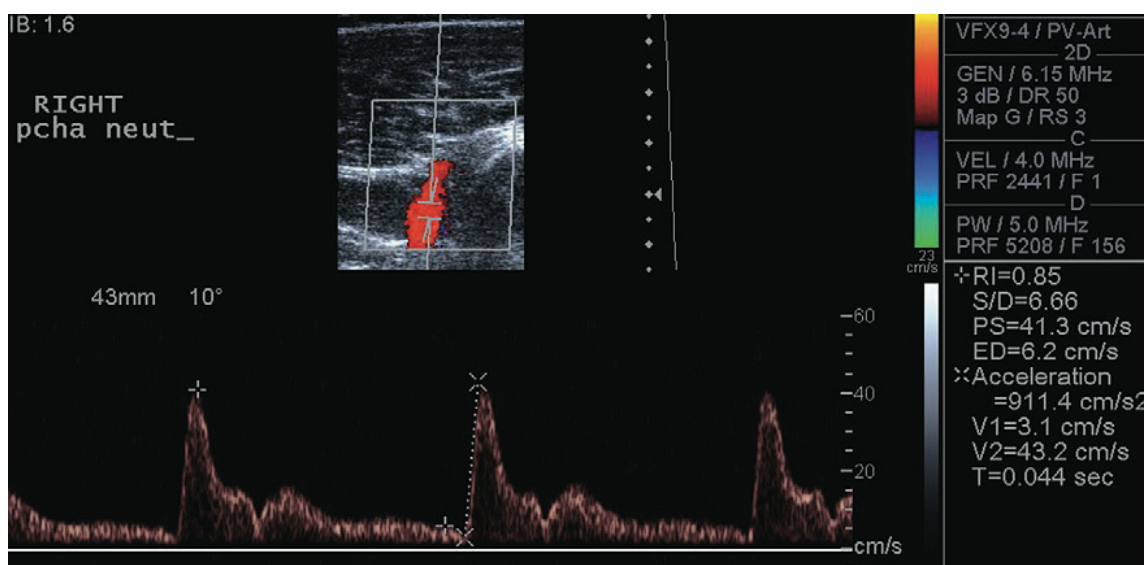


Figure 5-3 Typical Doppler values of the PCHA in neutral position. (PCHA, posterior circumflex humeral artery.)



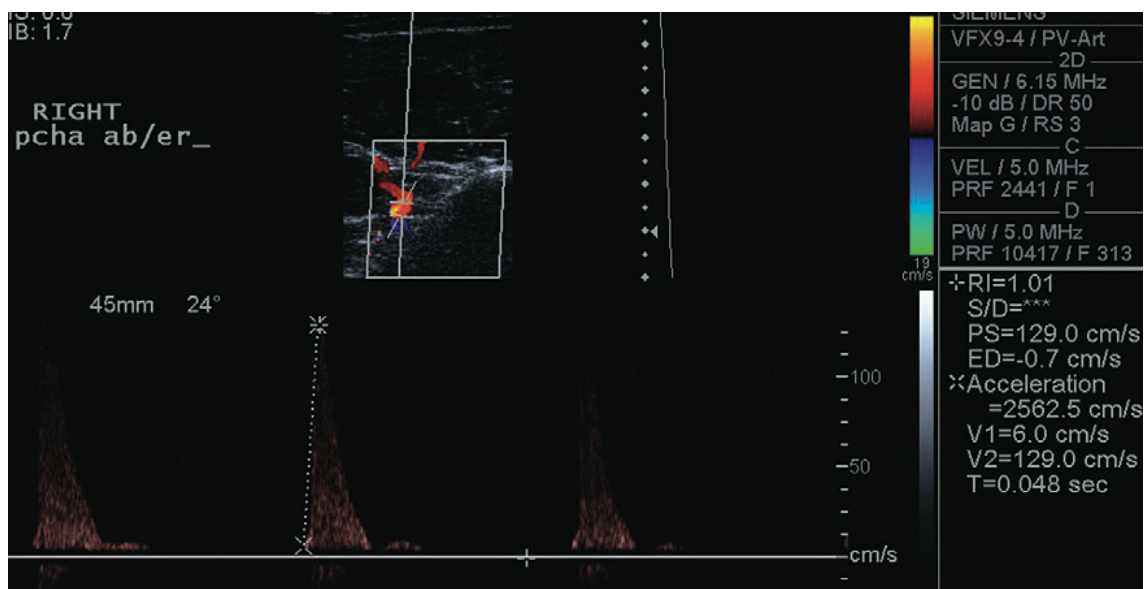


Figure 5-4 (a and b) Normal PCHA Doppler trace in neutral position. In b (below) PSV dramatically increases with ABER (129 cm/s), more than three times PSV (41.3 cm/s) in neutral position, indicative of a significant stenosis of the PCHA with ABER. (ABER, abduction and external rotation PCHA, posterior circumflex humeral artery; PSV, peak systolic velocity).

Table 5-2 Ultrasound characteristics of the PCHA according to arm position and dominance.

	Neutral	ABER
PSV Dominant arm	29.58 ( $\pm 8.69$ ) cm/sec	29.81 ( $\pm 19.76$ ) cm/sec
PSV Non-dominant arm	28.99 ( $\pm 9.38$ ) cm/sec	25.79 ( $\pm 16.80$ ) cm/sec
Resistive Index	0.92 ( $\pm 0.07$ )	0.93 ( $\pm 0.14$ )
Acceleration time	37.73 ( $\pm 9.34$ )	49.51 ( $\pm 31.38$ )

**Key:** ABER = Abduction and External Rotation PSV = Peak Systolic velocity

## 5.8 Discussion

We have assessed the PCHA in fifty volunteers with the arm in both neutral and ABER positions using normal ultrasound Doppler parameters. Ultrasound criteria for occlusion or

stenosis of the PCHA on ABER of the arm were met in 16% of asymptomatic volunteers. We have found significant stenosis or occlusion of the PCHA with abduction and external rotation of the arm in fifteen (16.13%) of 93 included shoulders. All included participants were asymptomatic. Eight of the 15 (8.60%) shoulders showed complete occlusion of the PCHA on ABER. Two (2.15%) shoulders showed at least a doubling of the PCHA PSV upon ABER and five (5.37%) shoulders demonstrated prolonged acceleration time of greater than 80 milliseconds without evidence of arterial thoracic outlet syndrome, indicating a significant stenosis within the proximal part of the quadrilateral space.

Our participants were healthy volunteers, and were excluded from participation if conditions that may affect PCHA impingement such as rotator cuff tendon tears or glenoid labral pathology were present. Doppler evidence of stenosis was taken to be at least a doubling of PSV representing an at least 50% stenosis of the PCHA or delayed acceleration time greater than 80msec without evidence of arterial thoracic outlet syndrome. We believe that our findings represent the prevalence of axillary neurovascular bundle impingement within the quadrilateral space upon ABER in the normal population, and that it is an uncommon phenomenon in asymptomatic shoulders.

The first report of QSS by Cahill and Palmer described the use of angiography to detect external impingement upon the neurovascular bundle in the quadrilateral space (10).

Impingement upon the PCHA was thought to be indicative of neurovascular bundle compression and thus pathognomonic of the condition. All asymptomatic shoulders showed a normal patent PCHA on abduction and external rotation (ABER), whereas abduction of as little as 60 degrees caused PCHA occlusion in symptomatic shoulders (10). They described the condition as practically always affecting the dominant extremity (10). Other subsequent reports have not remarked upon dominance or otherwise of the affected limb (29, 45, 84, 85, 191). We have found Doppler ultrasound evidence of PCHA occlusion of the non-dominant arm. Five of eight (62.50%) volunteers demonstrated complete loss of Doppler signal in the



PCHA on ABER of the non-dominant arm.

One recent study using MR angiography of one patient with QSS and six healthy volunteers found that PCHA was stenotic near the origin in 80% of the healthy volunteers(46).

Mochizuki et al have suggested based upon their single study that PCHA occlusion or stenosis on ABER is not a specific finding for QSS (46). There is hence considerable dispute regarding the association of PCHA compression on ABER and QSS. Brestas et al (2006) examined the PCHA of one patient with ultrasound and suggested that colour Doppler may help to identify the PCHA, and confirm compression of the neurovascular bundle with the arm in stress positions (45). Ultrasound colour Doppler is the preferred method of assessment of the PCHA as it does not require the patient to maintain the arm in the most uncomfortable position for an extended length of time, is non-invasive and requires no toxic contrast agents. Analysis of ultrasound Doppler frequency spectrum can provide quantitative information on vessel blood flow (114). In particular, when an artery diameter is reduced identifiable characteristics of this Doppler frequency spectrum will change (49). Typical parameters measured include PSV, RI and AT. PSV is considered most sensitive to arterial diameter reductions, but RI and AT have the advantage of not requiring angle correction (114). Visualisation of a large section of the PCHA is thus not required as it is to accurately calculate true velocity. EDV is required for the calculation of the RI.

Hyperabduction of the arm (beyond 90 degrees) can dramatically affect blood flow in the subclavian/axillary artery in a small percentage of asymptomatic individuals. Many asymptomatic people exhibit upper extremity pulse deficits with positional movements of the arm, and evidence of thoracic outlet arterial compression has been reported to be common in asymptomatic persons (48, 100). As the PCHA is a branch of the third part of the axillary artery, arterial thoracic outlet syndrome affecting flow in the axillary artery will also affect flow in the PCHA. Altered Doppler ultrasound characteristics of the PCHA in such a situation

would not be representative of external forces acting on the PCHA within the quadrilateral space.

It is thought that only chronic repetitive impingement upon the axillary neurovascular bundle gives rise to the atrophic changes and muscular atrophy characteristic of the condition (79, 85). Intermittent impingement such as might occur in those performing everyday activities for example amateur sports or office work is unlikely to give rise to QSS. The causative fibrous bands have been found in a percentage of cadavers with no apparent record of QSS (67). Those suffering QSS are normally young adult athletes undertaking repeated overhead actions such as throwers and swimmers (30, 79, 87). PCHA stenosis or occlusion on ABER could therefore still be present in those that do not suffer symptoms consistent with QSS. The results of our study have shown that axillary neurovascular impingement is detectable in the normal population, but uncommon. In a population of patients with symptoms consistent with QSS ultrasound may be used to exclude axillary neurovascular impingement and obviate further invasive and expensive testing.

A weakness of our study was the difficulty in proving the absence of a Doppler signal. The absence of a Doppler signal could be due to patient movement, poor technique or malpositioning of the ultrasound transducer. This occurs most frequently when the operator is inexperienced in the technique, but less so as the anatomical arrangements in neutral and ABER become better understood. Our study was conducted by one experienced sonographer and hence, we do not believe that our findings were affected by this issue. Absence of colour flow on ABER can be confirmed by repeating the action of moving from neutral to ABER, essentially performing a number of repeated samplings – one of the advantages of ultrasound over other modalities. The PCHA can also be followed as the subject abducts and externally rotates observing cessation of colour flow in real time.

Further work is required to prove the association between ultrasound-detected



occlusion/stenosis of the PCHA with ABER and patients with clinical QSS. The assumption that PCHA impingement always represents impingement of the axillary nerve may not be valid. Our study was performed with the patient seated in the erect position, whereas angiography and MR angiography are performed with the patient supine. Ideally a comparative study utilizing MR angiography, Doppler ultrasound and surgical cross-correlation should be performed to determine a reference standard. However, such a study will be difficult to perform due to the rare nature of QSS.

In summary, we have demonstrated that occlusion or stenosis of the PCHA upon ABER is detectable with ultrasound Doppler techniques. It is an uncommon finding in an asymptomatic population. Doppler ultrasound is able to quickly and safely assess the PCHA with ABER and may make angiography for the diagnosis of QSS in suspected sufferers unnecessary.

## ***Chapter 6* Ultrasound determination of the femoral head-neck alpha angle**

David John Robinson,<sup>1</sup> Steven Lee<sup>1</sup>, Paul Marks<sup>2</sup> and Michal Schneider-Kolsky<sup>3</sup>

<sup>1</sup>The Avenue X-ray and MRI, The Avenue Hospital, Windsor

<sup>2</sup> Imaging Associates Box Hill, Box Hill, Victoria, Australia;

<sup>3</sup>Department of Medical Imaging and Radiation Sciences, Faculty of Medicine, Nursing and Health Sciences, Monash University, Clayton, Victoria, Australia

*Ultrasound in Med & Biol* 44 (2) (2018) 495-501

**doi:** 10.1016/j.ultrasmedbio.2017.10.006

This chapter is an exact copy of the journal paper referred above comparing ultrasound measurements of the femoral head-neck alpha angle with an established modality, in this case CT.

This study demonstrates the usefulness of ultrasound in providing objective evidence of femoroacetabular impingement. The advantages of ultrasound are particularly relevant for young adult populations for whom early detection of FAI before major joint damage has occurred would have significant advantages. In this chapter, we compared an ultrasound measurement of the femoral head-neck alpha angle to an established standard. Thirty-nine hips were analysed and the femoral head-neck alpha angle calculated for both ultrasound and 3DCT. Results were compared using the Bland-Altman test of agreement between two methods of clinical measurement.

This manuscript demonstrates that ultrasound measurement of the alpha angle can provide

objective evidence of cam-type femoroacetabular impingement in symptomatic patients and can direct patients to more established imaging techniques where appropriate.

## 6.1 Declaration for Thesis Chapter

Declaration by candidate

In the case of Chapter 6, the nature and extent of my contribution to the work was the following:

<b>Nature of Contribution</b>	<b>Extent of Contribution</b>
Concept,	70 %
Collecting data,	100 %
Data analysis,	90 %
Writing published draft	90 %

The following co-authors contributed to the work. If co-authors are students at Monash University, the extent of their contribution in percentage terms must be stated:

<b>Name</b>	<b>Nature of Contribution</b>	<b>Extent of Contribution (%) for student Co-authors only</b>
A/Prof Michal Schneider	Intellectual input on data analysis and	N/A

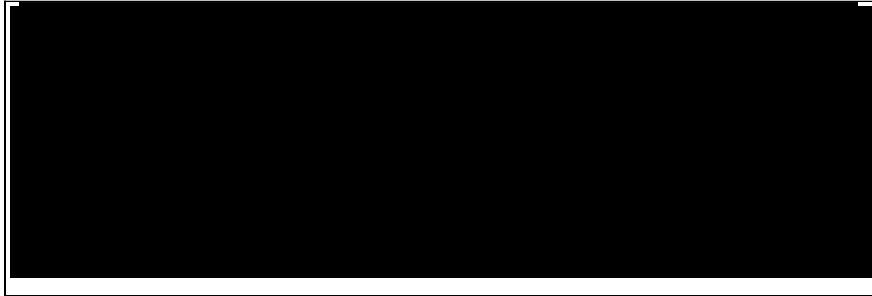
	manuscript editing	
Dr Steven Lee	Intellectual input on data collection and analysis, and manuscript editing	N/A
Dr Paul Marks	Intellectual input on study concept and manuscript editing	N/A

The undersigned hereby certify that the above declaration correctly reflects the nature and extent of the candidate's and co-authors' contributions to this work\*.

Candidate's Signature

	Date :  15 November 2018
---	--------------------------------

Main Supervisor's Signature

	<p>Date : 15 November 2018</p>
--	------------------------------------

# Ultrasound determination of the femoral head-neck alpha angle

## 6.2 Abstract

The femoral head-neck alpha angle is used to quantify the degree of femoral head asphericity in patients suspected of cam-type femoroacetabular impingement. The measurement was first performed using magnetic resonance imaging and, more recently, three-dimensional computed tomography (CT). We set out to determine whether the alpha angle could be reliably measured using ultrasound. Patients were recruited from a cohort presenting for CT of the hip. Alpha angles were calculated following the departmental protocol by institutionally accredited radiographers. After the CT, patients were imaged with ultrasound and the alpha angle calculated from the ultrasound image by a sonographer blinded to the CT result. Statistical comparison of the two methods was performed with the Bland-Altman test using SPSS (version 21.0, Chicago, USA), and a  $p < 0.05$  afforded significance. Twenty-eight patients were recruited. Eleven patients were bilateral examinations, providing 39 hips for analysis. There were 15 females and 13 males, with 21 right and 18 left hips examined. Average patient age ( $\pm$ standard deviation) was 40 y ( $\pm$ 13.9 y). Mean ( $\pm$ standard deviation) measurements for CT and ultrasound were  $62.5^\circ$  ( $\pm$ 14.2 $^\circ$ ) and  $64.5^\circ$  ( $\pm$ 12.6 $^\circ$ ), respectively. The mean absolute difference between the two methods was  $10.5^\circ$  (95% confidence interval  $6.9^\circ$ – $14.0^\circ$ ). Sensitivity of each individual ultrasound measurement was 91.3%. The specificity of ultrasound was 43.75%. The positive predictive value was 0.7, and the negative predictive value was 0.78. Overall accuracy of the ultrasound-derived alpha angle was calculated at 0.718. Ultrasound demonstrates good sensitivity and good negative predictive value in calculation of the femoral head-neck alpha angle compared with CT; however, specificity is low. Ultrasound measurement of the alpha angle can provide objective evidence of cam- type femoroacetabular impingement in symptomatic patients and can direct patients

to more established imaging techniques where appropriate.

(E-mail: [djrob6xx@gmail.com](mailto:djrob6xx@gmail.com))

© 2018 World Federation for Ultrasound in Medicine & Biology. Published by Elsevier Inc.

All rights reserved.

**Key Words:** Ultrasound, Musculoskeletal, Hip, Femoroacetabular impingement, Alpha angle.



## 6.3 Introduction

Femoracetabular impingement (FAI) has been postulated to be a cause of acetabular labral and articular cartilage damage to the hip (11). The sequelae of the condition and the damage that it causes are thought to contribute to early onset of osteoarthritis (OA) (15). Cam-type FAI is impingement of the antero-superior femoral head-neck junction upon the acetabular labrum as the result of an osseous *bump* at the superior end of the upper femoral epiphysis (5, 69, 129). The bony prominence causes an abnormality of the femoral head-neck contour, manifesting as a loss of sphericity of the femoral head, a shallow head-neck offset and impingement upon the acetabulum, in particular, with flexion of the leg upon the trunk with internal rotation (15). Symptoms of cam impingement occur at the limits of forward flexion and internal rotation where the loss of the normal femoral head-neck offset impacts upon and damages the acetabulum over time (15). Delay or misdiagnosis of cam-type FAI may result in potentially more severe joint damage or unnecessary medical and surgical treatments (15). Qualitative criteria such as a *pistol-grip* shape of the femoral head-neck junction cannot be used to quantify the severity of the condition (15). An attempt to provide an objective measurement of this femoral head *asphericity* coined the *alpha angle* was pioneered using magnetic resonance imaging (MRI) by Nötzli et al. (2002)(11).

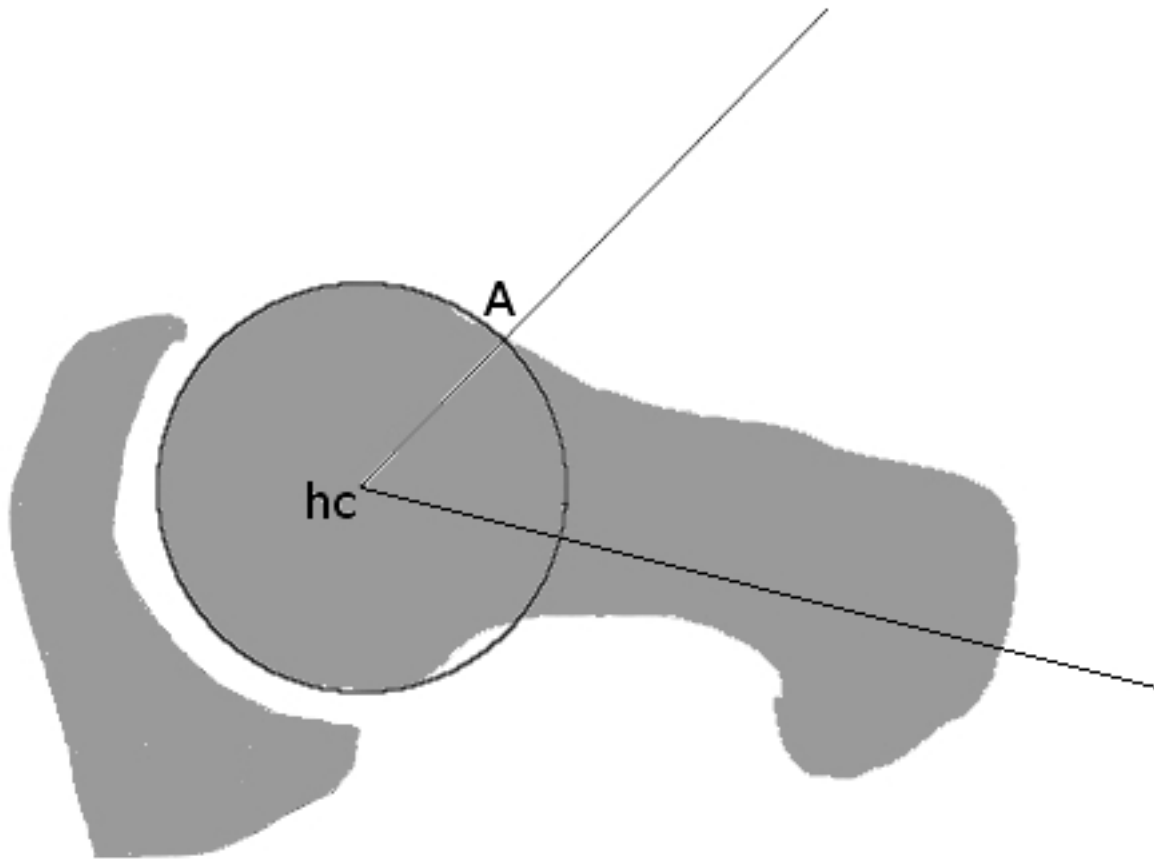


Figure 6-1: Diagram of the alpha angle calculation from the axial oblique image as described by Beaulè et al. (2005). A circular template is drawn over the femoral head. From the center of the femoral head template (hc) a straight line is drawn laterally along the long axis of the femoral neck parallel to the anterior bony cortex. A second line is then drawn from the center of the femoral head template to intersect the point where the femoral head-neck contour exits the circular template (point A). The resulting angle between the two lines is the alpha angle.

The alpha angle was subsequently modified for computed tomography (CT) by Beaulè et al. (2005) with a minor change in the placement of the femoral neck axis line (Figure 6-1) (11, 12). With the femoral neck axis line placed parallel to the anterior femoral neck cortex Beaulè et al. (2005) found that their data *closely reproduced* that of Nötzli et al.'s work (2002).

MRI and CT are the imaging modalities of choice for the evaluation of the hip for their ability to image intra-articular causes of symptoms. However, they are expensive, not always readily

available, and, in the case of CT, involve ionizing radiation. The ability to make a diagnosis of this abnormality, particularly among younger populations, before major joint damage occurs, using a non-ionizing, widely available, and cost-effective technique for early detection of cam-type FAI would be highly beneficial. Ultrasound can provide imaging of the soft tissues associated with the hip when looking for musculoskeletal disorders and effusions of the joint (14). Ultrasound can also provide images of the cortical surfaces of the anterior femoral head and neck equivalent to the oblique axial view described by Nötzli et al. (2002) and Beaulè et al. (2005) for MRI and CT, respectively. To date, no study has explored the usefulness of ultrasound in the quantification of femoral head asphericity using an identical method of measurement as an accepted reference standard.

We hypothesize that ultrasound-based calculations of the alpha angle are a clinically useful alternative to those obtained using a CT gold standard when the same measurement method is applied. Our aim was to demonstrate the usefulness of ultrasound in providing objective evidence of FAI when CT is not available or not appropriate.

Table 6-1: Indications for hip evaluation among 28 patients (39 hips) presenting for CT

Indication	Number of hips (% of 39)
Suspected FAI	14 (37%)
Groin/Hip/other pain	6 (16%)
Included as part of bilateral examination	5 (13%)
Dysplasia	3 (8%)
Avascular necrosis	3 (8%)
Post-surgery assessment	3 (8%)
Osteitis Pubis	2 (5%)
Osteoarthritis	1 (2%)
Labral tear	1 (2%)
History of # NOF	1 (2%)

Key:

FAI – femoroacetabular impingement

# NOF – Fractured neck of femur

## 6.4 Materials and Methods

Ethics approval for the study was received from the Monash University Human Research Ethics Committee. Participants were consecutively recruited from amongst patients attending the department for CT imaging of one or both hips for a variety of indications (Table 6-1). Written informed consent was obtained from all patients. We prospectively recruited 28 patients with a mean ( $\pm$ SD) age of 40 ( $\pm$ 13.9) y. Eleven patients had bilateral examinations, providing a total of 39 hip joints for analysis. The cohort consisted of 15 women and 13 men with measurements taken from 21 right hips and 18 left hips.

### *CT method*

A Toshiba Aquilion 16 TSX101-A Version 3.38 ER005 (Toshiba Medical Systems Corporation, Tochigi- Ken, Japan) was used to perform a 300-mm helical acquisition from above the acetabulum to below the lesser trochanter. Scan parameters were 135 kVP, 120–170 mA and 400-mm field of view. The reconstruction interval (slice thickness) was 2.5 mm. The data block was rotated to create a group of axial oblique images passing through the plane of the femoral neck, from which the alpha angle was calculated by an Institute of Radiography-registered radiographer according to the method described by Beaulè et al. (2005) (Figure 6-2).



Figure 6-2: Computed tomography axial oblique image of the right hip of a 36-y-old female referred for possible femoroacetabular impingement. Calculated alpha angle is 73°.

#### *Ultrasound method*

Ultrasound imaging was then performed immediately after the CT using a General Electric Logiq E9 (Wauwatosa, WI, USA) by the same sonographer with 15 y' experience in ultrasound of the musculoskeletal system. Imaging was performed with the patient positioned supine with the leg extended and with approximately 20 degrees of internal rotation. A linear ML6-15 MHz transducer was used to obtain a longitudinal image of the femoral head- neck junction with the cortical surface of the femoral head maximally exposed, and the distal attachment of the iliofemoral ligament visible on the image (Figure 6-3). Acoustic settings included 12-MHz center frequency, dynamic range at 60 dB, acoustic output 100% and virtual

convex for wide field of view and good resolution at depth. High cross- beam setting (spatial compounding) was used to improve lateral resolution and ensure good visualization of as much of the femoral head cortex as possible to aid drawing of the circular femoral head template. Three separate images were taken of each hip, with the transducer repositioned between each image. The three ultrasound images were exported to a separate workstation for analysis.

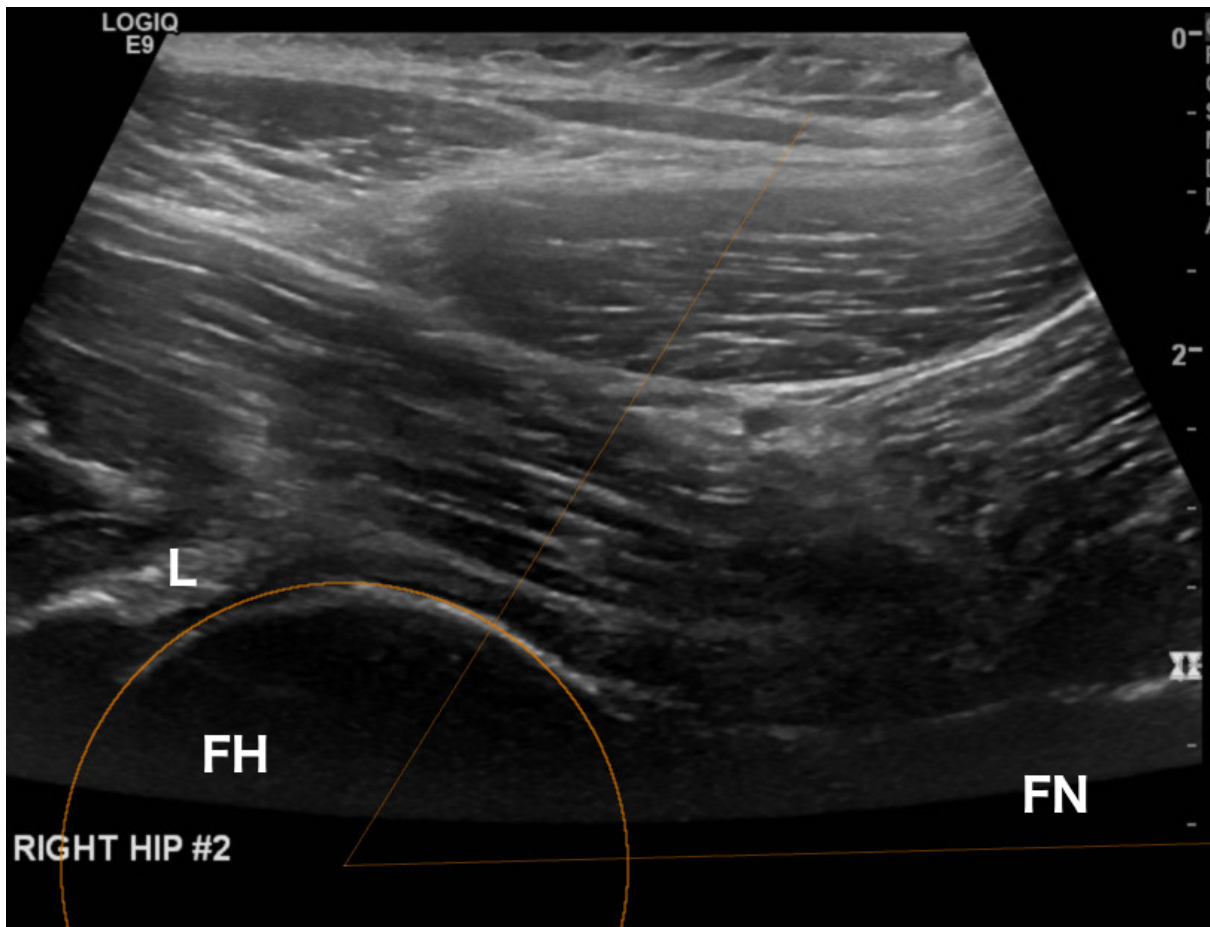


Figure 6-3: Ultrasound image of the anterior femoral head and neck used for calculation of the alpha angle. A circular template is fitted over the femoral head. A straight line is drawn from the center of the circular template along the femoral neck parallel to the anterior femoral neck. Another line is drawn from the center of the circular template to intersect the point where the femoral head-neck contour leaves the template. The angle between the two lines is the alpha angle. FH = femoral head; FN = femoral neck; L = acetabular labrum.

Ultrasound images were analyzed by the principal author blinded to the CT result using Gimp

for Windows 2.8.0 (Free Software Foundation, Boston, MA, USA), a GNU Public License image manipulation program. The alpha angle was calculated by drawing a circular template fitted closely over the femoral head using the ellipse-select tool on the computer. Care was taken to ensure that a true circle was drawn by ensuring that the width and height of each circle were equal. Composition guides (center lines) were turned on so that the center of the circle could be accurately located. The pixel address of the center was noted by placing the cursor over the marked center. The selected circle was then stroked (painted over the selected outline) to draw the femoral head template (Figure 6-3).

A straight line was then drawn from the pixel address of the center of the femoral head template laterally, parallel to the anterior femoral neck cortex. Another line was then drawn from the center to cross the femoral head circular template at the point where the femoral head outline leaves the circle, equivalent to point “A” in the description by Nötzli et al. (2002) (Figure 6-1). The angle between these two lines was then calculated using the Measure Tool on the computer software and noted as the ultrasound alpha angle. The alpha angle measurements were repeated for the other two ultrasound scans by the same investigator at intervals of greater than 48 h so that the result of previous calculations was not known. After the third image was analyzed, the investigator averaged the measurement of all three alpha angles. The mean alpha angle was used as the final ultrasound alpha angle.

The principle researcher was then un-blinded to the CT measurements and the CT and mean ultrasound alpha angle compared.

#### *Statistical analysis*

The average of the absolute difference between the three-repeated ultrasound alpha angles measurements and the CT reference standard for all hips were compared using the Bland-Altman test of agreement between two methods of clinical measurement. The null hypothesis was that no difference exists between ultrasound and CT calculations of the alpha angle.

An alpha angle  $>55^\circ$  obtained on the CT was classified as an abnormal test result (11).

Statistical analyses were carried out using SPSS (v 21.0, Chicago, IL, USA) and a  $p < 0.05$  afforded significance. The accuracy for ultrasound was calculated using the formula for observational error:

Equation 6-1 Formula for accuracy

$$Accuracy = \frac{(True\ Positive + True\ Negative)}{(True\ Positive + False\ Positive + True\ Negative + False\ Negative)}$$

## 6.5 Results

Mean ( $\pm$ SD) (range) measurements for CT and ultrasound were 62.5° degrees ( $\pm$ 14.2°) (37.7°–90.9°) and 64.5° degrees ( $\pm$ 12.6°) (44.4°–101.6°), respectively (Table 6-2).



Table 6-2: Measured alpha angle for each hip calculated from CT and three separate ultrasound images (N = 39) with mean difference between ultrasound and CT

Hip Number	CT alpha angle	US alpha angle #1	US alpha angle #2	US alpha angle #3	mean difference CT:US
1	46.7	50.00	54.00	52.00	-5.30
2	52.7	66.28	67.90	64.11	-13.40
3	65.2	62.50	51.32	54.18	+9.20
4	88.9	73.58	63.18	76.48	+17.82
5	61.7	57.34	65.39	66.33	-1.32
6	49.0	53.30	54.65	55.64	-5.53
7	56.8	62.69	63.44	58.91	-4.88
8	78.0	63.87	67.29	67.58	+11.75
9	66.2	75.47	75.34	79.63	-10.61
10	52.0	55.10	58.45	56.28	-4.61
11	48.4	48.97	52.87	32.83	+3.51
12	90.9	76.80	76.60	77.97	+13.78
13	64.6	62.83	55.11	61.05	+4.94
14	76.1	67.65	58.66	62.46	+13.18

15	67.4	65.39	80.14	68.35	-3.89
16	61.4	65.82	69.78	71.99	-7.80
17	53.6	64.56	56.11	57.82	-5.90
18	44.3	89.07	96.10	93.73	-48.67
19	63.1	59.19	71.63	75.38	-5.63
20	44.5	45.72	48.14	57.57	-5.98
21	50.5	58.32	65.72	61.60	-11.38
22	67.9	64.97	74.53	71.16	-2.32
23	89.2	79.31	79.97	85.48	+7.61
24	82.1	59.63	56.62	57.44	+24.20
25	67.6	65.02	68.02	66.10	+1.22
26	54.1	73.14	51.88	57.05	-6.59
27	49.4	73.60	53.92	47.69	-9.00
28	76.6	93.12	72.19	45.83	+6.22
29	48.3	102.62	102.31	99.81	-53.28
30	37.7	58.59	52.36	42.78	-13.54

31	45.7	47.22	42.34	43.65	+1.30
32	67.7	56.63	58.35	55.67	+10.79
33	87.0	81.49	83.32	77.67	+6.21
34	51.2	55.49	49.68	51.11	-0.89
35	48.7	60.81	58.07	44.33	-5.70
36	74.8	58.02	54.36	68.61	+14.47
37	61.8	59.40	57.66	64.33	+1.34
38	73.0	48.37	57.06	61.56	+17.34
39	71.7	86.37	94.02	86.88	-17.39

Key: CT = three-dimensional Computed Tomography; US - ultrasound

Large discrepancies of  $>45^\circ$  were noted in two cases where there was a history of femoral neck osteoplasty in patients of advanced y ( $>60$  y). We found 62/116 (53%) instances where ultrasound returned a greater value than CT with an average overestimation of  $12.4^\circ$ .

Ultrasound underestimated the CT on 54/116 (47%) occasions, with the average under-call being  $10.1^\circ$ . Average coefficient of variation for the three ultrasound measurements was 8.28% (1%–33.7%).

The mean of the absolute differences between the ultrasound-measured alpha angles and the CT measurements was  $10.5^\circ$  ( $p < 0.001$ ) (95% CI  $6.9^\circ$ – $14.0^\circ$ ) (Figure 6-4).

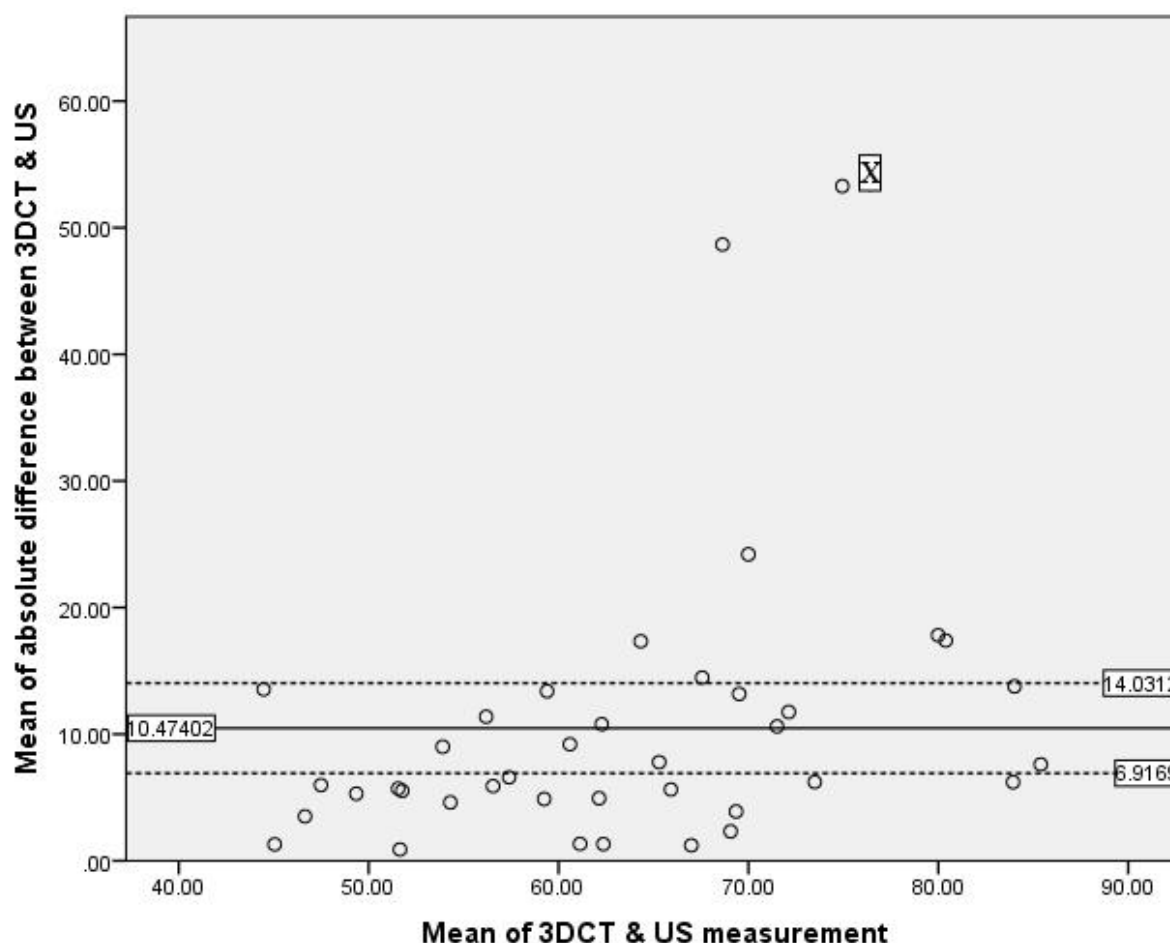


Figure 6-4 Results. Bland-Altman scatter plot of the mean of the computed tomography (CT) and ultrasound measurements of the alpha angle (X-axis) versus the mean absolute difference between the CT and the ultrasound measurements of the alpha angle (Y-axis). The null hypothesis of no difference

is represented as the X-axis at 0 difference. The 95% confidence intervals are drawn at 6.917 and 14.031 (*dashed lines*).

Twenty-three positive tests among all hips were obtained using the CT alpha angle result as the gold standard. Sixty-three of 69 (91.3%) individual ultrasound measurements resulted in a correct positive diagnosis (sensitivity of 91.3%). The specificity of ultrasound was 43.75% with 21 of 48 negative ultrasound measurements deemed to be truly negative. The positive predictive value (PPV) was 0.7 and the negative predictive value (NPV) was 0.78. Overall accuracy of the ultrasound-derived alpha angle was calculated at 0.718.

## 6.6 Discussion

In our study, we have, for the first time used CT as the reference standard and compared it with ultrasound to calculate the alpha angle using an identical method from the same image vector. Our results demonstrate that ultrasound could replicate the image vector used by CT, and that the sensitivity of ultrasound measurements was good with PPV = 0.7 and the NPV = 0.78. Overall accuracy of the ultrasound-derived alpha angle was calculated at 0.718.

Many attempts to radiologically characterize a *cam* deformity associated with FAI have been made using a variety of imaging modalities and methods (11, 12, 53, 139, 157). Ultrasound has been used to detect the presence or absence of a non-spherical head-neck junction in the evaluation of cam-type FAI by Buck et al. (2011) who found that the NPV of such a deformity was between 50%–80% (162). Nötzli et al. (2002) used MRI to quantify the degree of femoral head asphericity by measuring a femoral head-neck alpha angle. CT has been used to confirm the original findings of Nötzli et al. (2002), with the femoral neck axis line placed parallel to the anterior femoral neck bony cortex, rather than through the center of the narrowest part of the femoral neck (Figure 6-2) (12). Alpha angle calculations using the method of Beaulè from an axial oblique image have been widely adopted, including at our

facility, and these can be reproduced using ultrasound imaging (12, 161, 192). The plane of imaging described is regularly used to assess for hip joint effusion and is achievable even for a novice sonographer (Figure 6-3) (14, 193). We have used ultrasound to image the anterior aspect of the femoral head-neck junction to calculate the femoral head-neck alpha angle, using the original work of Nötzli et al. (2002) and Beaulè et al. (2005) as the gold standard. Ultrasound has been used in the past to calculate the femoral head-neck alpha angle and compared with MRI arthrography as the reference standard (161, 162). In a study of 50 patients with suspected cam-type FAI based upon clinical examination, ultrasound was compared with MRI arthrography and inter-rater agreement was evaluated between two readers (162). Reader one showed a strong significant relationship between ultrasound measurements and MRI (Pearson correlation coefficient (PCC) 0.891) (162). A second reader, however, showed only poor-to- moderate agreement (PCC 0.425) (162). The authors in that study used a different approach to measure the alpha angle on MRI and ultrasound, with the method of Nötzli et al. (2002) used for calculating the alpha angle in the MRI images, but a tangential line between the most distal insertion of the joint capsule and the femoral head contour was used as the femoral neck axis line for the ultrasound images (162). The poor inter-rater reliability demonstrated in this study is likely the result of using two different methods for calculation of the alpha angle for each modality.

In another study, 40 patients with a pre-surgical axial oblique MRI and a diagnosis of cam-type FAI were examined with ultrasound, with a mean alpha angle on MRI of 64.8° and on ultrasound of 61.2° in neutral position, and 65.6° with 20° of internal rotation (161). PCC in this study ranged 0.67–0.77 ( $p < 0.0001$ ) for neutral position and 20° of internal rotation respectively (161). Inter-observer reliability for ultrasound calculation of the alpha angle ranged 0.86–0.95 (161). In this study, the MRI alpha angle was calculated according to Nötzli et al's method; whereas on ultrasound, the femoral neck axis line was positioned parallel to the anterior visible surface of the femoral neck following the method of Beaulè et al. (2005)

(161). This discrepancy may have affected the resultant measurements but was not addressed by the author. A more accurate and reliable evaluation of ultrasound to calculate the alpha angle would be performed if the same method were used for both imaging modalities.

We have found that ultrasound can replicate the image vector used on CT to calculate the femoral head-neck alpha angle. Using the CT alpha angle result as the gold standard and using the same method for both modalities, the sensitivity of ultrasound was calculated at 91.3% and overall accuracy at 0.718. However, calculations of the alpha angle performed using ultrasound are significantly different than CT. Our study has shown an average discrepancy between the reference standard CT and ultrasound calculation of alpha angles of slightly more than 10° and low specificity of 43.75%.

Our study had several limitations. Ultrasound imaging was performed by a single sonographer. Hence, inter-observer reliability of the ultrasound alpha angle calculation could not be evaluated in this series, although Lerch et al. (2013) estimated inter-observer reliability of ultrasound- measured alpha angle at 0.86–0.95.

Two instances occurred in this series where very large differences were observed between the ultrasound and CT values of alpha angle. The largest difference exceeded 53° (Marked X in Figure 6-4). Both patients were older individuals (>60 y) with a history of femoral head-neck osteoplasty. In the case demonstrating the largest discrepancy, very minor osteophyte formation (mushrooming) has occurred, causing the bony contour to break the femoral head circular template on the ultrasound but not on the CT image (Figure 6-5). Bony cortical irregularities such as those related to advanced age or prior surgery may significantly reduce the accuracy of the ultrasound alpha angle calculation. Hence, ultrasound may not be suitable to patients of advanced y or those with a history of prior hip surgery or disease. We believe, however, that ultrasound calculation of the alpha angle would have its major application in younger individuals before major joint damage secondary to FAI, and who have had no prior hip disease.

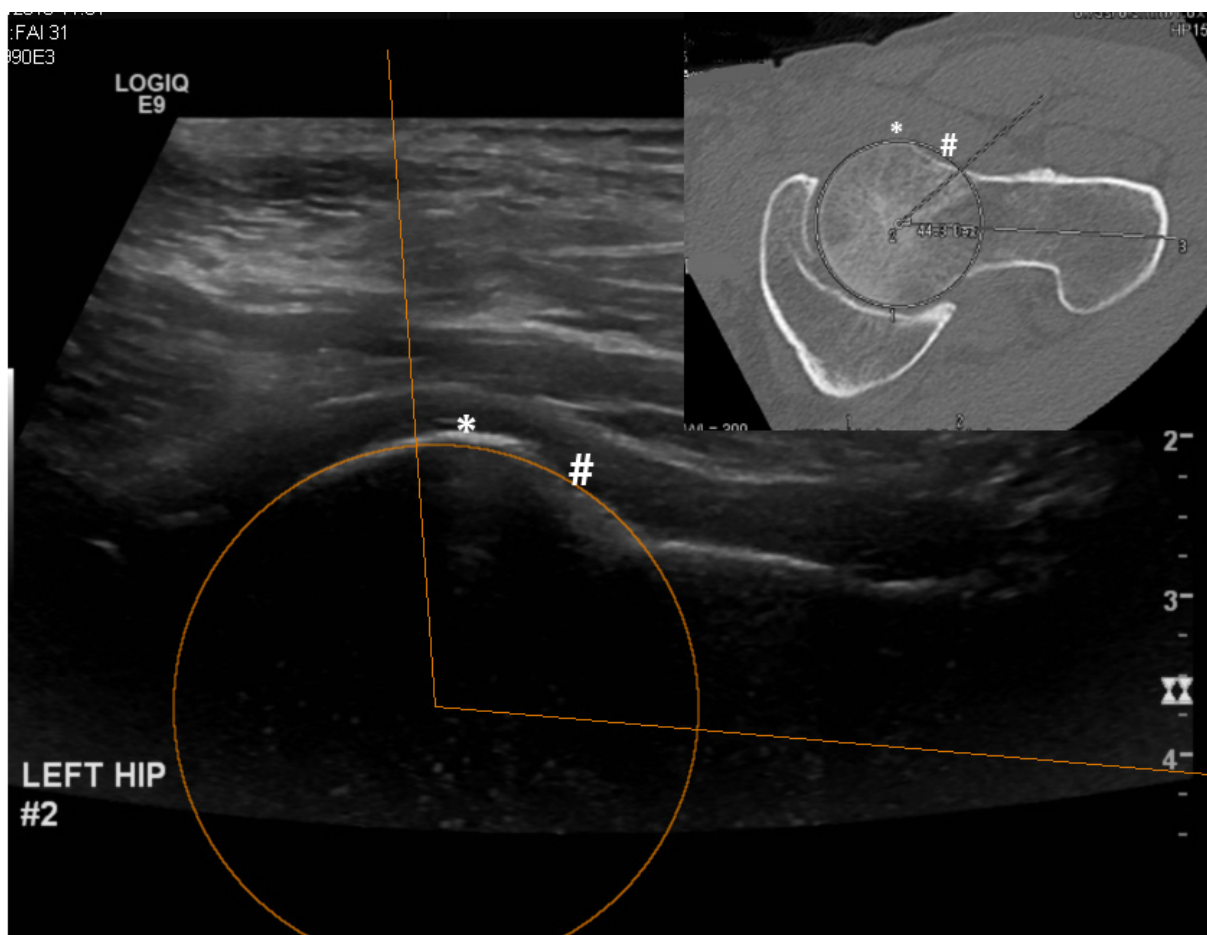


Figure 6-5 Left hip ultrasound and computed tomography (CT) (insert) performed for groin pain of a 63-y-old female with a history of femoral head-neck osteoplasty (#) for cam femoroacetabular impingement. Dramatic difference between the ultrasound and CT calculation of the alpha angle caused by very mild degree of mushrooming (\*) of the femoral head-neck junction causing the contour to exceed the femoral head template on the ultrasound but not on the CT image. The difference in the ultrasound and CT alpha angles exceeds 53° and is marked X on the Bland-Altman scatter plot (Figure 6-4).

Our technique has revealed a large range in the co-efficient of variation across the ultrasound measurements, ranging from 1% to almost 34%. Nötzli et al. (2002) found an intra-observer variation of  $\pm 3\%$  for their measurements of alpha angles when using MRI, indicating that placement of the base and inclination (to point A) lines have an acceptable error. Our technique involves placing the baseline parallel to the anterior cortical surface by visual approximation, perhaps giving rise to this larger variation. Variation in the ultrasound alpha angle may be reduced if a line is first drawn parallel to the anterior cortex and then translated



to intersect the center point of the femoral head template before calculation of the alpha angle.

## **6.7 Conclusion**

Young active patients with groin pain have a wide differential diagnosis including stress fractures of the femoral neck, iliopsoas tendonitis, tears of the adductor tendons and nerve entrapment syndromes. Ultrasound has many well-established advantages over CT and MRI, is better suited to preliminary screening and can be performed quickly as a general investigation of groin symptoms that might include as a differential diagnosis FAI. Ultrasound demonstrates good sensitivity and good NPV in calculation of the femoral head-neck alpha angle compared with CT. Ultrasound calculation of the alpha angle does, however, suffer poor specificity and perhaps further studies should be undertaken to refine the described technique. Ultrasound measurement of the alpha angle in young patients with no prior hip surgery or trauma can, however, provide objective evidence of cam-type FAI in symptomatic young patients and direct patients to more established imaging techniques where clinically appropriate.

## ***Chapter 7* Ultrasound Screening for Adverse Local Tissue**

### **Reaction after Hip Arthroplasty**

DAVID J. ROBINSON,<sup>\*</sup> STEVEN LEE,<sup>\*</sup> PAUL MARKS,<sup>y</sup> and MICHAL E. SCHNEIDER<sup>z</sup>

<sup>\*</sup>Healthcare Imaging Services, The Avenue X-Ray & MRI, The Avenue Hospital, Windsor, Victoria, Australia;

<sup>y</sup>Imaging Associates Box Hill, Box Hill, Victoria, Australia;

<sup>z</sup>Department of Medical Imaging & Radiation Sciences, Faculty of Medicine, Nursing and Health Sciences, Monash University, Clayton, Victoria, Australia

Ultrasound in Med. & Biol., Vol. 43, No. 7 (2017) pp. 1549–1556.

**doi:** 10.1016/j.ultrasmedbio.2017.02.001

This chapter is an exact copy of the journal paper referred above.

The final aim of this thesis is to demonstrate the usefulness of ultrasound in the characterisation of soft tissue findings around hip prostheses after hip arthroplasty. Small accumulations of wear debris adjacent to the prosthetic hardware can impinge upon the native bone, causing tissue destruction and necrosis, giving rise to aseptic loosening. Currently MARS MRI is the modality of choice for detection and monitoring of ALTR after hip joint arthroplasty. This modality is limited, however, by an inability to clearly visualise soft tissues adjacent to the prosthesis, as well as the issues pertaining to costs to patients and availability especially in rural, remote and/or underdeveloped countries. These same characteristics also

make the modality unsuitable to screening an asymptomatic population. This manuscript shows that ALTR development in asymptomatic well-functioning prostheses may be recognised earlier using ultrasound rather than MARS MRI. Ultrasound findings after hip arthroplasty can assist in the management of patients who may require a more frequent surveillance program.

## 7.1 Declaration for Thesis Chapter

Declaration by candidate

In the case of Chapter 7, the nature and extent of my contribution to the work was the following:

<b>Nature of Contribution</b>	<b>Extent of Contribution</b>
Concept,	80 %
Collecting data,	100 %
Data analysis,	90 %
Writing published draft	90 %

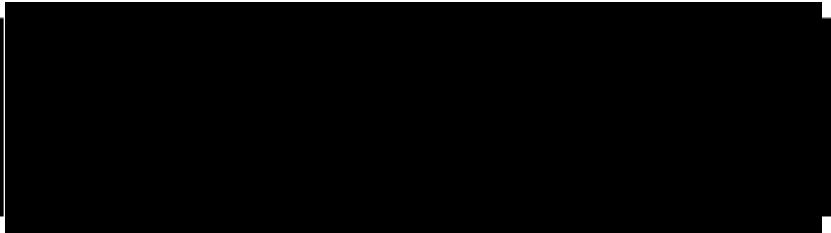
The following co-authors contributed to the work. If co-authors are students at Monash University, the extent of their contribution in percentage terms must be stated:

<b>Name</b>	<b>Nature of Contribution</b>	<b>Extent of Contribution (%) for student</b>
-------------	-------------------------------	---

		<b>Co-authors only</b>
A/Prof Michal Schneider	Intellectual input on data analysis and manuscript editing	N/A
Dr Steven Lee	Intellectual input on data analysis and collection, and manuscript editing	N/A
Dr Paul Marks	Intellectual input on manuscript editing	N/A

The undersigned hereby certify that the above declaration correctly reflects the nature and extent of the candidate's and co-authors' contributions to this work\*.

Candidate's Signature

	Date :  15 November 2018
---	--------------------------------

Main Supervisor's Signature

	<p>Date : 15 November 2018</p>
--	------------------------------------

# **Ultrasound Screening for Adverse Local Tissue Reaction after Hip Arthroplasty**

## **7.2 Abstract**

Early detection of adverse local tissue reaction (ALTR) to prosthetic hip wear debris is vital to improve the success of revision surgery. Magnetic resonance imaging with metal artefact reduction sequencing (MARS MRI) is considered the modality of choice to provide cross-sectional imaging of the soft tissues. The areas adjacent to the prosthesis are, however, not readily imaged using these protocols. Ultrasound has also been recommended as an imaging modality in the follow-up of hip replacement surgery. We decided to characterise the typical ultrasound findings in a group of patients undergoing routine biennial review of arthroplastic hips with particular reference to the hip capsule, femoral neck and iliopsoas bursa and tendon adjacent to the implant. Fifty-two patients with a mean ( $\pm$ SD) age of 60.4 ( $\pm$ 12) y were prospectively recruited. Twelve patients had bilateral hip prostheses, giving 64 hips for analysis. Mean ( $\pm$ SD) age of the prosthesis in situ was 8.2 ( $\pm$ 3.3) y. Data were grouped on the basis of the shape of the iliofemoral ligament. The median (range) maximal anteroposterior synovial thickness was 5 (2–8) mm in the normal concave iliofemoral ligament group and 7 (4–56) mm in the abnormal straight/convex iliofemoral ligament group ( $p = 0.001$ ). The anteroposterior iliopsoas tendon measurement was 5 (3–8) mm in the normal group and 5 (4–8) mm in the abnormal group ( $p = 0.065$ ). ALTR development in asymptomatic well-functioning prostheses may be recognised earlier using ultrasound rather than MARS MRI by carefully assessing the shape of the iliofemoral ligament. Ultrasound findings of an abnormal straight or convex ligament may be suggestive of early ALTR and warrant streaming of patients to a more frequent surveillance program.

### **Keywords**

### 7.3 Introduction

Hip replacement surgery is an increasingly common medical procedure in Western societies, with the rate increasing from 17,105 in 2001 to 44,419 in 2015 according to data from the Australian Joint Replacement Registry (3). Implant loosening without evidence of infection (aseptic loosening) is the most common reason for implant failure and subsequent revision surgery (16). Early implant failure is a concern because the success of revision hip replacement surgery may be reduced by the higher complication rate, soft tissue necrosis and reduction of femoral bone stock (17, 178, 194, 195). Adverse local tissue reaction (ALTR) to wear debris, mainly from the prosthetic bearing, may hasten aseptic loosening and result in early prosthetic failure (16). ALTR causing thickening of the soft tissues at the femoral neck of a resurfacing prosthesis may be a portent of osteolysis and impending femoral neck failure (13, 16, 18, 19, 38, 196).

Some symptomatic complications such as component suboptimal positioning, implant loosening and peri-prosthetic fracture can be optimally imaged with plain radiography (19, 196). Periodic follow-up of both symptomatic and asymptomatic patients, using cross-sectional imaging of the soft tissues, has also been recommended for the detection of ALTR around hip prostheses (13, 18, 19, 196). The role of follow-up with imaging has, however, been unclear with respect to asymptomatic well-functioning hip replacements. Current imaging protocols lack the sensitivity to detect ALTR in asymptomatic well-functioning prostheses, even though high rates of ALTR have been reported in this cohort (4, 18, 19, 196). Even asymptomatic, well-functioning prostheses should be periodically assessed with cross-sectional imaging to look for evidence of accumulating wear debris that may hasten aseptic loosening, femoral neck osteolysis and early prosthesis failure (4, 179).



Magnetic resonance imaging (MRI) with metal artefact reduction sequencing (MARS) algorithms have been suggested for the assessment of periprosthetic soft tissues (13, 18, 19, 196). MRI is, however, not optimal because the tolerability of some types of metal implants have to date not been evaluated (19, 196). MRI is a relatively expensive modality not widely available in all areas, has a prolonged scan time and is contraindicated in patients with some ferromagnetic implants, making MRI not always suitable for screening an asymptomatic well-functioning prosthesis (55). Further, the soft tissues adjacent to the native or prosthetic femoral neck are not readily imaged even with MARS MRI (54). There is a need to develop tolerable, low-cost imaging protocols for routine follow-up of all patients after hip replacement surgery.

Ultrasound (US) has been suggested as a cross-sectional imaging modality for assessment of the post-arthroplastic hip as it is readily available, relatively cost effective and radiation and artefact free (18, 19, 196). Only limited information is available in the literature on the usefulness of US screening of the asymptomatic hip prosthesis. We decided to characterize the typical US findings with particular reference to the shape of the anterior hip capsule, the presence of fluid or solid material about the femoral neck and the iliopsoas bursa and size of the iliopsoas tendon in a group of patients undergoing routine biennial review of arthroplastic hips.

## **7.4 Methods**

Ethics approval for the study was received from the Monash University Human Research Ethics Committee. Volunteers were consecutively recruited from patients attending the department for routine biennial review of their hip prosthesis. Patients were included if they were over 18 y of age and gave written informed consent to use their de-identified medical records for the research project. All patients, both symptomatic and asymptomatic for

prosthesis complications, were imaged using X- ray and ultrasound of one or both prosthetic hips.

#### **7.4.1 X-ray protocol**

A Phillips Optimus 65 (Hamburg, Germany) was used to obtain X-ray images of the pelvis and hips(s). An anteroposterior (AP) view of the pelvis centred on the symphysis pubis with the patient supine was performed at 73 kVP, 32 mAs. A horizontal beam lateral at 90 kVP and 160 mAs centred on the femoral neck of the prosthetic hip with a portable grid was also performed with the contralateral leg raised.

#### **7.4.2 Ultrasound protocol**

Ultrasound imaging was performed for all patients by the same operator (D.R.) using a GE Logiq E9 (Wauwatosa, WI, USA). A linear high-frequency broadband transducer (ML6-15) operating in harmonics mode at 15 MHz, 60 dB, low cross-beam and virtual convex field of view was used to image the anterior and posterior prosthesis at the level of the articulation and femoral neck. Images of the iliopsoas bursa and tendon superior and inferior to the prosthetic joint were also obtained. In corpulent patients, a 9 L linear transducer was used at 9 MHz harmonics and 69 dB, specifically to image the posterior prosthesis. The prosthetic acetabulum, femoral head and neck were imaged together in an anterior axial oblique plane approximately parallel to the plane of the iliofemoral ligament with the patient supine and leg extended with 15° of internal rotation (Figure 7-1). The maximum AP thickness of the pseudo-synovium was measured from the anterior aspect of the native or prosthetic femoral neck to the posterior aspect of the joint capsule. The measurement was performed two more

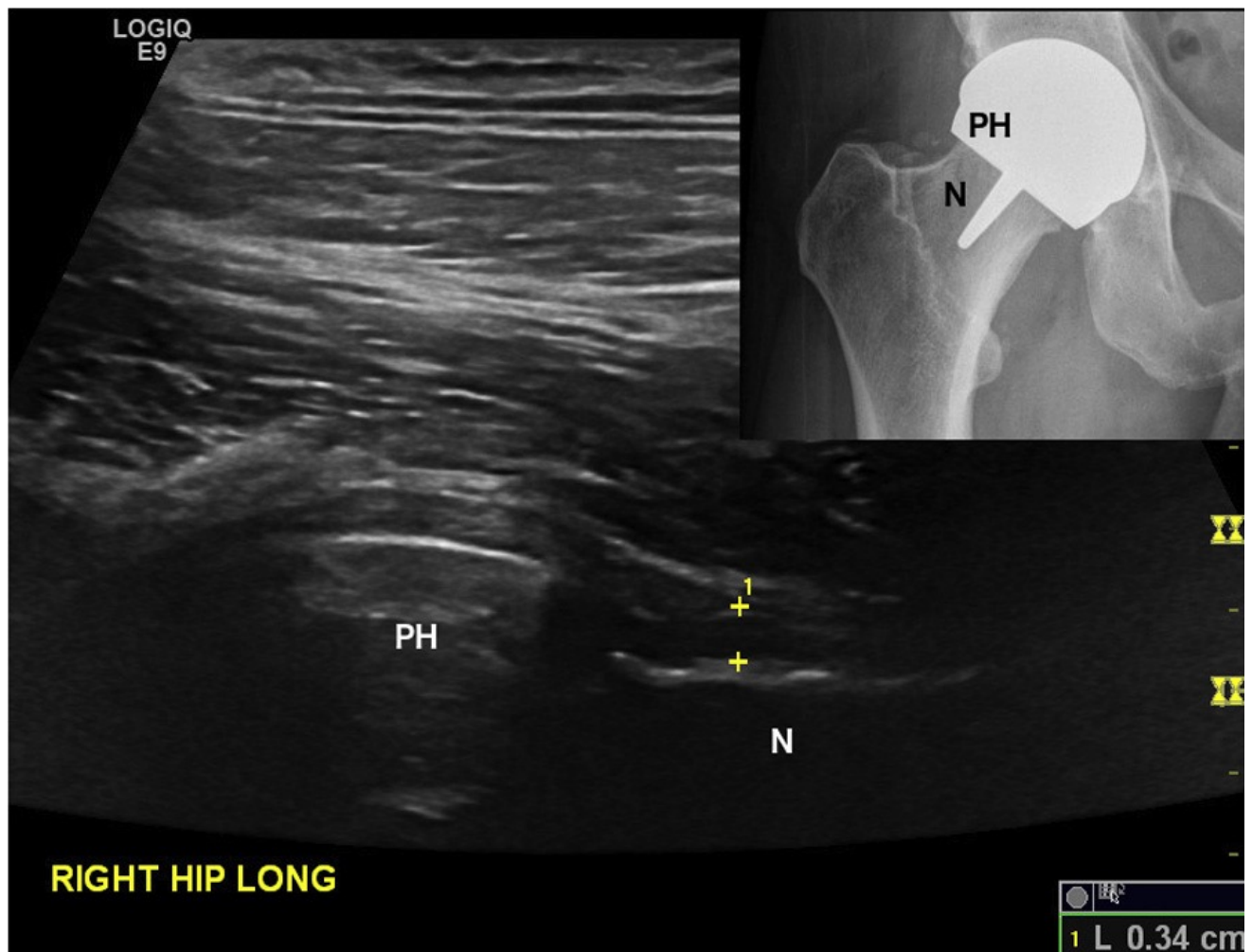


Figure 7-1: Anterior axial oblique ultrasound of a 44-y-old man with an asymptomatic right-sided MITCH resurfacing in situ for 5 y revealing the anterior recess with concavity of the iliofemoral ligament and maximal anteroposterior measurement 0.7 cm, considered within normal limits. Inset: Corresponding anteroposterior weight-bearing plain X-ray (cropped) revealing no adverse features. N = native femoral neck; PH = prosthetic femoral head.

times, and the average of the three measurements was taken and recorded as AP synovium.

The iliopsoas bursa and tendon were imaged in the transverse and sagittal planes at the level of the joint and superior to it, to just above the inguinal ligament. The maximal AP thickness of the iliopsoas tendon was measured at the level of the prosthetic joint with the leg in the same position as described above (Figure 7-2). This measurement was performed two more times, and the average of the three was taken as the final AP tendon measurement. Images were also obtained of the posterior prosthetic neck and acetabulum in an axial oblique plane

along the line of the long axis of the femoral neck where possible.

Patients whose blood metal ion levels were elevated or who reported symptoms attributable to the hip, such as groin pain and clicking, were assigned to a symptomatic subgroup. Patients who did not report pain attributable to the hip prosthesis and had normal blood metal ion levels were assigned to the asymptomatic group. X-ray and ultrasound results were analysed with the non-parametric  $\chi^2$  test of variance to compare the symptomatic and asymptomatic groups. AP synovium and maximal AP iliopsoas tendon measurements of the symptomatic and asymptomatic groups were compared using the Mann–Whitney U- test for non-parametric data. The AP synovium and AP iliopsoas tendon measurements were regrouped using a normal concave or (abnormal) straight/convex shape of the iliofemoral ligament as seen on US as the variable, and the analysis was repeated. Statistical analyses were carried out using SPSS (Version 21.0, IBM, Armonk, NY, USA), and a  $p < 0.05$  indicated significance.

Table 7-1 Patient demographic data according to implant type

Implant type	Number (%N)	No. of Males	Patient Age (y)	Time <i>In situ</i> (y)
Birmingham resurfacing (BHR)	45 (70%)	29	63.98 ( $\pm$ 12.36)	9.6 ( $\pm$ 2.61)
Stryker MITCH	10 (16%)	9	50.1 ( $\pm$ 7.06)	4.2 ( $\pm$ 1.68)
Articular surface replacement (ASR)	5(8%)	3	47.5( $\pm$ 14.03)	7.8 ( $\pm$ 1.17)
Total Hip replacement (THR)	3 (5%)	1	69( $\pm$ 1.63)	4 ( $\pm$ 2.16)
ADEPT resurfacing	1 (1%)	1	60	2
Total	64 (100%)	43	60.4( $\pm$ 12)	8.2( $\pm$ 3.3)

Key: In situ – number of years hip prosthesis in situ

## 7.5 Results

Fifty-two patients were prospectively recruited with a mean  $\pm$  standard deviation (SD) age of  $60.4 \pm 12$  y. Twelve patients had bilateral hip prostheses, yielding 64 hips for analysis. Mean ( $\pm$ SD) age of the prosthesis in situ was  $8.2 \pm 3.3$  y (Table 7-1). Twenty-four (38%) patients had signs or symptoms that could be attributed to the hip prosthesis, including elevated blood ion levels. The most common presenting symptom was groin pain (Table 7-2). The remaining 40 hips were considered to be asymptomatic.

Ultrasound was able to reliably image the periprosthetic soft tissues of all hips. Forty-three (67%) hips presented with a normal ultrasonic appearance ( $p < 0.001$ ). Fifty-three (83%) X-rays were classified as normal ( $p < 0.001$ ).

Ten of 20 (50%) symptomatic cases manifested some abnormality on one or both imaging modalities (Figure 7-3). Two of these were sonographically normal, but X-ray revealed radiographic bone lucency at the lateral acetabulum and proximal femoral shaft of an ASR (buttock pain) and an ADEPT THR (raised blood metal ion levels) respectively (Table 7-3).

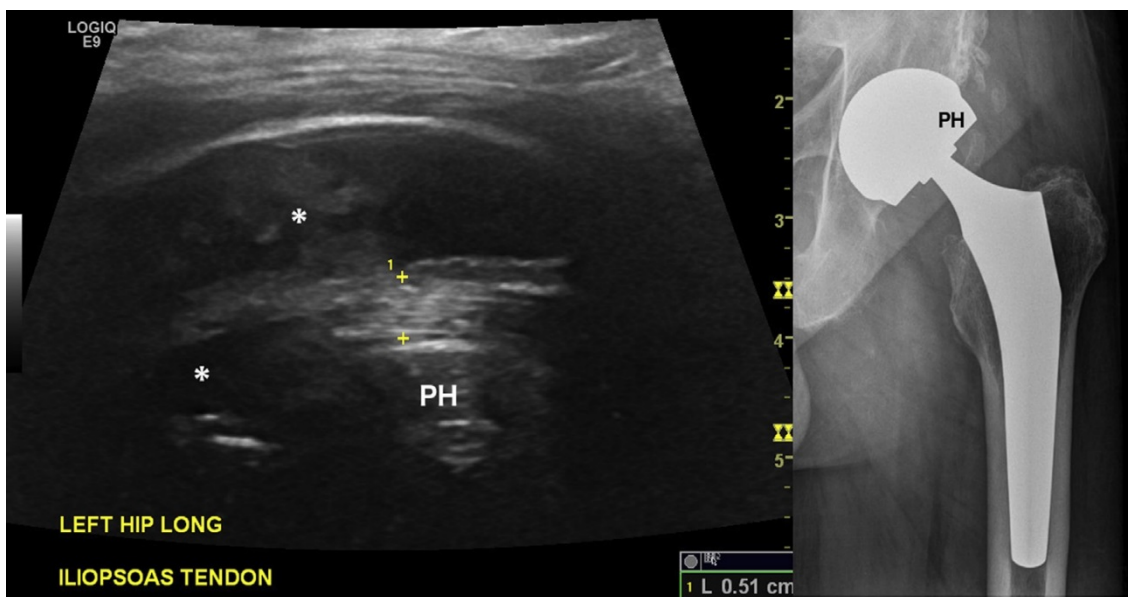


Figure 7-2: Anterior sagittal ultrasound of a 76-y-old male patient with an asymptomatic revision uncemented Accolade THR in situ for 7 y revealing the iliopsoas tendon in the longitudinal plane (between 1 cursors). The normal fibrillary pattern of the tendon is noted, and the anteroposterior measurement is approximately 5 mm. Note the large iliopsoas bursa surrounding the tendon filled with fluid and soft tissue echoes (asterisks). PH 5 prosthetic femoral head. Right inset: Corresponding anteroposterior plain X-ray (cropped) revealing moderate heterotopic bone formation, but no periprosthetic lucency or fracture.

In the asymptomatic group, 17 of 44 (39%) cases manifested some abnormality on imaging (Figure 7-4 and Figure 7-5). Two of these manifested some abnormality on X-ray but were normal on US. In both cases the abnormality was peri-articular heterotopic bone formation visualised only on the X-ray. Another patient with heterotopic bone formation also manifested

an unrelated small iliopsoas bursal effusion and thickened, heterogeneous iliopsoas tendon on US imaging. One patient manifested synovial thickening that was only visible posteriorly on US; however, the X-ray was normal (Figure 7-6).

The median (range) maximal AP synovial thickness was 5 (2–26) mm in the symptomatic group and 5 (3–56) mm in the asymptomatic group ( $p = 0.339$ ). The AP iliopsoas tendon measurement was 5 (3–6) mm in the symptomatic group and 5 (3–8) mm in the asymptomatic group ( $p = 0.355$ ) (Figure 7-2).

All hip data measurements were regrouped according to whether the normal concave shape of the anterior iliofemoral ligament was preserved, disregarding the presence or absence of symptoms. Hips in which the normal iliofemoral ligament concavity was preserved were labelled the normal group, and the remainder were labelled abnormal. AP synovium and AP iliopsoas tendon data were then re-analysed using this grouping. The median (range) maximal AP synovium measured 5 (2–8) mm in the normal (concave iliofemoral ligament) group and 7 (4–56) mm in the abnormal group ( $p = 0.001$ ). The AP iliopsoas tendon measurement was 5 (3–8) mm in the abnormal group and 5 (4–8) mm in the normal (concave iliofemoral ligament) grouping ( $p = 0.065$ ).

Table 7-2 Patients presenting for imaging of the post-arthroplastic hip with symptoms (N 5 26)

Symptom	Number of hips (% of 64)
Groin Pain	9 (14%)
Blood metal ions	6 (9%)
Other pain*	5 (8%)
Iliopsoas clicking/pain	2 (3%)
Sciatica	1 (2%)
Decreased range of motion	1 (2%)
Leg rash	1 (2%)

\* Other pain = buttock, thigh or trochanteric pain.

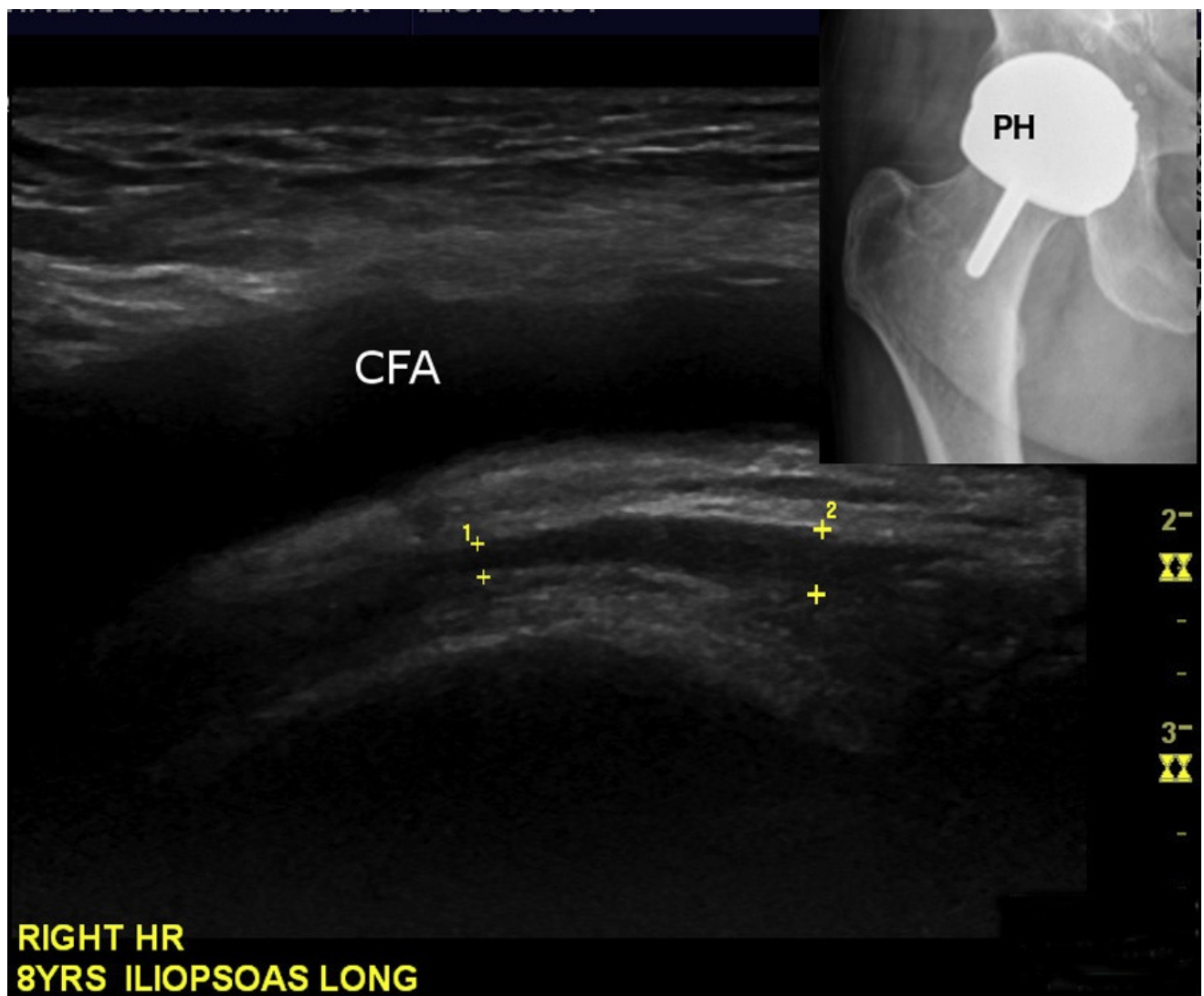


Figure 7-3: Anterior longitudinal ultrasound of a 75-y-old man with right-sided BHR in situ for 8 y presenting with iliopsoas symptoms, demonstrating a trace of fluid in the iliopsoas bursa (denoted by + cursors 1 and 2). The common femoral artery (CFA) is used as a sonographic window to aid detection of this small effusion lying just medial to the iliopsoas tendon (not shown). The prosthetic femoral head (PH) lies below this level. Inset: Corresponding weight-bearing anteroposterior X- ray (cropped) revealing satisfactory alignment.



Table 7-3 X-ray and US results of all implants found to have abnormal imaging (N = 24)

Hip type	Side	Time in situ (y)	Symptoms	X-ray finding	US finding
BHR	L	7	Nil	Moderate neck narrowing	Neck narrowing
BHR	L	8	Nil	NAD	Large iliopsoas bursa
BHR	R	10	Nil	Mild neck narrowing	NAD
BHR	L	10	Nil	NAD	Small iliopsoas bursa
BHR	L	8	Nil	Mild neck narrowing	Enlarged head-neck offset
BHR	L	12	Nil	Mild neck narrowing	Iliopsoas bursa fluid & synovial thickening
BHR	R	12	Nil	NAD	Moderate iliopsoas bursa
BHR	L	11	Nil	NAD	Moderate iliopsoas bursa
BHR	L	5	Nil	NAD	Small iliopsoas bursa
BHR	L	13	Nil	Mild heterotopic bone	NAD
BHR	L	11	Nil	Mild neck narrowing	NAD
MITCH	R	3	Nil	NAD	Synovial thickening posterior
BHR	L	13	Nil	Heterotopic bone	Small iliopsoas bursa/thick heterogeneous tendon
Accolade THR	R	7	Nil	NAD	Large joint and bursal effusion
BHR	R	12	Nil	NAD	Small iliopsoas bursa
BHR	L	10	Nil	NAD	Small iliopsoas bursa
BHR	R	14	Nil	Heterotopic bone	NAD
BHR	R	10	Pain	NAD	Moderate iliopsoas bursa
BHR	R	11	Pain	NAD	Large effusion
BHR	R	10	Groin pain	NAD	Synovial thickening 9mm
THR	R	2	Buttock pain	NAD	Posterior collection
BHR	R	13	Clicking	NAD	Small iliopsoas bursa
BHR	L	11	Pain post-fall	NAD	Large head-neck offset

BHR	R	7	Groin pain	NAD	Moderate iliopsoas bursa
ADEPT THR	R	2	Metal ions	Lucency, femoral stem	NAD
ASR	R	8	Buttock pain	Lucency, lateral acetabulum	NAD
ASR	R	10	Metal ions	NAD	Moderate iliopsoas bursa

ASR = articular surface replacement; BHR = Birmingham hip resurfacing; NAD = no abnormality detected; THR = total hip replacement;

## 7.6 Discussion

Wear debris and the subsequent cellular reactions in the implant bed are considered to be significant contributors to the development of periprosthetic osteolysis and aseptic loosening in both metal-on-metal and metal- or ceramic-on-polyethylene prosthetic hip bearings (16, 35). Wear particles originate predominantly from the prosthetic bearing and are shed directly into the synovial fluid from which they are removed by macrophages in the fluid and the pseudo- synovium lining the prosthetic joint (16). ALTR to wear debris can lead to significant soft tissue and bone damage, including necrosis and osteolysis, making revision surgery more difficult with additional post-surgical complications (17, 194, 195). Current protocols lack the sensitivity to detect ALTR in the asymptomatic well-functioning prosthesis (4). Early identification of a poorly performing prosthesis provides the option of early revision, which is thought to provide a better long-term outcome (18).

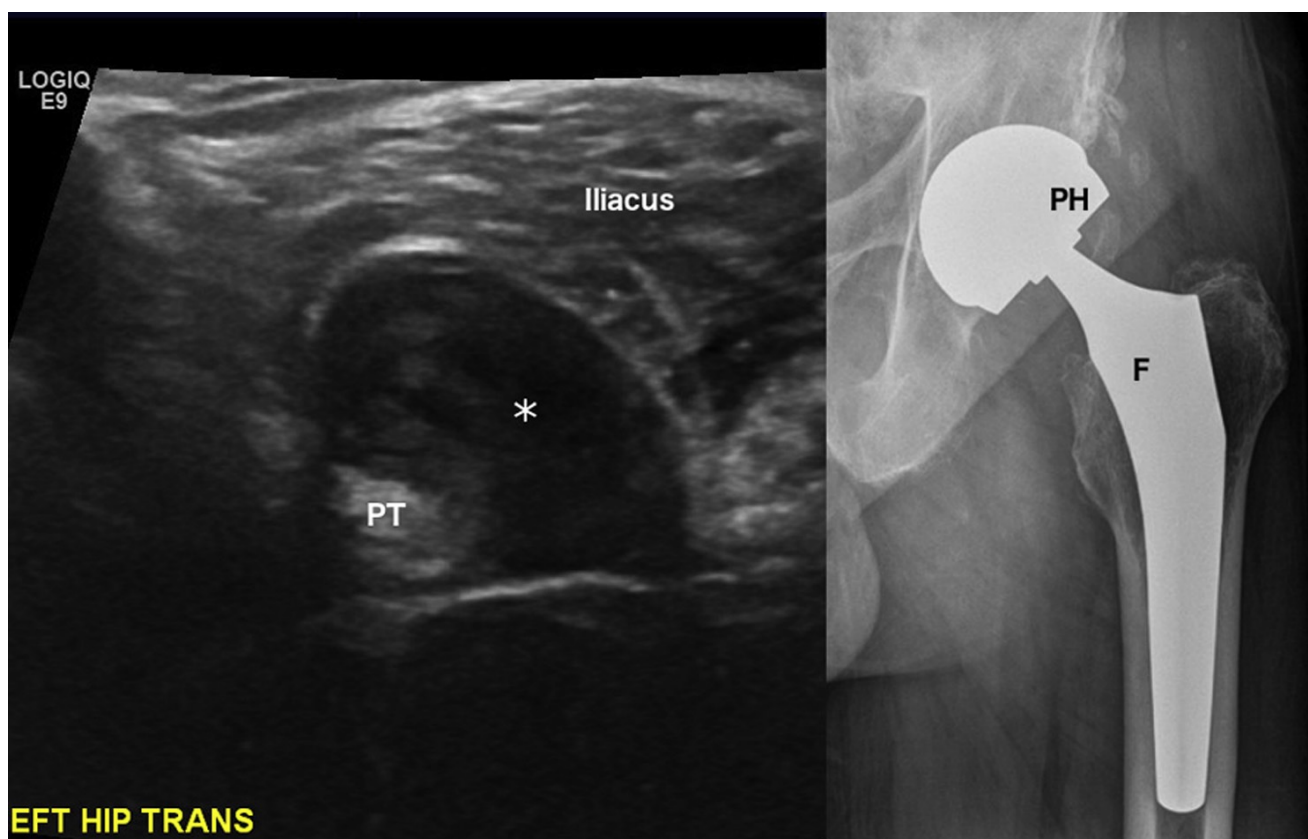


Figure 7-4: Ultrasound of a 77-y-old male patient with an asymptomatic revision left THR in situ for 8 y. Transverse view of the iliopsoas tendon and bursa above the level of the inguinal ligament. An enlarged iliopsoas bursa (asterisk) is noted with low-level echoes denoting the presence of thickened synovial tissue and/or wear debris displacing the iliacus muscle anteriorly (iliacus). PT = psoas tendon. Right inset: Anteroposterior weight-bearing X-ray (cropped) revealing normal alignment and no periprosthetic lucency or fracture.

Previous studies examining the utility of US in the follow-up of hip arthroplasty have focussed on large- diameter metal-on-metal implants and the presence of periprosthetic soft tumour masses and fluid collections, with results varying from poor to almost perfect agreement with MARS MRI (4, 54, 56, 181, 187, 188). Small-volume ALTR adjacent to the implant or native femoral neck in the case of resurfacing can, however, be missed on MRI even when using metal artefact reduction protocols. Such accumulations have been reported to progress if left untreated (179, 181). It is important to detect small but aggressively expanding ALTR as early as possible to minimise bone and soft tissue damage (187, 188). Ultrasound has previously been used in the investigation of the hip and immediate

surrounding soft tissue structures. The hip joint capsules of 6 adult cadaveric specimens, 58 healthy children and 105 children with unilateral transient synovitis were investigated with US by Robben et al. (1999), who found that a concave anterior capsule rules out effusion (193). In another study, Tormenta et al. (2012) examined the anterior hips of patients with symptomatic osteoarthritis using US and found an enlarged iliopsoas bursa in 19 of 860 patients (2.2%), indicating that US can detect associated findings of osteoarthritis with high reproducibility (197).

Increased soft tissue and/or fluid in cases of synovitis can be readily seen on US scanning in the anterior axial oblique plane (14, 193). Soft tissue thickening such as might be seen with intracapsular ALTR at the anterior recess will cause the normally concave iliofemoral ligament to become straight or convex with larger accumulations (193).

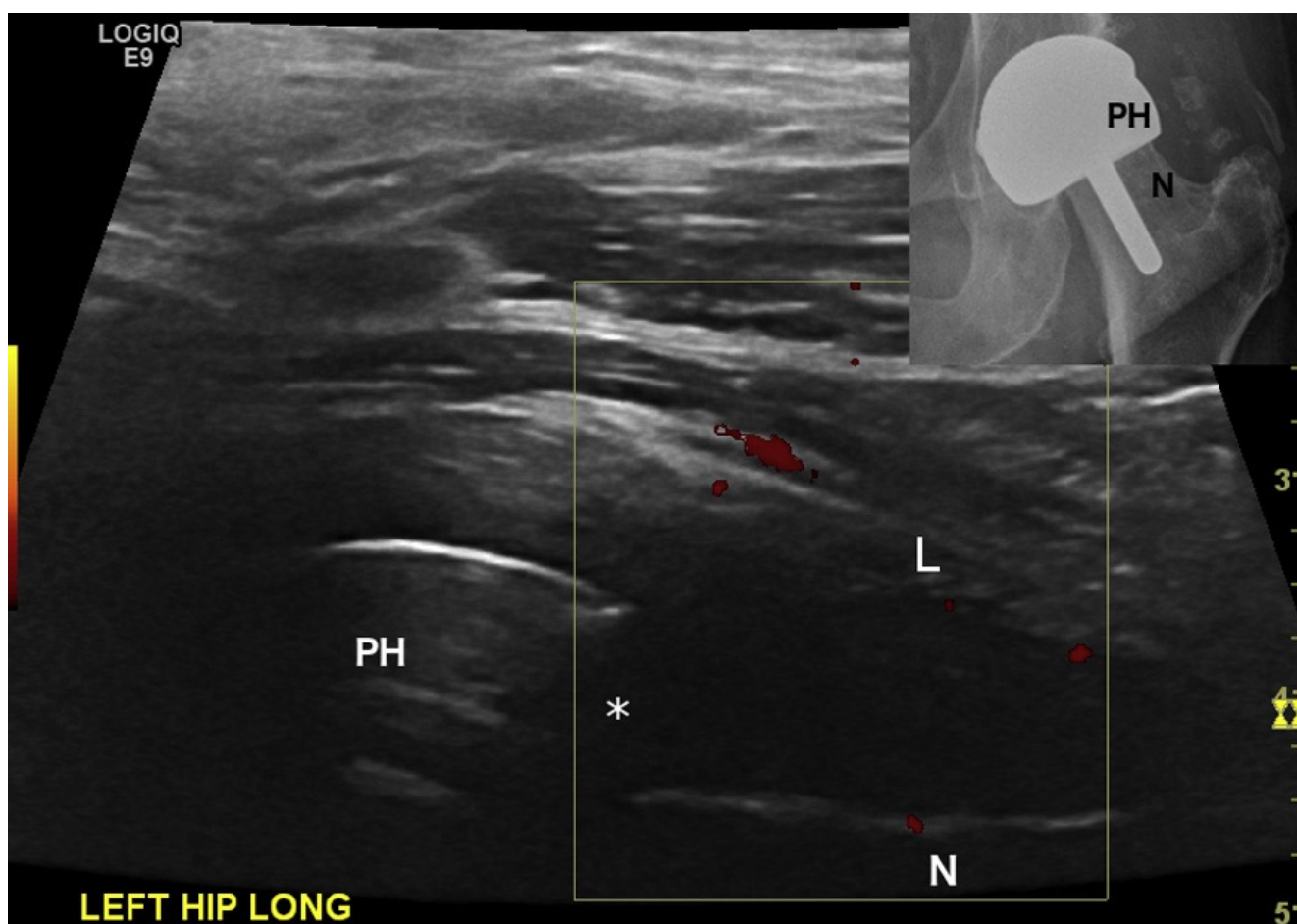


Figure 7-5: Anterior axial oblique ultrasound of a 65-y-old woman with an asymptomatic left BHR in situ for 7 y revealing a large “step” (asterisk) between the prosthetic head and native femoral neck,

suggesting femoral neck osteolysis. Colour box reveals no detectable vascularity. The head-to-neck gap is 9 mm (asterisk). The iliofemoral ligament (L) has lost the normal concavity and appears straight. Inset: Corresponding X-ray revealing a mild degree of femoral neck thinning. PH = prosthetic femoral head; N = native femoral neck.

The anterior joint capsule has been assessed in 152 asymptomatic metal-on-metal hip resurfacings with repeat US (188). In this study, a depth of fluid at the anterior joint line exceeding 15 mm was considered to be a pathologic effusion (188). The incidence of an effusion (grade 3 lesion) either progressing or developing to pseudo-tumour was found to be 43% (3/7) in this series (188). In another study, Siddiqui et al. (2014) evaluated 19 patients with metal-on-metal hip arthroplasties with either large-diameter bearing or who were symptomatic using MARS MRI as the imaging gold standard (54). A measurement of 4 mm between the femoral neck and the hip capsule was used as the threshold of normal according to the “joint expansion” pattern of Nishii et al. (2012) (54). Joint effusion using this classification was detected in 10 of 19 patients (53%) on US (average: 8 mm), none of which was detected by MARS MRI (54). Pseudo-tumour was found to be common (7/10) in the presence of joint effusion (54).

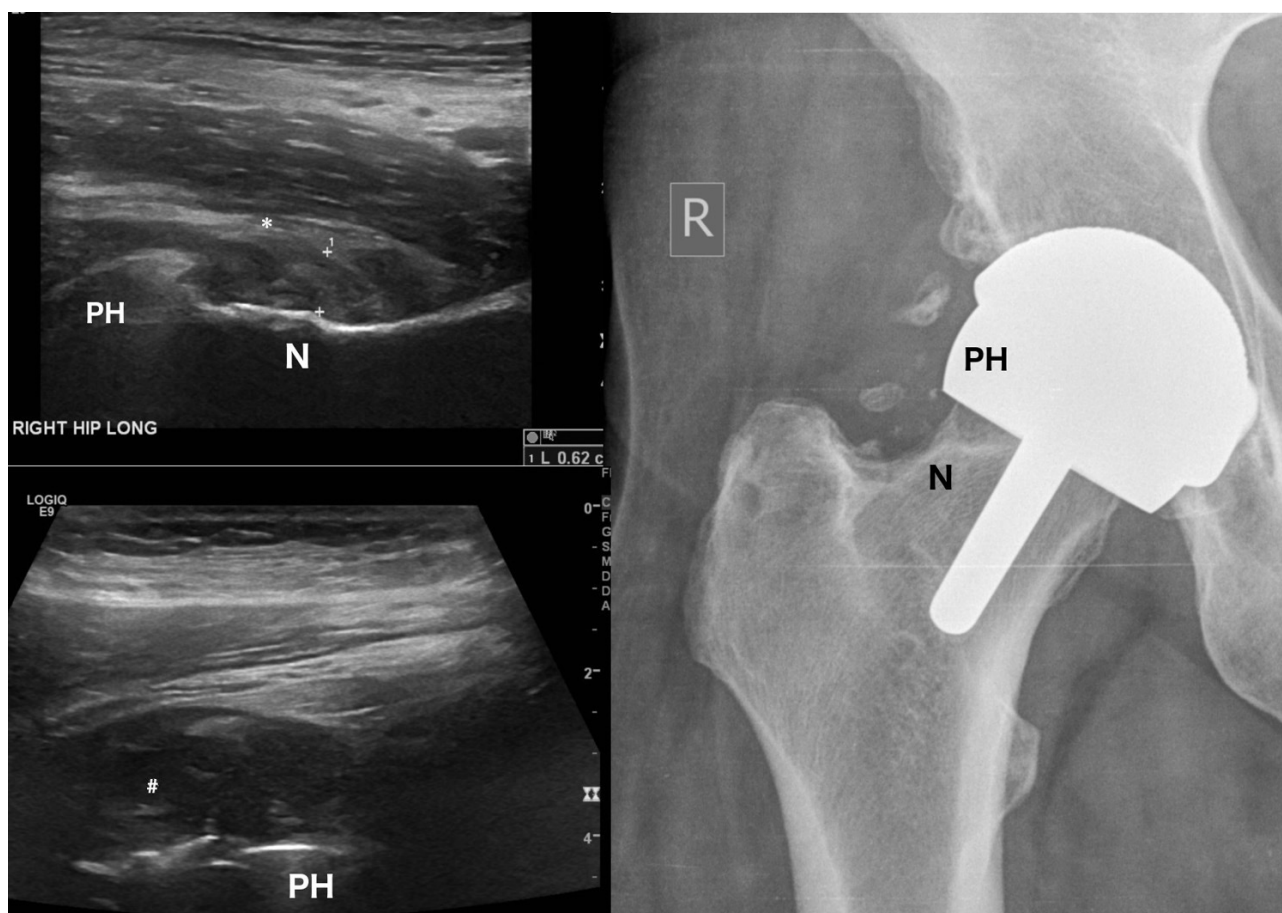


Figure 7-6: Sixty-seven-year-old female patient with an asymptomatic right BHR resurfacing in situ for 12 y. Axial oblique image of anterior recess reveals synovial tissue within normal limits at 6 mm (between 1 cursors). However, the iliofemoral ligament (asterisk in left upper image) is noted to be convex as it passes over the femoral head and neck. Posterior axial oblique of the posterior joint (left lower image) demonstrates marked synovial thickening (#). Right image: Anteroposterior X-ray (cropped) revealing normal alignment with no periprosthetic lucency or fracture seen. PH = prosthetic femoral head; N = native femoral neck.

We used an anterior axial oblique view of the anterior hip and measured the maximal AP thickness of the anterior synovial recess of the joint space of prosthetic hips and found that when symptomatic and asymptomatic groups are compared, there is no significant difference in the measurement (193). However, we found that when hips with a straight or convex iliofemoral ligament are compared with those with the normal concave pattern, a difference in the AP synovial measurement becomes apparent (7 mm vs. 5 mm, respectively,  $p < 0.001$ ). Changes in the shape of the iliofemoral ligament from concave to straight or convex is an

important sign of soft tissue thickening that may represent wear debris accumulating deep to the hip capsule (18, 19, 196). Wear debris may be present at the posterior or anterior recess in isolation; hence the posterior aspect of the prosthesis must be scanned as part of the routine imaging protocol. A normal anterior ligament shape or AP measurement does not preclude thickening or fluid posteriorly (16).

We found no statistically significant difference in iliopsoas tendon thickness between symptomatic and asymptomatic groups or between normal and abnormal iliofemoral ligament groupings. Larger fluid and/or synovial tissue collections can decompress anteromedially into the medial compartment containing the common femoral artery and vein and superiorly under the inguinal ligament into the pelvis and may present as a pelvic mass (78, 198). We found that the majority (9/13, 69%) of iliopsoas bursal effusions were present in asymptomatic patients.

There are several limitations to our investigation. US in this study was performed by a single sonographer (D.R.). Inter-observer reliability of US cannot therefore be determined from this series. Validation of the US findings, such as surgical confirmation, was performed in only one case to date, where a large ALTR was caused by trunnionosis. The false-positive and false-negative rates of US cannot be calculated. For patients who underwent prior US imaging of their prosthesis, the protocol used was different from that described here. Thus, no longitudinal data are available; however, all patients were part of a routine biennial review program and previous imaging had been considered normal. Abnormal findings observed in our cohort are yet to be re-imaged. Some minor abnormalities seen in this series may therefore not persist or progress. Approximately 20% of small US- detected lesions have, however, been reported to progress further, and these lesions require early identification and early follow-up to detect progression (188).

Our findings have further clarified the abnormal characteristics of a hip prosthesis imaged using US. ALTR development in asymptomatic well-performing prostheses may be



recognised earlier using US by carefully assessing the shape of the iliofemoral ligament. US findings of an abnormal straight or convex ligament may be suggestive of early ALTR and warrant streaming of patients to a more frequent surveillance program. Where a measurement of the femoral neck–joint capsule distance is performed, we suggest 7 mm as a threshold of normal. Small iliopsoas bursa effusions can be detected using the femoral artery as a sonographic window. Given the increasing and common use of hip replacement surgery, we believe that regular follow-up with imaging is warranted among all patients and suggest that US is better suited to the serial evaluation of asymptomatic well- functioning hip prostheses than any other cross-sectional imaging modality.

## ***Chapter 8* Discussion**

Our research has demonstrated that ultrasound can provide important imaging of impingement syndromes at the shoulder and hip. The ability of ultrasound to provide high resolution images of soft tissues around these anatomical structures enables imaging earlier in the disease process before symptoms become apparent. Other more invasive or radiation-based imaging methods may no longer be required. Ultrasound provides not only the ability to image impingements at the shoulder and hip, but also facilitates regular follow-up imaging and monitoring of disease progression, an improvement on currently accepted imaging methods.

### **8.1 Ultrasound as an angiography tool in the assessment of the PCHA**

Our novel approach to assessing the PCHA as it exits the quadrilateral space was able to reliably demonstrate the PCHA on colour Doppler, and allowed an assessment of the rate of occlusion with ABER in the normal population. We performed our sampling from a posterolateral approach on the arm in contrast to the trans-axillary approach described by other groups (45, 199). This technique does not require partial abduction of the arm to visualise the PCHA, and allows assessment of the Doppler characteristics of the PCHA in genuine neutral arm position, and comparison of these results with those with the arm abducted and externally rotated. Doppler sampling as the PCHA emerges from the quadrilateral space, downstream from any potential stenosis is a more conventional and well understood method of using ultrasound to test for occlusion and stenosis in any vessel (48).

The diagnosis of QSS using ultrasound involves angiographic confirmation of stenosis of the PCHA with ABER of the arm serving as a proxy for entrapment of the axillary nerve within the quadrilateral space (10, 45). Until now, x-ray angiography and MRA have been the modalities of choice in the assessment of the PCHA (10, 46). These modalities are invasive, expensive and not readily available or repeatable. There is no gold standard method of testing for PCHA stenosis on ABER. The only two previous studies using asymptomatic volunteers have been the angiography study reported by Cahill and Palmer (1983), and the MR angiography study reported by Mochizuki (1994) (10, 46). These two methods, namely angiography and MR angiography have numerous disadvantages, precluding their use to screen a large, asymptomatic population due to radiation dose concerns, cost and availability. There has, until now, existed some controversy over the relevance of impingement of the PCHA on abduction and external rotation (46). Axillary nerve entrapment must be an intermittent process, as it only occurs in abduction and external rotation - in a neutral arm position no entrapment occurs. It is only after repeated and prolonged compromise such as would occur in overhead athletes that neuropathy of the axillary nerve commences and symptoms become apparent. More recently, it has become apparent that repeated PCHA compromise in the quadrilateral space can also lead to PCHA degeneration and aneurysm formation (61). If the causative fibrous bands are common, then there must exist a rate of neurovascular bundle impingement amongst the general population that is asymptomatic, as not all would abduct and externally rotate the arm sufficiently often to cause a symptomatic neuropathy or aneurysm formation to develop (10, 46, 61, 67, 86). Most of the previous studies in the literature were limited by small sample sizes.

Our patient group is much larger than those previously described, with a wide range of ages and our results are more likely to be clinically relevant to a healthy population than the findings reported by Mochizuki et al, which were based on a very small sample size of only six volunteers (46). In our sample of healthy volunteers, PCHA compromise with arm in

ABER occurred in 15/93 (16.13%) compared to rates previously described between 0% and 80% (10, 46). We believe that this rate of PCHA stenosis or occlusion is more likely to be representative of the status in the general population. Our results show that axillary neurovascular impingement is detectable in the normal population, but that it is relatively uncommon.

Without external impingement upon the axillary neurovascular bundle there can be no axillary neuropathy, and hence QSS should not exist. Sonographic evidence of PCHA stenosis or occlusion confirms the existence of neurovascular bundle mechanical impingement with ABER and is a useful confirmation that QSS may be present, or that the patient is at risk of aneurysm development. Conversely, absence of PCHA stenosis or occlusion on ABER effectively rules out QSS as a diagnosis in a patient suffering symptoms consistent with QSS. Presenting symptoms consistent with QSS in these cases are more likely to have a more common pathology such as rotator cuff disease or subacromial bursitis.

Ultrasound is already widely used in the assessment of shoulder pain and is readily available, non-invasive and requires no contrast materials. The assessment of the PCHA with ultrasound is simple, quick and was well-tolerated by patients. We suggest that ultrasound could be a useful screening test for patients with symptoms consistent with QSS. The posterolateral approach that we have described provides maximal Doppler signal strength, maximizing the rate of visualization and successful acquisition of the Doppler trace. While the prevalence of arterial thoracic outlet syndrome in an asymptomatic population is low, it nevertheless must be ruled out as a cause or contributor to damped PCHA signal on ABER. Hence, we suggest that the distal subclavian artery should also be assessed in neutral and ABER.

Ideally, our technique would be tested not just with normal volunteers but also among patients

suffering with QSS. True sufferers of QSS are extremely rare and hence it is difficult to recruit patients for a comparative study using our technique and another independent technique. It would be ideal if patients suspected of QSS would be referred for ultrasound before the advent of fatty atrophy. Future studies should aim to recruit a group of patients with QSS well before significant fatty atrophy is demonstrated. These patients should then undergo angiography of the PCHA using both Doppler ultrasound and MR prior to surgical intervention. The findings of both modalities could then be directly compared and our ultrasound technique validated for diagnosis of QSS. Ideally, both modalities would be performed again after surgery to prove reconstitution of PCHA blood flow on ABER post quadrilateral space decompression. Elite overhead athletes such as throwers and swimmers could have ultrasound screening for PCHA compromise on ABER at a young age. Patients who record a positive result should be considered at risk for PCHA aneurysm formation and be periodically followed up to determine the rate at which PCHA impingement leads to PCHA aneurysm.

Ultrasound assessment of PCHA occlusion requires proof of absence of blood flow, something that is difficult to establish. The absence of a Doppler signal could be due to patient movement, poor technique or malpositioning of the ultrasound transducer. This occurs most frequently when the operator is inexperienced in the technique, but less so as the anatomical arrangements in neutral and ABER become better understood. Ultrasound has a low interoperator reliability when examining small peripheral vessels (48, 59). However, approaching the PCHA from behind with the artery passing directly toward the transducer maximises the Doppler shift and hence the signal strength and sensitivity to blood flow making detection of this relatively small peripheral vessel much simpler. The ability to repeat the ultrasound, and simplicity of the ultrasound examination conveys an advantage here in that the absence of blood flow in the PCHA can be confirmed in real time by repeating the

arm movement from neutral to ABER. The cessation of PCHA flow can be noted as it occurs – essentially by performing a number of repeated measurements. This is one of the considerable advantages that ultrasound has over other modalities. Ultrasound has been used in the assessment of aTOS where, in a similar method to that described here, the loss of blood flow is noted with abduction of the arm, and confirmed by repeating the test a number of times (51, 101, 102). It is not known if a false positive rate exists for angiography or MR angiography, but it must presumably exist as not all PCHA will opacify sufficiently in ABER to be visualised.

## **8.2 Comparison of measurement of the hip alpha angle between ultrasound and 3DCT**

It is now widely accepted that primary OA does not exist and that in fact all OA is secondary to damage to the joint from mild previously undetected hip dysmorphia (15, 33, 129).

We have used ultrasound to image the anterior aspect of the femoral head-neck junction to determine the ability of ultrasound to detect and characterize a cam lesion. The plane of imaging described is regularly used in the assessment of the hip for effusion. This ultrasound plane of imaging is already taught to novice sonographers. We used 3DCT as the reference standard and compared it with ultrasound to determine the degree of femoral head-neck contour abnormality using the alpha angle method devised by Nötzli et al (2002) (11). Using the CT alpha angle result as the gold standard and using the same method of calculation in both modalities, the sensitivity of ultrasound was calculated at 91.3% and overall accuracy at 0.718, with a large Coefficient of Variation (1-33.7%) of repeated measurement by a single operator. Inter-rater reliability of ultrasound measurement of the alpha angle was not tested in our study. Other imaging modalities have not performed well in determining the alpha angle.

X-ray derived alpha angles may vary by up to 30 degrees depending on radiographic

projection used and some views may miss the asphericity completely (147, 152). Other x-ray derived measurements of femoral head asphericity have poor agreement (149-151). A study using MRI found that the alpha angle determined from the conventional axial image was significantly different to that determined from a radial plane image ( $p < 0.001$ ) (157). Other studies utilising ultrasound have used different methods to calculate the alpha angle and compare those to angles obtained by MRI, resulting in poor inter-rater reliability or only moderate correlation (161, 162).

Detection of FAI prior to joint damage in elite athletes requires imaging modalities that can be used as methods of screening, where patients who are asymptomatic for the condition have imaging tests that are non-invasive and impart no radiation burden. Ultrasound is ideally suited for this purpose.

Symptomatic young athletes with groin pain potentially arising from FAI have a wide differential diagnosis that involves many soft tissue structures preferably imaged with ultrasound (126, 144, 200). Ideally, FAI could be detected in this cohort, often in teenage years when symptoms first appear and prior to the occurrence of advanced joint damage. Other modalities such as x-ray, CT and MRI are often held in reserve in this younger cohort due to radiation burden, invasiveness, cost and availability, factors which also favour ultrasound as the first line investigation. Ultrasound is known to be able to demonstrate the anterior femoral head-neck junction and we have shown that ultrasound can provide quantitative evidence of a cam lesion and is better suited than CT or MRI for the preliminary screening for the condition (193).

Our investigation has shown that in some cases there is a large discrepancy in the measured alpha angle between ultrasound and 3DCT. This mainly occurs in older patients with evidence of OA and in patients who have had prior osteoplasty. The bony cortical irregularities that

result cause the femoral head contour to break the femoral head circular template used for the alpha angle calculation on the ultrasound but not on the CT image. Bony cortical irregularities such as those related to advanced age or prior surgery may significantly reduce the accuracy of the ultrasound alpha angle calculation. Ultrasound calculation of the alpha angle would, however, have its major application in younger individuals who have not had surgical intervention.

Our results showed a large coefficient of variation in the ultrasound measurement, that we believe may have resulted from placement of the femoral neck baseline by visual approximation. Refining the technique for performing the alpha angle measurement could potentially reduce this variation.

It is difficult to justify surgical intervention to correct an anatomical abnormality before joint damage occurs as it is not clear that OA is an inevitable consequence of a mild abnormality (167, 201). Large scale studies demonstrating the progression of FAI to OA have not been performed due to the nature of the imaging studies used to characterise and quantify the degree of hip dysmorphia (5). Ultrasound, utilising our technique for quantifying the degree of anatomical abnormality, would be ideal in a prospective, longitudinal setting with the aim of examining the association between FAI and OA over time.

It has recently been discovered that many patients with FAI demonstrate generalized joint hypermobility (202). Microinstability of the hip has been cited as a cause of symptoms that occur in the presence of translation of the femoral head away from conformity with the acetabular fossa due to capsular laxity, leading to abnormal motion of the articular surfaces (203). The pathomechanics of hip microinstability are thought to involve anatomical abnormalities, repetitive forces/microtrauma across the hip (overuse in elite athletes) and capsular ligamentous laxity (202-204). The hip capsule is a key static constraint to



translation/subluxation of the hip through a wide range of physiological motion (205). Small translations of the femoral head can lead to large increases in cartilage pressure leading to cartilage degeneration, tears of the anterosuperior labrum, and OA similar to FAI (203, 206). The iliofemoral ligament is the primary structure controlling hip joint stability in anterior translation and external rotation of the hip (202).

It is generally accepted that hip microinstability may cause rim loading, further worsening of articular cartilage damage, and eventual degenerative changes of the hip joint in a similar way to FAI (203). The hip capsule is thickest anteriorly at the 1-2 o'clock position, corresponding to the iliofemoral ligament (205). The iliofemoral ligament can become stretched and focally lax, particularly after overuse in elite athletes and/or after arthroscopy (202, 204, 206-208). The iliofemoral ligament has been shown to be abnormally thinned in patients with microinstability (202). In the course of our investigations of the hip we have used ultrasound to image the hip anteriorly, with the plane of imaging corresponding approximately to the iliofemoral ligament. Further studies could compare ultrasound measurements of the thickness of the iliofemoral ligament with arthroscopic or MRI assessment of the iliofemoral ligament thickness amongst patients with FAI or microinstability. Ultrasound potentially has the ability to detect and quantify FAI secondary to cam lesions of the femoral head-neck junction, and at the same time, assess the thickness of the iliofemoral ligament for thinning that potentially represents hip instability.

Iliopsoas impingement in the native hip is a mechanical conflict between the iliopsoas tendon and the labrum, primarily in extension that can result in acetabular labral impingement producing distinct anterior labral lesions (175, 209, 210). The iliopsoas tendon directly overlies the anterior capsulolabral complex at 2-3 o'clock (175). This area is included when imaging the hip for simple effusions or FAI. Seven of 24 (29.2%) patients who required

revision hip arthroscopy for ongoing symptoms were found to have a “tight” iliopsoas tendon overlying and impinging upon a torn or inflamed anterior labrum (210). Soft tissues conditions adjacent to the hip like iliopsoas tendon impingement and bursal effusions are thus ideal candidates for ultrasound imaging.

### 8.3 Ultrasound ~~replacing MRI~~ for early ALTR detection

Regular periodical follow-up of hip prosthetic implants has been recommended even in asymptomatic well-functioning cases by a number of international organizations to detect ALTR (19, 178). Current imaging protocols lack sensitivity to detect ALTR in asymptomatic well-functioning prostheses even though high failure rates of up to 48.8% at six years for certain types of implant have been reported (4, 36, 178, 196). Small implant-related soft tissue lesions have been shown to progress in size over time (188). MRI and CT imaging are not optimal due to difficulty in detecting small ALTR close to the implant due to artefact from the orthopaedic hardware. The safety of MRI has not been established for all types of ferrous implants. It also has a prolonged scan time, and an inability to image soft tissues with sufficient accuracy.

We have used ultrasound to characterise the typical appearances after hip arthroplasty, demonstrating that soft tissue thickening such as might be seen with intracapsular ALTR will manifest on ultrasound imaging as capsular expansion similar to fluid accumulation in the native hip. The normally concave anterior iliofemoral ligament becomes straight or convex as ALTR accumulates deep to the hip capsule. Such changes in the shape of the iliofemoral ligament are therefore an important sign of soft tissue thickening that may represent wear debris accumulating adjacent to the implant. The median maximal (range) AP measurement of

the anterior hip capsule was seven millimetres (4 – 56mm) when an abnormal shape of the anterior capsule was taken into account. Our investigation has shown that an important sign of early ALTR occurs when the AP anterior hip capsule measurement exceeds seven millimetres.

Our investigation has also found that the majority of iliopsoas bursal effusions occur in asymptomatic patients, and that larger fluid and/or synovial tissue collections can decompress anteromedially into the medial compartment containing the common femoral artery and vein, and superiorly under the inguinal ligament into the pelvis which may present as a pelvic mass. We have demonstrated that fluid in the iliopsoas bursa is a pathological finding after hip arthroplasty. Ultrasound examinations must therefore include the portion of the iliopsoas bursa above the line of the hip joint, deep to the inguinal ligament.

In our study, all ultrasound examinations were performed by a single operator. The inter-observer reliability of ultrasound cannot therefore be determined from our series. No longitudinal data for our study is available to confirm progression of small ultrasound detected abnormalities. Further validation of our findings, such as surgical confirmation, has not been performed and the false-positive and false-negative rates of ultrasound cannot be calculated. It is known that approximately 20% of small ultrasound- detected lesions will progress further, and therefore small lesions detected in our study will be included as part of the regular ongoing monitoring of these prostheses (179, 181). The patient cohort that we have studied here should continue to be monitored periodically for the life of the implant to determine if small ALTR that we have detected progress further. Ultrasound should always be performed together with plain x-ray imaging as aseptic loosening that can also be responsible for pain cannot be demonstrated with ultrasound imaging.

Training of sonographers to perform the ultrasound imaging that we have described will not

be difficult, as many of the structures that are included in the standard examination are already taught to novice sonographers as part of musculoskeletal ultrasound imaging. Only a small extra component of anatomical recognition is required.

Persistent groin symptoms after hip arthroplasty are present in 0.4% up to 18% of patients and present a diagnostic dilemma (211). Causes include acetabular loosening, fracture, ALTR and iliopsoas tendonitis and impingement (211). We have developed ultrasound imaging criteria that can be applied ~~in situations where patients present with symptoms that are consistent with ALTR~~ when performing ultrasound imaging of the post arthroplastic hip. The development of ALTR giving rise to groin or hip pain can now be recognised ~~earlier on ultrasound than any other imaging modality~~ on ultrasound imaging, potentially earlier in the process due to the nature of ultrasound imaging and its relatively low cost and wide availability.

Tendonitis or impingement of the iliopsoas tendon post arthroplasty may also give rise to groin symptoms that may mimic ALTR or loosening prosthesis. Up to 3.9% of all hip arthroplasties will demonstrate symptoms of iliopsoas tendonitis (212). Iliopsoas impingement may result from a prominent or malpositioned acetabular component, retained cement, excessively long screws, an acetabular cage, a prominent femoral component collar, an oversized acetabular component or femoral head larger than the native femoral head (211). Iliopsoas tendonitis may also occur, however, without any structural problem being identified and may manifest as a snapping or clunking sensation without pain (211). Iliopsoas impingement should be included in the differential diagnosis of groin pain following hip arthroplasty. Impingement usually occurs between the tendon and the anterior edge of the acetabular cup overhanging the acetabular ring (212, 213). ~~Our study has shown that focal tendinopathy can be demonstrated using ultrasound, were the normal tendon fibrillary echo pattern is lost~~. Ultrasound, with its advantages of imaging soft tissue closely adjacent to orthopaedic hardware would be ideal to utilise in an investigation of the rate of iliopsoas

tendinitis post arthroplasty. These applications should be explored further in future studies in order to establish the position of ultrasound in the investigation of iliopsoas tendinopathy post arthroplasty compared to CT and MRI.

We have clarified the ~~abnormal~~ characteristics of a hip prosthesis when imaged using ultrasound. Sonographers can now recognise early ALTR development in asymptomatic well-performing prostheses by carefully assessing the shape of the iliofemoral ligament and the iliopsoas bursa above the joint line. The early detection of ALTR provides the opportunity to selectively stream asymptomatic, well-functioning prostheses to a more frequent imaging program when required, reducing health costs and improving outcomes.

Given the increasing and common use of hip replacement surgery, we believe that regular follow up with imaging is warranted among both symptomatic and asymptomatic patients and suggest that US is ~~better suited~~well-suited to the serial evaluation of all hip prostheses, ~~than any other cross-sectional imaging modality.~~

## ***Chapter 9 Conclusion***

Ultrasound is a proven soft tissue imaging modality that has excellent image resolution, can be viewed in real time, ~~is repeatable~~, is widely available and relatively inexpensive.

Ultrasound is increasingly utilised to investigate all types of maladies and sources of pain, including several impingement and entrapment syndromes previously investigated with other more expensive and invasive imaging modalities. Although operator dependency is considered a weakness of ultrasound, the examinations that we have described are performed as part of current ultrasound practice, and can be quickly learned by inexperienced operators ~~or can be repeated multiple times~~. The ultrasound techniques described require no specialist knowledge and can be learned quickly.

In Chapters 4 and 5 we have described a novel approach for the detection and evaluation of the PCHA for occlusion or stenosis in ABER in patients suspected of suffering QSS. Our technique can rule out external impingement upon the axillary neurovascular bundle in ABER, effectively eliminating QSS as a diagnosis in most cases. Doppler ultrasound of the PCHA is a non-invasive, simple-to-perform test of occlusion or stenosis of the PCHA in ABER. The ready availability of ultrasound in comparison to alternative techniques means ultrasound may obviate the need for MR angiography in many patients. Future studies could correlate the incidence of PCHA stenosis using our method with the later development of vascular QSS and PCHA aneurysm formation in overhead athletes.

In Chapter 6 we have assessed the ability of ultrasound to quantify the femoral head-neck sphericity by comparing to 3DCT, the established Gold Standard.

We have shown that ultrasound measurement of the alpha angle in young patients without prior hip surgery or trauma can provide objective evidence of cam-type FAI in symptomatic

individuals, enabling clinicians to reserve more expensive and/or radiation-based modalities for patients in whom a cam lesion has already been detected by ultrasound. Recent reports in relation to hip impingement have indicated that symptoms can be the result of impingement via a thickened iliofemoral ligament. Ultrasound would be ideal to investigate the association of symptoms with such a thickened area of soft tissue.

Chapter 7 investigates the application of ultrasound to assessment of the post-arthroplastic hip. ALTR development in asymptomatic well-performing prostheses may be recognised earlier using ultrasound by carefully assessing the shape of the iliofemoral ligament. Given the increasing and common use of hip replacement surgery, we believe that regular follow up with imaging is warranted among all patients with ultrasound. Our characterisation of new findings associated with the soft tissues about the arthroplastic hip will allow other sonographers to perform these examinations with confidence. Current interest in follow-up of hip arthroplasty involves assessment of the iliopsoas tendon for impingement with the orthopaedic hardware. Ultrasound is ideally suited for this purpose.

We have demonstrated that ultrasound is an excellent first-line imaging investigation in the detection, characterisation and quantification of impingement and entrapment syndromes of the shoulder and hip. Ultrasound has an advantage over other established imaging techniques in screening programmes, young patient cohorts and in routine or post-surgical follow up. Ultrasound has emerged as a key imaging modality in the assessment of several entrapment and impingement syndromes affecting the shoulder and hip.

## **Chapter 10** References

1. Ergen FB, Vudali S, Şanverdi E, Dolgun A, Aydingöz Ü. CT assessment of asymptomatic hip joints for the background of femoroacetabular impingement morphology. *Diagn Intervention Radiol*. 2014;20(3):271-6.
2. Brown SAN, Doolittle DA, Bohanon CJ, Jayaraj A, Naidu SG, Huettl EA, et al. Quadrilateral space syndrome: the Mayo Clinic experience with a new classification system and case series. *Mayo Clinic proceedings*. 2015;90(3):382-94.
3. Australian Orthopaedic Association. National Joint Replacement Registry Adelaide: School of Population Health University of Adelaide; 2015 [Available from: <https://aoanjrr.sahmri.com/hips>].
4. Matharu GS, Mellon SJ, Murray DW, Pandit HG. Follow-up of Metal-on-Metal Hip Arthroplasty patients is currently not evidence based or cost effective. *The Journal of arthroplasty*. 2015;30(8):1317-23.
5. Ganz R, Leunig M, Leunig-Ganz K, Harris WH. The etiology of osteoarthritis of the hip. an integrated mechanical concept. *Clinical orthopaedics and related research*. 2008;466(2):264-72.
6. Linker CS HC, Fritz RC. Quadrilateral space syndrome: Findings at MR imaging. *Radiology*. 1993;188:675-6.
7. Sanders TG TP. Paralabral cyst: An unusual cause of quadrilateral space syndrome. *Arthroscopy*. 1999;15(6):632-63.
8. Sainani NI, Lawande MA, Pawar A, Patkar DP, Pungavkar SA. Posterior ankle impingement syndrome due to Os Trigonum. *Applied Radiology*. 2011;40(12):28(3).
9. Bashir WA, Connell DA. Imaging of Entrapment and Compressive Neuropathies. *Semin Musculoskelet Radiol*. 2008;12(2):170-82.
10. Cahill BR, Palmer RE. Quadrilateral space syndrome. *Journal of Hand Surgery Am*. 1983;8(1):65-9.
11. Nötzli HP, Wyss TF, Stoecklin CH, Schmid MR, Treiber K, Hodler J. The contour of the femoral head-neck junction as a predictor for the risk of anterior impingement. *The Journal of bone and joint surgery (BR)*. 2002;84-B(4):556-60.
12. Beaulè PE, Zaragoza E, Motamedi K, Copelan N, Dorey FJ. Three-dimensional computed tomography of the hip in the assessment of femoroacetabular impingement. *Journal of orthopaedic research : official publication of the Orthopaedic Research Society*. 2005;23(6):1286-92.
13. Naraghi AM, White LM. Magnetic resonance imaging of joint replacements. *Semin Musculoskelet Radiol*. 2006;10(1):98-106.
14. Martinoli C, Bianchi S. Hip. In: Baert AL, Knauth M, Sartor K, editors. *Ultrasound of the musculoskeletal system*. Berlin: Springer; 2007.
15. Ganz R, Parvizi J, Beck M, Leunig M, Notzli H, Siebenrock KA. Femoroacetabular impingement: a cause for osteoarthritis of the hip. *Clinical orthopaedics and related research*. 2003(417):112-20.
16. Revell PA. The combined role of wear particles, macrophages and lymphocytes in the loosening of total joint prostheses. *Journal of the Royal Society Interface*. 2008;5(28):1263-78.



17. Amstutz HC, Ma SM, Jinnah RH, Mai L. The Classic: Revision of Aseptic Loose Total Hip Arthroplasties. *Clinical orthopaedics and related research*. 2004;420.
  18. MHRA U. Medical safety alert: Metal-on-metal (MoM) hip replacements - updated advice with patient follow ups United Kingdom: United Kingdom Medicines and Healthcare products Regulatory Agency; 2012 [Web page]. Available from: <https://www.gov.uk/drug-device-alerts/medical-device-alert-metal-on-metal-mom-hip-replacements-updated-advice-with-patient-follow-ups>.
  19. USFDA A. Medical devices: Information about Soft Tissue Imaging and Metal Ion Testing [Web page]. United States Food and Drug Administration; 2015 [updated 04/10/2015; cited 2015. Web page]. Available from: <http://www.fda.gov/MedicalDevices/ProductsandMedicalProcedures/ImplantsandProsthetics/MetalonMetalHipImplants/ucm331971.htm>.
  20. Dorlands' Illustrated Medical Dictionary. 29 ed: WB Saunders Co; 1994. Dorlands' Illustrated Medical Dictionary.
  21. Schon LC. Nerve entrapment, neuropathy and nerve dysfunction in athletes. *Orthopedic Clinics of North America*. 1994;25(1):47-59.
  22. Klaue K, Durnin CW, Ganz R. The acetabular rim syndrome.
- A clinical presentation of dysplasia of the hip. *The Journal of bone and joint surgery (BR)*. 1991;73-B(3):423-9.
23. Koes BW, Hendriksen IJM, Burdorf A, Verhagen AP, Miedema HS, Verhaar JAN. Prevalence and incidence of shoulder pain in the general population; a systematic review AU - Luime, JJ. *Scandinavian Journal of Rheumatology*. 2004;33(2):73-81.
  24. Beggs I. Shoulder Ultrasound. *Seminars in Ultrasound, CT and MRI*. 2011;32(2):101-13.
  25. Plomb-Holmes C, Clavert P, Kolo F, Tay E, Läderrmann A. An orthopaedic surgeon's guide to ultrasound imaging of the healthy, pathological and postoperative shoulder. *Orthopaedics & Traumatology: Surgery & Research*. 2018;104(8, Supplement):S219-S32.
  26. Dimachkie MM, Barohn RJ. Chapter 55 - Peripheral Neuropathies A2 - Tubbs, R. Shane. In: Rizk E, Shoja MM, Loukas M, Barbaro N, Spinner RJ, editors. *Nerves and Nerve Injuries*. San Diego: Academic Press; 2015. p. 857-88.
  27. Atroshi I, Gummesson C, Johnsson R, Ornstein E, Ranstam J, Rosén I. Prevalence of carpal tunnel syndrome in a general population. *JAMA*. 1999;282(2):153-8.
  28. Lafosse L, Samitier G, Petkin K, Lafosse T, Gupta A. Nerve entrapment syndromes in the shoulder: Diagnosis, principles, and different techniques for nerve decompression. *Sports Injuries: Prevention, Diagnosis, Treatment and Rehabilitation, Second Edition* 2015. p. 205-18.
  29. Francel TJ, Dellon AL, Campbell JN. Quadrilateral space syndrome: Diagnosis and operative decompression technique. *Plastic and Reconstructive Surgery*. 1991;87(5):911-6.
  30. Bencardino JT, Rosenberg ZS. Entrapment neuropathies of the shoulder and elbow in the athlete. *Clinical sports medicine*. 2006;25(3):465-87.
  31. Tannast M, Siebenrock KA, Anderson SE. Femoroacetabular Impingement: Radiographic diagnosis - What the radiologist should know. *AJR*. 2007;188(6):1540-52.
  32. Ganz R, Parviz iJ, Beck M, Leunig M, Notzli H, Siebenrock KA. Femoroacetabular impingement. A cause for osteoarthritis of the hip. *Clinical orthopaedics and related research*. 2003;112-20.
  33. Murray RO. The aetiology of primary osteoarthritis of the hip. *British Journal of Radiology*. 1965;38(455):810-24.
  34. (HICA) HICA. The growing cost of hip and knee replacements Templestowe: HICA; 2014 [Available from: <http://www.hica.com.au/health-insurance-news/the-growing-cost-of-hip-and-knee-replacements>].

35. Witzleb W-C, Hanisch U, Kolar N, Krummenauer F, Guenther K-P. Neo-capsule tissue reactions in metal-on-metal hip arthroplasty. *Acta Orthopaedica*. 2007;78(2):211-20.
  36. Langton DJ, Jameson SS, Joyce TJ, Gandhi JN, Sidaginamale R, Mereddy P, et al. Accelerating failure rate of the ASR total hip replacement. *Journal of Bone & Joint Surgery, British Volume*. 2011;93-B(8):1011-6.
  37. Hing CB, Young DA, Dalziel RE, Bailey M, Back DL, Shimmin AJ. Narrowing of the neck in resurfacing arthroplasty of the hip: a radiological study. *J Bone Joint Surg (Br)*. 2007;89(B)(8):1019-24.
  38. Kohan L, Field C, Kerr D, Ben-Nissan B. Femoral neck remodelling after hip resurfacing surgery: a radiological study. *ANZ Journal of Surgery*. 2014;84(9):639-42.
  39. USFDA. Medical devices: Information about Soft Tissue Imaging and Metal Ion Testing 2015 [updated 04/10/2015; cited 2015. Available from: <http://www.fda.gov/MedicalDevices/ProductsandMedicalProcedures/ImplantsandProsthetics/MetalonMetalHipImplants/ucm331971.htm>.
  40. (AOANJRR) AOANJRR. Annual Report 2017
- Hip, Knee & Shoulder Arthroplasty. Adelaide; 2016.
41. Clohisy JC, Carlisle JC, Beaulé PE, Kim Y-J, Trousdale RT, Sierra RJ, et al. A systematic approach to the plain radiographic evaluation of the young adult hip. *J Bone Joint Surg (Am)*. 2008;90(Suppl 4):47-66.
  42. Martinoli C, Bianchi S, Pugliese F, Bacigalupo L, Gauglio C, Valle M, et al. Sonography of entrapment neuropathies in the upper limb (wrist excluded). *J Clin Ultrasound*. 2004;32(9):438-50.
  43. Nazarian LN. The Top 10 Reasons Musculoskeletal Sonography Is an Important Complementary or Alternative Technique to MRI. *American Journal of Roentgenology*. 2008;190(6):1621-6.
  44. Cahill BR PR. Quadrilateral space syndrome. *Journal of Hand Surgery*. 1983;8:65-9.
  45. Brestas PS, Tsouroulas M, Nikolakopoulou Z, Malagari K, Drossos C. Ultrasound findings of teres minor denervation in suspected quadrilateral space syndrome. *Journal of clinical ultrasound*. 2006;34(7):343-7.
  46. Mochizuki T, Isoda H, Masui T, Ohkawa Y, Takahashi M, Takehara Y, et al. Occlusion of the posterior circumflex humeral artery: Detection with MR angiography in healthy volunteers and in a patient with quadrilateral space syndrome. *American journal of Roentgenology*. 1994;163(3):625-7.
  47. Tao M, Eisenberg N, Jaskolka J, Roche-Nagle G. Coil embolization of a posterior circumflex humeral aneurysm in a volleyball player. *Vasa - European Journal of Vascular Medicine*. 2016;45(1):67-70.
  48. Dean RH, Yao JST, Brewster DC. Current diagnosis and treatment in vascular surgery. 1 ed. Norwalk, Connecticut: Appleton and Lange; 1995.
  49. Kohler TR, Nance DR, Cramer MM, Van den burghe N, Strandness DEJ. Duplex scanning for diagnosis of aortoiliac and femoropopliteal disease: a prospective study. *Circulation*. 1987;76(5):1074-80.
  50. Cossman DV, Ellison JE, Wagner WH, Carroll RM, Treiman RL, Foran RF, et al. Comparison of contrast angiography to arterial mapping with color-flow duplex imaging in the lower extremities. *Surgery*. 1989;10:522-9.
  51. Demondion X, Herbinet P, Van Sint JS, Boutry N, Chantelot C, Cotten A. Imaging assessment of thoracic outlet syndrome. *Radiographics*. 2006;26(6):1735-50.
  52. Seifert H. Diagnostic value of duplex scanning in peripheral vascular disease. *Vascular Medicine Review*. 1990;1:21-33.

53. Clohisey JC, Nunley RM, Otto RJ, Schoenecker PL. The frog-leg lateral radiograph accurately visualised hip cam impingement abnormalities. *Clinical orthopaedics and related research*. 2007;462:115-21.
54. Siddiqui IA, Sabah SA, Satchithananda K, Lim AK, Cro S, Henckel J, et al. A comparison of the diagnostic accuracy of MARS MRI and ultrasound of the painful metal-on-metal hip arthroplasty. *Acta Orthopaedica*. 2014;85(4):375-82.
55. Daivajna SC, Duncan CP, Masri BA, Garbuz DS. Ultrasound: Optimal screening test for pseudotumor detection. *Seminars in Arthroplasty*. 2015;26(3):121-4.
56. Sdao S, Orlandi D, Aliprandi A, Lacelli F, Sconfienza LM, Randelli F, et al. The role of ultrasonography in the assessment of peri-prosthetic hip complications. *Journal of Ultrasound*. 2014;18(3):245-50.
57. Williams PL, Warwick R, editors. *Gray's Anatomy*. 36 ed. Edinburgh: Churchill Livingstone; 1980.
58. Diercks RL. Proximal Humerus. In: Bain GI, Itoi E, Di Giacomo G, Sugaya H, editors. *Normal and Pathological Anatomy of the Shoulder*: Springer; 2015. p. 29-33.
59. Bernstein EF. *Vascular Diagnosis*. 4 ed: Mosby; 1993 Jan. 1058 p.
60. Van de Pol D, Alaeikhanehshir S, Kuijer PPFM, Terpstra A, Pannekoek-Hekman MJC, Planken RN, et al. Reproducibility of the SPI-US protocol for ultrasound diameter measurements of the Posterior Circumflex Humeral Artery and Deep Brachial Artery: an inter-rater reliability study. *Eur Radiol*. 2016;26(8):2455-61.
61. Van de Pol D, Maas M, Terpstra A, Pannekoek-Hekman M, Alaeikhanehshir S, Kuijer PPFM, et al. Ultrasound assessment of the posterior circumflex humeral artery in elite volleyball players: Aneurysm prevalence, anatomy, branching pattern and vessel characteristics. *Eur Radiol*. 2017;27(3):889-98.
62. Anatomy.tv the world's most detailed model of human anatomy online [Internet]. Primal Pictures Ltd. 2001-present [cited 2015].
63. Nimura A, Akita K, Sugaya H. Brachial Plexus. In: Bain GI, Itoi E, Di Giacomo G, Sugaya H, editors. *Normal and Pathological Anatomy of the Shoulder*: Springer; 2015. p. 309 - 13.
64. Galley IJ. Axillary Nerve. In: Bain GI, Itoi E, Di Giacomo G, Sugaya H, editors. *Normal and Pathological Anatomy of the Shoulder*: Springer; 2015. p. 315 - 30.
65. Loomer R, Graham B. Anatomy of the Axillary Nerve and its' relation to inferior capsular shift. *Clinical orthopaedics and related research*. 1989(243):100-5.
66. Blum A, Lecocq S, Louis M, Wassel J, Moisei A, Teixeira P. The nerves around the shoulder. *European Journal of Radiology*. 2013;82(1):2-16.
67. McClelland D, Paxinos A. The anatomy of the quadrilateral space with reference to quadrilateral space syndrome. *Journal of shoulder and elbow surgery*. 2008;17(1):162-4.
68. Sato T, Sato N. Clinical relevance of the hip joint: Part I – Review of the anatomy of the hip joint. *International Musculoskeletal Medicine*. 2015;37(4):141-5.
69. Stulberg SD, Cordell LD, Harris WH, Ramsey PL, MacEwen GD. Unrecognized childhood hip disease. A major cause of idiopathic osteoarthritis of the hip. *The Hip Proceedings of the third open scientific meeting of the hip society*. 1975:212-28.
70. Kelly BT, Bedi A, Robertson CM, Dela Torre K, Giveans MR, Larson CM. Alterations in internal rotation and alpha angles are associated with arthroscopic cam decompression in the hip. *The American journal of sports medicine*. 2012;40(5):1107-12.
71. Walters B, Cooper H, Rodriguez J. New Findings In Hip Capsular Anatomy: A Cadaveric Study of the Ligamentous and Muscular Contributions to the Hip Capsule. *Arthroscopy: The Journal of Arthroscopic & Related Surgery*. 2013;29(12, Supplement):e200.
72. Rylander L, Froelich JM, Novicoff W, Saleh K. Femoroacetabular impingement and acetabular labral tears. *Orthopedics*. 2010;33(5):342-52.

73. Huang R, Diaz C, Parvizi J. Acetabular labral tears: focused review of anatomy, diagnosis, and current management. *The Physician and sportsmedicine*. 2012;40(2):87-93.
74. Kim YT, Azuma H. The nerve endings of the acetabular labrum. *Clinical orthopaedics and related research*. 1995(320):176-81.
75. Van Dyke JA, Holley HC, Anderson SD. Review of iliopsoas anatomy and pathology. *Radiographics*. 1987;7(1):53-84.
76. Meaney JF, Cassar-Pullicino VN, Etherington R, Ritchie DA, McCall IW, Whitehouse GH. Ilio-psoas bursa enlargement. *Clinical Radiology*. 1992;45(3):161-8.
77. Loneragan R, Anderson J, Taylor J. Distended iliopsoas bursa: case reports and anatomical dissection. *Australasian Radiology*. 1994;38(4):331-5.
78. Bianchi S, Martinoli C, Keller A, Bianchi-Zamorani MP. Giant iliopsoas bursitis: sonographic findings with magnetic resonance correlations. *Journal of Clinical Ultrasound*. 2002;30(7):437-41.
79. Safran MR. Nerve injury about the shoulder in athletes, part 1: suprascapular nerve and axillary nerve. *The American journal of sports medicine*. 2004;32(3):803-19.
80. Hung CY, Chang KV, Chen PT, Ho YT, Han DS, Chen WS, et al. Sonoelastography for the evaluation of an axillary schwannoma in a case of quadrilateral space syndrome. *Clinical Imaging*. 2014;38(3):360-3.
81. Lester B, Jeong GK, Weiland AJ, Wickiewicz TL. Quadrilateral space syndrome: Diagnosis, pathology and treatment. *American Journal of Orthopedics (Belle Mead NJ)*. 1999;28(12):718-22.
82. McKowen HC, Voorhies RM. Axillary Nerve entrapment in the quadrilateral space: case report. *J Neurosurg*. 1987;66(6):932-4.
83. Bencardino JT RZ. Entrapment neuropathies of the shoulder and elbow in the athlete. *Clinical sports medicine*. 2006;25:465-87.
84. Chautems RC, Glauser T, Waeber-Fey M, Rostan O, Barraud GE. Quadrilateral space syndrome: Case report and review of the literature. *Annals of vascular surgery*. 2000;14(6):673-6.
85. Linker CS, Helms CA, Fritz RC. Quadrilateral space syndrome: findings at MR imaging. *Radiology*. 1993;188(3):675-6.
86. Chen D, Cai P, Lao G, Gu Y. Quadrilateral Space Syndrome. *Chinese Medical Journal (Engl)*. 1995;108(2):109-12.
87. Sanders TG, Tirman PF. Paralabral cyst: an unusual cause of quadrilateral space syndrome. *Arthroscopy : the journal of arthroscopic & related surgery : official publication of the Arthroscopy Association of North America and the International Arthroscopy Association*. 1999;15(6):632-7.
88. Sofka CM, Haddad ZK, Adler RS. Detection of muscle atrophy on routine sonography of the shoulder. *J Ultrasound Med*. 2004;23(8):1031-4.
89. Wilson L, Sundaram M, Piraino DW, Ilaslan H, Recht MP. Isolated teres minor atrophy: manifestation of quadrilateral space syndrome or traction injury to the axillary nerve? *Orthopedics*. 2006;29(5):447-50.
90. de Mooij T, Duncan AA, Kakar S. Vascular injuries in the upper extremity in athletes. *Hand Clinics*. 2015;31(1):39-52.
91. Atema JJ, Ünlü Ç, Reekers JA, Idu MM. Posterior circumflex humeral artery injury with distal embolisation in professional volleyball players: A discussion of three cases. *European Journal of Vascular and Endovascular Surgery*. 2012;44(2):195-8.
92. Schulte KR, Warner JJP. Uncommon causes of shoulder pain in the athlete. *Orthopedic Clinics of North America*. 1995;26(3):505-8.
93. Okino S MH, Matoba M. The quadrilateral space syndrome. *Neuroradiology*. 1995;37:311-2.

94. Poole GV, Thomae KR. Thoracic outlet syndrome reconsidered. *American Surgery*. 1996;62(4):287-91.
95. Conn JJ. Thoracic outlet syndromes. *Surg Clin North Am*. 1974;54(1):155-64.
96. Demondion X, Vidal C, Herbinet P, Gautier C, Duquesnoy B, Cotten A. Ultrasonographic assessment of arterial cross-sectional area in the thoracic outlet on postural maneuvers measured with power Doppler ultrasonography in both asymptomatic and symptomatic populations. *J Ultrasound Med*. 2006;25(2):217-24.
97. Sanders RJ, Hammond SL, Rao NM. Clinical update: Diagnosis of thoracic outlet syndrome. *J Vasc Surg*. 2007;46(3):601-4.
98. Czihal M, Banafsche R, Hoffmann U, Koeppel T. Vascular compression syndromes. *Vasa - European Journal of Vascular Medicine*. 2015;44(6):419-34.
99. Wadhvani R, Chaubal N, Sukthankar R, Shroff M, Agarwala S. Color Doppler and duplex sonography in 5 patients with thoracic outlet syndrome. *J Ultrasound Med*. 2001;20(7):795-801.
100. Gergoudis R, Barnes RW. Thoracic outlet arterial compression: Prevalence in normal persons. *Angiology*. 1980;31(8):538-41.
101. Longley DG, Yedlicka JW, Molina E.J., Schwabacher S, Hunter DW, Letourneau JG. Thoracic outlet syndrome: Evaluation of the subclavian vessels by color duplex sonography. *AJR*. 1992;158(3):623-30.
102. Stapleton C, Herrington L, George K. Sonographic evaluation of the subclavian artery during thoracic outlet syndrome shoulder manoeuvres. *Man Therapy*. 2009;14(1):19-27.
103. Australia Co. Medicare Benefits Schedule Book Category 2: Australian Government Department of Health; 2014 [Medicare Benefits Schedule]. Available from: <http://www.health.gov.au/mbsonline>.
104. Amin MF, Berst M, el-Khoury GY. An unusual case of the quadrilateral space impingement syndrome caused by a bone spike. *Skeletal radiology*. 2006;35(9):956-958.
105. Kim S-H. Pathoanatomy of Glenohumeral Instability. In: Bain GI, Itoi E, Di Giacomo G, Sugaya H, editors. *Normal and Pathological Anatomy of the Shoulder*: Springer; 2015. p. 115-22.
106. Sofka CM, Lin J, Feinburg J, Potter HG. Teres minor denervation on routine magnetic resonance imaging of the shoulder. *Skeletal radiology*. 2004;33:514-8.
107. Cothran RL, Helms CA. Quadrilateral Space Syndrome: Incidence of imaging findings in a population referred for MRO of the shoulder. *AJR*. 2005;184:989-92.
108. Ashry R, Schweitzer ME, Cunningham P, Cohen J, Babb JC, A. Muscle atrophy as a consequence of rotator cuff tears: should we compare the muscles of the rotator cuff with those of the deltoid? *Skeletal radiology*. 2007;36:841-5.
109. Middleton WD, Teefey SA, Yamaguchi K. Sonography of the rotator cuff: Analysis of interobserver variability. *American Journal of Roentgenology*. 2004;183(5):1465-8.
110. Ellegaard K, Wieland I, Warming S, Juul-Kristensen B. Intra-rater and inter-rater reliability of the standardized ultrasound protocol for assessing subacromial structures AU - Hougs Kjær, Birgitte. *Physiotherapy Theory and Practice*. 2017;33(5):398-409.
111. Taljanovic MS, Gimber LH, Becker GW, Latt LD, Klauser AS, Melville DM, et al. Shear-Wave Elastography: Basic Physics and Musculoskeletal Applications. *Radiographics*. 2017;37:855-70.
112. Gilbert F, Klein D, Weng AM, Köstler H, Schmitz B, Schmalzl J, et al. Supraspinatus muscle elasticity measured with real time shear wave ultrasound elastography correlates with MRI spectroscopic measured amount of fatty degeneration. *BMC musculoskeletal disorders*. 2017;18(1).
113. Ooi CC, Malliaras P, Schneider ME, Connell DA. "Soft, hard, or just right?" Applications and limitations of axial-strain sonoelastography and shear-wave elastography in the assessment of tendon injuries. *Skeletal radiology*. 2014;43(1):1-12.

114. Gent R. Applied physics and technology of diagnostic ultrasound. Prospect, South Australia: Milner publishing; 1997.
115. Martinoli C, Derchi LE, Rizzatto G, Solbiati L. Power Doppler sonography: general principles, clinical applications, and future prospects. *Eur Radiol.* 1998;8(7):1224-35.
116. Myers K, Clough A. Making sense of vascular ultrasound. London: Arnold Publishers; 2004.
117. Martinoli C, Bianchi S, Prato N, Pugliese F, Zamorani MP, Valle M, et al. US of the shoulder: non-rotator cuff disorders. *Radiographics.* 2003;23(2):381-401.
118. Jager KA, Phillips DJ, Martin RL, Hanson C, Roederer GO, Langlois YE, et al. Noninvasive mapping of lower limb arterial lesions. *Ultrasound in Medicine and Biology.* 1985;11:515-21.
119. Zierler RE, Zierler BK. Duplex sonography of lower extremity arteries. 3rd ed. Sydney: W.B. Saunders Company; 1992.
120. Strandness DEJ. Hemodynamics of arterial stenosis and occlusion: Lippincott Williams and Wilkins; 2002.
121. Reimers K, Reimers CD, Wagner S, Paetzke I, Pongratz DE. Skeletal muscle sonography: a correlative study of echogenicity and morphology. *J Ultrasound Med.* 1993;12(2):73-7.
122. Campbell SE, Adler R, Sofka CM. Ultrasound of muscle abnormalities. *Ultrasound Quarterly.* 2005;21(2):87-94.
123. Strobel K, Hodler J, Meyer DC, Pfirrmann CW, Pirkel C, Zanetti M. Fatty atrophy of supraspinatus and infraspinatus muscles: accuracy of US. *Radiology.* 2005;237(2):584-9.
124. Elmslie RC. Remarks on Aetiological Factors in Osteoarthritis of the Hip Joint. *BMJ.* 1933;7(1):1-3.
125. Solomon L. Patterns of osteoarthritis of the hip. *J Bone Joint Surg (Br).* 1976;58-B(2):176-83.
126. Murray RO, Duncan C. Athletic activity in adolescence as an etiological factor in degenerative hip disease. *Journal of Bone and Joint Surgery - Series B.* 1971;53B(3):406-19.
127. Stulberg SD, Harris WH. Acetabular dysplasia and the development of osteoarthritis of the hip. Charnley J, editor. St Louis: C. V. Mosby Co; 1974.
128. Wedge JH, Wasylenko MJ, Houston CS. Minor anatomic abnormalities of the hip joint persisting from childhood and their possible relationship to idiopathic osteoarthritis. *Clinical orthopaedics and related research.* 1991(264):122-8.
129. Harris WH. Etiology of osteoarthritis of the hip. *Clinical orthopaedics and related research.* 1986(213):20-33.
130. Eijer H, Myers SR, Ganz R. Anterior femoroacetabular impingement after femoral neck fractures. *Journal of Orthopaedic Trauma.* 2001;15(7):475-81.
131. Siebenrock KA, Wahab KHA, Werlen S, Kalhour M, Leunig M, Ganz R. Abnormal extension of the femoral head epiphysis as a cause of cam impingement. *Clinical orthopaedics and related research.* 2004(418):54-60.
132. Carney BT, Weinstein SL. Natural history of untreated chronic slipped capital femoral epiphysis. *Clinical orthopaedics and related research.* 1996(322):43-7.
133. Goodman DA, Feighan JE, Smith AD, Latimer B, Buly RL, Cooperman DR. Subclinical slipped capital femoral epiphysis: Relationship to osteoarthritis of the hip. *The journal of bone and joint surgery (Am).* 1997;79-A(10):1489-97.
134. Reynolds D, Lucas J, Klaue K. Retroversion of the acetabulum. A cause of hip pain. *The Journal of bone and joint surgery (BR).* 1999;81-B(2):281-8.
135. Leunig M, Casillas MM, Hamlet M, Hersche O, Notzli H, Slongo T, et al. Slipped capital femoral epiphysis: early mechanical damage to the acetabular cartilage by a prominent femoral metaphysis. *Acta Orthop Scand.* 2000;71(4):370-5.

136. Clohisy JC, Knaus ER, Hunt DM, Leshner JM, Harris-Hayes M, Prather H. Clinical presentation of patients with symptomatic anterior hip impingement. *Clinical orthopaedics and related research*. 2009;467(3):638-44.
137. Philippon MJ, Maxwell RB, Johnston TL, Schenker M, Briggs KK. Clinical presentation of femoroacetabular impingement. *Knee Surgery, Sports Traumatology, Arthroscopy*. 2007;15(8):1041-7.
138. Nogier A, Bonin N, May O, Gedouin JE, Bellaiche L, Boyer T, et al. Descriptive epidemiology of mechanical hip pathology in adults under 50 years of age. Prospective series of 292 cases: Clinical and radiological aspects and physiopathological review. *Orthopaedics & traumatology, surgery & research : OTSR*. 2010;96(8 Suppl):S53-8.
139. Ito K, Minka M-An, Leunig M, Werlen S, Ganz R. Femoroacetabular impingement and the cam-effect. A MRI-based quantitative anatomical study of the femoral head-neck offset. *The Journal of bone and joint surgery (Br)*. 2001;83-B(2):171-6.
140. Audenaert E, Vigneron L, Pattyn C. A method for three-dimensional evaluation and computer aided treatment of femoroacetabular impingement. *Computer aided surgery : official journal of the International Society for Computer Aided Surgery*. 2011;16(3):143-8.
141. Beck M, Kalhor M, Leunig M, Ganz R. Hip morphology influences the pattern of damage to the acetabular cartilage: femoroacetabular impingement as a cause of early osteoarthritis of the hip. *J Bone Joint Surg (Br)*. 2005;87-B(7):1012-8.
142. Macfarlane RJ, Haddad FS. The diagnosis and management of femoro-acetabular impingement. *Ann R Coll Surg Engl*. 2010;92(5):363-7.
143. Byrd JW. Femoroacetabular Impingement in Athletes: current concepts. *The American journal of sports medicine*. 2014;42(3):737-51.
144. Imam S, Khanduja V. Current concepts in the diagnosis and management of femoroacetabular impingement. *International Orthopaedics*. 2011;35(10):1427-35.
145. Ejnisman L, Philippon MJ, Lertwanich P. Femoroacetabular impingement: the Femoral Side. *Clinics in sports medicine*. 2011;30(2):369-77.
146. Laborie LB, Lehmann TG, Engesaeter IO, Eastwood DM, Engesaeter LB, Rosendahl K. Prevalence of radiographic findings thought to be associated with femoroacetabular impingement in a population-based cohort of 2081 healthy young adults. *Radiology*. 2011;260(2):494-502.
147. Meyer DC, Beck M, Ellis T, Ganz R, Leunig M. Comparison of six radiographic projections to assess femoral head/neck asphericity. *Clinical orthopaedics and related research*. 2006;445:181-5.
148. Domayer SE, Ziebarth K, Chan J, Bixby S, Mamisch TC, Kim YJ. Femoroacetabular cam-type impingement: diagnostic sensitivity and specificity of radiographic views compared to radial MRI. *European Journal of Radiology*. 2011;80(3):805-10.
149. Clohisy JC, Carlisle JC, Trousdale R, Kim Y-J, Beaulé PE, Morgan P, et al. Radiographic evaluation of the hip has limited reliability. *Clinical orthopaedics and related research*. 2009;467(3):666-75.
150. Dudda M, Albers C, Mamisch TC, Werlen S, Beck M. Do normal radiographs exclude asphericity of the femoral head-neck junction. *Clinical orthopaedics and related research*. 2009;467(3):651-9.
151. Konan S, Rayan F, Haddad FS. Is the frog lateral plain radiograph a reliable predictor of the alpha angle in femoroacetabular impingement? *The journal of bone and joint surgery (Br)*. 2010;92-B(1):47-50.
152. Pollard TCB, Villar RN, Norton MR, Fern ED, Williams MR, Simpson DJ, et al. Femoroacetabular impingement and classification of the cam deformity: the reference interval in normal hips. *Acta Orthopaedica*. 2010;81(1):134-41.



153. Bellaiche L, Lequesne M, Gedouin JE, Laude F, Boyer T, French Arthroscopy S. Imaging data in a prospective series of adult hip pain in under-50 year-olds. *Orthopaedics & traumatology, surgery & research : OTSR*. 2010;96(8 Suppl):S44-52.
154. Barton C, Salineros M, Beaulé P. Validity of the alpha angle measurement on plain radiographs in the evaluation of Cam-type Femoroacetabular Impingement. *Clinical orthopaedics and related research*. 2011;469(2):464-9.
155. Brian P, Bernard S, Flemming D. Femoroacetabular Impingement: screening and definitive imaging. *Seminars in Roentgenology*. 2010;45(4):228-37.
156. Carlisle JC, Zebala LP, Shia DS, Hunt D, Morgan PM, Prather H, et al. Reliability of various observers in determining common radiographic parameters of adult hip structural anatomy. *The Iowa orthopaedic journal*. 2011;31:52-8.
157. Rakhra KS, Sheikh AM, Allen D, Beaulé PE. Comparison of MRI alpha angle measurement planes in femoroacetabular impingement. *Clinical orthopaedics and related research*. 2009;467(3):660-5.
158. James SLJ, Ali K, Malara F, Young D, O'Donnell J, Connell DA. MRI Findings of Femoroacetabular Impingement. *American Journal of Roentgenology*. 2006;187(6):1412-9.
159. Robben SGF, Lequin MH, Diepstraten AFM, den Hollander JC, Entius CAC, Meradji M. Anterior Joint Capsule of the Normal Hip and in Children with Transient Synovitis: US Study with Anatomic and Histologic Correlation1. *Radiology*. 1999;210:499-507.
160. Leekam RN, Matzinger MA, Mustard RA, Grosman H. Enlarged iliopsoas bursa simulating neoplasm on sonographic examination. *J Ultrasound Med*. 1985;4(9):493-4.
161. Lerch S, Kasperczyk A, Warnecke J, Berndt T, Ruhmann O. Evaluation of Cam-type femoroacetabular impingement by ultrasound. *International Orthopaedics*. 2013;37(5).
162. Buck FM, Hodler J, Zanetti M, Dora C, Pfirrmann CWA. Ultrasound for the evaluation of femoroacetabular impingement of the cam type. Diagnostic performance of qualitative criteria and alpha angle measurements. *European Journal of Radiology*. 2011;21(1):167-75.
163. Matsuda DK. The case for cam surveillance: the arthroscopic detection of cam femoroacetabular impingement missed on preoperative imaging and its significance. *Arthroscopy - Journal of Arthroscopic and Related Surgery*. 2011;27(6):870-6.
164. Pollard TCB. A perspective on femoroacetabular impingement. *Skeletal radiology*. 2011;40(7):815-8.
165. Jung KA, Restrepo C, Hellman M, AbdelSalam H, Morrison W, Parvizi J. The prevalence of cam-type femoroacetabular deformity in asymptomatic adults. *Journal of Bone and Joint Surgery - Series B*. 2011;93 B(10):1303-7.
166. Agricola R, Bessems JH, Ginai AZ, Heijboer MP, van der Heijden RA, Verhaar JA, et al. The development of Cam-type deformity in adolescent and young male soccer players. *The American journal of sports medicine*. 2012;40(5):1099-106.
167. Hartofilakidis G, Bardakos NV, Babis GC, Georgiades G. An examination of the association between different morphotypes of femoroacetabular impingement in asymptomatic subjects and the development of osteoarthritis of the hip. *Journal of Bone and Joint Surgery - Series B*. 2011;93 B(5):580-6.
168. Harris-Hayes M, Royer NK. Relationship of acetabular dysplasia and femoroacetabular impingement to hip osteoarthritis: a focused review. *PM and R*. 2011;3(11):1055-67.e1.
169. Emara K, Samir W, Motasem el H, Ghafar KA. Conservative treatment for mild femoroacetabular impingement. *Journal of orthopaedic surgery (Hong Kong)*. 2011;19(1):41-5.



170. Clohisy JC, St John LC, Schutz AL. Surgical treatment of femoroacetabular impingement. a systematic review of the literature. *Clinical orthopaedics and related research*. 2010;468(2):555-64.
171. Sionek A, Czubak J, Polaczek P, Czwojdzinski A. Osteochondroplasty as a treatment of femoroacetabular impingement. *Ortopedia, traumatologia, rehabilitacja*. 2010;12(6):504-10.
172. Harris WH. Traumatic arthritis of the hip after dislocation and acetabular fractures: treatment by mold arthroplasty. An end-result study using a new method of result evaluation. *Journal of Bone and Joint Surgery (Am)*. 1969;51(4):737-55.
173. Philippon MJ, Egnisman L, Ellis HB, Briggs KK. Outcomes 2 to 5 years following Hip Arthroscopy for Femoroacetabular Impingement in the patient aged 11 to 16 years. *Arthroscopy - Journal of Arthroscopic and Related Surgery*. 2012;28(9):1255-61.
174. Byrd JW. Arthroscopic hip surgery for the treatment of femoroacetabular impingement. *Orthopedics*. 2011;34(3):186.
175. Bardakos NV, Vasconcelos JC, Villar RN. Early outcome of hip arthroscopy for femoroacetabular impingement: the role of femoral osteoplasty in symptomatic improvement. *Journal of Bone and Joint Surgery - Series B*. 2008;90(12):1570-5.
176. Fabricant PD, Heyworth BE, Kelly BT. Hip arthroscopy improves symptoms associated with FAI in selected adolescent athletes. *Clinical orthopaedics and related research*. 2012;470(1):261-9.
177. Nikolaou VS, Bergeron SG, Huk OL, Zukor DJ, Antoniou J. Evaluation of persistent pain after hip resurfacing. *Bulletin of the NYU Hospital for joint diseases*. 2009;67(2):168-72.
178. UK MHRA. Medical safety alert: Metal-on-metal (MoM) hip replacements - updated advice with patient follow ups [Web page]. United Kingdom: United Kingdom Medicines and Healthcare products Regulatory Agency; 2012 [Web page]. Available from: <https://www.gov.uk/drug-device-alerts/medical-device-alert-metal-on-metal-mom-hip-replacements-updated-advice-with-patient-follow-ups>.
179. Almousa SA, Greidanus NV, Masri BA, Duncan CP, Garbuz DS. The natural history of inflammatory pseudotumors in asymptomatic patients after metal-on-metal hip arthroplasty. *Clin Orthop Relat Res*. 2013;471(12):3814-21.
180. USFDA C. Medical devices: Metal on Metal hip implants [Web page]. United States Food and Drug Administration; 2015 [updated 04/10/2015. Web page]. Available from: <http://www.fda.gov/MedicalDevices/ProductsandMedicalProcedures/ImplantsandProsthetics/MetalonMetalHipImplants/default.htm>.
181. Nishii T, Sakai T, Takao M, Yoshikawa H, Sugano N. Ultrasound screening of periarticular soft tissue abnormality around metal-on-metal bearings. *The Journal of arthroplasty*. 2012;27(6):895-900.
182. Martinoli C BS. Hip. In: Baert AL KM, Sartor K, editor. *Ultrasound of the musculoskeletal system*. Berlin: Springer; 2007.
183. Nikolaou V, Bergeron SG, Huk OL, Zukor DJ, Antoniou J. Evaluation of persistent pain after hip resurfacing. *Bulletin of the NYU Hospital for joint diseases*. 2009;67(2):168-72.
184. Rezig R, Copercini M, Montet X, Martinoli C, Bianchi S. Ultrasound diagnosis of anterior iliopsoas impingement in total hip replacement. *Skeletal radiology*. 2004;33(2):112-6.
185. Lachiewicz PF, Kauk JR. Anterior Iliopsoas impingement and tendinitis after total hip arthroplasty. *J Am Acad Orthop Surg*. 2009;17(6):337-44.
186. Kolmert L, Persson BM, Herrlin K, Ekelund L. Ileopectineal bursitis following total hip replacement. *Acta Orthopaedica Scand* 1984;55(1):63-5.
187. Lainiala O, Elo P, Reito A, Pajamaki J, Puolakka T, Eskelinen A. Good sensitivity and specificity of ultrasound for detecting pseudotumors in 83 failed metal-on-metal hip replacements. *Acta Orthopaedica*. 2015;86(3):339-44.

188. Low AK, Matharu GS, Ostlere SJ, Murray DW, Pandit HG. How Should We Follow-Up Asymptomatic Metal-on-Metal Hip Resurfacing Patients? A Prospective Longitudinal Cohort Study. *The Journal of arthroplasty*. 2016;31(1):146-51.
189. Okino S, Miyaji H, Matoba M. The quadrilateral space syndrome. *Neuroradiology*. 1995;37(4):311-2.
190. Robinson DJ, Marks P, Schneider-Kolsky ME. Ultrasound of the posterior circumflex humeral artery. *Journal of Medical Imaging and Radiation Oncology*. 2010;54(3):219-23.
191. Cormier PJ, Matalon TA, Wolin PM. Quadrilateral space syndrome: a rare cause of shoulder pain. *Radiology*. 1988;167(3):797-8.
192. Hogervorst T, Bouma H, De Boer SF, De Vos J. Human hip impingement morphology: An evolutionary explanation. *Journal of Bone and Joint Surgery - Series B*. 2011;93 B(6):769-76.
193. Robben SGF, Lequin MH, Diepstraten AFM, den Hollander JC, Entius CAC, Meradji M. Anterior joint capsule of the normal hip and in children with transient synovitis: US study with anatomic and histologic correlation. *Radiology*. 1999;210(2):499-507.
194. Grammatopoulous G, Pandit H, Kwon YM, Gundle R, McLardy-Smith P, Beard DJ, et al. Hip resurfacings revised for inflammatory pseudotumour have a poor outcome. *Journal of Bone & Joint Surgery, British Volume*. 2009;91-B(8):1019-24.
195. Munro JT, Masri BA, Duncan CP, Garbuz DS. High complication rate after revision of large-head metal-on-metal total hip arthroplasty. *Clin Orthop Relat Res*. 2014;472(2):523-8.
196. USFDA B. Information for Orthopaedic Surgeons: United States Food and Drug Administration; 2015 [updated 04/10/2015. Available from: <http://www.fda.gov/MedicalDevices/ProductsandMedicalProcedures/ImplantsandProsthetics/MetalonMetalHipImplants/ucm241667.htm> - 3a.
197. Tormenta S, Sconfienza L, Iannessi F, Bizzi E, Massafra U, Orlandi D, et al. Prevalence study of iliopsoas bursitis in a cohort of 860 patients affected by symptomatic hip osteoarthritis. *Ultrasound in Medicine and Biology*. 2012;38(8):1352-6.
198. Janus C, Hermann G. Enlargement of the iliopsoas bursa: unusual cause of cystic mass on pelvic sonogram. *J Clin Ultrasound*. 1982;10(3):133-5.
199. Van De Pol D, Maas M, Terpstra A, Pannekoek-Hekman M, Kuijer PPFM, Planken RN. B-mode sonographic assessment of the posterior circumflex humeral artery: The SPI-US protocol - A technical procedure in 4 steps. *Journal of Ultrasound in Medicine*. 2016;35(5):1015-20.
200. Stoller DW, editor. *Stoller's atlas of orthopaedics and sports medicine*. Baltimore: Lippincott Williams and Wilkins; 2008.
201. Emara K, Samir W, Motasem eH, Ghafar KA. Conservative treatment for mild femoroacetabular impingement. *Journal of orthopaedic surgery (Hong Kong)*. 2011;19(1):41-5.
202. Devitt BM, Smith BN, Stapf R, Tacey M, O'Donnell JM. Generalized joint hypermobility is predictive of hip capsular thickness. *Orthopaedic Journal of Sports Medicine*. 2017;5(4).
203. Han S, Alexander JW, Thomas VS, Choi J, Harris JD, Doherty DB, et al. Does Capsular Laxity Lead to Microinstability of the Native Hip? *The American journal of sports medicine*. 2018;46(6):1315-23.
204. Philippon MJ, Patterson D, Fagrelus T, Briggs KK. Hip Arthroscopy: Recent progress and future directions. In: Haddad FS, editor. *The Young Adult Hip in Sport*. London: Springer.
205. Philippon MJ, Michalski MP, Campbell KJ, Rasmussen MT, Goldsmith MT, Devitt BM, et al. A quantitative analysis of hip capsular thickness. *Knee Surgery, Sports Traumatology, Arthroscopy*. 2015;23(9):2548-53.

206. Martin HD, Savage A, Braly BA, Palmer IJ, Beall DP, Kelly B. The Function of the Hip Capsular Ligaments: A Quantitative Report. *Arthroscopy - Journal of Arthroscopic and Related Surgery*. 2008;24(2):188-95.
207. Cvetanovich GL, Harris JD, Erickson BJ, Bach Jr BR, Bush-Joseph CA, Nho SJ. Revision Hip Arthroscopy: A Systematic Review of Diagnoses, Operative Findings, and Outcomes. *Arthroscopy: The Journal of Arthroscopic & Related Surgery*. 2015;31(7):1382-90.
208. Telleria JJM, Lindsey DP, Giori NJ, Safran MR. An Anatomic Arthroscopic Description of the Hip Capsular Ligaments for the Hip Arthroscopist. *Arthroscopy: The Journal of Arthroscopic & Related Surgery*. 2011;27(5):628-36.
209. Blankenbaker DG, Tuite MJ. Non-Femoroacetabular Impingement. *Semin Musculoskelet Radiol*. 2013;17(03):279-85.
210. Heyworth BE, Shindle MK, Voos JE, Rudzki JR, Kelly BT. Radiologic and Intraoperative Findings in Revision Hip Arthroscopy. *Arthroscopy: The Journal of Arthroscopic & Related Surgery*. 2007;23(12):1295-302.
211. Henderson RA, Lachiewicz PF. Groin pain after replacement of the hip: aetiology, evaluation and treatment. *J Bone Joint Surg Br* 2012;94:145e51. *J Bone Joint Surg (Br)*. 2012;94-B(2):145-51.
212. Ueno T, Kabata T, Kajino Y, Inoue D, Ohmori T, Tsuchiya H. Risk Factors and Cup Protrusion Thresholds for Symptomatic Iliopsoas Impingement After Total Hip Arthroplasty: A Retrospective Case Control Study. *The Journal of arthroplasty*. 2018.
213. Trousdale RT, Cabanela ME, Berry DJ. Anterior Iliopsoas Impingement After Total Hip Arthroplasty. *The Journal of arthroplasty*. 1995;10(4):546-9.

## **Appendix 1 Ultrasound of the Posterior Circumflex Humeral Artery**

Volunteers for the studies detailed in Chapters four and five of this thesis were the same sample. They were recruited consecutively from attendees to the radiology clinic for imaging not involving the shoulder, or accompanying another patient having imaging performed. If volunteers were older than 18 years, and agreed to participate they were included.



**MONASH** University  
Medicine, Nursing and Health Sciences

## Explanatory Statement

### Investigators:

Mr. David Robinson

Dr. Michal Schneider-Kolsky

Dr. Paul Marks

### **Research Project:**

### **Ultrasound of the Posterior Circumflex Humeral Artery**

This information sheet is for you to keep.

The research staff at the Department of Medical Imaging & Radiation Sciences at Monash University, Dr. Michal Schneider-Kolsky, and Dr. Paul Marks and Mr. David Robinson at the Avenue Hospital will be conducting this project.

#### **Introduction.**

Your doctor has referred you to our clinic to have an ultrasound scan. This scan will take a few minutes to complete, and the results will be provided to your doctor, together with the images that we make.

Additionally, we are undertaking an investigation into the appearances on ultrasound of a small artery at the back of the shoulder. This artery is of interest in the diagnosis of a condition called Quadrilateral Space Syndrome (QSS).

Historically, this artery has been investigated using MRI and Arteriography, however very little is known about its' appearances on ultrasound. We aim to characterise this artery's' appearance using ultrasound, and hopefully make the diagnosis of QSS simpler.

This information will be important for the physicians of patients with shoulder pain, and for sonographers who

might perform scans in the diagnosis of QSS.

While the data collected will be important for the sonographers and referring medical staff, there will be no direct benefit to those people participating in this study.

### **What is involved?**

You will be given a questionnaire to complete prior to your shoulder scan. The questionnaire covers three sections: Section 1 asks you a few questions about yourself. Section 2 deals with any medical problems you may have had with your shoulders, and section 3 asks some questions about any symptoms that you may be experiencing now.

Completion of the questionnaire will take only a few minutes. The ultrasound scan will take only a few minutes, and there will be no further requirements placed upon you.

Apart from answering the questionnaire and undertaking an ultrasound scan, participation in this study will not cause you any further inconveniences.

There will be no financial rewards to the patients participating in this study.

### **Participation is voluntary**

Participating in this study is completely voluntary – you are under no obligation to consent to participation and you may withdraw at any stage, or avoid answering questions which are felt to be too personal or intrusive.

### **Confidentiality/results**

All aspects of the study, including results, will be strictly confidential and only the researchers will have access to information on participants. The data collected will not identify your personal details. All data collected will be summarised and no individual will be identified.

### **Storage of data**

Storage of the data collected will adhere to the University regulations and kept on University premises in a locked cupboard/filing cabinet for 5 years. A report of the study may be submitted for publication, but individual participants will not be identifiable in such a report.

### **Questions about the study and the results**

If you have any queries or would like to be informed of the aggregate research finding, please contact Dr. Michal Schneider-Kolsky on 99051348 or Fax 99058149. The findings will be accessible for 5 years. You can ask Dr. Schneider-Kolsky to send you the final report once the study is completed. Please indicate your interest to one of the investigators at the time of your scan.

### **What if I have a complaint?**

Should you have any complaint concerning the manner in which this research project is conducted, please do
--

not hesitate to contact the Monash University Standing Committee on Ethics in Research Involving Humans at the following address:

The Secretary

The Standing Committee on Ethics in Research Involving Humans (SCERH)

Building 3D

Research Grants & Ethics Branch

Monash University VIC 3800

[REDACTED]

[REDACTED]

Thank you for considering participation in this research project.

**Dept of Medical Imaging & Radiation Sciences**

Faculty of Medicine, Nursing and Health Sciences

Monash University

Wellington Road

Clayton 3800

[REDACTED]

[REDACTED]

ABN 12 377 614 012 CRICOS provider number 00008C

## Department of Medical Imaging &amp; Radiation Science

## Patient Questionnaire

## Research Project:

## Ultrasound of the Posterior Circumflex Humeral Artery

**Investigators:**

Dr Michal Schneider-Kolsky

Dr. Paul Marks

Mr. David Robinson (Research student)

**S1. Please provide us with some information about yourself:**

1. Are you male or female? Male Female (circle)
2. How old are you? \_\_\_\_\_ years
3. Which arm is your **dominant** arm (i.e. which arm do you use to write)  
Right Left (circle)
4. Do you or have you ever participated in any sport at “elite” level? Yes (detail) No

**S2. We would like to enquire about the medical history of your shoulder**

5. Have you ever had an operation on **either** shoulder?      Left      Right      Never (circle)
- a) Detail the operation \_\_\_\_\_
- b) When was the operation carried out?



6. Have you had shoulder pain before today?                      Yes                      No (go to S3)
- a) Which shoulder                      Left                      Right
- b) Did you have a scan of the shoulder                      Yes                      No
- c) What type of scan (circle all that apply)                      X-Ray   CT                      MRI                      Ultrasound
- d) What was the diagnosis

---



---

- e) What treatment were you given? (e.g. rest, physiotherapy, anti-inflammatories, Cortisone injection)

---



---



---

**S3. We would like to ask you if you currently have shoulder pain**

7. Are you having shoulder pain right now?                      Left                      Right                      Neither
- a) For how long have you had pain?                      \_\_\_\_\_

8. Do you have shoulder pain                      At work                      At sport                      Always                      Never

- a)                      What activity gives you pain? (i.e. Golf, Tennis, Gardening, Cleaning)

---

- b) Rate the level of pain that you experience undertaking this activity.

(no pain at all) 0 1 2 3 4 5 6 7 8 9 10 (worst possible pain)

*Thank you for your time!*



## Consent Form

### Ultrasound of the Posterior Circumflex Humeral artery

**NOTE: This consent form will remain with the Monash University researcher for their records**

I agree to take part in the Monash University research project specified above. I have had the project explained to me, and I have read the Explanatory Statement, which I keep for my records. I understand that agreeing to take part means that I am willing to:

I agree to participate in the survey by the researcher ☐ Yes ☐ No

**and**

I understand that my participation is voluntary, that I can choose not to participate in part or all of the project, and that I can withdraw at any stage of the project without being penalised or disadvantaged in any way.

**and**

I understand that any data that the researcher extracts from the study for use in reports or published findings will not, under any circumstances, contain names or identifying characteristics.

**and**

I understand that any information I provide is confidential, and that no information that could lead to the identification of any individual will be disclosed in any reports on the project, or to any other party.

**and**

I understand that the data will be destroyed after a 5-year period unless I consent to it being used in future research.

**Participants' name**

---

**Signature**

---

**Date**

---

## Suggested Amendments

### Exclusion criteria

Volunteers were excluded if they were having any imaging procedure of the shoulder performed.

### Pulsatility Index (PI)

While PI is a well-understood measure of vascular resistance, it is not commonly utilised in the determination of peripheral artery stenosis. Its' major application is in assessing vascular resistance in pregnancy.

### Number of males and females

There were 33 females and 17 males.

### Students t-test

This should read paired t-test. It was assumed all t-tests were Students' t tests, including paired and unpaired as the test statistic follows a Student's *t*-distribution under the null hypothesis.

### Results table.

	<u>Neutral</u>	<u>ABER</u>
<u>PSV Dominant arm</u>	<u>29.58 (±8.69) cm/sec</u>	<u>29.81 (±19.76) cm/sec</u>
<u>PSV Non-dominant arm</u>	<u>28.99 (±9.38) cm/sec</u>	<u>25.79 (±16.80) cm/sec</u>
<u>Resistive Index</u>	<u>0.92 (±0.07)</u>	<u>0.93 (±0.14)</u>

<u>Acceleration time</u>	<u>37.73 (<math>\pm 9.34</math>)</u>	<u>49.51 (<math>\pm 31.38</math>)</u>

### **Reliability of scanning method**

This publication was a “technical article” describing a new method for insonating the PCHA.

This paragraph refers to our method of obtaining Doppler signals from the PCHA when compared to a previously described method of placing the transducer in the axilla, which necessitates abduction of the arm, ruling out assessment of the PCHA in true neutral position.

It is acknowledged that the word “reliability” here is slightly misleading as it does not refer to a statistical analysis, but rather that the technique is simple to execute repeatedly.

## **Appendix 2 Ultrasound determination of the femoral head-neck alpha angle**



# **MONASH University**

**Monash University Human Research Ethics Committee (MUHREC)**

Research Office

### **Human Ethics Certificate of Approval**

**Date:** 2 August 2012

**Project Number:** CF12/2103 – 2012001144

**Project Title:** Ultrasound of femoroacetabular impingement

**Chief Investigator:** Dr Michal Schneider-Kolsky

**Approved:** From: 2 August 2012      **To:** 2 August 2017

---

#### **Terms of approval**

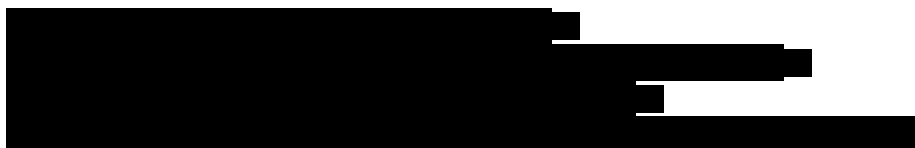
1. The Chief investigator is responsible for ensuring that permission letters are obtained, if relevant, and a copy forwarded to MUHREC before any data collection can occur at the specified organisation. **Failure to provide permission letters to MUHREC before data collection commences is in breach of the National Statement on Ethical Conduct in Human Research and the Australian Code for the Responsible Conduct of Research.**
2. Approval is only valid whilst you hold a position at Monash University.
3. It is the responsibility of the Chief Investigator to ensure that all investigators are aware of the terms of approval and to ensure the project is conducted as approved by MUHREC.

4. You should notify MUHREC immediately of any serious or unexpected adverse effects on participants or unforeseen events affecting the ethical acceptability of the project.
5. The Explanatory Statement must be on Monash University letterhead and the Monash University complaints clause must contain your project number.
6. **Amendments to the approved project (including changes in personnel):** Requires the submission of a Request for Amendment form to MUHREC and must not begin without written approval from MUHREC. Substantial variations may require a new application.
7. **Future correspondence:** Please quote the project number and project title above in any further correspondence.
8. **Annual reports:** Continued approval of this project is dependent on the submission of an Annual Report. This is determined by the date of your letter of approval.
9. **Final report:** A Final Report should be provided at the conclusion of the project. MUHREC should be notified if the project is discontinued before the expected date of completion.
10. **Monitoring:** Projects may be subject to an audit or any other form of monitoring by MUHREC at any time.
11. **Retention and storage of data:** The Chief Investigator is responsible for the storage and retention of original data pertaining to a project for a minimum period of five years.



Professor Ben Canny  
Chair, MUHREC

cc: Mr David John Robinson, Dr Steven Lee



ABN 12 377 614 012 CRICOS Provider #00008C



## Explanatory Statement

01/08/2012

**Title:** Ultrasound of femoroacetabular Impingement

**This information sheet is for you to keep**

My name is **David Robinson** and I am conducting a research project with **Dr. Steven Lee** and **Dr. Michal Schneider-Kolsky** (Senior Lecturer) in the Department of **Medical Imaging and Radiation Sciences** towards a PhD at Monash University.

You are invited to take part in this study. Please read this Explanatory Statement in full before making a decision to participate.

### **Why were you chosen for this research?**

You have been chosen to participate because you have been referred for an imaging procedure on your hip. You therefore qualify for the first of two research groups of this project.

### **The aim/purpose of the research**

I am conducting this research to find out if ultrasound may be able to be used as an alternative to CT scanning for femoroacetabular (FAI) of the hip. FAI is when part of the leg bone impacts against the bone of the pelvis, over time causing osteoarthritis of the hip joint.

### **Possible benefits**

There will be no direct benefits to you in taking part in this study. The study may prove that ultrasound can be used to assess FAI in place of other imaging modalities. This will make imaging cheaper, more readily available and safer as no radiation is used.

### **What does the research involve?**

The study involves a short ultrasound scan of your hip immediately before the CT scan. You will have to partially undress and lie on an ultrasound scanning couch while the scan takes place.

### **How much time will the research take?**

The ultrasound scan will take no more than five to ten minutes.

### **Inconvenience/discomfort**

You should experience no more than mild pressure over the front of your hip during the scan. As no x-rays are used, there will not be any side effects at all arising from the scan.

### **Payment**

There will be no financial reward for participation in this research. There will be no cost to you or Medicare if you participate in this research.

**Being in this study is voluntary and you are under no obligation to consent to participation. However, if you do consent to participate, you may withdraw from further participation at any stage. You will only be able to withdraw however, prior to the ultrasound scan being completed. Once data from the scan has been collected, you will not be able to withdraw as all data will be non-identifiable.**

### **Confidentiality**

Personal data that we collect in this research will not include names, address or phone numbers. We will collect basic demographic data only such as date of birth, gender and previous injury history from your medical record provided by your medical practitioner, and already in our practice records.

### **Storage of data**

Data collected will be stored in accordance with Monash University regulations, kept at The Avenue X-ray & MRI in a locked cupboard in the office of the investigator or on a password-protected computer.

### **Use of data for other purposes**

Your data will not be used for any other purpose.

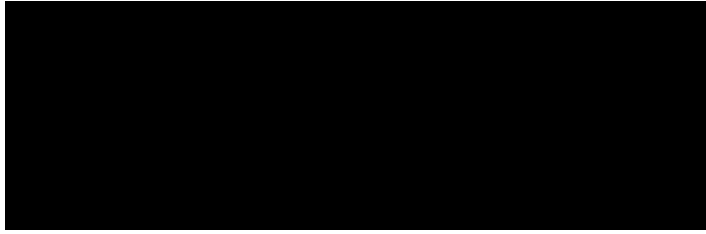
### **Results**

If you would like to be informed of the aggregate research finding, please contact **David Robinson** on [REDACTED]

If you would like to contact the researchers about any aspect of this study, please contact the Chief Investigator	If you have a complaint concerning the manner in which this research CF12/2103 – 2012001144 is being conducted, please contact:
Dr. Michal Schneider-Kolsky Senior Lecturer Faculty of Medicine, Nursing and Health Sciences Department of Medical Imaging and Radiation Sciences Monash University [REDACTED]	Executive Officer Monash University Human Research Ethics Committee (MUHREC) [REDACTED] [REDACTED] [REDACTED] [REDACTED] [REDACTED]

Thank You





**David Robinson**



## Consent Form

**Title:** Ultrasound of Femoroacetabular Impingement

**NOTE:** This consent form will remain with the Monash University researcher for their records

I understand that I have been asked to take part in the Monash University research project specified above. I have had the project explained to me, and I have read the Explanatory Statement, which I keep for my records.

<b>I understand that:</b>	<b>YES</b>	<b>NO</b>
<b>I will be asked to undergo a short ultrasound scan of my hip</b>	<input type="checkbox"/>	<input type="checkbox"/>
<b>My medical record will be used for basic demographic data only and will be completely anonymised</b>	<input type="checkbox"/>	<input type="checkbox"/>

I understand that my participation is voluntary, that I can choose not to participate in part or all of the project, and that I can withdraw at any stage of the project without being penalised or disadvantaged in any way

**and**

I understand that any data that the researcher extracts from the scan for use in reports or published findings will not, under any circumstances, contain names or identifying characteristics with my signed consent below

**and**

I understand that data from the scan will be kept in secure storage and will be accessible to the research team only. I also understand that the data will be destroyed after a five year period unless I consent to it being used in future research

**and**

I will remain anonymous at all times in any reports or publications from the project.

**Participants name:**

---

**Signature:** \_\_\_\_\_

**Date:** \_\_\_\_\_

## Suggested Amendments

**Results contingency table:** Ultrasound determination of the Femoral Head-Neck alpha angle

	# CT Positive (gold standard)	# CT Negative (gold standard)
Ultrasound Positive	63	27
Ultrasound Negative	6	21

### IntraClass Correlation Coefficient

This measure was not included as it would inconvenience our volunteers to ask them to return for repeat measurements. All measurements were performed at the same sitting. For this reason the CoV was used. We acknowledge that the ICC would benefit the overall findings of the thesis.

### Doppler Settings

<u>Settings</u>	<u>Frequency</u>	<u>Pulse repetition Freq.</u>	<u>Wall Filter</u>	<u>Sample Volume size</u>
<u>Colour Doppler</u>	<u>3 - 5.0 MHz</u>	<u>2 - 4 MHz</u>	<u>Level 1</u>	<u>Variable</u>
<u>Spectral Doppler</u>	<u>4 - 5 MHz</u>	<u>2 - 4 MHz</u>	<u>Variable</u>	<u>2-3mm</u>

It should be noted that on the machine in question (Siemens Sonoline Antares) color and spectral Frequency and PRF are dynamically variable depending upon what depth the sample box is placed.

## Appendix 3 Ultrasound of the Iliopsoas Bursa

### Explanatory Statement

01/08/2012

**Title:** Ultrasound of the Iliopsoas Bursa

**This information sheet is for you to keep**

My name is **David Robinson** and I am conducting a research project with **Dr. Steven Lee** and **Dr. Michal Schneider-Kolsky** (Senior Lecturer) in the Department of **Medical Imaging and Radiation Sciences** towards a PhD at Monash University.

You are invited to take part in this study. Please read this Explanatory Statement in full before making a decision to participate.

#### **Why were you chosen for this research?**

You have been chosen to participate because you qualify into one of the two research groups because you have had a hip replacement and been referred for an ultrasound of your hip.

#### **The aim/purpose of the research**

I am conducting this research to document and describe typical appearances of a fluid sac in front of the hip on ultrasound after hip replacement.

#### **Possible benefits**

Ultrasound is a cheaper and safer method of scanning the soft tissues surrounding the hip after hip replacement surgery but typical appearances on ultrasound are not generally well known. Results of the scan will be forwarded to your referring practitioner.

#### **What does the research involve?**

The study involves a short ultrasound scan of your hip. You will have to partially undress and lie on an ultrasound scanning couch while the scan takes place.

#### **How much time will the research take?**

The ultrasound scan will take no more than five to ten minutes.

#### **Inconvenience/discomfort**

You should experience no more than mild pressure over the front of your hip during the scan. As no x-rays are used, there will not be any side effects at all arising from the scan.

## Payment

There will be no financial reward for participation in this research. There will be no cost to you or Medicare if you participate in this research.

**Being in this study is voluntary and you are under no obligation to consent to participation. However, if you do consent to participate, you may withdraw from further participation at any stage. You will only be able to withdraw however, prior to the ultrasound scan being completed. Once data from the scan has been collected, you will not be able to withdraw as all data will be non-identifiable.**

## Confidentiality

Personal data that we collect in this research will not include names, address or phone numbers. We will collect basic demographic data only such as date of birth, gender and previous injury history from your medical record provided by your medical practitioner, and already in our practice records.

## Storage of data

Data collected will be stored in accordance with Monash University regulations, kept at The Avenue X-ray & MRI in a locked cupboard in the office of the investigator or on a password-protected computer.

## Use of data for other purposes

Your data will not be used for any other purpose.

## Results

If you would like to be informed of the aggregate research finding, please contact **David Robinson** on [REDACTED]

If you would like to contact the researchers about any aspect of this study, please contact the Chief Investigator	If you have a complaint concerning the manner in which this research CF12/2103 – 2012001144 is being conducted, please contact:
Dr. Michal Schneider-Kolsky Senior Lecturer Faculty of Medicine, Nursing and Health Sciences Department of Medical Imaging and Radiation Sciences Monash University [REDACTED] [REDACTED]	Executive Officer Monash University Human Research Ethics Committee (MUHREC) [REDACTED] [REDACTED] [REDACTED] [REDACTED] [REDACTED]

Thank You



**David Robinson**

## Consent Form

**Title:** Ultrasound of the Iliopsoas Bursa

**NOTE:** This consent form will remain with the Monash University researcher for their records

I understand that I have been asked to take part in the Monash University research project specified above. I have had the project explained to me, and I have read the Explanatory Statement, which I keep for my records.

<b>I understand that:</b>	<b>YES</b>	<b>NO</b>
<b>I will be asked to undergo a short ultrasound scan of my hip</b>	<input type="checkbox"/>	<input type="checkbox"/>
<b>My medical record will be used for basic demographic data only and will be completely anonymised</b>	<input type="checkbox"/>	<input type="checkbox"/>

I understand that my participation is voluntary, that I can choose not to participate in part or all of the project, and that I can withdraw at any stage of the project without being penalised or disadvantaged in any way

**and**

I understand that any data that the researcher extracts from the scan for use in reports or published findings will not, under any circumstances, contain names or identifying characteristics with my signed consent below

**and**

I understand that data from the scan will be kept in secure storage and will be accessible to the research team only. I also understand that the data will be destroyed after a five year period unless I consent to it being used in future research

**and**

I will remain anonymous at all times in any reports or publications from the project.

**Participants name:**

---

**Signature:** \_\_\_\_\_

**Date:** \_\_\_\_\_



## **Suggested Amendments**

### **Exclusion criteria**

As volunteers were recruited from consecutive patients presenting for followup imaging of hip prostheses, only those who did not sign informed consent were excluded.

### **Ultrasound measurements**

All three ultrasound measurements were performed at the same session by the same sonographer, after repositioning the transducer.

### **Threshold of normal**

The median maximal (range) AP measurement of the anterior hip capsule was seven millimetres (4 – 56mm) when an abnormal shape of the anterior capsule was taken into account.